Experimental Investigation of Leakage-Induced Pipe Erosion Outside of Pipe Leaks

Prepared by:

Stefan Pike

For:

Prof. J. E. van Zyl

In partial fulfilment of the requirements for:

Master of Science in Engineering

Submission Date:	23 May 2016
Institution:	University of Cape Town
Faculty:	Engineering and the Built Environment
Department:	Civil Engineering

Plagiarism Declaration

1. I know that plagiarism is wrong. Plagiarism is to use another's work and to pretend that it is one's own.

2. I have used the Harvard Convention for citation and referencing. Each significant contribution to and quotation in this report form the work or works of other people has been attributed and has been cited and referenced.

3. This report is my own work

4. I have not allowed and will not allow anyone to copy my work with the intension of passing it as his or her own work.

Student number: PKXSTE001 Name: Stefan Pike

Date: 23 May 2016 Signature: Signed by candidate

Abstract

The problem of water loss from water distribution systems is an issue that faces municipalities worldwide. A large proportion of water loss is a result of leakage. With increasing water scarcity across the globe, it is imperative to conserve water resources, and hence reduce leakage in water distribution systems as best we can. Leaks develop in various different forms, and they form in pipes of all materials.

It has been observed in numerous cases around the world that pipe material has been removed from the pipe surfaces adjacent to leaks in excavated failed water distribution pipe specimens. It was proposed by various researchers that this pipe material was being removed as a result of abrasive soil action caused by the pipe leak itself. When pressurised water distribution pipes fail, they emit high velocity jets of water into the surrounding soil bed. Research has shown that high velocity jets of water entering a granular soil bed have the ability to fluidise the bed, allowing the granular particles to move freely. This fluidisation mechanism is known as internal fluidisation. The concept of internal fluidisation offers an explanation for the erosion of pipe material adjacent to pipe leaks.

In this study, the removal of pipe material adjacent to leaks due to internal fluidisation has been termed "leakage-induced pipe erosion." This phenomenon has received minimal attention from researchers in the past. Leakage-induced pipe erosion has the potential to aggravate small existing leaks. There are two main implications of aggravating small leaks; firstly, where water authorities do not utilise active leak detection programmes, aggravating the initial leak conditions of small leaks can result in increased long term water losses. Secondly, in water distribution systems where the water authority does implement active leak detection programmes, aggravating small leaks increases the probability of finding and repairing them.

This aim of this study was to experimentally investigate the influence of various factors on the leakage-induced erosion process. Five main factors were investigated, namely bedding material grain size, cover depth, leakage flow rate, initial leak orientation and pipe material. An experimental setup was designed and manufactured in order to provide a controlled environment in which to investigate the factors affecting leakage-induced pipe erosion.

It was demonstrated in this study that small leaks have the ability to develop into larger leaks due to the erosion process. It was found in this study that of the five aforementioned factors, the orientation of the initial leak has the greatest influence on the rate of leakage-induced pipe erosion. It was also found that larger grain sizes and larger flow rates increased the rate of leakage-induced pipe erosion significantly. It was further demonstrated that of the three pipe materials that were tested, uPVC was the most susceptible to the erosion, while steel and HDPE exhibited more resistance to the soil abrasion. It was also found in this study that the cover depth of the soil bed had a small effect on the rate of leakage-induced pipe erosion within the tested range of bed heights.

Acknowledgements

I would like to express my gratitude and thank the following people who have assisted me throughout this research project. These people have provided me with support and expertise without which this project would not have been possible.

My supervisor, Prof. J. E. van Zyl, for his expert advice and guidance throughout the research project.

The Water Research Commission for the financial support required for tuition and research.

The Civil Engineering Department's senior technician, Mr. Charles Nicholas, for manufacturing the majority of the experimental setup and pipe samples used in this investigation.

Prof. C.Clayton for his expertise and advice on geotechnical matters.

Dr. D. Kalumba for his expertise and advice on soil mechanics and soil classification tests.

The laboratory manager, Mr Nooredien Hassen his team of laboratory assistants who helped with all logistical and management issues, and were always more than willing to assist with laboratory operations.

My family for their continuous support and encouragement.

Table of Contents

List of Figures

List of Tables

1. Introduction

1.1 Subject and Motivation

The problem of water loss from water distribution systems is an issue that faces municipalities worldwide. A large proportion of water loss is a result of leakage. Leaks develop in various different forms, and they form in pipes of all materials.

Potable water is a valuable resource, which is growing scarcer. It has been postulated that up to two thirds of the world's population will be affected by water scarcity in the foreseeable future (Alcamo et al., 2000; Rijsberman, 2006; Seckler et al., 1990; Vörösmarty et al., 2000; Wallace, 2000; Wallace & Gregory, 2002). Yang et al. (2003) report that the minimum amount of water that a country needs in order to sufficiently fulfil its agricultural, commercial, industrial and domestic demands is 1500m^3/capita/year. Table 1-1 below illustrates the African and Asian countries that are predicted to have dropped below this minimum threshold by the year 2030. As well as the obvious financial losses and health and sanitation issues that arise from water scarcity, a lack of water places pressure on economic and industrial sectors (Marunga, Hoko & Kaseke, 2006). In a country with water resources as scarce as South Africa's, we can ill afford to waste what we have.

Table 1-1: List of Countries in Africa and Asia having Renewable Freshwater Resources below the Calculated Threshold of 1500 [m3 /(capita year)] by the Year 2030 (Yang et al. 2003)

Afghanistan	Egypt	Kenya	**Niger**	**Tanzania**
Algeria	**Eritrea**	Korea Republic	**Nigeria**	**Togo**
Burkina Faso	**Ethiopia**	Lebanon	**Pakistan**	Tunisia
Burundi	**India**	Libya	Rwanda	**Uganda**
Cape Verde	**Iran**	**Malawi**	Saudi Arabia	Emirates
Comoros	Israel	Maldives	**Somalia**	Yemen
Cyprus	Jordan	Morocco	South Africa	Zimbabwe

***Bold names are the countries entering the water deficit country list after the year 2000**.

It has been observed in various failed pipe specimens, that the external pipe surfaces adjacent to pipe leaks have been scoured or eroded (Negonga, 2013; Pike, 2013; de Kater, 2014; Mohsin & Majid, 2014; van Thienen, 2014). It has been confirmed by a previous study that this scouring phenomenon is a result of an internal soil fluidisation mechanism, whereby a high velocity jet of water is emitted by the pipe leak, thus fluidising the adjacent soil, and causing soil abrasion on the external pipe surface (Pike, 2013). By removing pipe material from around the leak, even small leaks can be exacerbated and hence have the potential to become more severe problems. Alternatively, this pipe material removal can be seen in a positive light, as it can exacerbate small leaks making them easier to detect.

The phenomenon whereby pipe material is removed from the pipe surface has been termed leakage-induced pipe erosion in this study. Unless stated otherwise, the terms "erosion" and "scour" will hereinafter be used to refer to leakage-induced pipe erosion. This

phenomenon has received limited research and is generally poorly understood. The motivation for this investigation is to gain a deeper understanding of this scouring phenomenon so that it can potentially be better managed in the future.

1.2 Scope and Objectives

The topic of leakage-induced pipe erosion due to soil agitation is a complex issue. There are a multitude of factors influencing this mechanism, and hence this study will be limited investigating the effects of what have been identified to be the most critical factors, namely soil particle size, soil cover depth, leakage flow rate, leak orientation and pipe material. These factors will be further discussed in Section 3.4.

The goal of this study is to experimentally investigate the influence of the various factors on the leakage-induced erosion process.

The specific objectives required to achieve this goal are the following:

1. Obtain the current state of knowledge in the field of leakage-induced pipe erosion based on literature, and define the most critical factors that affect the erosion mechanism.
2. Design and manufacture an experimental setup to test the effects of the five aforementioned parameters on the erosion mechanism.
3. Experimentally measure the erosion and quantify the effects that various parameters have on the scouring process.
4. Interpret the experimental results in the context of the current understanding of the knowledge.

The limitation to this study in terms of the proposed experimental setup, is that the leaking pipes shall be buried in a bounded domain (cubic container that is closed on 5 sides and open on the top), rather than an unbounded domain as one would expect to find in the field (an environment in which water is free to move through the granular material in any direction indefinitely).

2. Literature Review

2.1 Introduction

The topic of the effect of leakage-induced pipe erosion is one that has received limited attention by researchers in the past. Previous research has been limited to experimental investigations on the fluidised zone of bedding material outside of pipe leaks (van Zyl et al., 2013; Alsaydalani & Clayton, 2014; Bailey, 2015), leakage-induced pipe erosion caused by pipes situated within the fluidization zones of adjacent pipes (Majid, Mohsin & Yusof, 2011; Majid & Mohsin, 2013), and two undergraduate level exploratory studies investigating leakage induced pipe erosion where the leaking pipe causes damage to itself (Negonga, 2013; Pike, 2013) This literature review aims to synthesise literature from various fields of research in order to develop an understanding of the current state of knowledge.

This chapter will begin with an introduction of why water loss from leakage is a problem the. This is followed by a discussion of different leak types and factors affecting leak hydraulics. The literature review will then look at factors affecting the abrasive processes, followed by a discussion of typical bedding materials and pipe materials used in the construction of South African water distribution systems. Soil-leak interactions will then be discussed, which will include a description of the internal soil fluidisation mechanism. Various wear and abrasion mechanisms will then be explored, after which the abrasion resistance of pipe materials will be reviewed. The review of the literature will be concluded with a discussion of previous work that has been done in the field of leakage-induced pipe erosion.

2.2 Water Losses in Water Distribution Systems

Water losses from water distribution networks contribute to a sizable quantity of wastage of potable water. Total water loss from a water distribution system is defined as the volume difference between the water leaving the supply point (water treatment plant), and the volume of water consumed by the users (Dumbleton, 1996; Seago, Bhagwan & Mckenzie, 2004). Water losses comprise two components, namely apparent losses and real losses (Seago, Bhagwan & Mckenzie, 2004). Apparent losses are those which reach the consumer, but are not recorded by the water utility, e.g. illegal connections (theft), meter errors, and administration errors (Lambert & Hirner, 2000). The real losses are the physical water losses between the system input and the consumer's meter. These consist of water lost through leaks, bursts and overflows (Seago, Bhagwan & Mckenzie, 2004).

While Seago et al. (2004) state that apparent losses can be the most expensive losses, Lahlou (2001) states that real losses are the most substantial component of water loss. It should be noted that Seago et al. (2004) explain that in South Africa and other developing countries, illegal connections and meter tampering are major concerns. Lahlou (2001), however, is written from the perspective of a developed country, where issues such as illegal

connections are less prominent. It remains, however, that real losses form a large proportion water loss across the globe.

Mckenzie et al. (2012) suggest that South Africa's 36.8% of total non-revenue water depicted, in Figure 2-1, is in line with the global average. It is suggested, however, that this is well above that of developed countries. Figure 2-1 shows South Africa's national water balance in terms of percentages of the total system input volumes for 2009/2010. As it can be seen in Figure 2-1, real losses i.e. bursts and leaks account for over a quarter of South Africa's potable water resource allocation. This large proportion of real losses suggests that there is a potential for research and improvements in the field of reducing physical losses.

It should be noted that the data for the study by Mckenzie et al. (2012) was obtained by sending questionnaires to 237 South African water authorities, of which 132 returned comprehensible data sets. It was suggested in the study that the lack of responses and poor quality of data could be a result of poor record keeping, or fabricated results. This suggests that the proportion of non-revenue water in South Africa is potentially greater than that shown in Figure 2-1.

Figure 2-1: South African National Water Balance 2009/2010 (Mckenzie et al., 2012)

2.3 Leak Types

Water distribution pipes have various different modes of failure, which result in different failure patterns. Mora-Rodríguez et al. (2014) report that O'Day et al. (1986) classify types of pipe failures into three categories, namely circumferential cracks caused by longitudinal stress, longitudinal cracks caused by radial stress, and cracks at pipe connections as a result of cross-sectional tension. These leak types are illustrated in Figure 2-2 below.

Mora-Rodríguez et al. (2014) further stated that Rajani et al. (1996) report that in Canada, an average of 70% of pipe failures are circumferential cracks, while the remaining 30% are longitudinal cracks, holes, and leaks through service connections. It should be noted that Canadian water distribution systems comprise predominantly metal pipes. Metal pipes are susceptible to stress due to axial mechanisms, such as thermal expansion/contraction and soil heave caused by large temperature differentials in winter. In addition to these main classifications, other more minor breaks must also be taken into consideration, such as corrosion holes and leaks from connections (Mora-Rodríguez et al., 2013).

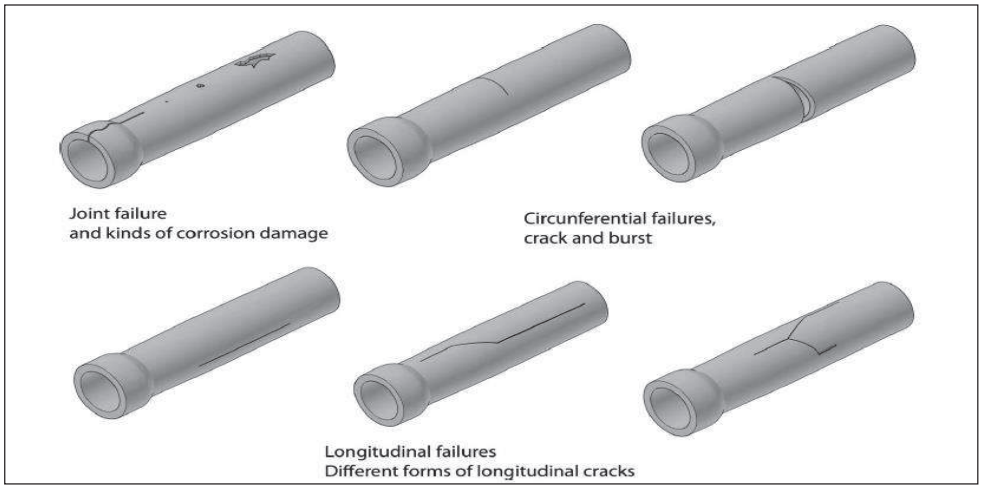

Figure 2-2: Types of Failures in Pipes (Mora-Rodríguez et al., 2013)

2.4 Leakage and Pressure

Leaks in water distribution systems are broadly characterised into two categories; bursts and background leaks (van Zyl & Clayton, 2007). Structural failure in the pipes result in bursts and are generally relatively easily detected and fixed. Bursts are easily detected because they tend to become visible at the ground surface, as well as consumers noticing a lack of pressure in their water delivery (van Zyl et al., 2013). Conversely, background leakages are small leaks along the pipe network that continuously discharge water. These leaks are too small to detect even with the active leakage detection equipment. Consequently, long-lasting background leaks have the potential to waste far more water than a pipe burst.

Research has determined that water pressure is a major factor that contributes to increasing leakage in water distribution networks. (Marunga, Hoko & Kaseke, 2006; Walski et al., 2009; Cassa, van Zyl & Laubscher, 2010; Mutikanga, Sharma & Vairavamoorthy, 2013). The volume of water exiting the orifices of leaking pipes can be calculated by the Orifice Equation (Equation 2.1). This expression can be derived from first principles using the principle of energy conservation. Equation 2.1 describes the conversion potential of the internal pressure energy to kinetic energy. The discharge coefficient, C_d, indicates the proportion of energy loss through the orifice, i.e. the discharge coefficient is theoretically

equal to 1 if there are no energy losses through the orifice (Greyvenstein & van Zyl, 2005; Walski et al., 2009; Guo et al., 2013; van Zyl et al., 2013):

$$Q = C_d A\sqrt{2gh} \tag{2.1}$$

Where Q= Flow rate; C_d= Discharge coefficient; A=Orifice area; g= Acceleration due to gravity; h= Pressure head differential over orifice.

However, practitioners tend to use a more general, empirical version of Equation 2.1 for characterising the leakage in a system, as shown below in Equation 2.2 (Lambert, 2001):

$$Q = c \cdot h^{N_1} \tag{2.2}$$

Where c=Leakage coefficient; and N_1=Leakage exponent

The need for this equation is a result of the observations that in practice, the flow rate does not always vary with the square root of the system's pressure head as theory would suggest. Various researchers report that this value ranges from 0.5-2.79 as summarised by Walski et al. (2009) in Table 2-1.

The effect of a change in pressure on leakage flow rate can is described by Equation 2.3 below as per Walski et al., (2006). This equation can be derived from Equation 2.2. If the N1 Equation (Equation 2.2) is expressed at two different pressures, it can be expressed as shown in Equations 2.3 (a) and 2.3 (b). Dividing 2.3 (b) by 2.3 (a) and solving for Q_2, we get Equation 2.3.

$$Q_1 = c \cdot {h_1}^{N_1} \tag{2.3 a}$$

$$Q_2 = c \cdot {h_2}^{N_1} \tag{2.3 b}$$

$$Q_2 = Q_1 \left(\frac{P_2}{P_1}\right)^{N_1} \tag{2.3}$$

Where Q_2 = Final Leak Rate; Q_1 = Initial Leak Rate; P_2 = Final Pressure; P_1 = Initial Pressure; N_1= Exponent Relating Flow and Pressure

Table 2-1: Values of Leakage Exponents found by various Researchers, as reported by (Walski et al., 2009)

Reference	Values	Conditions
Ogura (1979)	1.39-1.72	Slits
Hikki (1981)	0.5	Drilled holes
May (1994)	0.5 fixed area 1.5 size = f(P) 2.5 long	Fixed area Size = f(Pressure) Longitudinal
Lambert (2001)	0.52-2.79	Literature
Farley and Throw (2003)	0.70-1.68 0.63-2.12 0.52-2.79	UK (1977) Japan (1979) Brazil (1999)
Thornton and Lambert (2005)	0.5-1.6	Function of ILI
Walski et al. (2006)	0.66-0.76	Drilled holes
Greyvenstein and VanZyl (2007)	0.52 1.38-1.85 0.79-1.04 0.41-0.53 0.67-2.3	Round Hole Longitudinal PVC Longitudinal AC Circumferential Corrosion steel
Noack and Ullanicki (2007)	0.5 – 1.0	f(soil permeability)

Van Zyl & Clayton (2007) explain that the exponent of 0.5 only gives accurate results for large Reynold's numbers i.e. for turbulent flow, while for smaller Reynold's numbers (laminar flow), Equation 2.2 tends to be written with the coefficient as a function of the Reynold's number, or with the exponent as a constant that is greater than 0.5.

As explained by Greyvenstein & van Zyl (2005), due to N_1's exponential nature, it is imperative that N_1 is determined correctly since it is the overriding factor in the leakage expression (Equation 2.2). Walski et al. (2009) further explain that a reason for the variation in exponent values is due to the changing orifice size with changing pressure, i.e. an increase in internal pipe pressure can increase the orifice size. This expanding orifice effect creates an apparent exponent value of greater than 1 (Walski et al., 2009). Adding to that statement, Greyvenstein and van Zyl (2005) state that an increase in pressure can also cause small cracks or fractures in the pipe that were not leaking at low pressures to open up and start leaking at higher pressures.

For buried pipes, the nature and size of an individual leak tend to have a greater effect on the leakage flow rate than the porous media flow through the soil (van Zyl & Clayton, 2007; Walski et al., 2009). In terms of the "nature and size" of the orifice, Greyvenstein & van Zyl (2005) explore the effect of different pipe materials (Asbestos cement, steel and uPVC) as well as types of leaks (round holes, circumferential cracks, longitudinal cracks and corrosion clusters) on the leakage exponent. From this work, it was suggested that the leak type was a better indicator of the leakage exponent than the pipe material for individual leaks, as shown by the results in Table 2-1 above. This is because the formation of the leak can have an effect on the pipe's structural strength, for example, the longer the length of a circumferential crack, the more susceptible it may be to expansion as a result of increased longitudinal forces.

The research by Greyvenstein & van Zyl (2005) concluded that steel pipes with corrosion clusters had the greatest leakage exponent. Greyvenstein & van Zyl (2005) report that this result contrasts that which was reported by Farley & Trow (2003), who claim that plastic pipes would have the largest leakage exponent. The explanation that was offered for this discrepancy by Greyvenstein and van Zyl was that the corrosion in the steel pipes reduced the support material around the hole and hence compromised the pipe's structural integrity.

Based on a synthesis of data from the available literature, it is suggested by Lambert (2001), however, that the best guidance for predicting average N_1 values for sectors of distribution systems depends on pipe material and Infrastructure Leakage Index (ILI) as described by Figure 2-3. The ILI is a dimensionless ratio that describes the severity of leakage in a particular water distribution system. It is defined as the ratio of the current annual real losses to the unavoidable annual real losses (the theoretical minimum achievable leakage in a system) (Seago, Bhagwan & Mckenzie, 2004). Figure 2-3 indicates that systems comprising metal pipes tend to have lower N1 values than plastic pipes. It further suggests that the N1 values of metal pipe systems decrease with increasing ILIs. It is interesting to note that Figure 2-3 indicates that water distribution systems comprising of entirely plastic

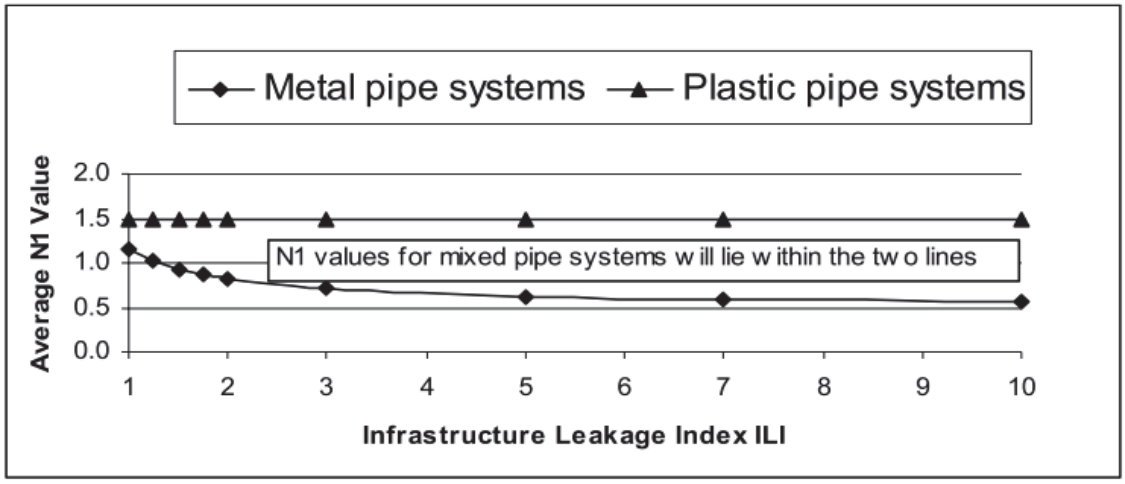

Figure 2-3: Best Available Guidance on Predicting N1 values for Individual Sectors (Lambert 2001)

materials will have an N1 value of 1.5.

However, these are not the only influencing factors. Other factors that affect the leakage exponent include leak hydraulics, pipe material behaviour, soil hydraulics and water demand (Coetzer, et al., 2008; Greyvenstein & van Zyl, 2005). Although it was previously mentioned that the media surrounding the leak had a lesser effect on the leakage exponent than the nature of the leak, the effect of surrounding media was investigated by Coetzer et al. (2008). The leakage exponent of a circular orifice was determined experimentally for water leaking into air, water, and glass beads which represent an idealised soil with spherical

particles. From this experiment, it was determined that the leakage exponent for water leaking into air was approximately 0.5, however, the exponent was significantly lower than the theoretical value of 0.5 for leaks submerged in water and beads, 0.41 and 0.43 respectively due to local effects. This is illustrated in Figure 2-4. It is important to note that there is no significant difference between the curves for leaks into water and granular media, suggesting that soil hydraulics is not the cause of large variations in N1 values. While the difference between N1 values of leaks into air and leaks into water and granular media are noteworthy, the difference is small enough to confirm that the nature of the leak is a more significant factor than the external leak conditions.

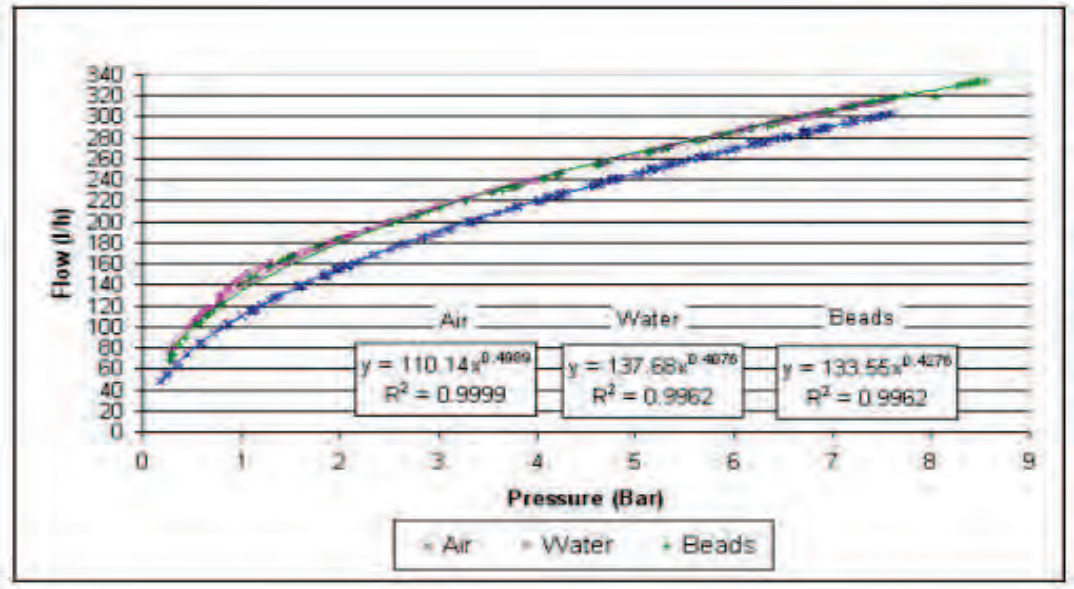

Figure 2-4: Results for a 2 mm hole in an uPVC pipe discharging into air, water and glass beads (Coetzer et al., 2008)

2.5 Bedding Materials

As stated in South African Bureau of Standards (1983), bedding material for water pipes under pressure should comprise free draining, granular non-cohesive material. The bedding material should be uniformly graded between 0.6mm and 19mm. This granular material forms the bedding cradle as shown in Figure 2-5, which is required to fill the full width of the trench. As shown in Figure 2-5 below, the bedding cradle requires a minimum cover depth of 100mm with aforementioned granular material.

It is further stated that a compacted selected fill blanket (shown in Figure 2-5) should be laid to a minimum height of 300mm above the top of the pipe. The fill blanket must have a plasticity index of no greater than 6, and must be free from vegetation and stones exceeding 30mm (SABS, 1983).

The main fill, or backfill above selected fill blanket is defined as any approved filling material laid above the selected fill blanket (SABS, 1983). The standard is not specific about material type or required depth of main fill.

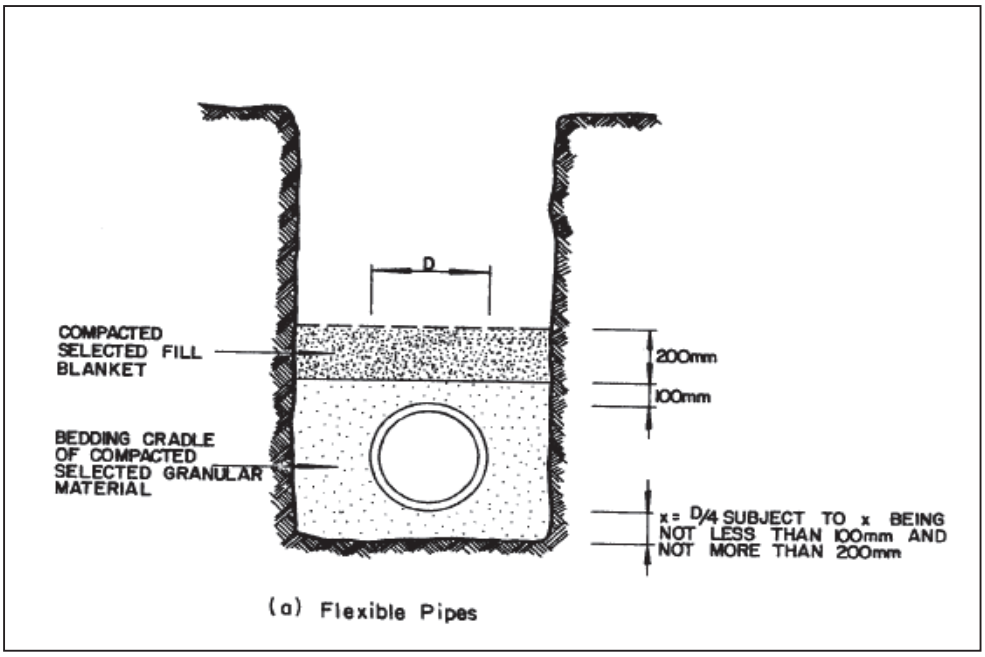

Figure 2-5: Bedding Conditions- Source: (South African Bureau of Standards, 1983)

2.6 Material Removal Mechanisms

2.6.1 Archard's Law of Abrasive Wear

Wear is defined as a process whereby material is gradually removed from surfaces of solids subject to contact and sliding (Zmitrowicz, 2006). Wear can occur in a multitude of situations, and can present itself in a various forms and patterns, such as abrasion, fatigue, ploughing, corrugation, erosion and cavitation (Zmitrowicz, 2006). In terms of wear, fatigue is the process where surface material is weakened by cyclic loading. Ploughing occurs when two surfaces strike each other obliquely, resulting in an abrasive groove/grooves on the weaker surface. Corrugations are typically multiple adjacent longitudinal grooves with periodic wave-like cross sections. Cavitation is a form of wear that takes place in fluid flow systems, where negative pressure vapour bubbles form and collapse upon a solid surface, causing damage to the surface (Kato & Adachi, 2001; Zmitrowicz, 2006).

Based on the previous definition, wear can be a result of mechanical, physical and/or chemical phenomena, however, literature tends to treat wear of solids as a mechanical process, thus excluding chemical processes such as oxidation and corrosion (Zmitrowicz, 2006). Wear is often measured in terms of mass of material removed from a solid, volume of removed material, or the reduction in dimensions of the solid body.

Archard's Law of abrasive wear predicts the volume of material that is removed due to friction between two sliding bodies. The mechanical wear is as dependent on the sliding conditions (normal pressure and sliding velocity), and the properties of the interacting materials (Zmitrowicz, 2006). Archard's Law is described by Equation 2.4.

$$V_{removed} = k \cdot \frac{P_N \cdot L}{H} \tag{2.4}$$

Where $V_{removed}$ = Volume of removed material (m^3); P_N= Normal pressure (Pa); L = Sliding distance (m); H = Brinell hardness of the softer material (Pa); k = Dimensionless wear coefficient

Dividing this equation by the time taken for the two bodies to pass each other (assuming constant velocity), we get that the rate of material removal is proportional to the product of the normal pressure and the relative velocity between the two bodies, as shown in Equation 2.5.

$$\frac{dV_{removed}}{dt} = k \cdot \frac{P_N \cdot v}{H} \tag{2.5}$$

Where $dV_{removed}/dt$ = rate of material removal; v = Relative velocity between bodies.

2.6.2 Chemical Mechanical Polishing (CMP)

Chemical mechanical polishing (CMP), also known as chemical mechanical planarization, is a process of smoothing surfaces using a combination of chemical and mechanical forces. This process is utilised, among other fields, in the semiconductor industry for oxide dielectric and metal layer planarization (Luo & Dornfeld, 2001). As illustrated in Figure 2-6, the process of CMP uses a rotating polishing pad/table covered with a colloidal slurry to polish the surface of a wafer. The wafer is pressed face down onto the polishing table by a wafer carrier which is rotated about an axis as shown in Figure 2-6.

The slurry typically contains an abrasive silica grit, with a particle size in the order of nanometres, suspended in a reactive chemical agent that is chosen to fit the specific wafer material being processed. The thickness of the slurry layer is normally in the order of micrometres (Luo & Dornfeld, 2001). The material is removed from the wafer as a result of both the chemical reaction between the slurry and the wafer material, and the repetitive rolling and sliding of the abrasive particles against the wafer surface (Luo & Dornfeld, 2001).

It is said that the most basic model to describe the rate of material removal due to CMP was developed by Preston (1927), and generally shows good correlation to experimental results when considering the significant input variables such as slurry flow rate, pressure, velocity and friction force (Maury et al., 1997; Luo & Dornfeld, 2001). Equation 2.6 shows

Preston's equation. This equation is an empirical equation describing how downward pressure and velocity influence the rate of material removal from a wafer surface.

$$\frac{dz}{dt} = k_p \cdot P_N \cdot v \tag{2.6}$$

Where dz/dt = Change in thickness over time; k_p = Preston coefficient; P_N = Normal pressure; v = relative velocity between abrasive and surface being polished

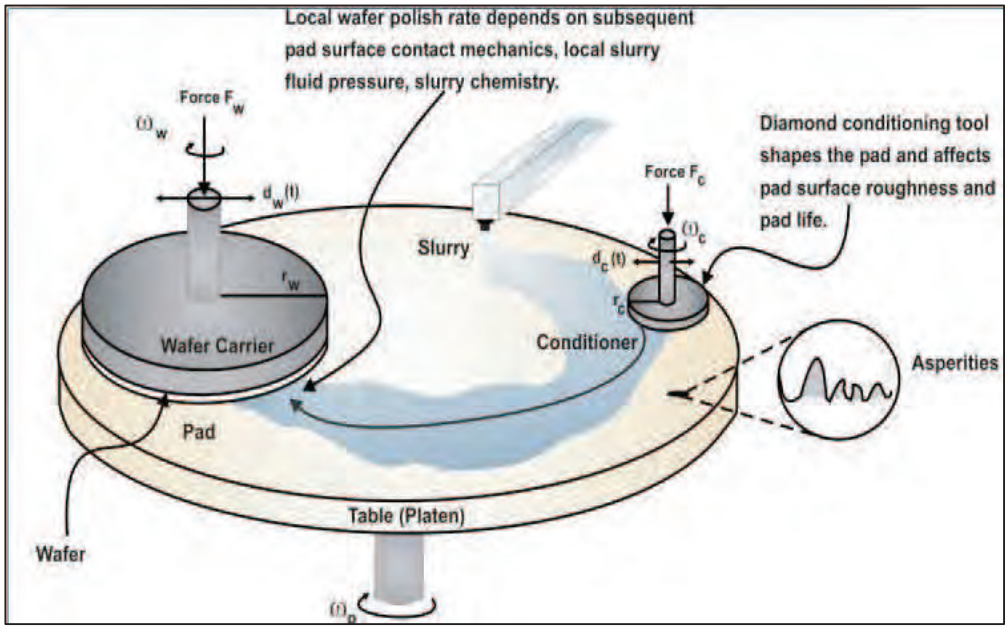

Figure 2-6: Schematic Representation of CMP Apparatus (Borucki, 2000)

Due to the complex nature of the Preston coefficient, k_p, is a constant used to account for all other factors that may influence the rate of material removal, such as abrasive material, polishing material, type of lapping, chemical effects etc. This equation suggests that the rate of material removal is proportional to the product of the downward pressure and the abrasive velocity. It is said, however, that this equation has its limitations, since it does not accurately account for factors such as grit size, polishing pad roughness, pad hardness, number of abrasive particles and chemical effects, but rather assumes the combined effects of these factors with the Preston coefficient (Luo & Dornfeld, 2001). Furthermore, Luo & Dornfeld (2001) state that in recent times, several efforts have been made to modify Preston's equation to account for various elements of CMP, however, most models have been quite rough, and are similar to Preston's equation, with the only process parameters included being pressure and velocity. Luo & Dornfeld (2001) further state that most alternative models appear to agree well with certain cases of the CMP, they tend not to be globally robust.

Luo & Dornfeld (2001) explain that that the Preston equation is most accurate when the polishing pad is of similar or greater hardness than that of the abrasives. This is because the wafer and the polishing pad are separated by the abrasives during hard pad polishing, while the wafer and polishing pad contact each other directly when the polishing pads are softer.

Typically the polishing pads are made of polyurethane polymers for CMP applications, making them much softer than the abrasive particles.

Although the Preston equation predicts a different parameter to the previously discussed Archard's Law (Equation 2.4), i.e. thickness instead of volume, it should be noted that there is a significant resemblance between the two equations. It can be seen that both models predict that the rate of material removal, be it thickness or volume, is proportional to the product of the normal pressure and relative velocity of the interacting bodies.

2.6.3 Abrasion Mechanisms

The rate of abrasive wear on a pipe surface when an aggregate is flowing in a pipe is dependent on the velocity and quantity of flow, size and shape of particles (Goddard, 1994). Abrasion on surfaces by sands and gravels is a phenomenon that is brought about by individual particles. As explained by Zok & Miserez (2007), abrasion is a poorly understood mechanism for the following reasons:

- Abrasion involves the interaction of two or more bodies, e.g. sand and a PVC surface. The bodies are generally two (or more) different materials, and hence abrasion is a function of system properties rather than material properties (Yang & Hlavacek, 1999; Zok & Miserez, 2007).
- There are many mechanisms that cause abrasion such as plastic deformation and cracking under single or multiple (fatigue) load cycles.
- Even for seemingly simple geometric configurations, such as two flat contacting plates, the stresses in the contact regions are complex because of surface imperfections.

Various idealised contact scenarios, under normal loading, or a combination of normal and tangential loading, are shown in Figure 2-7. Figures 2-7 (a) and (b) depict idealised blunt abrasive contact at the onset of yielding; Figures 2-7 (c) and (d) illustrate the formation of cracks prior to yielding. It is also stated that for sharp abrasive contacts, that even for low loads, yielding is unavoidable. This suggests that sharp abrasives will either cause plastic penetration (Figure 2-7 (e)), or form cracks within the plastic zone (Figure 2-7 (f)).

In the context of abrasive water jet cutting, Gent et al. (2012) explain that when abrasives strike a ductile surface, plastic deformation of gouging and shearing can occur.

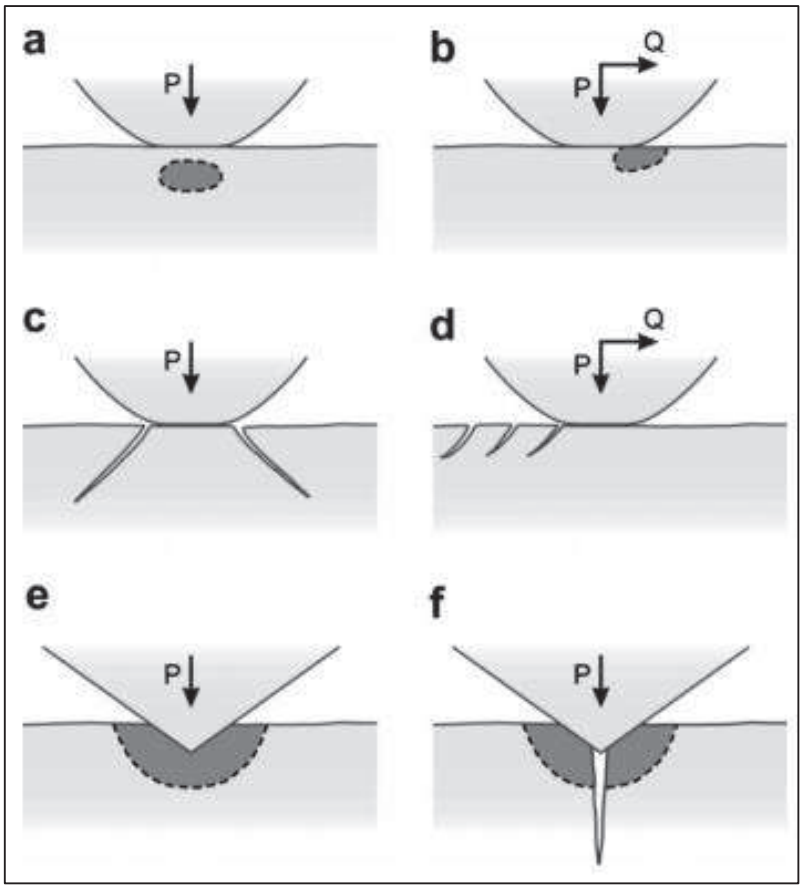

Figure 2-7: Idealised Damage mechanisms at Contacts with Blunt and Sharp Abrasives (Zok & Miserez, 2007)

They further state that if the abrasives have a great enough impact velocity, they can also cause exfoliation at the point of impact. Furthermore, the abrasive materials must be harder than the material being cut in order to for the water jet cutting to be successful. This is because the relative hardness between the abrasive and the target material is the property that best enables the abrasive to cut through the other material. Gent et al. (2012) report that the harder the abrasive material, the greater its cutting capacity.

Bouzid & Bouaouadja (2000) state that there are a number of parameters that influence the abrasion process in sand blasting applications. Sand blasting is a process that entails firing granular material at a surface, where the granular material strikes the surface and causes abrasive wear. The parameters that affect this abrasion process are the following:

- The nature and properties of the particles (size, shape, hardness, toughness). Hardness refers to a material's resistance to wear, while toughness refers to the strain energy stored by a body up until the point of fracture.

- The nature and properties of the surface target (hardness, toughness, state of superficial stress)
- The sand blasting procedure variables (flow velocity, impact angles, temperature variations) (Bouzid & Bouaouadja, 2000).

2.6.4 Scouring of Soil beds around Structures in Open Channel Flow

2.6.4.1 Time Development of Scour

The scour of loose soil beds around foundations of structures in open channels has been the leading cause of bridge failures in the United States in the last 30 years (Briaud et al., 2001). In general, structures placed in open channels (bridges, piers, abutments etc.) cause disturbances in the water flow. These disturbances can cause vortices, which have the potential to remove particulate material from alluvial beds around structures, as illustrated in Figure 2-8. Figure 2-8 shows the flow patterns and typical scour patterns that have been observed around circular piers.

This type of scour is generally classified as either clear-water scour, or live-bed scour.

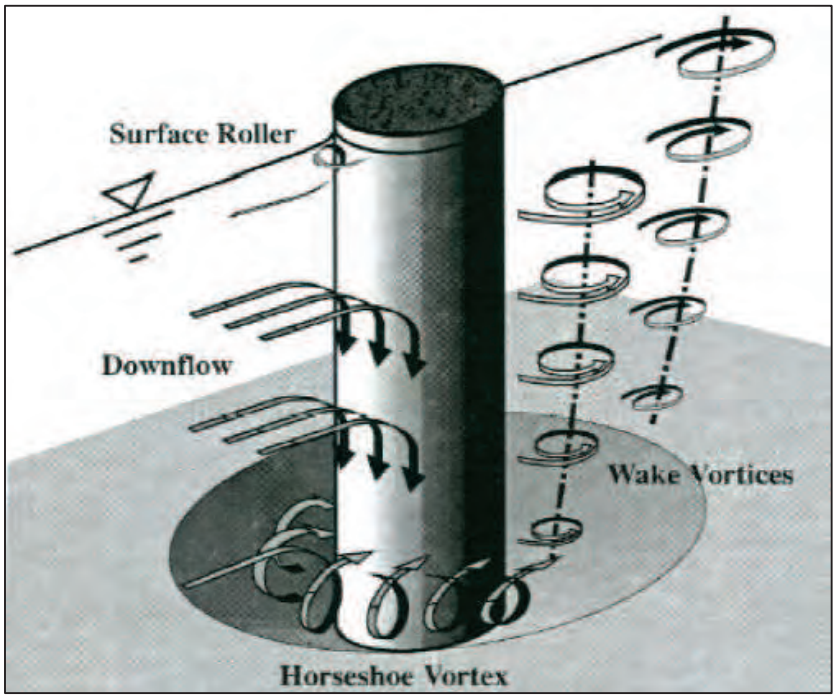

Figure 2-8: Illustration of the Flow and Scour Pattern at a Circular Pier (Melville & Coleman, 2000)

Clear-water scour occurs when the bed material upstream of the infrastructure is at rest, and therefore does not enter the scour hole. In this case, the maximum scour depth is reached when the water flow can no longer remove bed material from the scour hole (Raudkivi & Ettema, 1983). Live-bed scour is the case where bed material is being transported by the

flow, and is continually being deposited and removed from the scour hole (Raudkivi & Ettema, 1983). Figure 2-9 gives a schematic graphical depiction of how the scour depth develops over time in the cases of both clear-water and live-bed scouring. It should be noted that in both cases, the depth initially increases rapidly, after which the rate of development decreases with increasing time, until an equilibrium depth is reached. Barbhuiya & Dey (2004) state that numerous researchers believe that the time-dependency of the development of this scour depth is logarithmic in nature.

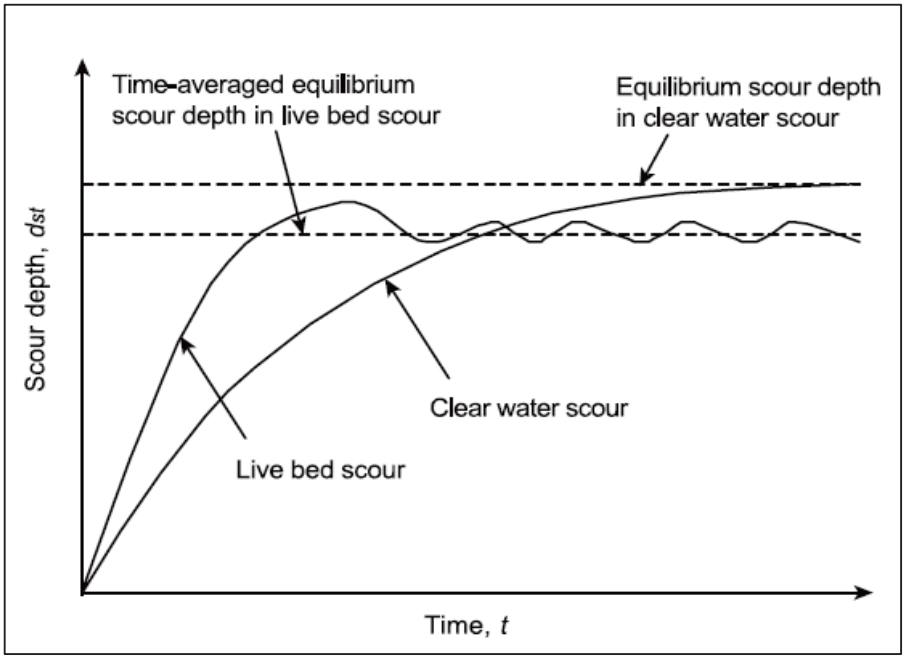

Figure 2-9: Time-dependent Development of Scour Depth around Abutments (Raudkivi & Ettema, 1983)

Barbhuiya and Dey (2004) further state that for this reason, many researchers argue that true equilibrium scour depth may not exist. Anderson (1963) states that "by virtue of the logarithmic character of the development of the scour region with time, a practical equilibrium is reached after a relatively short time, after which the increase in the depth and extent of scour becomes virtually imperceptible". The upper-most layers are removed quickly since they are in direct contact with the flowing water. As more and more material is removed, the exposed surface of the scour hole moves further away from dynamic action of the flowing water. Raudkivi & Ettema (1983) state that the maximum scour depth is reached when the flow can no longer remove particles from the scour hole.

Since the time-dependent development of this scour phenomenon often presents itself in a logarithmic form, it is common to plot the scour depth against time on a logarithmic time scale. As shown in Figure 2-10, a compilation of scour development data from 6 different studies has been illustrated graphically. The dimensionless ratio of scour depth (d_s) to the length of the abutment perpendicular to the flow direction (l) is plotted against time on a logarithmic scale. This ratio was used to normalise the rate of scour between studies, since it is known that the abutment length has a significant influence on the maximum scour depth.

Plotting logarithmically shaped data on a logarithmic time scale simplifies the analysis of the data, for example, Cardoso & Bettess (1999) used this strategy to analyse their data from experiments that were designed to investigate the time-dependence of scour depth development as shown in Figure 2-11. In this case, this strategy was used to identify the equilibrium phase of their tests, i.e. the portion of the data in Figure 2-11 where the gradient of the trend line flattens out.

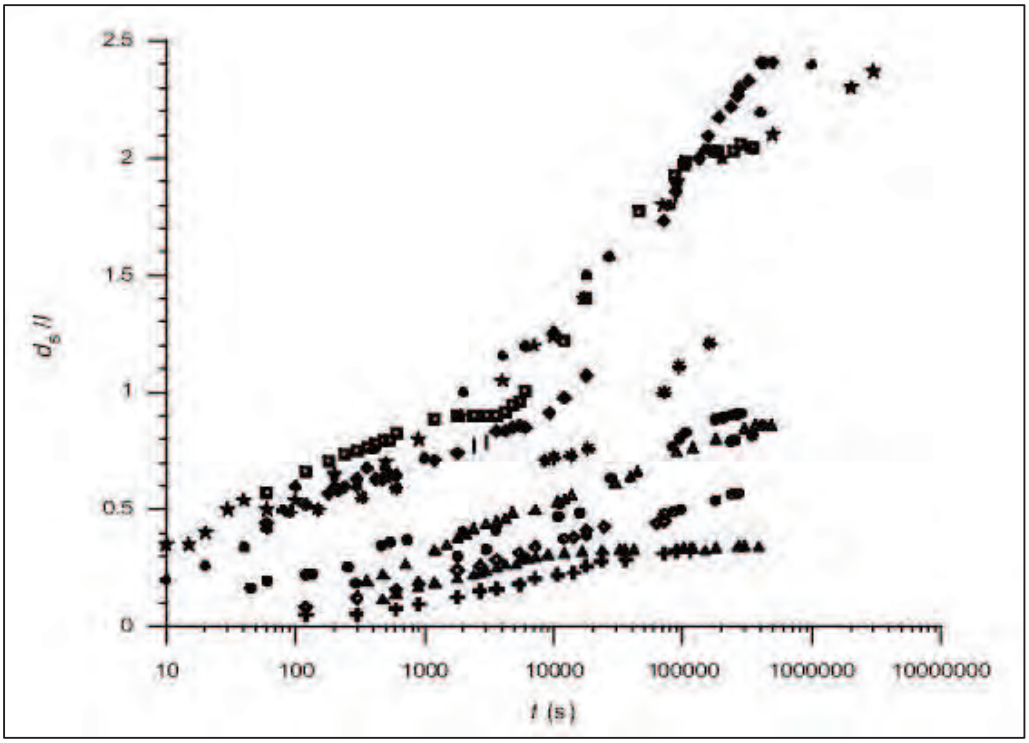

Figure 2-10: Compilation of Time-Dependent Scour Development Data from 6 Studies (Barbhuiya & Dey, 2004)

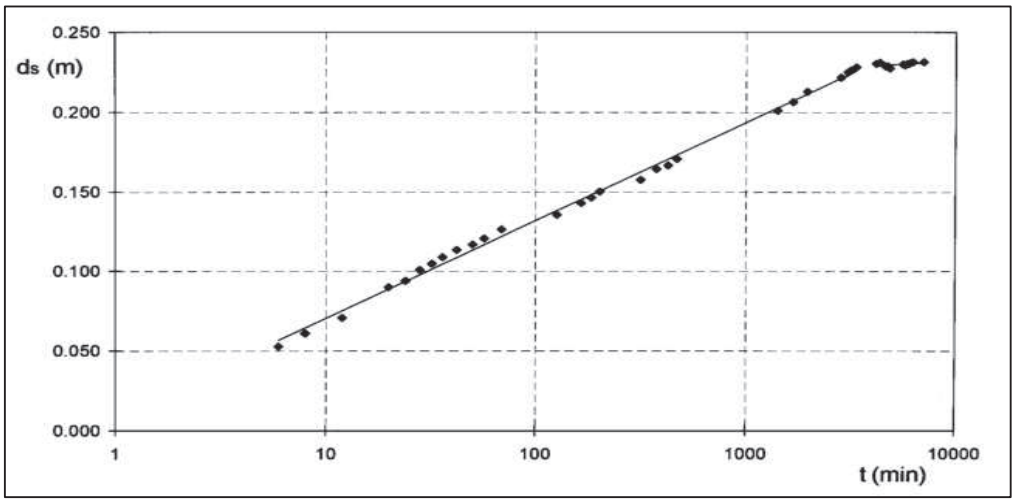

Figure 2-11: Time Evolution of Scour Depth

2.6.4.2 Inter-Granular Scour Mechanisms

Two mechanisms have been proposed for erosion of soil beds around infrastructure in free flowing water, namely sliding and rolling (Briaud et al., 2001). For both proposed mechanisms, electrostatic and electromagnetic forces between particles are neglected, since these analyses are for sand and gravel particles only.

The theory of the sliding mechanism assumes that spherical soil particles exert a shear force parallel to the erosion surface that is proportional to the resultant force of the water on the particle. An increase in water velocity increases the shear stress imposed by the water on the particles, which eventually exceeds the frictional force between two particles and causes the particles to slide across one another. The critical shear stress τ_c is the threshold shear stress at which erosion between granular particles is initiated, as illustrated below in Figure 2-12 (Briaud et al., 2001). With respect to Figure 2-12 (a) below, Equations 2.7 and 2.8 can be derived by considering equilibrium at the moment when the frictional forces are overcome. This model considers the submerged weight of the individual particles, with no external forces being applied by surrounding soil. The shear stress between the two particles is also dependent on the soil's friction angle, ϕ, a shear strength parameter of soil derived from the Mohr-Coulomb failure criterion, commonly used in geotechnical engineering (Craig, 2004).

$$\tau_c \cdot A_e = W \cdot tan\phi \tag{2.7}$$

Where A_e= Effective friction area of water on particle; W= Submerged weight of particle; ϕ= Friction angle of the interface between two particles.

Or, if spherical particles are assumed, equation 2.7 can be manipulated to give the following equation:

$$\tau_c \cdot \alpha \frac{\pi \cdot {D_{50}}^2}{4} = (\rho_s - \rho_w) \cdot g \cdot \frac{\pi \cdot {D_{50}}^3}{6} \cdot tan\phi \tag{2.8 a}$$

Solving for τ_c,

$$\tau_c = 2 \cdot \frac{(\rho_s - \rho_w) g \cdot tan\phi}{3\alpha} \cdot D_{50} \tag{2.8 b}$$

Where ρ_s= Soil density; ρ_w= Water density; g= Acceleration due to gravity; D_{50}= Median diameter representative of soil particle size distribution; α= Ratio of effective friction area over the maximum cross section of spherical particle.

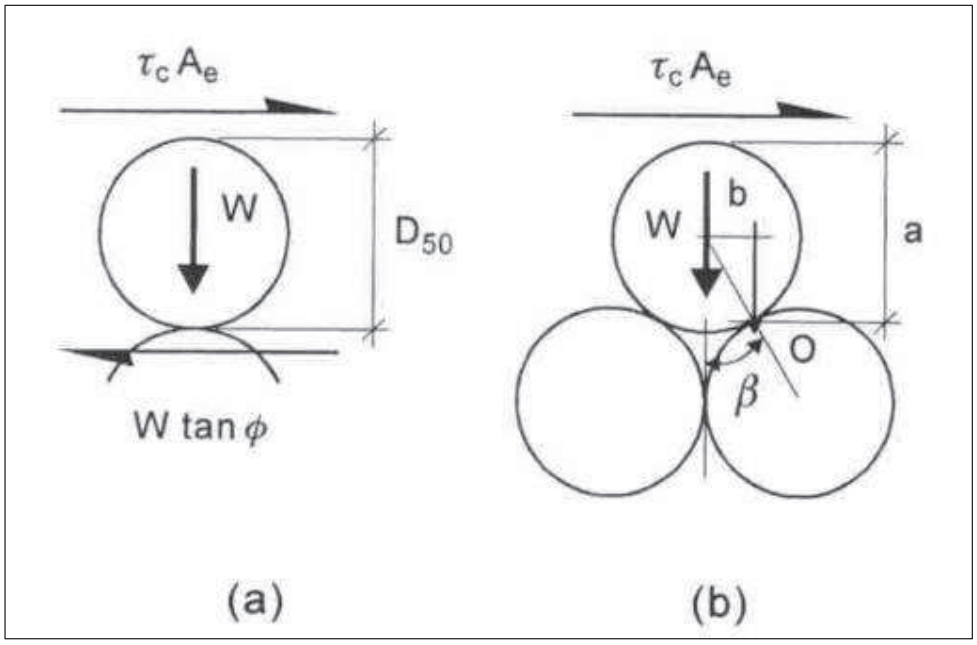

Figure 2-12: Forces Applied to Soil Grain during Inter-granular Scour (Briaud et al. 2001)

Equation 2.8 (b) suggests that the critical shear stress is linearly proportional to the particle diameter. Briaud et al. (1999)showed experimentally for sands that the following empirical equation gives an approximation for the critical shear stress:

$$\tau_c(\mathrm{N/m^2}) \simeq D_{50}(\mathrm{mm}) \tag{2.9}$$

Briaud et al. (2001) further suggest that sliding is not the eroding mechanism for sands in free flowing water, or at least not the only responsible mechanism. By considering Equations 2.8 and 2.9, and assuming "reasonable values for ρ_s, ρ_w, g and ϕ", a value of 6 can be calculated for α. This value is much higher than one would expect, and hence Briaud et al. (2001) concluded that sliding is not the mechanism for the erosion of sands in free flowing water.

Alternatively, a rolling mechanism has been proposed by Briaud et al. (2001) where it is again assumed that the soil particles are spherical, and the resultant force exerted by the water on the particles is a shear force parallel of the eroding surface. It is further assumed that the particle rotates around the point of contact with underlying particles. At the initial stage of rotation, taking moment equilibrium around point O in Figure 2-12 (b), the following equations can be derived:

$$\tau_c \cdot A_e \cdot a = W \cdot b \qquad 2.10\ (a)$$

Where *a* and *b* are the distances defined in Figure 2-12(b)

Or, if spherical particles are assumed, equation 2.7 can be manipulated to give the following equation:

$$\tau_c \cdot \alpha \frac{\pi \cdot {D_{50}}^2}{4} \cdot \left(\frac{D_{50}}{2} + \frac{D_{50} \cdot cos\beta}{2}\right) = (\rho_s - \rho_w) \cdot g \cdot \frac{\pi \cdot {D_{50}}^3}{6} \cdot \frac{D_{50}}{2} \cdot sin\beta \qquad 2.10\ (b)$$

Solving for τ_c;

$$\tau_c = \frac{2(\rho_s - \rho_w) \cdot g \cdot sin\beta}{3\alpha \cdot (1 + cos\beta)} \cdot D_{50} \qquad 2.11$$

Again it can be seen that the shear stress is linearly proportional to D_{50}, and this relationship is illustrated from experimental data in Figure 2-13 below. Furthermore, it is explained by Briaud et al. (2001) that rolling is most likely the erosion mechanism involved in this experiment. Using Equations 2.9 and 2.11, and again assuming reasonable values for ρ_s, ρ_w, g and for α=1, it can be calculated that β equals 10^o-12^o, which is said by Briaud et al. (2001) to be indicative of a loosely packed sand bed, what is what is described in the testing process when using the Erosion Function Apparatus (EFA) (Briaud et al., 2001). Briaud et al. (2001) further recommend that these theoretical models are more useful for understanding the erosion mechanisms than for accurate predictions, and experimental data should be favoured in determining τ_c. Moreover, these models are not applicable for fine

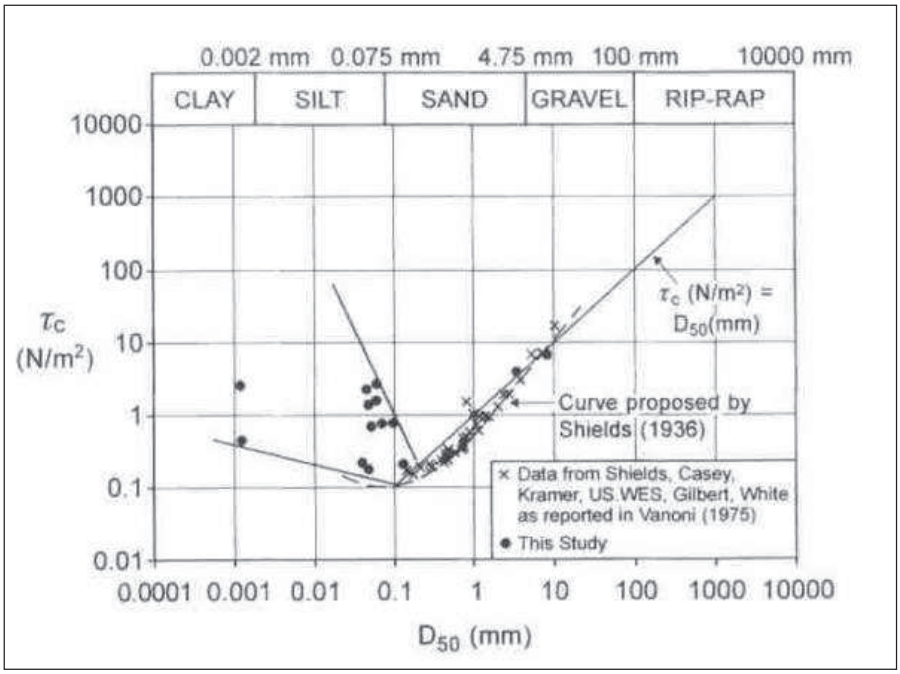

Figure 2-13: Critical Shear Stress versus Mean Soil Diameter (Briaud et al. 2001)

grained soils, and D_{50} is not an adequate parameter for predicting the shear stress in such materials due to their interparticle electrostatic and electromagnetic forces as demonstrated by Figure 2-13. Figure 2-13 shows the experimental results on different sized soil particles, zshowing that Equation 2.9 works well for sands and gravels, but not for silts and clays (Briaud et al., 2001).

2.6.5 Abrasive Properties of Granular Particles in Abrasive Water Jet Cutting

High velocity granular particles cause erosion by means of various mechanisms. Abrasive water jet cutting is a process whereby abrasive materials are entrained in a high velocity jet of water. Olsen, Olsen & Gidley (2013) state that the water is pressurized to between 1300 and 6200 bar. The water is then forced through an orifice of between 0.18 and 0.4mm diameter, creating water jet speeds of up to 960km/hour.

As shown in Figure 2-14, the water jet flows past the inlet for the abrasives, creating a vacuum and pulling the abrasives into the jet. The abrasives are then mixed into the water in the mixing tube, after which the mixture exits the nozzle at speeds great enough to cut through target materials that can be as hard as granite, and most metals. This process has been used in industrial applications for high precision cutting and machining purposes. Since it causes no heat damage, it is particularly useful as it does not alter the inherent material properties of the object being cut.

During the process of abrasive water jet cutting, Gent et al. (2012) explain that the cutting process is a combination of cutting, shearing, cracking, crack propagation, exfoliation, cavitation, and plastic deformation. Exfoliation is the process whereby material is removed from the target material layer by layer, due to the scraping action of the abrasive material. Gent et al. (2012) continue to state that the angle at which the abrasive materials strike the surface will determine the extent to which each of these elements will have an effect.

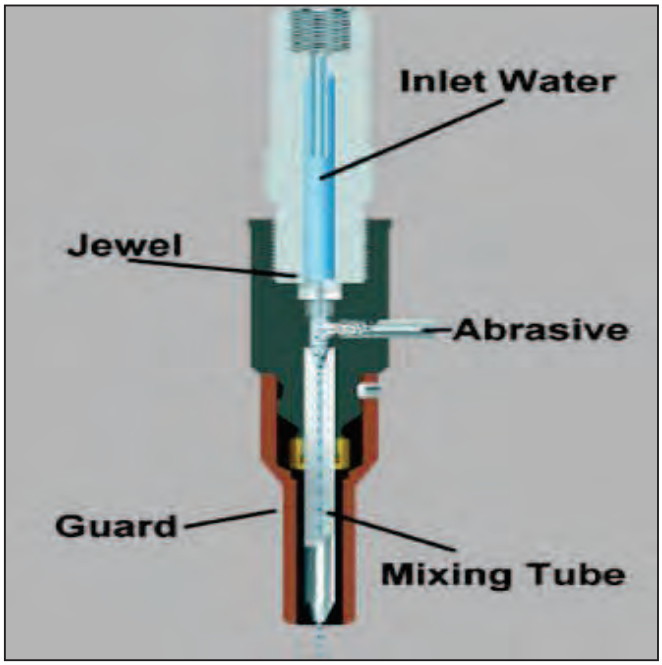

Figure 2-14: Abrasive Water Jet Cutting Apparatus (Olsen, Olsen & Gidley, 2013)

The energy imparted on the target object by the abrasive material is a function of the particle's mass (size and density), velocity, and resistance to fragmentation (Gent et al., 2012). Note that the measure of the resistance to fragmentation is Bond Work Index (BWI). A material's BWI is defined as the energy required to reduce one short ton (907kg) of that material from a notional infinite size to a D_{80} size of 100μm, as determined by the Bond Standard Grindability test (Levin, 1989).

In abrasive water jet cutting, Gent et al. (2012) note that in general, an increase in the abrasive's particle size generally leads to an increase in the depth of the cut. This phenomenon is more prominent in brittle materials than in ductile materials; however, it is further mentioned that above a certain particle size, the effect is opposite, i.e. the cut gets shallower with increasing particle size (Gent et al., 2012).

In an experiment conducted by Gent et al. (2012), the rate of erosion for various materials in an abrasive water jet cutting application were tested, and the various material properties were then compared to the rate of erosion. The graphic results are shown in the figures below.

Figure 2-15 shows the relationship between the abrasive's particle size and the rate of erosion at a constant abrasive feed rate. This test shows that the rate of erosion increases logarithmically with increasing particle size. This suggests that the rate of increase of erosion decreases with increasing particle size i.e. a small increase in particle size in the lower ranges (150-300 microns) increases the rate of erosion more than a small particle size increase in the larger ranges (500-700 microns).

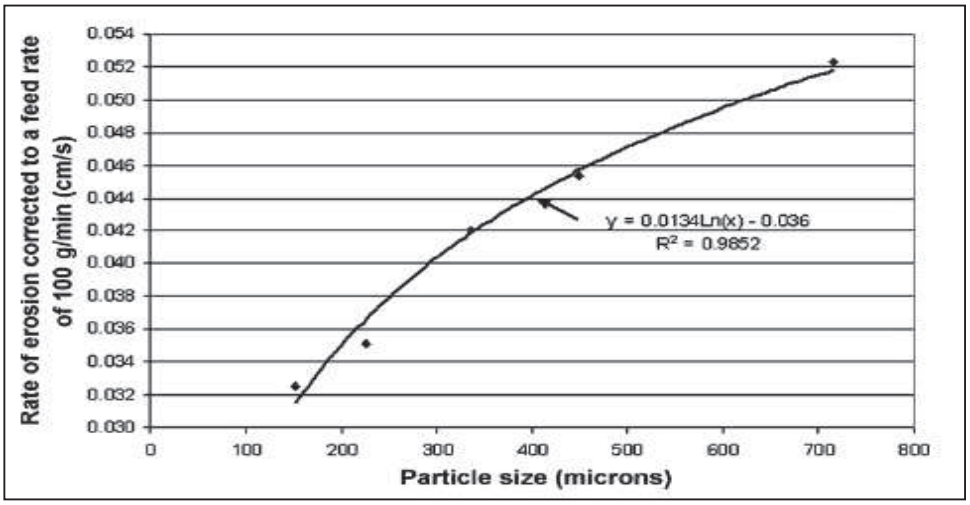

Figure 2-15: Rate of Erosion vs. Particle Size (Gent et al., 2012)

Figure 2-16 shows the relationship between the abrasive's particle density and the rate of erosion at a constant abrasive feed rate. This yields a quadratic relationship, where the rate of erosion increases rapidly when the particles' density increases, but the rate of erosion continues to increase at a decreasing rate in the larger range of the particle density.

Figure 2-17 shows the relationship between the abrasive's particle Bond Work Index (BWI) and the rate of erosion at a constant abrasive feed rate. The BWI is a measure of a material's resistance to fragmentation. This yields a cubic relationship, in which the gradient of the graph within the lower ranges of the bond work index is relatively steep, and hence increasing the Bond Work Index slightly, increases the rate of erosion rapidly.

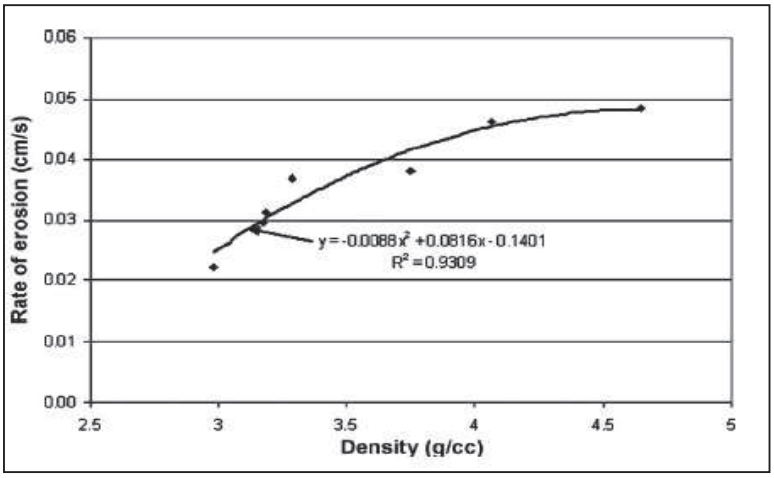

Figure 2-16: Rate of Erosion vs. Particle Density (Gent et al., 2012)

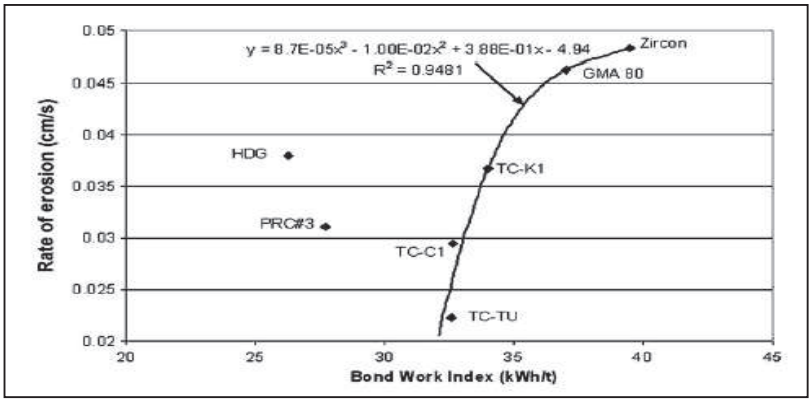

Figure 2-17: Rate of Erosion vs. Bond Work Index (Gent et al., 2012)

Figure 2-18 shows the relationship between the abrasive's particle Vicker's Hardness and the rate of erosion at a constant abrasive feed rate. This produces a linear relationship, i.e. the rate of erosion increases by a fixed amount for every unit increase of Vicker's Hardness.

As suggested by the gradients of these graphs, it can be noted that the two most critical abrasive properties, i.e. the properties that will produce the best abrasive result by small material property, improvements are the Bond Work Index and the Vickers Hardness. While the study by Gent et al. (2012) did make mention of the particle roundness/angularity, it was reported by the authors results for the angularity test were "dubious," and were were not reported in the study.

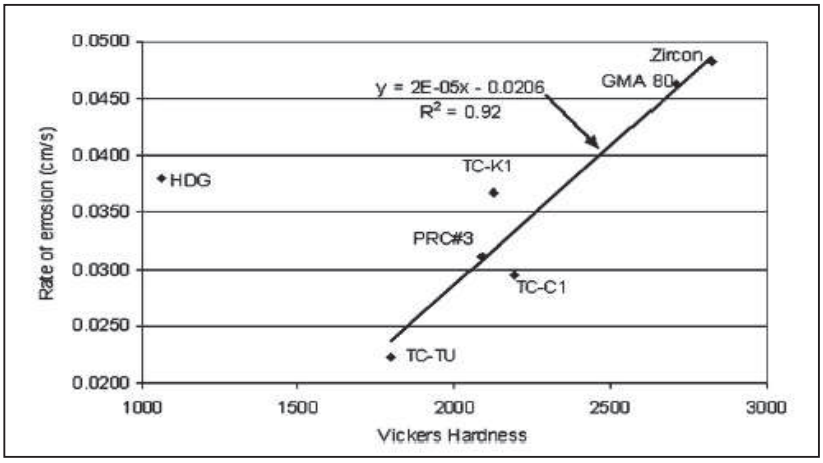

Figure 2-18: Rate of Erosion vs. Vickers Hardness (Gent et al., 2012)

2.6.6 Effect of Impact Angle

In the experiment carried out by Bouzid & Bouaouadja (2000), it was clearly shown that more damage is done to the surface when abrasives strike a surface more perpendicularly than acutely. In this experiment, sand was blasted against the glass surfaces for various durations, at varying impact angles. The results shown below in Figure 2-19 indicate that abrasives striking a brittle surface perpendicularly cause the most abrasion in terms of total roughness.

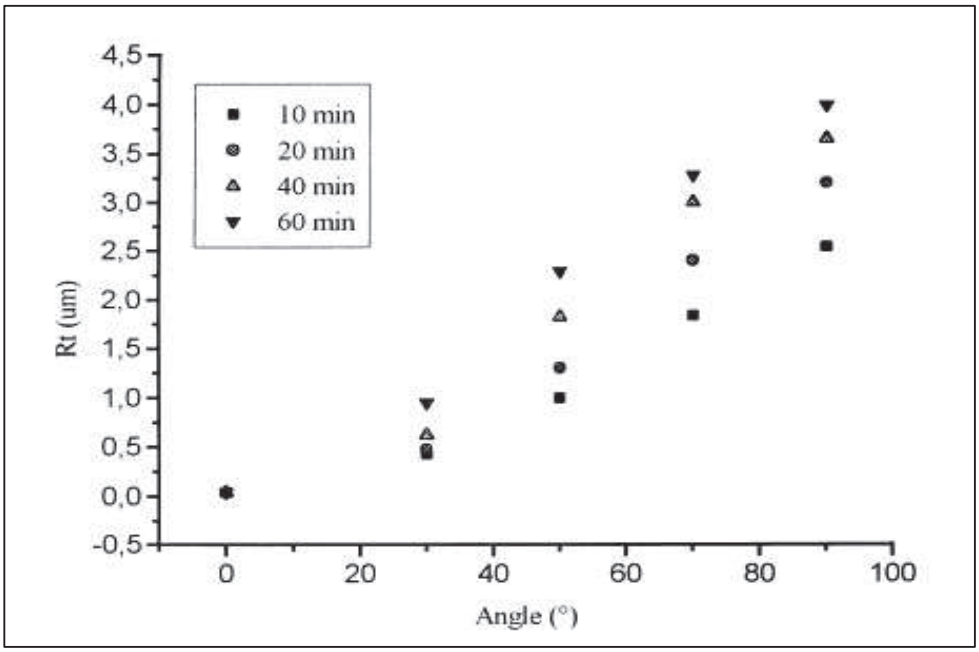

Figure 2-19: Variation of the total roughness (Rt) vs. the impact angles (Bouzid & Bouaouadja, 2000)

2.7 Abrasion Resistance of Pipe Materials

Water distribution systems can be constructed from various pipe materials. Common pipe materials found in South Africa include cast iron, steel, fibre cement, uPVC and polyethylene (CSIR, 2011). These various pipe materials exhibit different physical properties from each other, including resistance to abrasion.

It was reported by Goddard (1994) that Haas & Smith (1975) demonstrated that different pipe materials erode at different rates. In Haas & Smith's (1975) study, a closed loop of the test pipe had an abrasive material pumped through the pipe at a constant flow rate. Using this setup, five pipe materials were tested, those materials being steel, aluminium, polyethylene, ABS (Acrylonitrile butadiene styrene) and acrylic. The test was run at two different velocities (2.1m/s and 4.6m/s) using two sand types with different sized particles (D_{50}=0.58mm and D_{50}=0.31mm). The wear rates are measured in terms of loss of thickness in the pipe wall (mm) over a given period of time (the time period is not specified in Goddard's (1994) report). The numerical results of this test are shown in Table 2-2, and illustrated graphically in Figure 2-20. This method of testing shows that larger abrasive grain sizes and greater flow rates increased the rate of erosion in pipes. It also suggests that out of the 5 materials that were tested (and shown Table 2-2), that aluminium is the most susceptible to erosion damage, followed by acrylic, then ABS, then steel, with polyethylene showing the most erosion resistance.

Table 2-2: Wear Rates of Plastics and Metals under Abrasive Slurries (Goddard 1994)

	Wear Rates (mm)			
Material	**Coarse Sand**		**Fine Sand**	
	2.1m/s	**4.6m/s**	**2.1m/s**	**4.6m/s**
Steel	0.65	1.81	0.04	0.02
Aluminium	1.81	7.48	0.14	0.86
Polyethylene	0.06	0.46	-	0.06
ABS	0.36	2.07	0.07	0.51
Acrylic	0.99	4.10	0.17	1.42

Furthermore, Goddard (1994) demonstrated that different pipe materials exhibit different wear rates using a test in which a 1m pipe sample is tilted back and forth at a constant rate with an abrasive slurry inside of it. Figure 2-21 illustrates how the erosion progresses for different materials with increasing load cycles. Counter-intuitively, this graph suggests that PVC and HDPE are less erodible than concrete, asbestos cement, and glass fibre-reinforced plastics.

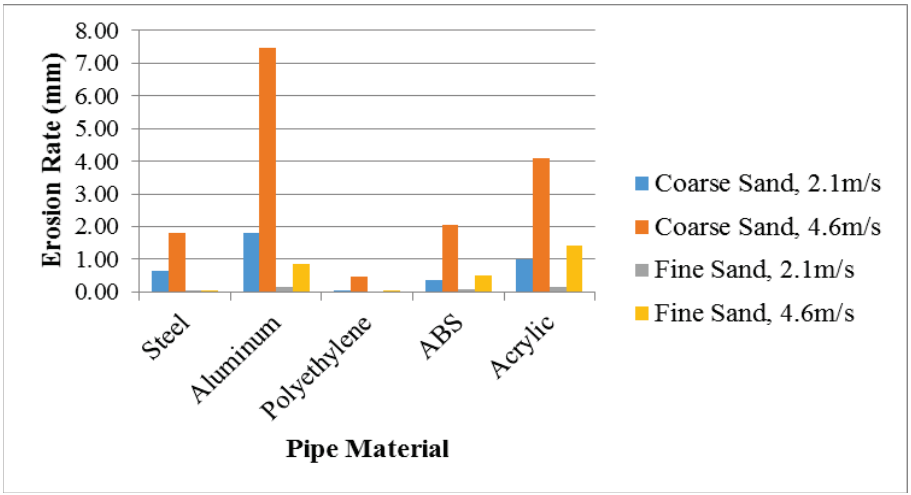

Figure 2-20: Wear Rates of Plastics and Metals under Abrasive Slurries (Goddard 1994)

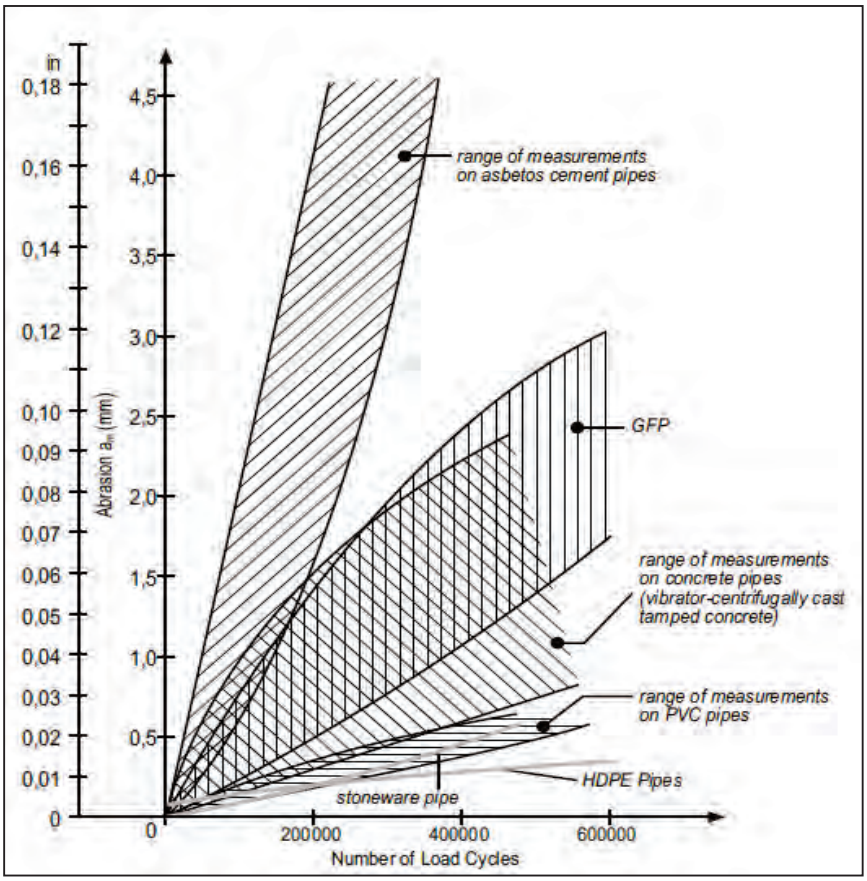

Figure 2-21: Average Abrasion Values for Pipes Made of Various Materials (Goddard 1994)

It has also been demonstrated by ADS (2012) that PVC exhibits less abrasion resistance than polypropylene (PP) and high density polyethylene (HDPE). This was found using the standard Taber Abrasion Test (ASTM D4060-14, 2014). For this test, a sample of the testing material is mounted on a Taber Abrader, and is subjected to rub-wear action of an abrading wheel as shown in Figure 2-22. This abrasion mechanism produces crossed arc erosion patterns, thus simulating abrasion from all angles (ADS, 2012). The test is run for 40hours, allowing for 500 revolutions of the specimen. While the Taber Abrasion Test does not accurately simulate the motion of abrasive particles flowing through a pipe, it is a standardised test for testing abrasion resistance of materials. The specimen's mass is recorded before and after the test so that the loss of mass can be calculated. The results of this test are shown graphically in Figure 2-23.

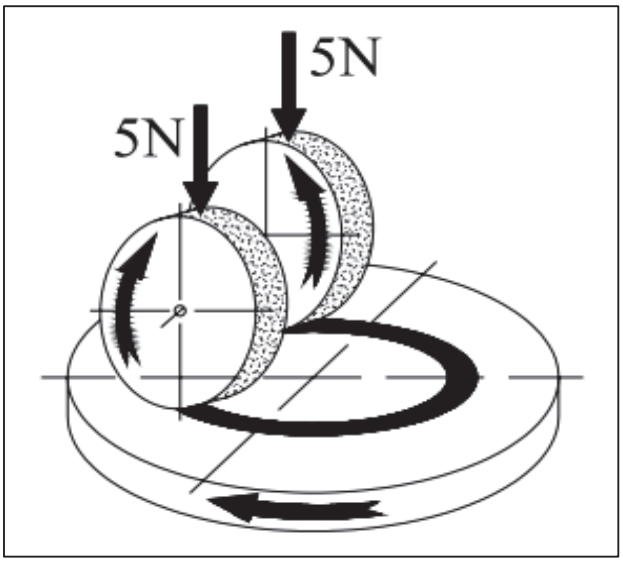

Figure 2-22: Principle of a Taber Abrasion Test (Stabik, Makselon & Tomanek, 2007)

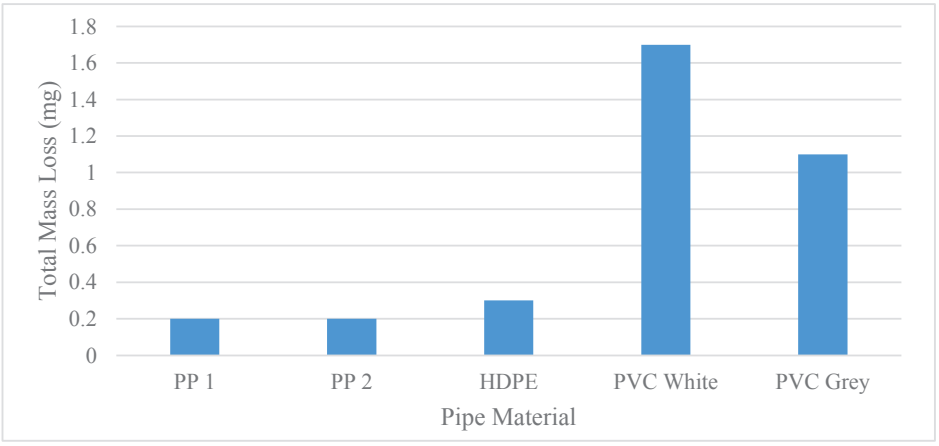

Figure 2-23: Taber Abrasion Test Results for Loss of Material Mass (ADS 2012)

Despite the different tests and measures of abrasion resistance, in both the cases of Figures 2-21 and 2-23, it can be seen that HDPE is less erodible than PVC. Furthermore, it is interesting to note that when comparing Figures 2-20 and 2-23, it appears to be a common trend that the polymeric materials (ABS, Polypropylene, polyethylene, HDPE, PVC), tend to show a greater resistance to erosion than some other materials, such as aluminium and asbestos cement.

Yang & Hlavacek (1999) explain that "polymers usually have poor resistance to abrasive sliding attack because of their relatively low levels of hardness and strength, high plasticity, and low thermal conductivity." Wiebking (1998) states that fillers or additives are substances added to PVC for a number of reasons, including bulking up of resin, increasing stiffness and strength, and improving impact performance . Common fillers include calcium carbonate, titanium dioxide, and calcined clay. Yang & Hlavacek (1999) explain that fillers can improve wear resistance of polymers that can be explained by one of two hypotheses:

1. Fillers may be more resistant to abrasion than the base material, and hence take more of the abrasive load. This proposition came about as a result of observations of high concentrations of fillers being noticed on the surface of the composite materials after long periods of exposure to abrasion.
2. The physical and chemical changes to the composite material could increase the strength of the intermolecular forces, thus increasing the materials' adhesion properties. A more detailed description is provided by Yang & Hlavacek, (1999), which is beyond the scope of this study.

In a study conducted by Ha et al. (1998), it was reported that the abrasion resistance of PVC increases with increasing TPU (thermoplastic polyurethane) content, as illustrated graphically by Figure 2-24. The apparatus and test procedures were not described in detail in this paper, but it is said that the test specimens were prepared and tested in accordance with the KS (Korean Standards) M 6534 method, with a sample size of 16 mm in diameter and 2-3mm in thickness.

Yang & Hlavacek (1999), report that "SiC and Al_2O_3 show the highest improvement on the wear resistance." In general, the more additives in a PVC blend, the greater its wear resistance properties (Ha et al., 1998; Yang & Hlavacek, 1999).

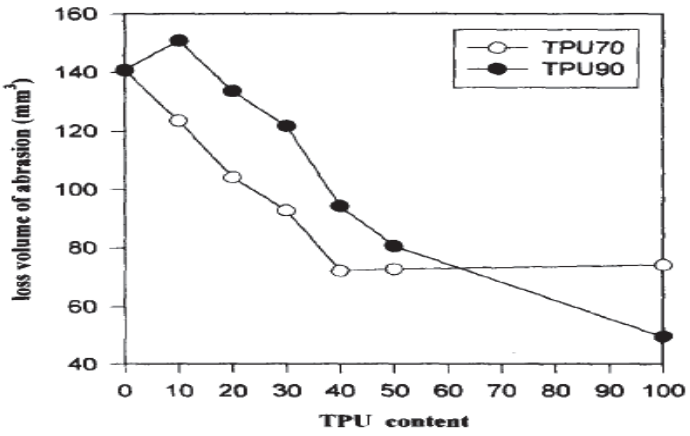

Figure 11 Abrasion resistance of the PVC/TPU90 blends and the PVC/TPU70 blends

Figure 2-24: Abrasion Resistance with Varying TPU contents (Ha et al., 1998)

2.8 Soil-Leak Interaction

2.8.1 Soil-Leak Hydraulics

It is generally accepted that the head loss in water flowing through a granular medium can be calculated by Darcy's Law as shown below in Equation 2.12 (Craig, 2004):

$$Q = KA \cdot \left(\frac{h_s}{L}\right) \tag{2.12}$$

Where Q= Volumetric flow rate; K= Hydraulic conductivity; A= Cross sectional flow area; h_s= Head loss; L= Length of flow path.

This law, however, assumes low flow rates through the granular medium, and hence the velocity component is negligible. The law only holds true for laminar flow (Reynolds, 1883, as cited by Clayton & van Zyl, 2007). Typically, the velocity of laminar flow through soils range from 10^{-2} m/s for clean coarse sand to 10^{-8} m/s and smaller for clays. However, the Orifice (Equation 2.1) predicts high velocities exiting the orifice (van Zyl & Clayton, 2007).

Yang et al. (2014) experimentally examined the effects of porous media on intrusion flow i.e. external water entering a pipe through an orifice. In this experiment, a pipe section with a round orifice was covered with a porous medium in a closed container. Pressurised water was pumped into the container creating a pressure differential between the exterior and the interior of the pipe (which was at atmospheric pressure), to drive the intrusion flow. The results from the control experiment where the surrounding medium was water showed that the orifice equation (Equation 2.1) was suitable for modelling intrusion flow through an orifice; however, the addition of a porous medium decreased the discharge coefficient. It was reported by the authors that the change in discharge coefficient was dependent on factors such as orifice size, flow regime and permeability of porous media.

While Equations (2.1) and (2.2) relate the leakage flow rate to pressure, Guo et al. (2013) suggest that leakage from a buried pipe should also take the hydraulic conductivity of soil into consideration to overcome the incompatibility between the high velocities predicted by Equations 2.1 and 2.2 and the low velocities predicted by Equation 2.12. Guo et al. (2013) derived an equation for leaking longitudinal cracks submerged in a bedding material as shown by Equation 2.13.

$$Q = 2\pi K\left(\frac{P_i}{\gamma_w} - h_{wt}\right) \cdot ln^{-1}\left[\frac{4\pi}{\beta}\left(\frac{h_{wt}}{r} - sin\alpha\right)\right] \quad (2.13)$$

Where K= Hydraulic conductivity; P_i= Internal pressure; γ_w= Specific weight of water; h_{wt}= Height of groundwater table above pipe centreline; β= Open angle of the crack; r= Pipe radius; α= Crack angle from the horizontal (Shown in Figure 2-26 below).

This equation was derived starting with a combination of the continuity equation and Darcy equation (Equation 2.12). This resulted in a second order differential equation, where the hydraulic head was set at 0m at the ground water table, and the hydraulic head just inside of the crack was the sum of the internal pressure head and the elevation above the origin (with respects to Figure 2-25 (a)), to give the boundary conditions. However, the second boundary condition is complex and cannot exist because of the flow through the crack, so an approximate solution to this boundary condition was deemed to be more reasonable and practical. The approximation made use of an equivalent circumference method, and then used a Möbius transformation to transfer the semi-infinite aquifer into a circular domain. The equivalent circumference method approximates the line crack as a permeable column located at the centre of the crack, as shown in Figure 2-25(b). This allows the groundwater table to be modelled as a concentric circle around the crack using a Möbius transformation, as shown in Figure 2-25(b). This transformation allows the governing equations and boundary conditions to be expressed in polar coordinates. Substituting the boundary conditions into the governing equations, Guo et al. (2013) found Equation 2.13 to describe the flow through a longitudinal crack into a granular medium. The validity of this equation was then verified by means of numerical modelling on MATLAB. The results of the analytical solution and numerical simulations were compared. It was concluded that Equation 2.13 gives an approximation for calculating the steady state leakage from longitudinal cracks from pressurised buried pipes, with a better understanding of the parameters involved than more commonly used N_1 equation (Equation 2.2).

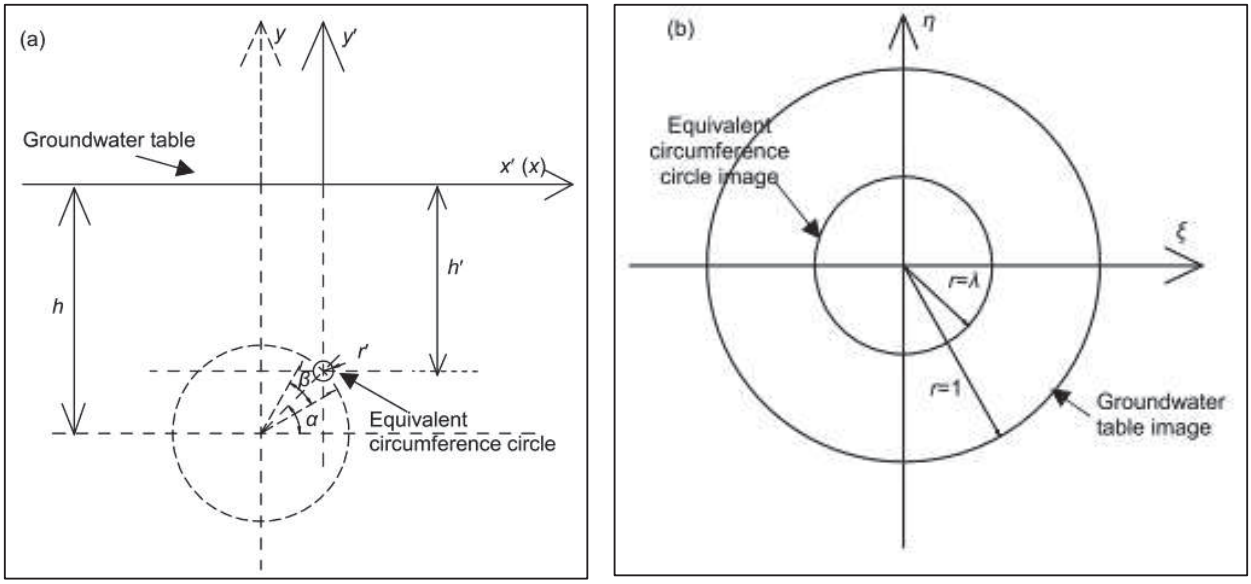

Figure 2-25: Equivalent Circumference Method for Approximating a Linear Crack and Groundwater Table (Guo et al., 2013)

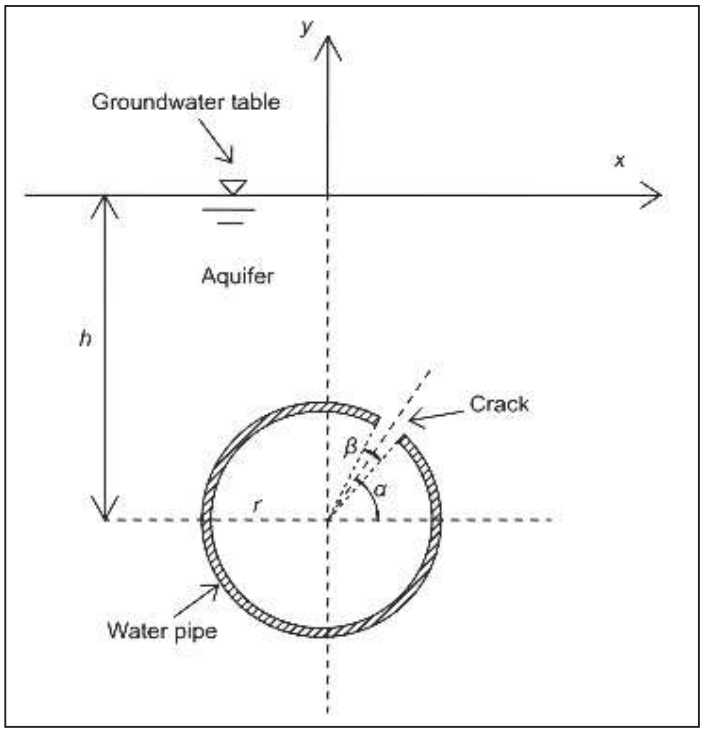

Figure 2-26: Parameters of Equation 2-13 (Guo et al., 2013)

A dimensionless Soil/Orifice number (also referred to as "OS number"), can be used to categorize leaks from water distribution pipes (Walski et al., 2006). This number is the ratio of the head loss from the orifice, and the head loss from the soil. As explained by Walski et al. (2006), this number can be derived from the Bernoulli energy equation in combination with Darcy's Law of head loss. The OS number of a leak is described by the following equation:

$$OS = \frac{KAQ}{2gL}\left(\frac{1}{C_d \cdot A_0}\right)^2 = \frac{h_0}{h_s} \quad (2.14)$$

Where K= Hydraulic Conductivity of the Soil; A= Area of the Flow in the Soil; Q= Flow Rate; g= Acceleration due to gravity; L= Length of the flow Path in the Soil; C_d= Orifice Discharge Coefficient; A_0= Area of the Orifice; h_0= Head Loss due to Flow through Orifice; h_s= Head Loss due to Flow in Soil.

Walski et al. (2006) went on to verify experimentally whether this OS number was a meaningful indicator of flow type. To obtain a range of OS numbers, leaks were simulated into soil beds at various different flow rates, into two soil beds of different heights. The soil matrix was also secured with a pressure plate so as to prevent the expansion of the soil matrix, and hence prevent fluidisation at higher flow rates. Walski et al. (2006) state that without the pressure plate, low OS numbers could not be created, implying that the soil matrix is not likely to control leakage for many situations. This study concludes that for OS values greater than 4, orifice head loss dominates, and for low OS numbers (smaller than 0.2), soil head loss is the dominant factor. Walski et al. (2006) then go on to explain that for most real world cases, OS numbers tend to be high, and hence the orifice equation is sufficient in calculating head loss. A low OS number would have to occur in a tightly compacted material (low conductivity), without fluidisation occurring.

2.8.2 Internal Soil Fluidisation

Alsaydalani & Clayton (2014) define internal soil fluidisation as the process whereby granular soil transforms into a fluid-like state as a result of a fluid being pumped into a granular bed. This phenomenon occurs when granular solids are subjected to a fluid flow which creates drag force sufficient to support the weight of the particles (Niven & Khalili, 1998). The soil is separated by the fluid and expands, thus allowing the soil itself to behave as a fluid, creating a zone of fluidisation. Richards & Reddy (2007) explain that particles are progressively dislodged from the soil matrix through tractive forces produced by intergranular seeping water. They then go on to explain that the mobilising tractive forces are balanced by the shear resistance of grains and the weight of the soil particles. In terms of initiating fluidisation in a granular bed from an orifice, it has been discovered that the size of the fluidisation zone is independent of the orifice size, but is rather more critically affected by the flow rate out of the orifice (van Zyl et al., 2013). An example of where this might occur is

when a jet of water from a leaking pipe shoots into the surrounding soil, as shown in Figure 2-27.

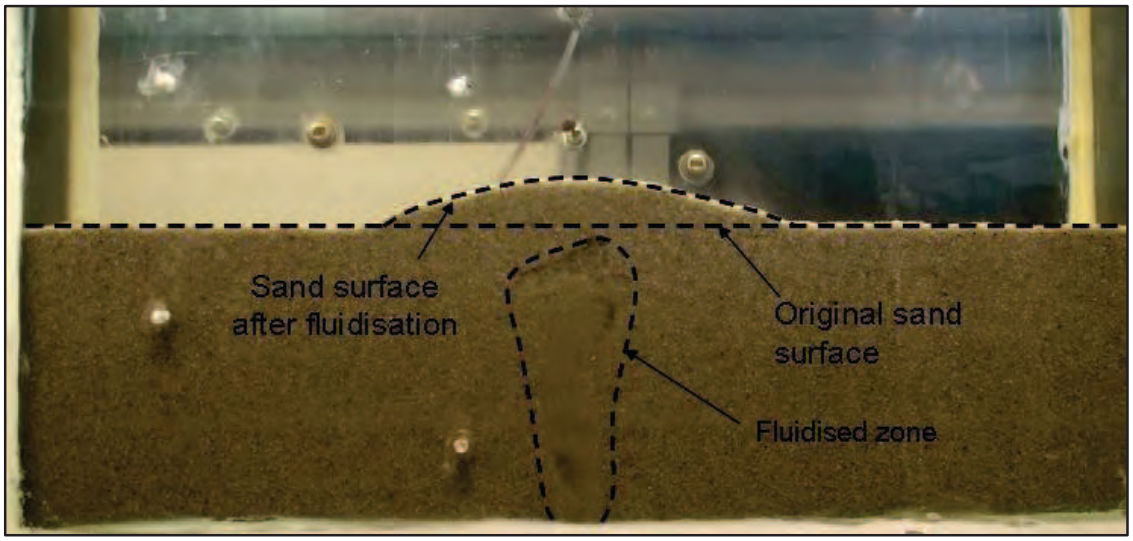

Figure 2-27: Illustration of Fluidisation Zone from Vertical Water Jet (Ma, 2011)

It was found that fluidisation did not occur when the flow rate of the fluid jet was too low (Alsaydalani & Clayton, 2014). Alsaydalani & Clayton (2014) demonstrated this in an experiment in which a linear crack was simulated under controlled laboratory conditions. In this experiment, water was pumped through an aperture of known width into a bed of granular material. The pressure upstream of the aperture was increased incrementally while the corresponding flow rates were recorded. The results of this experiment, shown graphically in Figure 2-28, show that when the upstream pressure is low (line section A-B in Figure 2-28), the flow rate of water through the sand bed increases approximately linearly with pressure, suggesting Darcy flow. In this range of flow rates, fluidisation has not yet been initiated, and the crack is occluded by the granular particles. Line section B-C in Figure 2-28 represents the onset of fluidisation. There is a sudden rapid increase in flow rate with a small increase in pressure as a result of the soil particles moving away from the crack, and removing the occlusion effect. After the onset of fluidisation, line segment C-D shows that the flow rate increased more gradually with increasing pressure. It was reported that by visual inspection, the volume of the fluidised zone continued to increase with increasing pressure during this phase. This suggests that the additional energy from the increased pressure head was being converted into velocity head (Alsaydalani & Clayton, 2014).

Alsaydalani & Clayton (2014) further suggested that both the depth of the granular bed and the grain size of the material have an effect on the pressure required to initiate fluidisation. Figure 2-29 shows their predictions for the pressures at the onset of fluidisation for different bed heights, and for two different grain sizes. These predictions are based on Ergun's Equation (Equation 2.15):

$$\frac{\Delta P}{L} = A\frac{\mu}{{\varphi^2}_s d^2_p}\cdot\frac{(1-\varepsilon)^2}{\varepsilon^3}U + B\frac{\rho_w}{\varphi_s d_p}\cdot\frac{(1-\varepsilon)}{\varepsilon^3}U^2 \qquad (2.15)$$

Where ΔP= Pressure drop over flow path; L= Length of flow path; μ = Dynamic viscosity; d_p = Particle diameter; ρ_s = Solid density; ρ_w = Water density; φ_s = Particle shape factor (sphericity); ε = Porosity; U = Superficial fluid velocity; A and B are constants calculated by Ergun to be equal to 150 and 1.75, respectively.

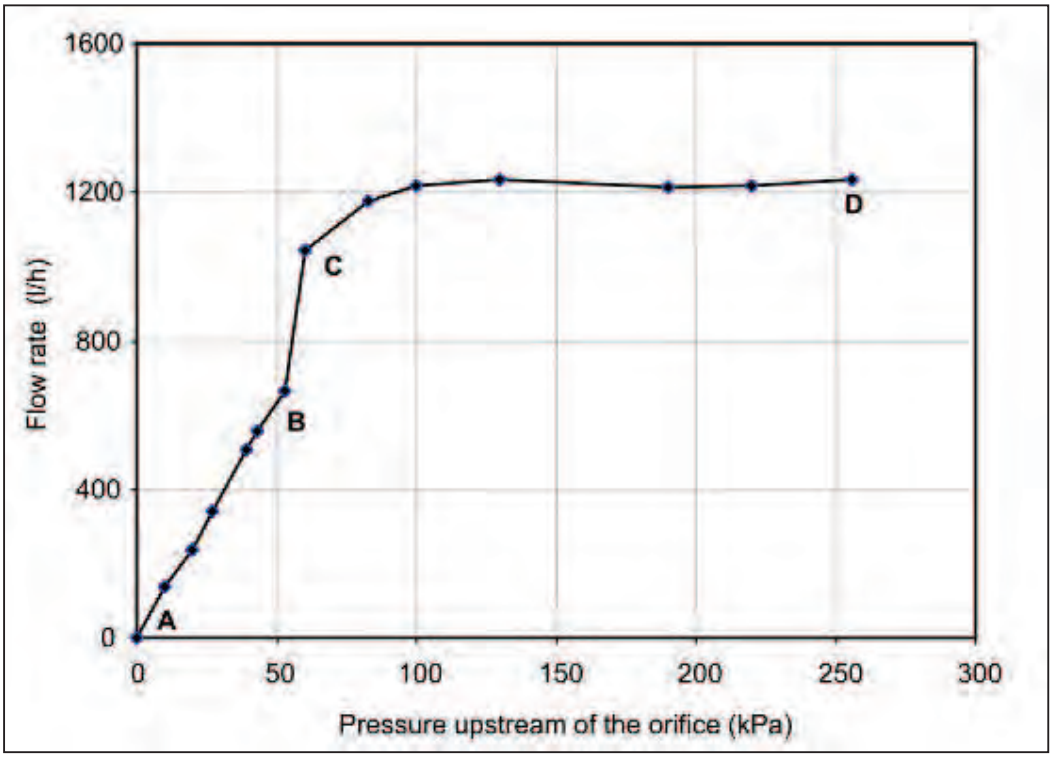

Figure 2-28: Pressure-flow rate relationship when water was injected into a 300-mm bed of 0.9-mm silica sand through an orifice opening of 0.336 mm (Alsaydalani & Clayton, 2014)

The superficial fluid velocity is the velocity of the fluid, calculated as if it were the only thing flowing in the given cross-sectional area, i.e. assuming no fluid-particle interaction.

Figure 2-29 suggests that the pressure required to initiate fluidisation increases with increasing bed depth. It further suggests that a granular bed comprised of larger grain sizes requires larger pressures, and hence flow rates, in order to induce fluidisation. It was then verified experimentally by Alsaydalani & Clayton (2014) that this was in fact the case. It was further observed experimentally, and by Ergun's model, that granular beds comprised of more spherical particles will fluidise at greater pressures.

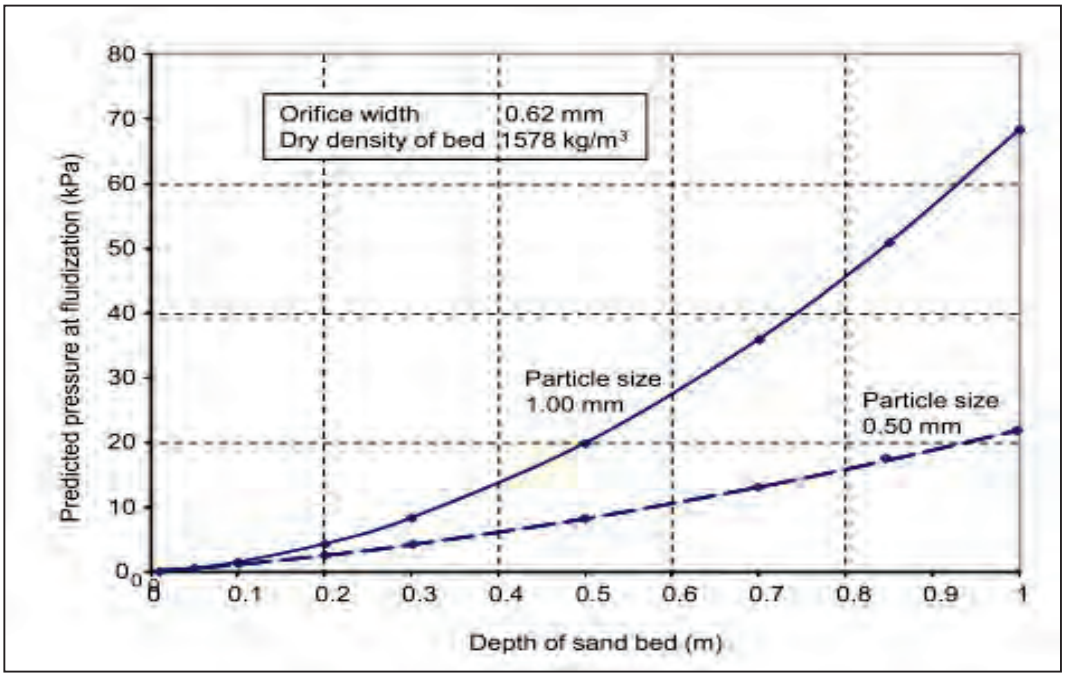

Figure 2-29: Predicted pressures at the onset of fluidization over upward facing orifices, as a function of bed thickness, and particle size (Alsaydalani & Clayton, 2014)

This concept of soil fluidisation allows for the basis of the hypothesis that a leak in a pipe may cause scouring of the pipe wall around the leak itself. Van Zyl et al. (2013) showed experimentally that a vertical jet of water shooting into a granular matrix forms a mechanism in which a vertical fluidisation zone is formed. Around the fluidisation zone, a "mobile bed zone" is created. In this mobile bed zone, granular particles that were moved to the top of the fluidisation zone sink back down towards the orifice, as shown in Figure 2-30. Figure 2-30 shows the geometry of the fluidisation and mobile bed zones for different flow rates out of leaking orifices in an experimental setup with an idealised soil medium. The idealised soil medium was ballotini, which is uniformly shaped and sized glass beads. The three orifice flow rates creating the three fluidisation zones are 130 l/h, 220 l/h and 320 l/h for images (a), (b) and (c) respectively.

As shown in Figure 2-30, the size of the fluidisation zone is dependent on the flow rate out of the orifice. Van Zyl et al. (2013) reported, however, that even with the larger pressure heads within the pipe, the fluidisation zone did not break through the open surface of the granular material.

In order to accurately describe flow of water through a granular bed as a result of a vertical water jet, a set of experimental apparatus was designed to measure the magnitude and direction of the water velocities at different points in a bed of ballotini, which simulates an idealised granular material (Bailey, 2015). This apparatus comprised of a glass tank filled with ballotini, and a vertically orientated orifice positioned in the centre of the base of the tank.

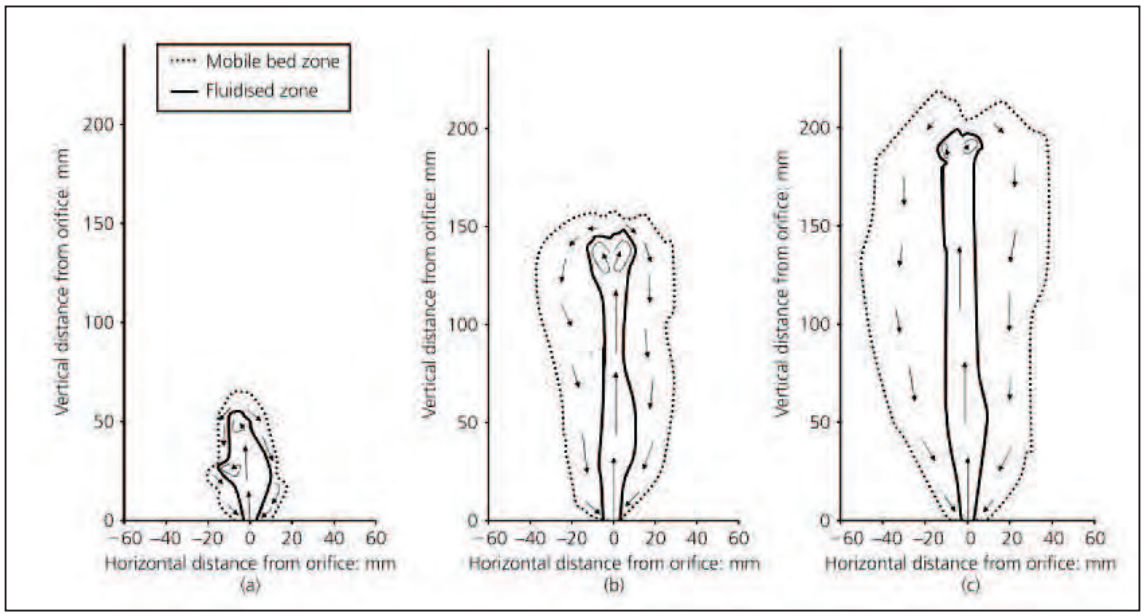

Figure 2-30: Fluidisation Mechanism (van Zyl et al., 2013)

When water was flowing out of the orifice, the pressures and velocities of the fluid flow within the ballotini bed were measured with Straight and L-type pitot tubes. The pitot tubes were connected to a site tube, where the pressure and velocity heads at the point of the pitot tube was represented by an increase in water level. The straight pitot tubes were used to measure the vertical velocity heads, while the L-type pitot tubes were used to measure the horizontal velocity heads. Figure 2-31 below shows a vector diagram of the resultant fluid velocities measured at various points in the ballotini bed, with an orifice flow rate of 2 l/min (120 l/h). In this figure, the orifice is positioned at the co-ordinates (0; 0), and the x and y axes represent the horizontal and vertical distances from the orifice respectively. The length of each vector in Figure 2-31 is proportional to its magnitude. This figure shows that the fluid velocity is at a maximum vertically above the orifice in the upward direction (the initial orientation of the orifice), after which the fluid tends to filter outwards into the granular bed. It is also interesting to note that the fluid velocity immediately adjacent to the orifice is relatively high, and towards the orifice, as indicated by the blue ellipse in Figure 2-31.

Since the fluid ultimately permeates the granular bed while the motion of the dynamic ballotini is restricted to the mobile bed zone, it is suggested by Bailey (2015) that the path of the soil particles is unlikely to follow the flow patterns of the fluid. Bailey (2015) observed the movement of the soil particles in the fluidised zone and mobile bed zone by simulating a leak in the ballotini bed adjacent to the glass sidewall as shown in Figure 2-32. The right hand side of Figure 2-32 shows the flow lines of the ballotini particles . Figure 2-32 shows that the ballotini particles rapidly move vertically upwards in the fluidised zone, and then more gradually make their way back down toward the orifice in the mobile bed zone (Bailey, 2015), similar to the findings of van Zyl et al. (2013).

Figure 2-32 suggests that the ballotini particles adjacent to the orifice in the mobile bed zone merges with the fluidised zone horizontally, causing the particles to scrape along the bottom of the tank before re-entering the fluidisation zone.

Using the orifice adjacent to the glass sidewall, it was further observed by Bailey (2015) that the an increase in surcharge pressure in the granular bed decreases the height of the fluidisation zone. Figure 2-33 shows the effect of an additional pressure applied to the bed's surface on the height of the fluidisation zone. In this case, the additional pressure was applied by hand. Practically, an increase in granular bed height could cause this same effect on the fluidised zone.

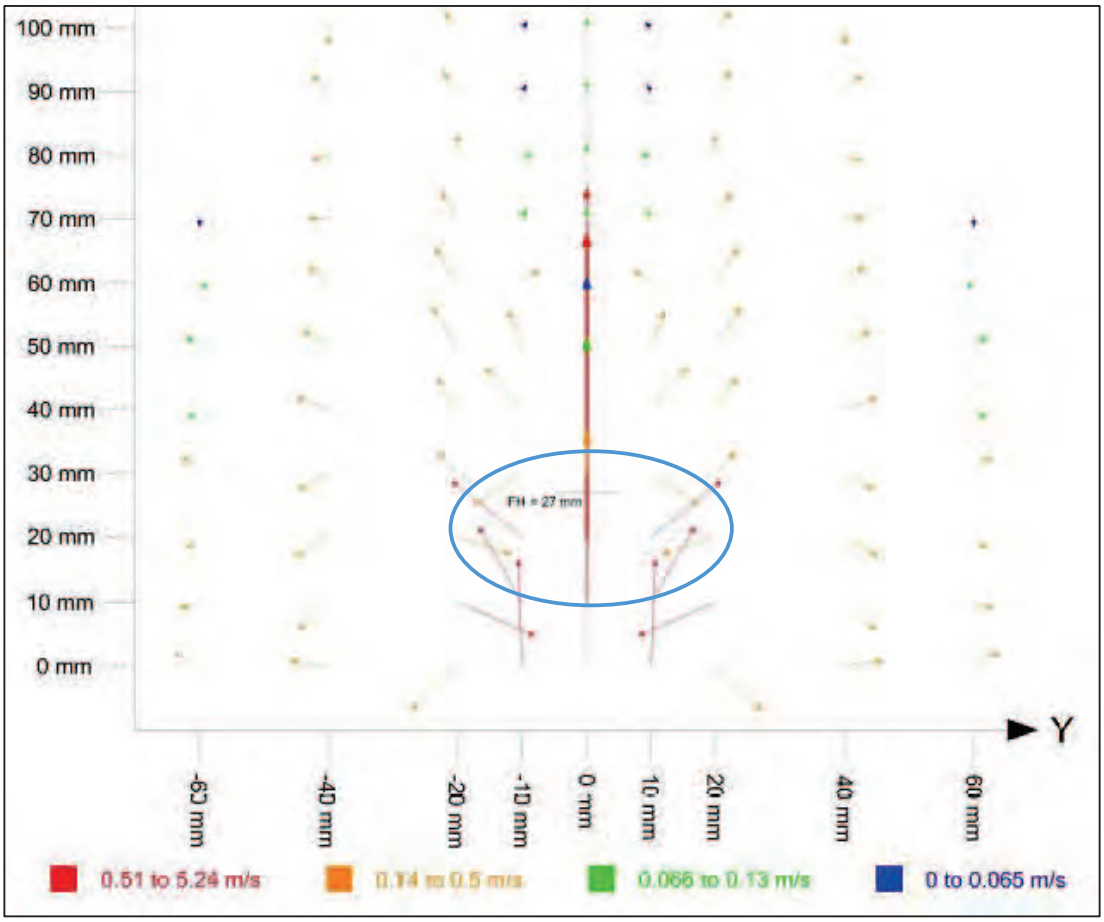

Figure 2-32: Velocity Vectors of Water Flowing through a Ballotini Bed (Adapted from Bailey, 2015)

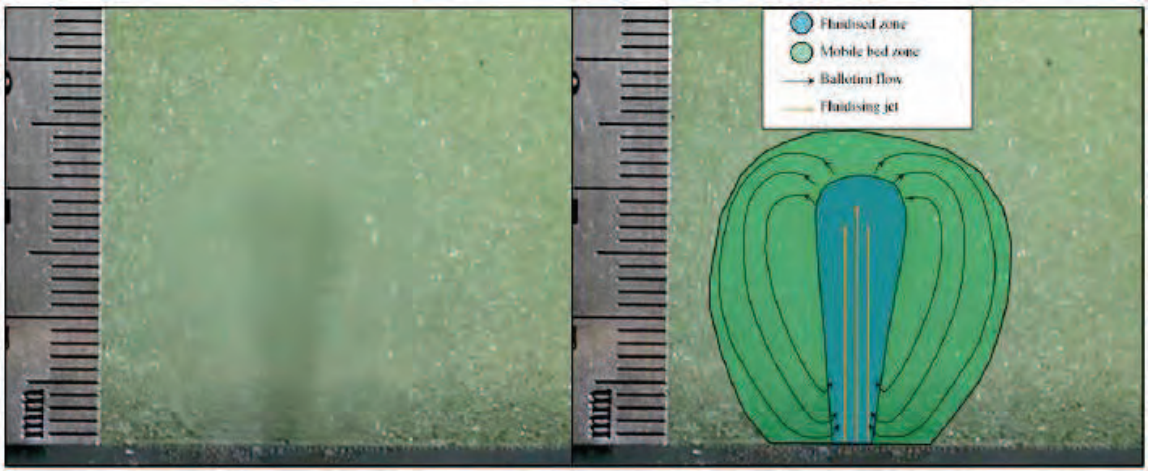

Figure 2-31: Influence Zone for Vertical Water Jet Flowing into Ballotini Bed at 2 l/min (Bailey, 2015)

Figure 2-33: Effect of Surcharge Pressure on Fluidised Zone (Bailey, 2015)

2.9 Previous Work on Scouring Outside Pipe Leaks

2.9.1 Evidence of Leakage-Induced Pipe Erosion

Evidence of leakage-induced pipe erosion has been observed in numerous failed pipe samples from around the world. Figures 2-34 to 2-37 give examples of suspected leakage-induced pipe erosion obtained from literature and personal communications. Figure 2-34 shows a uPVC socket joint that has failed due to excessive angular deflection, after which the failure has been exacerbated by erosion from the high-pressured leaking water. It is suggested that the material removed from around the leak has been removed as a result of leakage-induced pipe erosion after the pipe had cracked, since cracking from deflection would generally result in a linear crack without a loss of pipe material.

Figure 2-35 shows a leak whose surrounding pipe material has been removed as a result of erosion caused by the leak itself. It is suspected that a leak was initially formed, after

Figure 2-34: Failure in PVC-U socket due to excessive angular deflection of spigot, aggravated by erosion from pressurised leaking water (Water Services Association of Australia, 2012)

Figure 2-35: Pipe leak that has been aggravated by leakage induced erosion from the Netherlands (de Kater, 2014)

which the leaking water scoured away the adjacent pipe material causing the indentation that can be observed in this image. This indentation has caused the pipe wall to be locally thinned, which could potentially cause the pipe to burst. It can also be observed that the pipe wall thickness has been decreased to a point where a second orifice has been formed (to the right of the large orifice). This demonstrated how leakage-induced pipe erosion can exacerbate an initial leak condition. It can also be observed in Figure 2-35 that the indented region appears to be smooth and polished. This pipe sample was found in the Netherlands, and the image was obtained through personal communications (de Kater, 2014).

Figure 2-36 shows a PVC pipe with a longitudinal crack found in the Netherlands (van Thienen, 2014). In this image, it can be seen that there are clear indentations in regions adjacent to the crack at either end. It is clear that pipe material has been removed to cause these indentations. It is uncommon for pipe material to be removed from the pipe due to longitudinal cracking, suggesting that a different mechanism caused the removal of the material. The smoothness of these indentations suggests that they were caused by soil abrasion. These indentations have caused the crack width on the external surface of the pipe to widen.

It can also be observed in Figure 2-36 that the external surface of the pipe has a black coating as a result of spending time in anoxic underground conditions. It can be seen that the black coating has been removed adjacent to the crack, exposing the colour of the original pipe material. This coating has been removed by the abrasive action of soil in the fluidised zone around the leak.

The left hand image in Figure 2-37 shows cracked asbestos cement (AC) pipe sample from The City of Cape Town Municipality. This image shows a smoothed, indented region adjacent to the crack, where water was presumably leaking parallel to the pipe's surface. It appears that material has been removed from this pipe sample as a result of abrasive wear.

In the right hand image of Figure 2-37, it can be seen that a longitudinal crack has formed in an AC pipe. This pipe sample was also found by The City of Cape Town Municipality. In the region identified by the red circle, it appears that material has been removed from the original pipe surface. This indented region appears relatively smooth. The indentation has also locally widened the crack, thus aggravating the initial leak.

Figure 2-36: Evidence of Scouring around Longitudinal Crack in PVC Pipe (van Thienen, 2014)

Figure 2-37: Failed Asbestos Cement Pipe Samples from The City of Cape Town (Pike, 2013)

2.9.2 Failure Analysis of Natural Gas Pipes (Majid, Mohsin, Yaacob & Hassan, 2010)

It has been observed that damage can be caused to buried pipes that are situated in the fluidisation zone of adjacent leaking pipes. Majid et al. (2010) performed a case study in which an asbestos water reticulation pipe and two natural gas pipelines (Medium Density Polyethylene and Carbon Steel) were laid parallel to one another, and arranged as shown in Figure 2-38. The study came about as the result of the failure of the gas pipes, hence the need

to identify the most probable cause of failure. The water pipe was carrying water at an estimated 10 bar, while the steel and MDPE pipe were carrying gas at 18 bar and 3.45 bar respectively. The wall thicknesses of the carbon steel, MDPE and asbestos pipes were 5.6mm, 11.4mm, and 10mm respectively.

Upon excavation, it was found that all three pipes showed signs of damage or leakage. A visual inspection found no indication of third party damage or construction malpractices. The condition of the carbon steel pipe immediately after excavation, before oxidation took place, is shown in Figure 2-39. This pipe's protective coating had been removed in the vicinity of the leak, and the surface surrounding the leak was described as clean, smooth and shiny. The leak was approximately 10mm in diameter situated in the centre of the area that had had its coating removed.

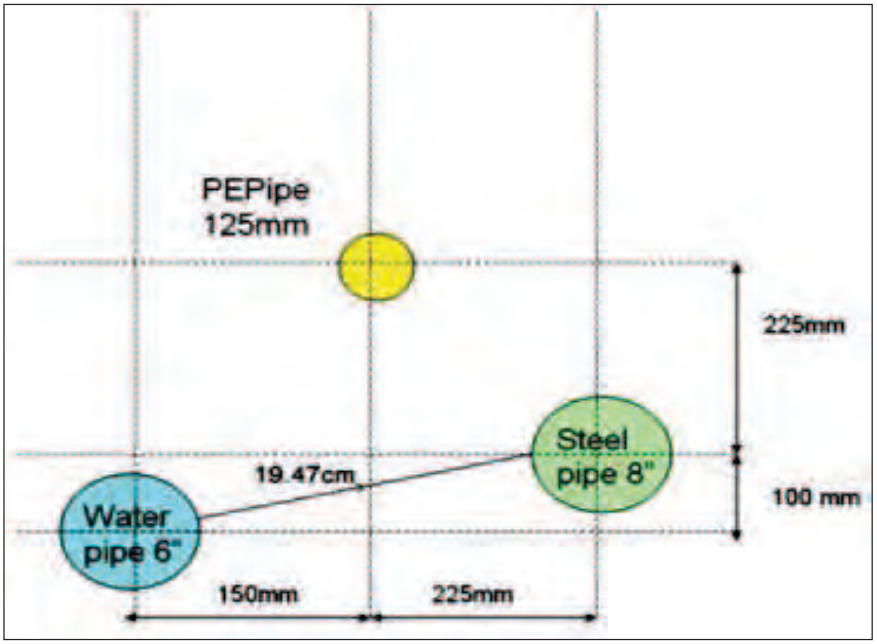

Figure 2-38: Arrangement of Pipes prior to Failure (Majid et al., 2010)

Figure 2-40 shows MDPE and carbon steel pipes having been repositioned in a laboratory, in the same relative positions in which they were found after excavation. This figure shows that a large portion of the MDPE pipe has been removed, presumably by the impact of high velocity soil caused by the leaking high pressure gas pipeline.

The failure mechanism of the asbestos water could not be analysed since the failed pipe specimen was not obtained. It was suspected, however, that the failure was likely caused by a crack in the pipe, probably longitudinal in nature, based on pipe material properties and behaviour.

Figure 2-39: Condition of Carbon Steel Pipe Immediately after Excavation (Majid et al., 2010)

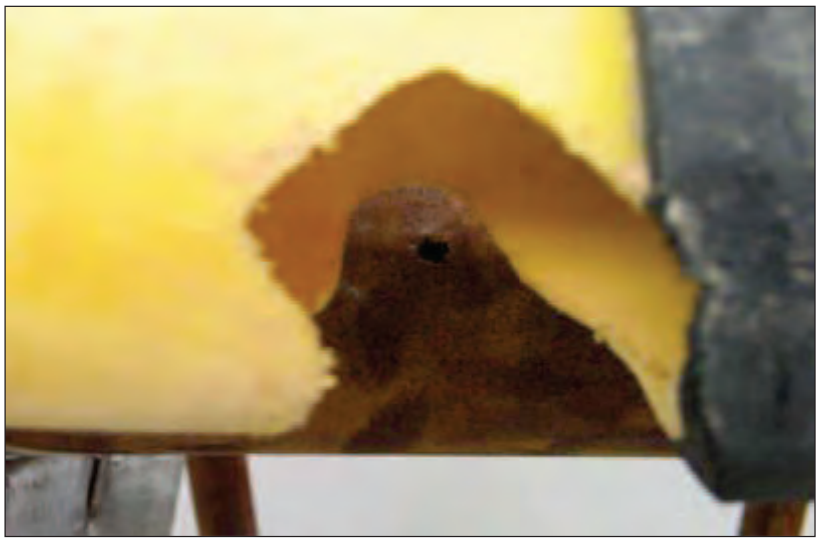

Figure 2-40: Laboratory Replication of Field Conditions of Soil Abraded Gas Pipe (Majid et al., 2010)

Having considered numerous possible failure scenarios, it was suggested that it was most likely that the water pipe failed first, thus causing a fluidisation zone below the MDPE pipe, and hence removed some of the support material from beneath it. This soil fluidisation caused abrasion on the carbon steel pipe, thus causing the steel pipe to fail, following which the pressurised leaking gas removed further support material from beneath the MDPE pipe. The MDPE pipe then dropped low enough to enter the fluidisation zone of the carbon steel pipe, after which the soil abrasion process commenced on the MDPE pipe.

2.9.3 Multiple Failures of API 5L X42 Natural Gas Pipeline (Majid & Mohsin, 2013)

A case study by Majid & Mohsin (2013) found that a mild steel water pipe (steel grade 430) had ruptured at a welded joint, causing erosive failure to an adjacent carbon steel pipe (grade API 5L X42) conveying natural gas.

The gas pipeline was buried 1.8m below the ground surface, positioned above the water pipeline which was at a depth of 2.25m below the surface, configured as shown in Figure 2-41.

The carbon steel gas pipeline had a coal-tar based enamel coating, with fibre-glass inner and outer linings. Prior to failure, this pipeline was conveying gas at an average of 17 bar.

The mild steel water pipeline had a bitumen based enamel coating, also with fibre-glass inner and outer linings. Prior to failure, this pipeline was conveying water at an average of 9 bar.

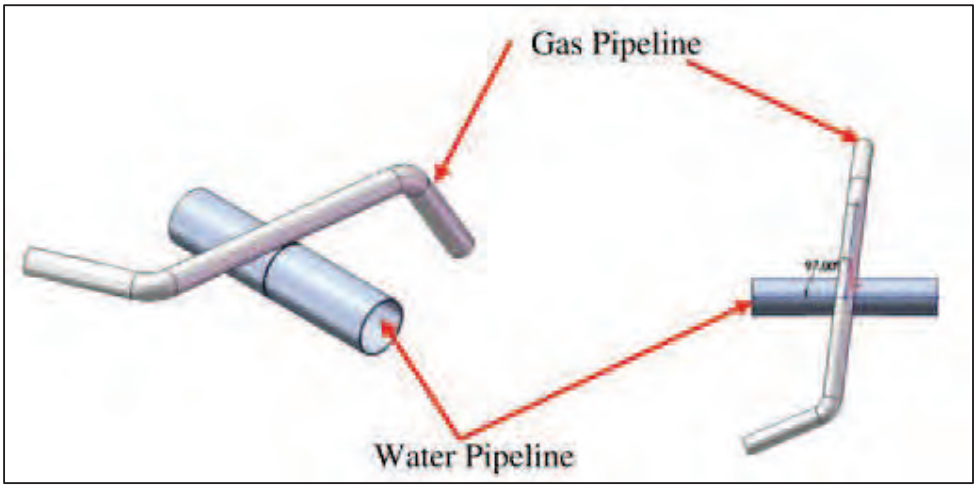

Figure 2-41: Configuration of Water and Gas Pipeline (Majid & Mohsin, 2013)

Upon excavation, three separate holes were observed on the underside of the carbon steel gas pipeline in line with the leaking weld joint of the steel water pipe, as shown in Figure 2-42. It was thought to be likely that the failed weld joint of the water pipeline caused a high velocity jet of soil and water to strike the gas pipeline, causing the damage shown in Figure 2-42. It was observed that to the right of orifice 1 (in Figure 2-42 (a)), that the eroded surface was rough, while the surface to the left of this orifice was smooth.

It was suggested by the authors that the difference in surface conditions was a result of two different erosion media, namely water on the smooth surface, and a sandy slurry on the rough surface. Due to the localised removal of the protective coating on the gas pipeline, it was deduced that the failure was caused by soil erosion.

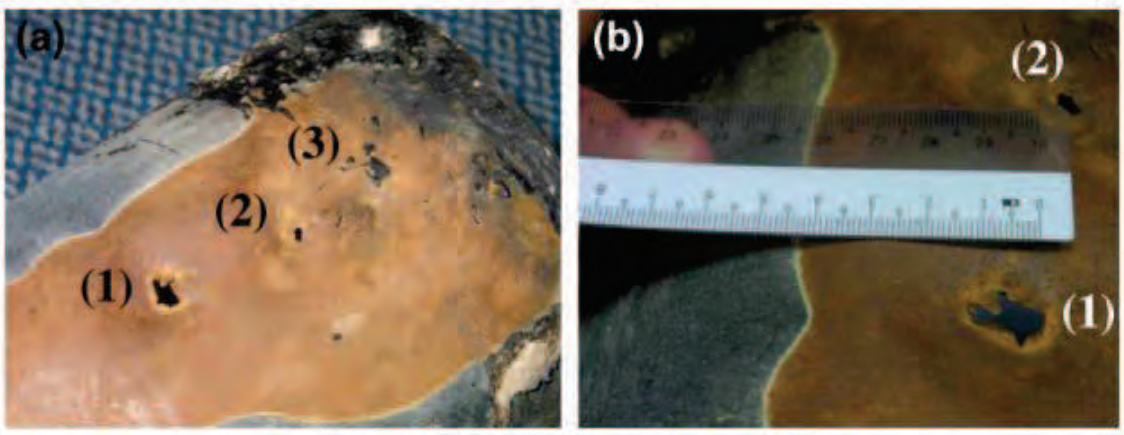

Figure 2-42: Ruptured Holes on Gas Pipeline Surface (Majid & Mohsin, 2013)

2.9.4 Experimental and Computational Failure Analysis of Natural Gas Pipe (Majid, Mohsin & Yusof, 2012)

The laboratory investigation by Majid, Mohsin & Yusof (2012) placed a carbon steel (API 5L X42) pipe specimen in the fluidisation zone of a buried, horizontal simulated water leak. In this experiment, a carbon steel pipe specimen was buried in a sand filled tank at a depth of 1m. To position the pipe in the soil bed, a number of small holes were drilled into the pipe surface through which water could be discharged, thus fluidising the soil bed and allowing the pipe sample to be lowered into the tank and buried. The bedding material was graded between 200 and 600μm. The pipe sample was positioned 300mm away from a 5mm diameter orifice which was orientated horizontally. The internal pressure of the water jet was set to 10 bar. After 100 hours of exposure to the jetting, it was observed that there were two zones which displayed different scour patterns as shown in Figure 2-43. At the centre of the scour pattern there was an inner ring where the surface was indented and smooth. The outer ring displayed rough, ripple-like scour patterns.

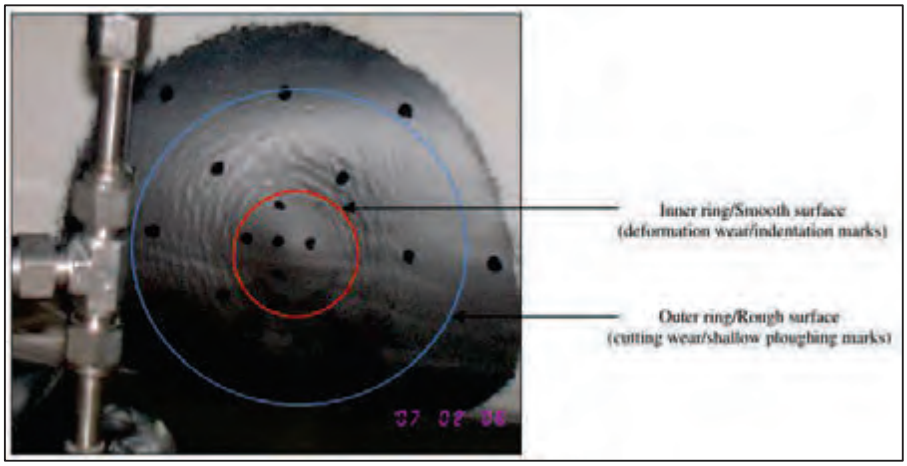

Figure 2-43: Pipe surface after 100 Hours of Jetting (Majid, Mohsin & Yusof, 2012)

The authors suggested that at the centre of the jet (point of impact), water was the main erosion media, with finer and fewer sand particles impacting the surface, causing horizontal tunnelling as shown in Figure 3-44. It is said that abrasive particles striking a surface at 90°tend to cause craters and indentation, as seen in the inner ring of this erosion pattern, while oblique impact angles tend to cause grooves, known as shallow ploughing. As shown in Figure 3-44, the outer ring of the erosion pattern will experience particle impact at oblique angles. This explains the ripple effects in this region.

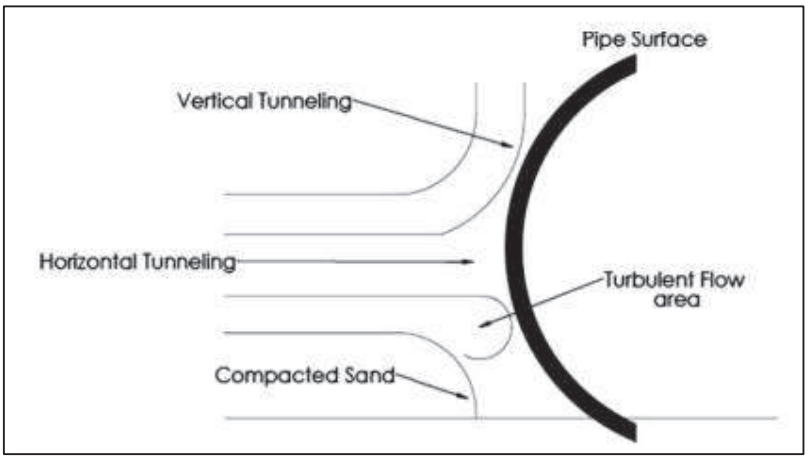

Figure 2-44: Tunnel Profiling (Majid, Mohsin & Yusof, 2012)

2.9.5 Scouring Patterns of Pipes outside Leaks due to Soil Agitation (Pike, 2013)

A laboratory study was conducted by Pike (2013) to investigate the response of uPVC pipes placed in the fluidisation zone of a pressurised leaking pipe, similar to the aforementioned case studies (Majid et al., 2010; Majid & Mohsin, 2013). The aim of this investigation was primarily to determine the rate at which a uPVC pipe would erode when placed in the fluidisation zone of an adjacent leaking buried pipe. This experiment had two pipes fixed at 120mm away from each other (external wall to external wall), with the leaking pipe below (referred to as "bottom pipe"), and an unpressurised pipe vertically above the leak (referred to as "top pipe"). Figure 3-45 shows the configuration of the experiment. The leakage flow rate was approximately 350 litres/hour. The leaking pipe had an internal pressure of 2 bar. This test was performed twice; once with a medium grain size sand (Malmesbury sand impact test), and once with a coarse sand blasting grit (Alcab 16 impact test).

The scour pattern formed on the top pipe is shown in Figure 2-46 below, while the progression of the scour dimensions is shown in the Figure 2-47. Figure 2-47 shows the development of the scour-affected region (scour diameter) created by the two tests with the aforementioned abrasives. The scour diameter is defined as the circular indented region of the pipe surface, which can be seen in Figure 2-46. It can be seen from Figure 2-47 that the scour diameter grew at a greater rate for the Alcab 16 impact test than for the Malmesebury sand

impact test. This suggests that the larger grain size of the abrasive particles increase the rate of erosion.

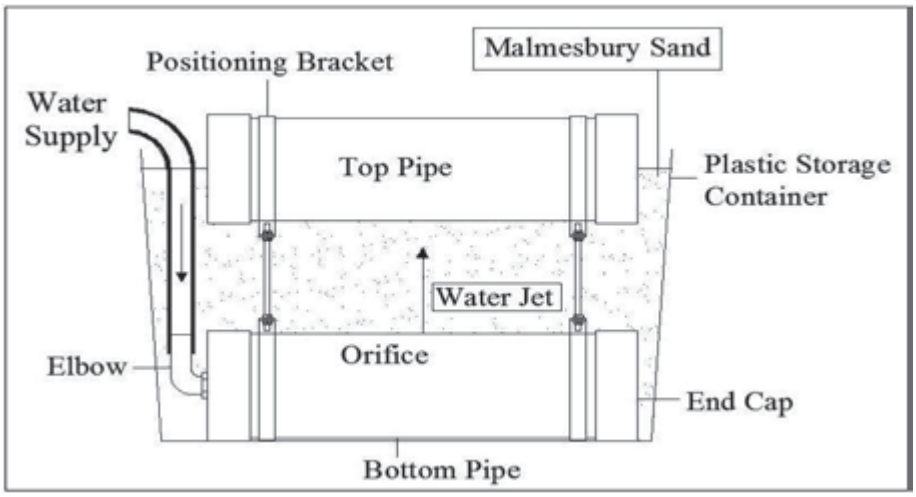

Figure 2-45: Experimental Setup of Malmesbury Sand and Alcab 16 Impact Tests (Pike, 2013)

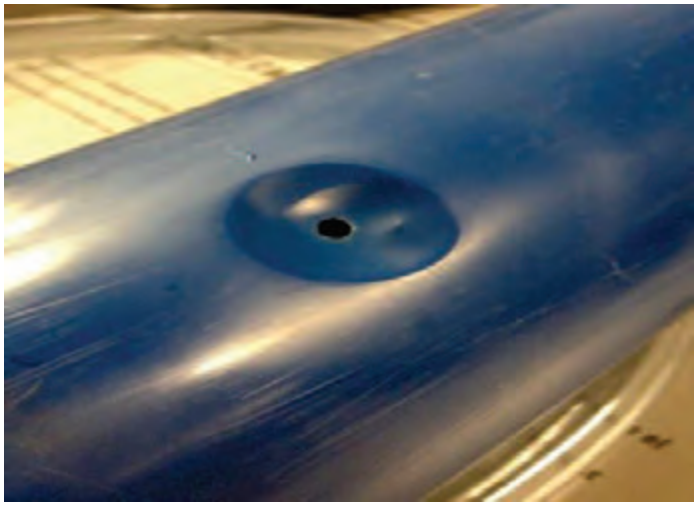

Figure 2-46:New orifice formed from direct Impact of buried leaking Pipe (Pike, 2013)

In this study, it was also observed that the abrasive action of a jet on a target pipe could erode through the pipe wall, creating a new orifice in the top pipe, as shown in Figure 2-46. Figure 2-47 also show the point in the process at which the new orifices on the top pipes were first observed during the testing period as well as their sizes. There are two data points for the Alcab 16 orifice diameter, since the test was continued after the new orifice was first observed, thus showing its growth. While Majid & Mohsin (2013) observed a rough and a smooth portion of the pipe surface, the surface condition in this experiment in the scour-affected zone was completely smooth and despite the granular slurry. It is suggested that the discrepancy between the observed surface conditions after abrasive action can be attributed to

the different pipe materials and coatings, since these materials may respond differently to abrasive action.

Pike (2013) also investigated the effects of leakage-induced pipe erosion where leaks in pipes cause damage to their own pipe surface. Laboratory experiments were performed to

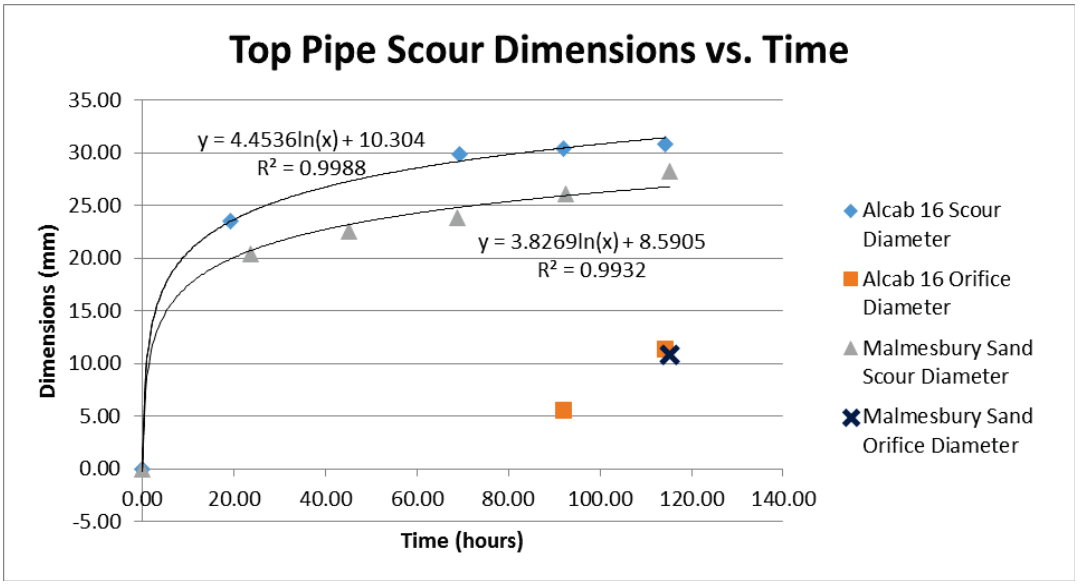

Figure 2-47: Progression of Scour Patterns for PVC Pipes in Fluidisation Zone (Pike 2013)

investigate this phenomenon in uPVC pipes. The experiments examined the effects of vertical leaks and inclined leaks from circular orifices. Three experiments were conducted to examine the erosive damage caused by vertically leaking jets on the leaking pipes themselves. The three tests were, as named by the author, the vertical leak test, the Alcab 16 impact test, and the Malmesbury sand impact test. The vertical leak test had an initial orifice diameter of 3mm, an average leakage flow rate of 250 litre/hour, and leaked into a 200mm deep Malmesbury sand bed. This test showed that the orifice on the external wall widened over time. The final orifice condition is shown in Figure 2-48. Figure 2-49 shows an approximation of the cross-section of the orifice at the end of the experiment. It was observed that the orifice widened on the external surface of the pipe, but the size of the orifice on the internal surface remained unchanged with a diameter of 3mm over the duration of the test, as indicated in Figure 2-49.

The bottom pipes in the Alcab 16 and the Malmesbury sand impact tests also leaked vertically into a granular bed, as shown in 2-45. These pipes exhibited similar scour patterns to that of the vertical leak test, as shown in the right hand image in Figure 2-50. The orifices, however, widened at a greater rate for the Alcab 16 and the Malmesbury sand impact tests than the vertical leak test due to greater flow rates, and different granular material in the case of the Alcab 16 impact test. None of the three vertically leaking tests were run for longer than 50 days. As shown in Figure 2-50, the laboratory created scour pattern (on the right) bears a similarity to that which was found on a portion of the failed pipe sample (on the left), despite the field specimen's longitudinal crack.

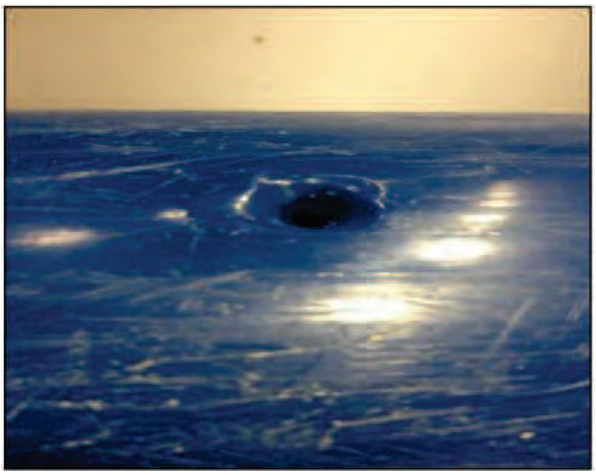

Figure 2-48: Orifice Condition of Vertical leak Test after 45.7 Days of Scouring(Pike, 2013)

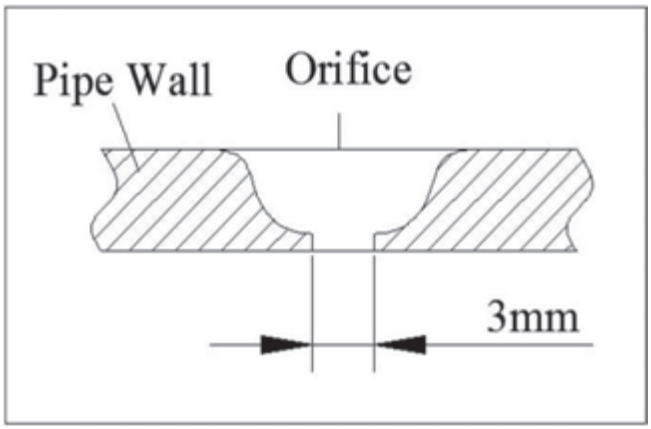

Figure 2-50: Approximate Shape of Vertical Leak Test Orifice Cross-Section after Scouring

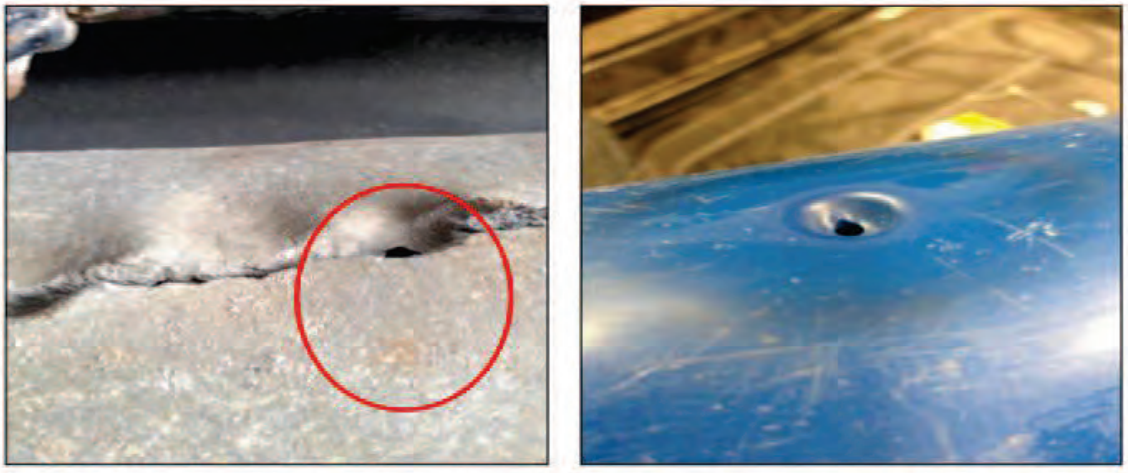

Figure 2-49: Comparison between Field Sample and Laboratory Experiment (Pike, 2013)

An inclined leak test was also performed, where a 3mm diameter orifice was orientated at a 45° angle to the horizontal. This test had a leakage flow rate of approximately 400 litres/hour, and leaked into ab 200mm deep bed of Alcab 16 sandblasting grit. This test yielded a more elongated scour pattern as shown below in Figure 2-51 (a). This orifice orientation affected a larger area than those with vertically leaking orientations. In this test,

the leak was aggravated to a point where a second orifice was formed as a result of the scouring, and can be seen in Figure 2-51 (b).

Furthermore, it was observed that the abrasion mechanism was not a result of the water jet pushing the sand along the pipe surface, but rather a result of the jet sucking sand into the jet. This was observed when the orifice was cleared of bedding material as the water jet broke through the bed's surface, but there was still granular material nearby. This observation was made at the moment of initiating the leakage while the orifice was exposed, but granular material was present in the near vicinity as depicted in the left hand image of Figure 2-52. The water was turned off, and granular material was piled up on either side of the orifice. When the water was turned on and the orifice began to leak, it could be observed that the granular material was drawn toward the orifice from the base of the pile, as indicated by the red arrows in the central image in Figure 2-52. This caused the particles to be dragged along the pipe surface before entering the water jet, after which they would be deposited on top of the pile of granular material, as shown in the right hand image in Figure 2-52. It was observed that particles were drawn toward the orifice from the left and the right (as seen in Figure 2-52), but the particles were being moved at a greater rate on the right hand side of the orifice. This soil movement bears a similarity to the soil motion described by Figure 2-32, where the ballotini in the immediate vicinity of the orifice was sucked horizontally toward the outlet.

For the Alcab 16 impact test, the Malmesbury sand Impact test, and the inclined leak test, it was found that the volume of pipe material was removed from the pipe surface approximately linearly with respect to time. This trend was observed regardless of whether the damage was caused by the leaking orifice or a result of an impact from a nearby leaking pipe.

Figure 2-51: Scour Patterns from Inclined Leak Test (Pike, 2013)

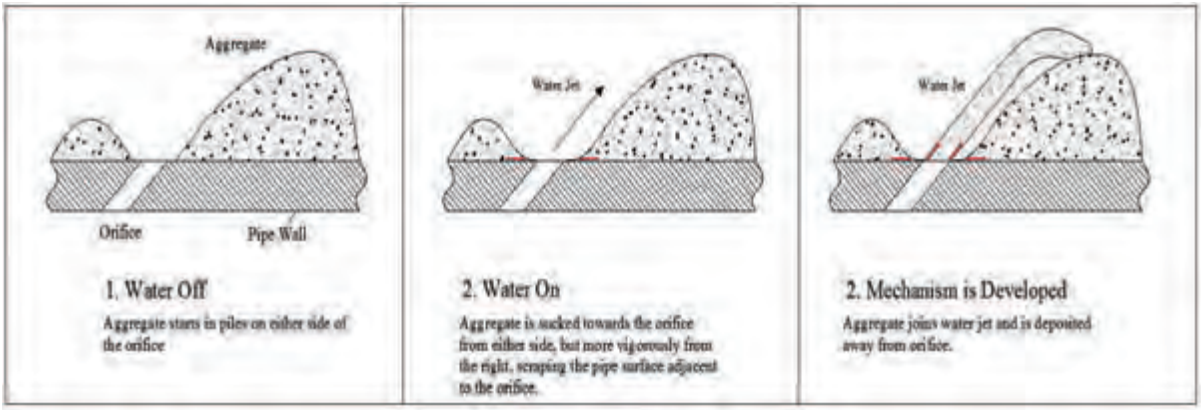

Figure 2-52: Inclined Leak Test Scour Mechanism (Pike, 2013)

2.9.6 Investigation of the Effects of Soil Material Grade and Flow Rate on the Scouring of PVC Water Distribution Pipes due to Soil Fluidisation (Negonga, 2013)

Negonga (2013) conducted a set of experiments investigating the effect of the leakage induced erosion where a simulated leaking saddle connection ejected a high velocity water jet horizontally along the pipe surface as shown in Figure 2-53. These experiments tested the effects of three different bedding materials and three different leakage flow rates. Figure 2-54 shows the scour pattern caused by this leak orientation, where the water would have been flowing from right to left on this figure. As it can be seen in Figure 2-54, the erosive action scoured through the entire pipe wall to create a second orifice, thus aggravating the initial leak condition. The straight edge that can be observed on the right hand side of the scour pattern in Figure 2-54 was caused by the saddle from which the pipe was leaking.

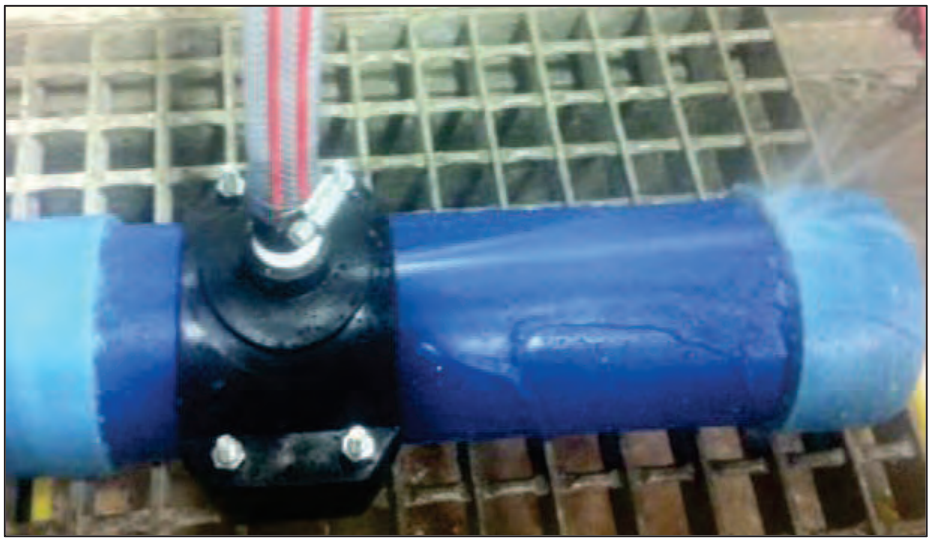

Figure 2-53: Induced Saddle Leak (Negonga, 2013)

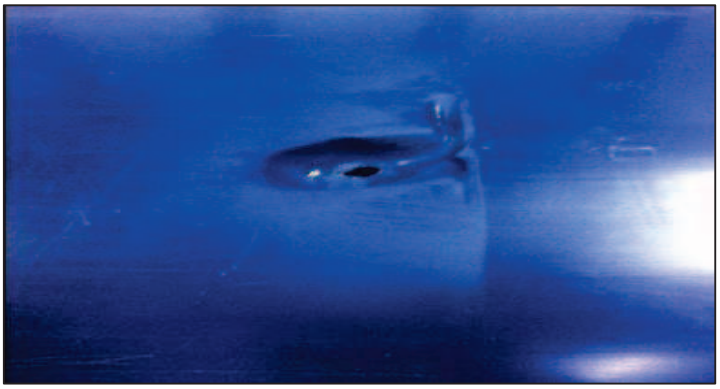

Figure 2-54: Pipe Condition adjacent to Saddle after Scouring (Negonga, 2013)

The key findings from this set of experiments were the following:

1. The rate of erosion increased with increasing sand particle size as illustrated in 2-5. For this experiment, the D_{60} values of the sands are recorded in Table 2-3.
2. The rate of scour was linearly proportional to the flow rate. To test this, the volume of removed material was measured for each test specimen after four days of exposure to the scouring process. Various tests were run with the same bedding material, but with differing flow rates, as shown in Figure 2-55.
3. Finally, it was concluded that the relationship between volume of pipe material removed and time was quadratic, and that the rate at which material was removed decreased over time (as illustrated in Figure 2-56). It would appear that the scouring is limited to a specific area of influence, and as more material was removed, the rate of removal decreased. The weakness of this model mathematically, however, is that if the function is extrapolated beyond the time period for which the tests were run, it would suggest that at some point in the future, removed material will begin to decrease i.e. pipe material will be added back to the pipe. Otherwise, if this quadratic model is to be validated, it could be proposed that once the trend line reaches its maximum value, material ceases to be removed.

Table 2-3: Bedding Material Grain Sizes (Negonga, 2013)

Material	D_{60} (mm)
Alcab F16	1.5
Filter Sand	0.95
Alcab F60	0.24

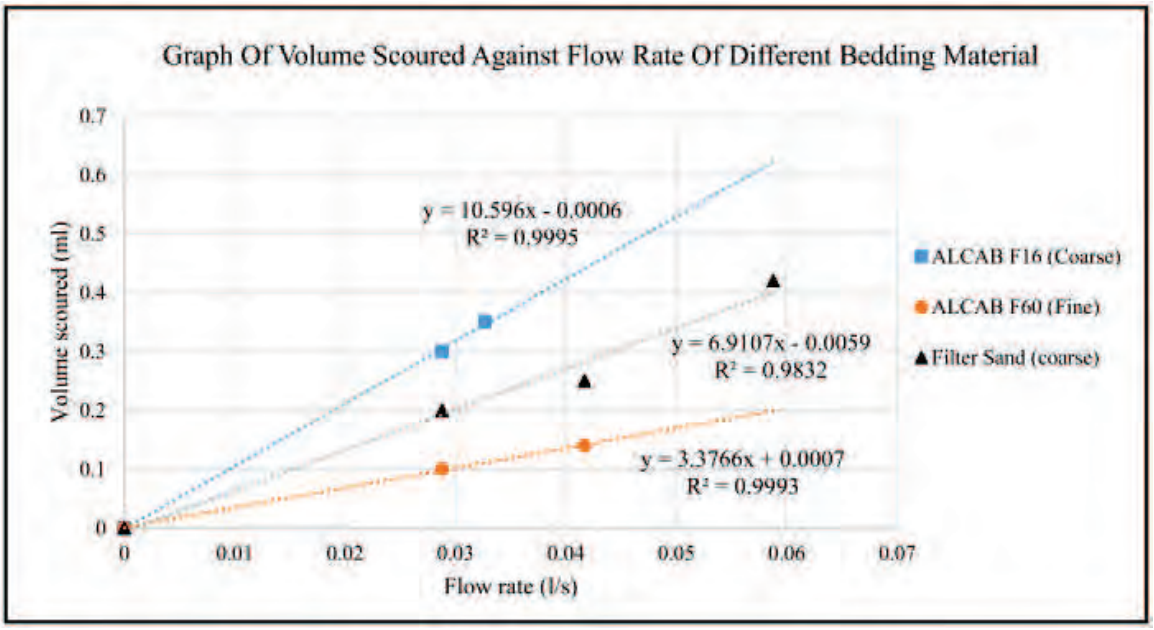

Figure 2-55: Effect of Flow Rate on Rate of Erosion (Negonga, 2013)

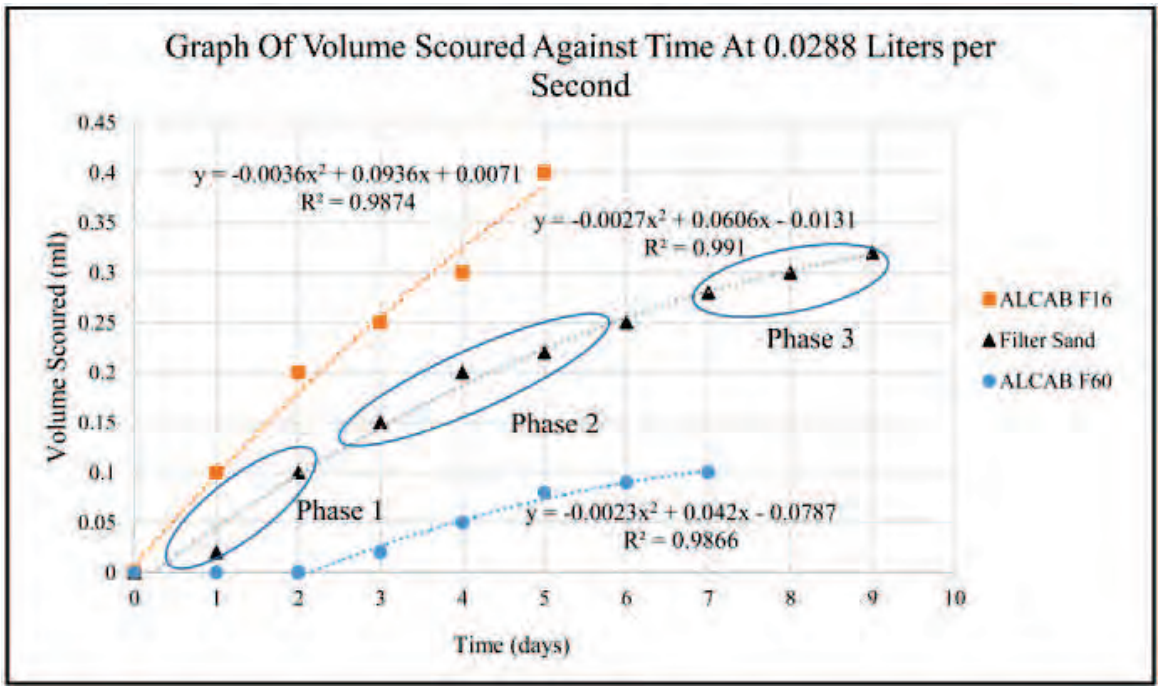

Figure 2-56: Comparison of Scour rates for different Particle Sizes (Negonga, 2013)

3. Methodology

3.1 Introduction

An experimental investigation was performed in order to examine the effects of various factors on leakage-induced pipe erosion. This chapter aims to provide a detailed description of the experimental setups and methodologies that were used to investigate this phenomenon. This chapter will begin by describing the general experimental setup and methods of data collection. Following this, there will be a brief section stating the experiments that were performed, after which there will be individual sections dedicated to each experiment. The sections for the individual experiments will include the finer details of each experiment, as well as a justification for each experiment based on the literature.

3.2 Experimental Setup

The experiments that were performed were intended to simulate realistic field conditions that would be conducive to the formation of the leakage-induced pipe erosion mechanism. The general experimental setup included a pressurised water supply that would deliver water to a pipe sample buried in a sand bed, as shown schematically in Figure 3-1. The buried pipe sample was closed on both sides with end caps, and had a manufactured leak on its upper-most surface. The leak would shoot a high velocity water jet into the surrounding sand medium, thus initiating the scouring process. Three setups of this nature were run simultaneously.

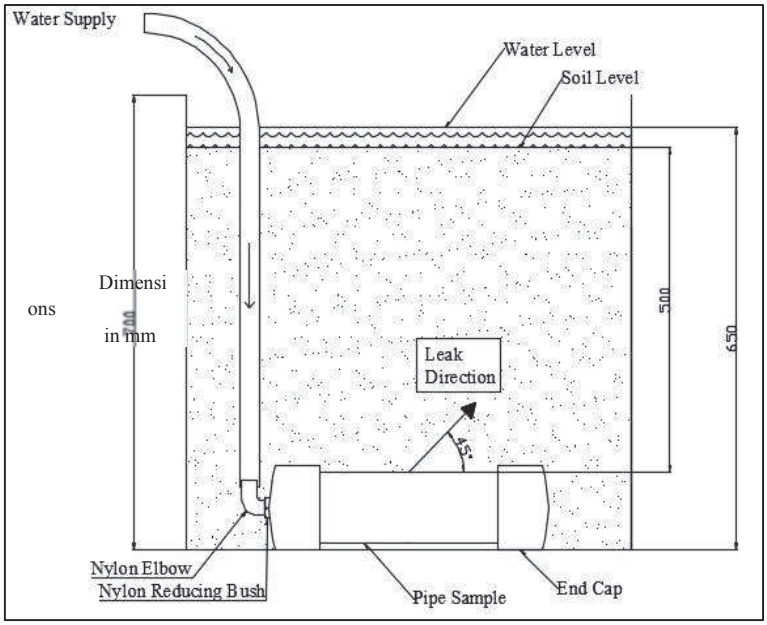

Figure 3-1: Schematic Representation of Buried Pipe Sample in Control Experiment

This set of experiments made use of the municipal water supply as shown in Figure 3-1 and 3-2. The pressure of this water supply fluctuated between approximately 5 and 6 bar. A reinforced hose, partially shown in Figures 3-2 and 3-3, conveyed the municipal water into a 110mm diameter uPVC pipe, which distributed the water between the three experiments that were run simultaneously, as shown in Figure 3-3. This large diameter pipe will hereinafter be referred to as “the delivery pipe”. The purpose of the delivery pipe was to provide an equal pressure between the three draw offs. As shown in Figure 3-4, the municipal pipeline was connected to a pressure-reducing valve (PRV), which then connected to the uPVC delivery pipe with a saddle. The pressure reducing valve on the delivery pipe served the purpose of stabilising pressure within the distribution pipe to eliminate pressure and flow rate fluctuations during the experiments. This PRV was set to 4 bar, which is below the minimum municipal pressure so that the pressure in the distribution pipe remained stable regardless of the external pressure fluctuations.

Figure 3-2: Municipal Water Supply

Figure 3-3: Delivery Pipe Feeding into Three Setups

The delivery pipe distributed water between the three setups as shown in Figure 3-3, and was connected to each setup as shown in Figure 3-5. A saddle connected the delivery pipe to an adjustable PRV equipped with a pressure gauge. The purpose of the PRV on each draw-off was to accurately adjust the flow rate into the pipe samples. The PRV was connected to a mechanical flow meter with a straight, rigid connecting pipe. The flow meter was used to set the flow rate to the desired flow rate for each experiment, and monitor the flow rate throughout each experiment. A shut off valve was then placed on the downstream side of the flow meter, followed by a detachable hose connector as shown in Figure 3-5. This hose connector was necessary for quick and easy disconnection of the pipe specimen, since the pipe sample was removed and inspected regularly.

A flexible reinforced hose connected the detachable hose connector to the pipe sample as shown below in Figures 3-5 and 3-6. The hose connected to a nylon elbow (shown in Figure 3-7). The elbow had an insert fitting to connect to the hose on one side, and a male

thread to connect to a nylon female to male reducing bush on the other. The end cap had a tapped hole, so that the bush could be screwed securely into the end cap. End caps were fitted to both ends of the pipe sample and secured in place with 16 bar rated PVC glue.

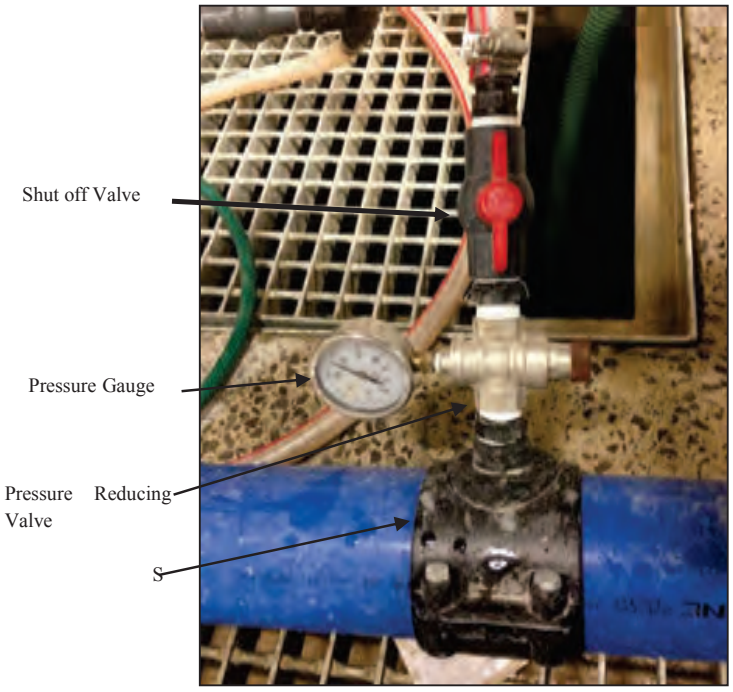

Figure 3-4: Municipal Pipeline connected to Delivery Pipe

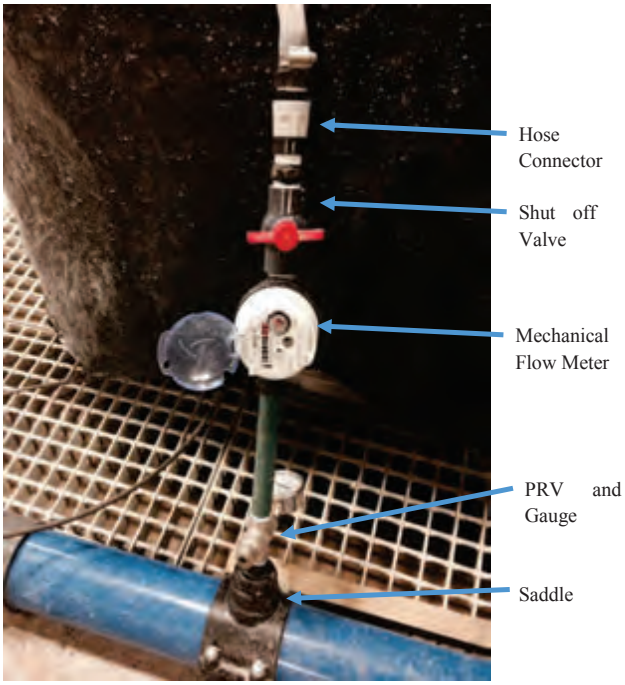

Figure 3-5: Delivery Pipe to Experiment Connection

As shown in Figure 3-6, the pipe sample was placed in a 700x700x700mm aluminium box. The purpose of this box was to contain the experiment, and to give the pipe a controlled environment in which to leak. These dimensions were selected so that the depth to width ratio of the soil bed could be kept to a maximum of 1:1. It was important not to exceed this ratio so that the side walls of the container did not reduce the soil load on the pipe. As stated by American Concrete Pipe Association (2011), the earth loads on pipes in narrow trenches is equal to the weight of the soil in the trench minus the vertical shear force between the backfill material and the trench walls. For pipes with diameter less than 750mm, it is said that that the trench width at which the shear forces on the trench wall need not be considered is approximately equal to the depth of the backfill (American Concrete Pipe Association, 2011).

Aluminium was selected for the box since this is a corrosion resistant material. Figure 3-6 also shows the pipe sample strapped down with rubber straps. These straps' primary purpose was to hold the pipe in place, and ensure that the leak remained on top of the pipe during the sand loading process. Lastly, Figure 3-6 shows that bricks were placed on the bottom of the container prior to sand loading. These bricks were used for the sole purpose of reducing the volume of sand required to fill the box. The height of the bricks when laid in this

manner was lower than the upper-most surface of the pipe so as not to interfere with the soil-leak interaction.

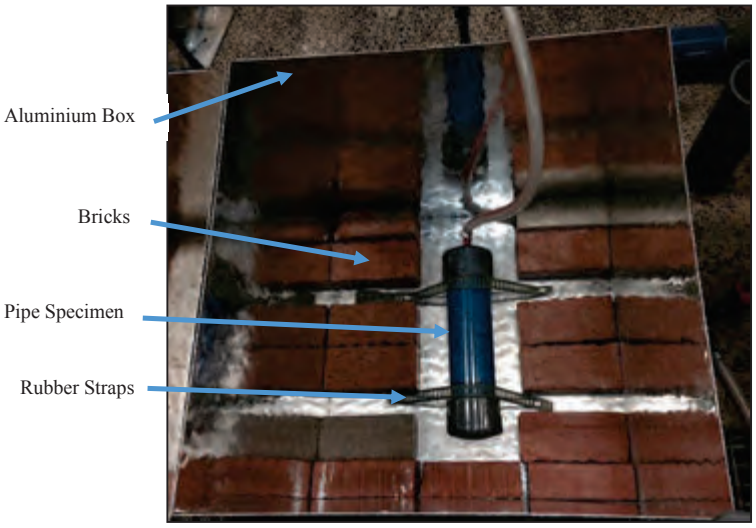

Figure 3-6: Pipe Sample fixed securely into Testing Box

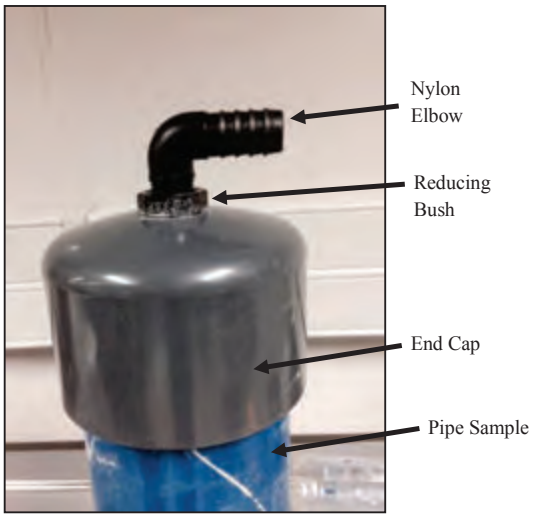

Figure 3-7: Water Supply to Pipe Sample Connection

A stainless steel supporting frame was manufactured for the aluminium box as shown in Figure 3-8. This frame served two functions; firstly, the frame prevented the boxes' walls from buckling under the loads of the sand and water when they were full. Secondly, the frame enabled the boxes to be lifted and tipped using a gantry, as shown in Figure 3-9. This tipping process was used for the excavation of the pipe samples since the pipe samples needed to be excavated and inspected regularly. Two holes were drilled into the frame, where a winching cable could be connected to the frame with D-shackles. The gantry could then lift the box with the winching cable, and tip the box over its tipping point, after which the sand would be caught in the lifting bag shown in Figure 3-10.

Once the pipe had been excavated and inspected, it would be placed back into the box and strapped into place. The pipe sample would be connected back to the delivery pipe, and the pipe sample would be filled with water before being re-buried. This step was necessary to ensure that no air would enter the system and disrupt the mechanism when the leaking process resumed.

Figure 3-10 shows a lifting bag filled with sand, being lifted by the gantry. Once the pipe had been placed back in its original position and filled with water, the sand would be lifted in this manner to re-bury the pipe sample. This lifting bag has a spout on the bottom which could be closed with a drawstring. The bag would be positioned directly above the box, and the spout would be opened, allowing the sand to be poured back into the box to bury the pipe.

A permanent mark was made on the inside of each box on all four walls at the required soil surface level for each experiment. When re-burying the pipe, the sand would be poured slowly from the lifting bag onto the pipe. Enough sand was poured into the box to exceed the height of the level markers. The box was then struck several times until the sand had settled down to the level of the aforementioned mark on the inside of the box. The striking of the box served to ensure a consistent degree of compaction of the soil bed after each inspection. The sand surface would then be levelled to the height of the aforementioned permanent mark with a hand trowel, and the box was then be filled with water until the sand bed was fully saturated. It was assumed that the same bulk density of the sand bed was achieved after each inspection since the same volume of sand that was emptied from the box was used to refill the box, after which the sand was levelled to the same height.

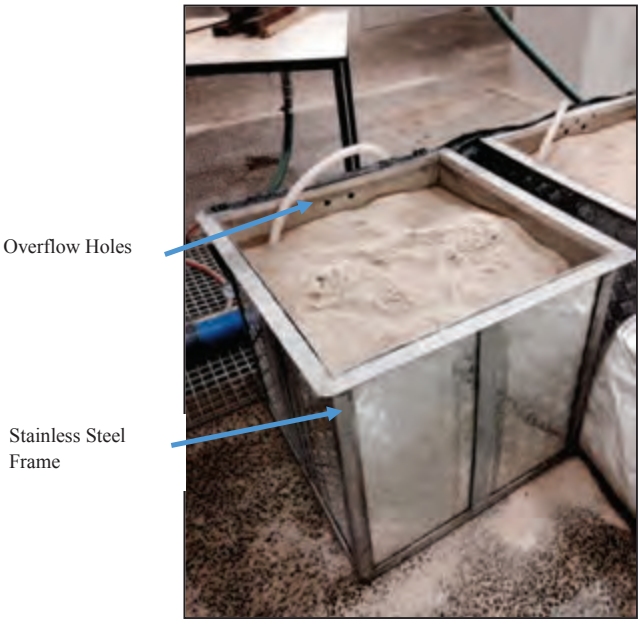

Figure 3-8: Stainless Steel Support Frame

Figure 3-9: Tipping the Box using a Gantry

Figure 3-10: Lifting Bag filled with Sand

3.3 Data Collection

3.3.1 Timing of Data Collection

In order to examine the effects of the leakage-induced erosion, the pipes were excavated and inspected at regular intervals. During the initial stages of each experiment, the pipes were inspected daily at 20 hour intervals. The time intervals were recorded with an accuracy of ±1 minute, for example, if the test, i.e. all three setups, was turned on at 12h45 on the first day, it would be turned off at 08h45 the following day. A timing error of 1 minute had a negligible effect on the analysis of the data. Running the experiments in 20 hour intervals allowed the experiments to run for the majority of each day, allowing four hours for excavation, inspection, and general equipment maintenance. Collecting data at these uniform intervals also allowed the different experiments to be compared after the same amount of exposure to the scouring process. Once the trends had been observed in the formation of the erosion patterns, the time intervals between excavations were increased so as to run the experiments for a greater portion of each day.

3.3.2 Measurements of Linear Dimensions

These experiments aimed to quantify the rate of formation of erosion patterns caused by leakage-induced erosion. Various linear dimensions were measured in order to best describe the progression of the scour patterns. For all of the experiments, the depth of the erosion into the pipe wall was measured using Vernier Callipers with an error of ±0.02mm as shown in Figure 3-11. This measurement is critical to the investigation, because once the erosion depth equalled the pipe wall thickness, the orifice size began to increase, thus exacerbating the initial leak. Furthermore, the thinning of the pipe wall could increase the likelihood of a burst, since the pipe wall will be locally weakened. It was unlikely that a burst would occur in the experiments performed in this study since the maximum pressures in the class 9 pipe specimens was 5 bar.

To measure the scour depth, the depth gauge on the Vernier Callipers was inserted into the eroded indentation, while the bottom end of the main scale was aligned with a straight-edged ruler indicating the original pipe surface, as demonstrated in Figure 3-11. This method of measurement was subject to random observational errors due to the orientation and alignment of the Vernier Callipers. It was found that when measurements were repeated using this method, the difference between the maximum and minimum measurements was less than 0.06mm.

The length and width of the erosion pattern in the horizontal plane were measured with Vernier Callipers as shown in Figure 3-12 below. While these dimensions are less critical in predicting further pipe failure, they give a good description of the scour-affected region of the pipe surface. For each experiment, with the exception of those experiments where the leak orientation was vertical, the long dimension of the scour pattern (in the longitudinal direction of the pipe) will hereinafter be termed “Dimension A,” while the shorter dimension (in the transverse direction) will hereinafter be termed “Dimension B,” as shown in Figures 3-12(a)

and 3-12(b) respectively. As it will later be discussed, vertically orientated leaks from round holes form circular scour patterns, and hence only the scour diameter was measured. Since the scour patterns formed smooth, polished surfaces, there were no clear-cut edges to the patterns. This made it difficult to measure Dimensions A and B accurately. Dimensions A and B were measured from the visually apparent edges of the indentation. It is suggested that these measurements give an estimation of the size of the scour-affected region rather than an exact size due to potential error in the visual determination of the scour patterns' edges.

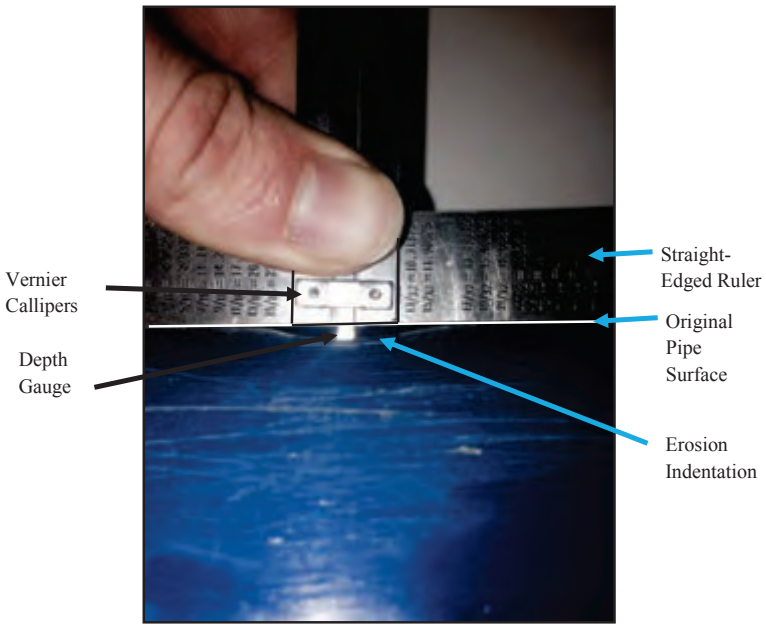

Figure 3-11: Measurement of Depth of Erosion into Pipe Wall

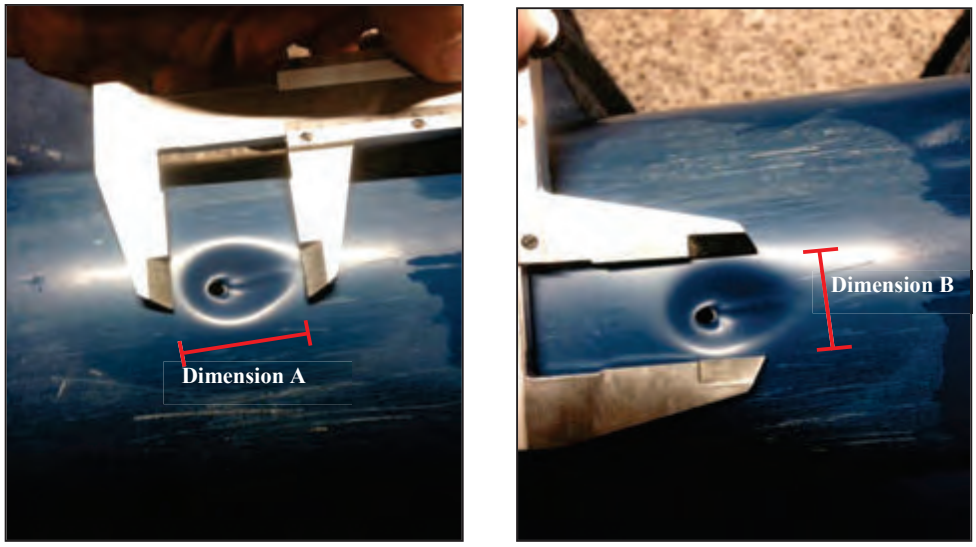

Figure 3-12: Measurement of Scour Patterns' Linear Dimensions

3.3.3 Volumetric Measurements

The volume of the material that was removed from pipe surface was measured at each inspection. This measurement gives an indication of the severity of the erosion. In order to measure the volume of the removed material, multi-purpose glazing putty was inserting into the void. As shown in Figure 3-13, the excess putty would be smoothed off using a modified end cap. The end cap had its circular surface removed so that it could slide along the length of the pipe sample, and had an arc of the cylindrical wall removed, as shown in Figure 3-13, so that it could slip onto the pipe. The modified end cap fitted snugly around the pipe, which, when dragged over the void, compressed the putty into the void, and allowed the top surface of the putty to take on the original pipe surface's profile, as shown in Figure 3-14. It was assumed that the putty's density did not change during this process, since the excess putty was forced through the orifice, therefore the putty could not withstand any excess pressure.

It was assumed that the putty took on the exact shape of the void below its upper-most surface, even though the putty deformed as it was removed. It can also be observed in Figure 3-14 that there are longitudinal scratches on the pipe's surface. These scratches are visible on pipe samples from several tests. It should be noted that these scratches are a result of this volumetric measurement process, and not a result of the leakage-induced pipe erosion process. These scratches are created when sand particles are caught under the modified end cap during this measurement process, and are scraped along the pipe surface.

Figure 3-13: Modified End Cap for Smoothing the Putty

Figure 3-14: Putty Taking on the Original Pipe Profile

Once the putty had been smoothed to fit the void, it was removed and weighed on a Mettler Toledo PB303-S digital analytical balance which was accurate to 0.001 grams. As shown in Appendix C, a repeatability analysis was performed to determine the accuracy of this method of measurement. A medium sized void (in the context of this study) was selected for this repeatability analysis. This analysis showed that for 10 measurements on the same void, the range of putty masses (the difference between the maximum and minimum

measured masses) was 0.037g which represented 4.9% of the mean (mean= 0.754g), and that the standard deviation for this sample was 0.012g.

Using the putty's specific gravity of S = 2.07 (calculated in Appendix B) the volume of the putty, i.e. the volume of the removed pipe material could be calculated by the following equation:

$$V_V = \frac{m}{S \cdot \rho_w} \tag{3.1}$$

Where V_V = Volume of Void; m = Mass of Putty; S = Specific Gravity; ρ_w = Water Density

3.3.4 Reported Measurements

Upon the analysis of the data, it was observed that there were correlations between the measured dimensions, i.e. Dimension A, Dimension B, scour depth and scour volume. As shown in Figure 3-15, the scour volume was linearly proportional to the scour depth. Figure 3-15 shows the scour depth plotted against the scour volume for seven selected experiments. Since there was a proportional difference between scour volume and scour depth, the graphs of the time-dependent progressions for each of these measurements were similar in shape for each experiment. For this reason, it was deemed unnecessary to report both the scour volume and scour depth findings in the results chapter. The Dimensions A and B had similar linear relationships to the scour depth. For this reason, all four of the measured dimensions will be discussed in the results section of Experiment 1 (Section) only to illustrate the measured dimensions. Following Experiment 1, only the progression of the scour volume will be reported and discussed for the subsequent experiments. The numerical and graphical representations of the developments of Dimension A, Dimension B and scour depth over time can be found in Appendix A.

The regression analysis carried out in the results is primarily for descriptive purposes. The trend lines fitted to the data are intended to give a sense of rate of growth of the dimensions.

3.4 Experimental Design

The nature of the leakage-induced pipe erosion mechanism is highly complex. There are a large number of factors that can play a role in both the formation of the scour pattern, and the rate of the erosion's progress. Based on the literature, it was decided to test five factors that were hypothesised to be the most influential on the rate of erosion. The following five factors were investigated:

- Sand grain size
- Flow rate

- Depth of soil cover
- Pipe material
- Initial leak orientation

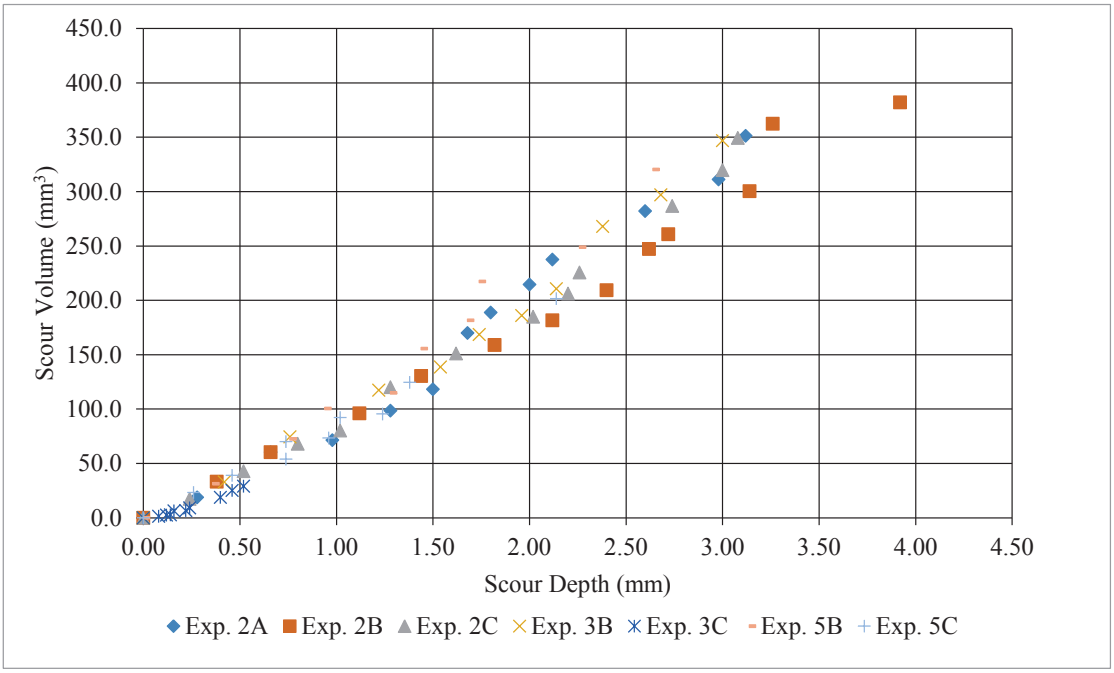

Figure 3-15: Relationship between Scour Depth and Scour Volume

These factors were selected for one of two reasons; firstly, based on the literature, it was suggested that they were either the most critical factors that affect the rate of erosion. Gent et al. (2012) reported that the particle grain size had a significant effect on the rate of erosion in the cate of abrasive water jet cutting. Van Zyl et al. (2013) stated that the leakage flow rate had the most significant effect on the formation of the fluidised zone. Pike (2013) and Negonga (2013) found that the initial leak orientation changed the shape of the scour pattern and rate of the material removal.

The second reason that the remaining factors were chosen, i.e. depth of soil cover and pipe material, was they are parameters that can easily be controlled when installing a water distribution pipeline. A full justification for the choice to test each of these parameters will be provided in Sections 3.5.1-3.5.6, which describes each experiment in detail.

Factors that were not examined in this investigation included the following:

- Soil particle hardness
- Soil particle angularity

- Soil particle density
- Soil bulk density
- Initial orifice size
- Initial leak shape
- Soil bed hydraulic conductivity
- Pipe class
- Temperature

3.4.1 Control Experiment

A control experiment has been designed against which all other parameter variations can be compared. The standard experiment was run under the conditions described in Table 3-1. In order to test the effects of each of the previously listed influencing factors, three tests were performed for each influencing factor. In each experiment, the influencing factor was varied to a different degree in each of the three tests. The operating conditions for the control experiment were selected to be the median flow rate, grain size and angle of leak orientation that were used for the tests to test those parameters. The 45° leak orientation was selected specifically because the literature suggests that this orientation is most likely to cause orifice enlargement (Pike, 2013). The maximum cover depth that the box would allow, 500mm, was selected so as to ensure that the fluidisation zone would not break through the soil's surface for the test where the initial leak orientation was positioned vertically upwards.

Table 3-1: Control Experiment Parameters

Flow Rate (l/h)	Grain Size (D_{50}) (mm)	Cover Depth (mm)	Pipe Material -	Leak Orientation (°)	Orifice Diameter (mm)
400	1.6	500	uPVC	45	3

As it was discussed in the literature, leaks present themselves in various forms. This study will focus on small leaks from round orifices. This orifice type has been selected because in order to formulate theory on a topic as complex as leakage-induced erosion, it is necessary to start off with the simplest possible case. Furthermore, small leaks are the most likely leak types to experience the effects of leakage-induced erosion since they are difficult to detect, and therefore they are exposed to the erosion mechanisms for long durations. Furthermore, it was found by van Zyl et al. (2013) that the size and shape of the orifice has a

negligible effect on the fluidisation mechanism for small leaks, while the leakage flow rate has a significant influence.

uPVC was selected for the control experiment since it is known that this material is susceptible to this erosion mechanism, as it has been shown in the literature (Negonga, 2013; Pike, 2013). Furthermore, it is a commonly used pipe material in modern water distribution systems.

3.4.2 Experimental Planning

Three experiments were run simultaneously to examine the effect of each of the factors listed in Section 3.4 above. Table 3-2 below describes the experiments that were carried out. In each experiment, one parameter was varied from the control experiment. The control experiment in each set has been highlighted with bold text in Table 3-2. As it can be seen in the first column of Table 3-2, the experiments have been assigned set numbers. Each set of experiments is a group of experiments designed to investigate the effect of a particular parameter on the erosion, i.e. the parameter in column number 2 of Table 3-2. Each set of experiments will be run simultaneously.

In the first row of Table 3-2, it can be seen that the experiments have been assigned an identification, either A, B or C. This identification will serve the purpose of a quick referencing system to refer to individual experiments for the remainder of this study, for example, when subsequently referring the experiment in which standard conditions were used with the exception of the flow rate which was 200 l/h, this experiment can be referred to as Experiment 3C.

Table 3-2: Details of the Experiments Performed

	Experiment ID	**A**	**B (Control)**	**C**
Set	**Varied Parameter**			
1	Grain Size – D_{50} (mm)	2.1	**1.6**	0.75
2	Cover Depth (mm)	400	**500**	300
3	Flow Rate (l/h)	600	**400**	200
4	Leak Angle (°)	0	**45**	90
5	Pipe Material	Steel	**uPVC**	HDPE

The values in Table 3-2 that have been highlighted in bold text in column B represent the standard test conditions. The standard test with the conditions described in Table 3-1 was performed with each set of tests. This was necessary to demonstrate repeatability in the testing procedure.

Columns A and C are the parameters that have been varied for each experiment. It can be assumed that the standard conditions were used in each experiment, with the exception of the parameter that is indicated for each individual experiment unless otherwise stated, as is the case with the pilot experiment.

3.5 Individual Experiments

3.5.1 Pilot Experiment and Shape of Suspended Zone

A pilot experiment was performed with the primary intention of testing the functionality of the apparatus. This set of experiments did not run under the standard conditions that were described in Table 3-1, but rather under the conditions described in Table 3-3 below. This set of experiments differed fundamentally from the standard test conditions in terms of the leak orientation. For all three tests in the pilot experiment, the initial leak condition was vertically upwards (90°). The flow rate was also slightly lower than that of the control experiment. The parameter that differed between the three tests in the pilot experiment was grain size, as described by Table 3-4. As shown in Table 3-4, it should be noted that the pilot experiment is denoted as Experiment 6, and shall hereinafter be referred to as such.

To inspect the pipe samples for the duration of the pilot experiment, the boxes were drained with a hose pipe siphon and the pipe samples were excavated manually with a shovel, as opposed to tipping the containers with the gantry as described in Section 3.2.

Table 3-3: General Parameters of Pilot Experiment

Average Flow Rate (l/h)	Grain Size (D_{50}) (mm)	Cover Depth (mm)	Pipe Material -	Leak Orientation (°)	Orifice Diameter (mm)
370	Varied	500	uPVC	90	3

Table 3-4: Description of the three Tests Conducted in the Pilot Experiment

Set	Experiment ID	A	B	C
6	Grain Size – D_{50} (mm)	2.10	1.60	0.75

The three sand types that were used for the pilot experiment differed only in median grain diameter size, D_{50}, but not in composition. These were the same three sands used in Experiment 1. The three sands used for this experiment were silica sands, originating from the Consol Industrial Mineral mine in Philippi, Western Cape, South Africa (Consol, 2014). This mine excavates natural silica deposits from a depth of up to 20m below ground level. All three sands were silica sands, the chemical compositions of which can be found in Appendix B. These sands were selected so as to maintain approximately the same particle density, Bond Work Index, hardness and angularity across the three experiments. This type of sand is also a relatively hard material, thus giving the experiments the best possible chance of initiating the scouring process.

Figure 3-16 shows magnified images of samples of each of the three sands. Figures 3-16 (a), (b), and (c) correspond to the sands with D_{50} = 2.10mm, 1.6mm and 0.75mm respectively. It can be seen that the sands in Figures 3-16 (a) and (b) are made up of a combination of both angular and smoothed particles, while it appears that the sand in Figure 3-16 (c) is comprised predominantly of smoothed, more rounded particles.

Figures 3-17 (a) and (b) shows microscopic images of the angular particles found in samples of the sands with D_{50} = 2.10mm and 1.6mm respectively. These images were taken using a scanning electron microscope. It can be seen that these particles have sharp corners and edges, as well as microscopic roughness on their surfaces.

Figures 3-18 (a), (b) and (c) show examples of the rounded, smoothed particles found in the sands with D_{50} = 2.10mm, 1.6mm and 0.75mm respectively. Although these particles have rounded edges, it can be observed that there are microscopic roughnesses on the particles' surfaces.

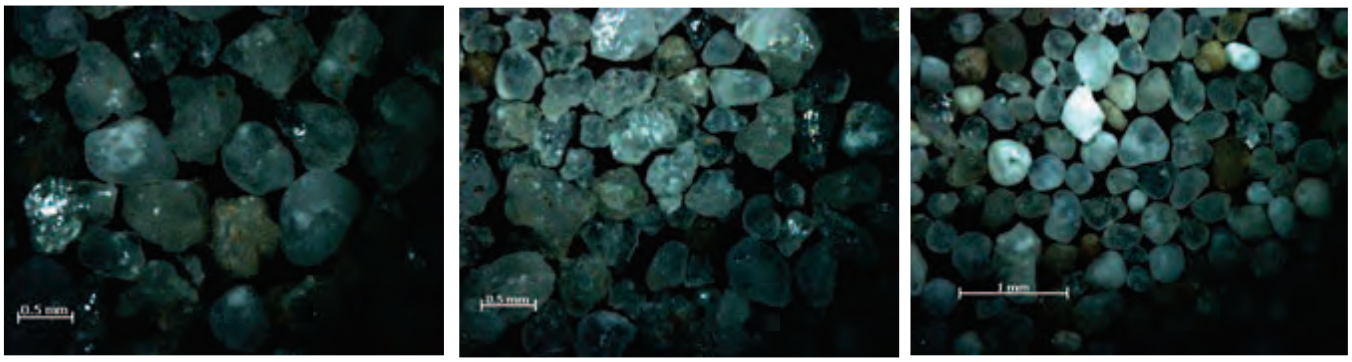

Figure 3-16: Different Sands used for Experiments

The physical properties of these three sands can be found in Table 3-5, and the methods of determining these properties are described in detail in Appendix B. The D_{50}, D_{60} and D_{10} were determined from the standard sieve analysis test. Figure 3-19 below shows the grading curve from the sieve analysis for each of the three sand types. Figure 3-19 also illustrates the D_{50} for each sand type with the dashed black lines.

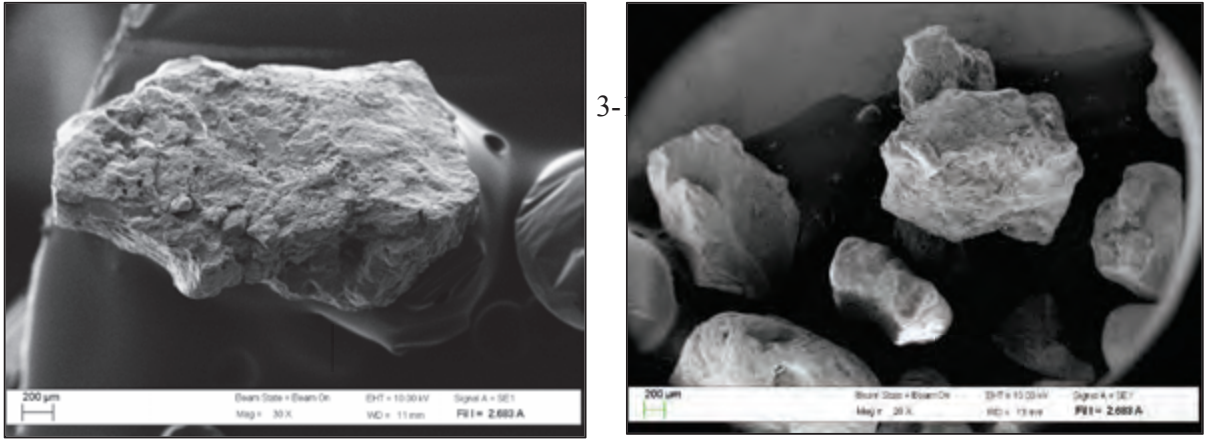

Figure 3-17: Microscopic Image of Angular Particles

The particle density was determined using the Small Pyknometer Method, as described in BS 1377-2 (British Standards Institution, 1990). The calculations for this test are shown in Appendix B.

The particle form factor given in Table 3-5 is the Scalene Ellipsoid Equivalent Sphericity (SEES), a form factor developed to differentiate between platy and bulky particles (Clayton, Abbireddy & Schiebel, 2009). This factor describes the sphericity of the particle, where an SEES of 1 represents a perfectly spherical particle, and smaller values represent lesser degrees of sphericity. The calculations for the SEES can be found in Appendix B.

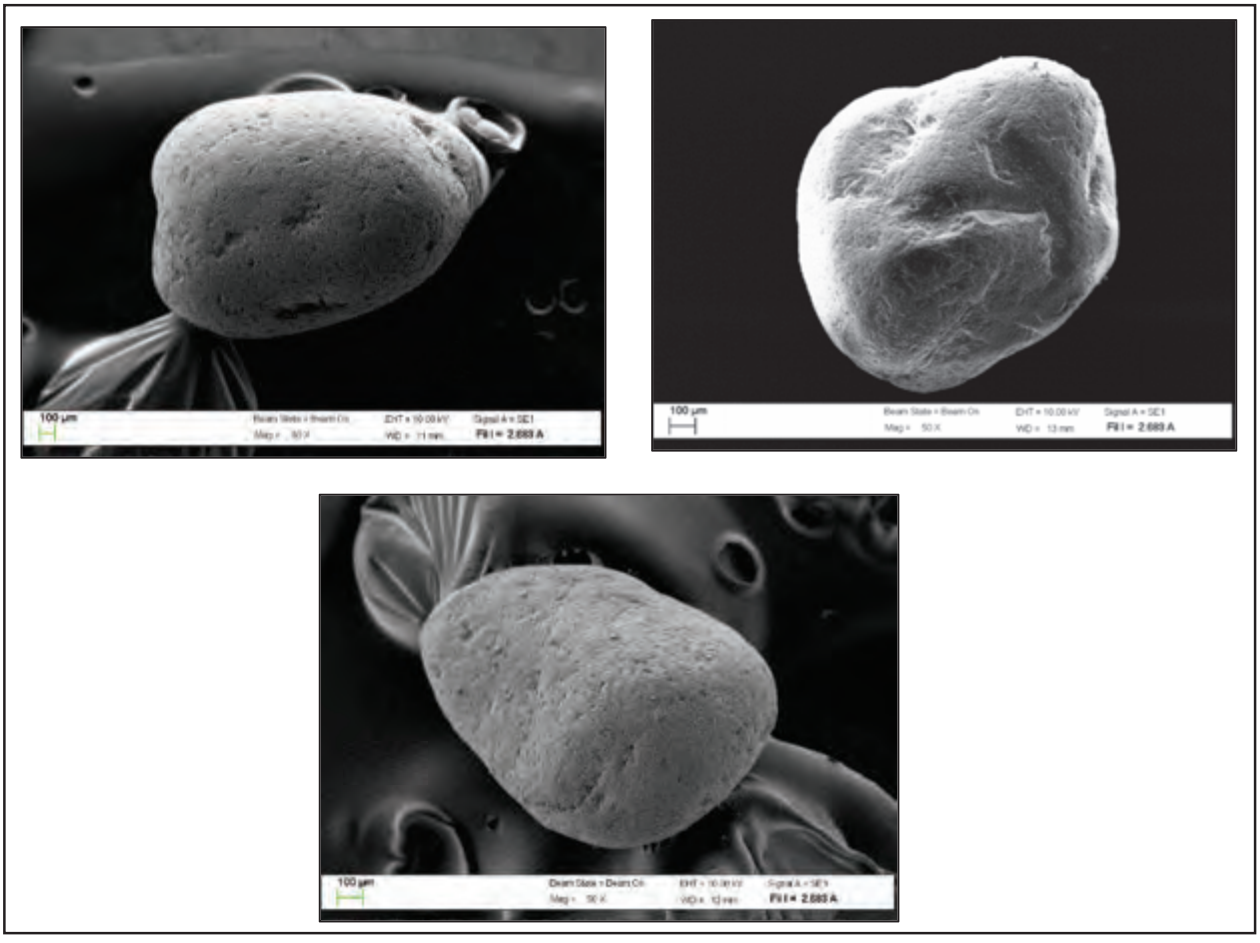

Figure 3-18: Microscopic Images of Rounded Particles

The dry maximum dry bulk density, minimum void ratio and minimum porosity were determined using *Method A* as described in ASTM International D4254 : 2015, the calculations of which can be found in Appendix B.

The permeability of the soils was determined using the Constant Head Method. The test was carried out in accordance with ASTM International-D2434 : 2006, the calculations of which can be found in Appendix B.

Table 3-5: Properties of Sands used in Pilot Experiment

Sand Property	Units	Sand 1	Sand 2	Sand 3
D_{50}	mm	2.1	1.6	0.75
Particle Density	kg/m^3	2690	2661	2690
Coefficient of Uniformity (D_{60}/D_{10})	-	1.77	1.62	1.48
Maximum Dry Bulk Density	kg/m^3	1580	1643	1790
SEES Form Factor	-	0.57	0.49	0.56
Minimum Void Ratio	-	0.70	0.62	0.50
Minimum porosity	%	41.25	38.26	33.46
Permeability	cm/s	1.75	0.44	0.16

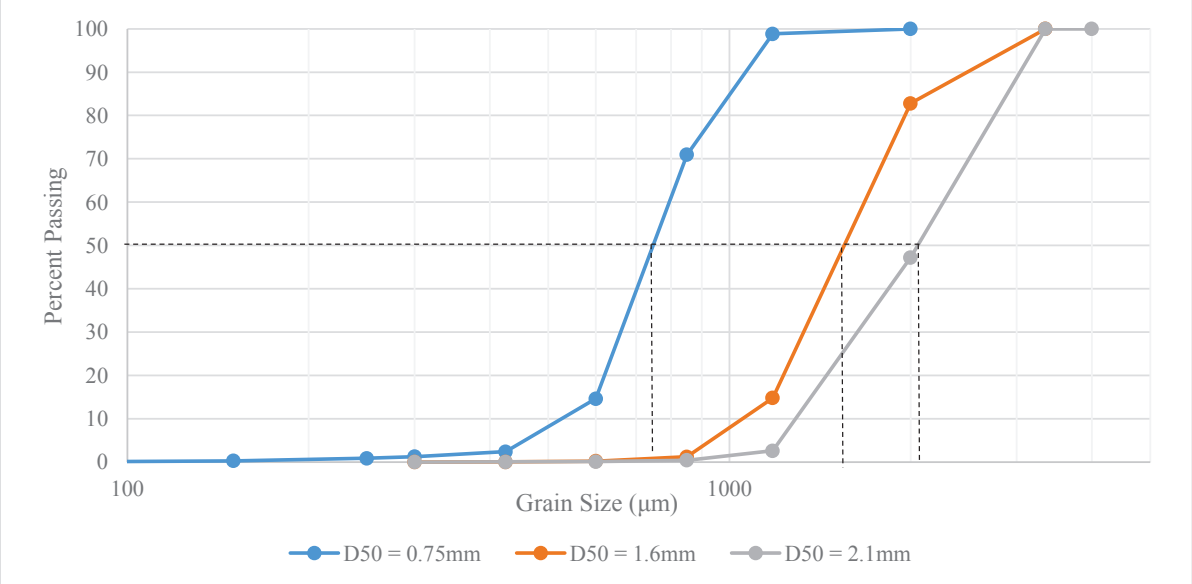

Figure 3-19: Sieve Analysis of Sands used in Pilot Experiment

3.5.1.1 Development of Mobile Bed Zone

In addition to the measured parameters discussed in Section 3.3 (linear and volumetric measurements), it was observed during the excavation process that a region of sand directly above the orifice had been discoloured during the run of the test. Upon further investigation, it was discovered that a horizontal cross section through this region presented an almost perfectly circular zone of discoloured sand as shown below in Figure 3-20. It was assumed that this discoloured zone represented the mobile bed zone of the fluidisation mechanism. It is assumed that the turbulent motion of the soil particles removed the darker dust-like particles from the coarser grains, leaving behind only the pale, silica crystals.

Based on this this discovery, a three dimensional image of the mobile bed zone could be constructed by measuring the diameter of the discoloured cross-section and plotting it against its height above the orifice.

In order to perform these measurements, the soil first needed to be drained so that the soil was dry enough to hold itself firmly in place while excavating carefully around it. The soil was drained by placing a hose pipe into the container prior to filling the container with soil. One end of hose pipe had filter cloth covering its opening, and this end was placed at the bottom of the container. The other end was placed outside of the container so that the water in the soil could be siphoned out.

The diameter of these circular cross sections was measured at a number of different heights. As shown in Figure 3-21, the discoloured region had a very definitive outline rather than a gradual change in colour. To measure the heights, a straight bar was placed on the edges of the container such that the bar passed over the discoloured zone as shown in Figure 3-22. The bottom edge of this bar gave the level of the top of the container. The distance between the bottom of this bar and the level of the discoloured zone was then measured. A layer of soil would then be scraped away, and the process would be repeated to get another height and corresponding diameter. The height of each diameter above the orifice could then be calculated by subtracting the measured distance and the pipe diameter from the box height.

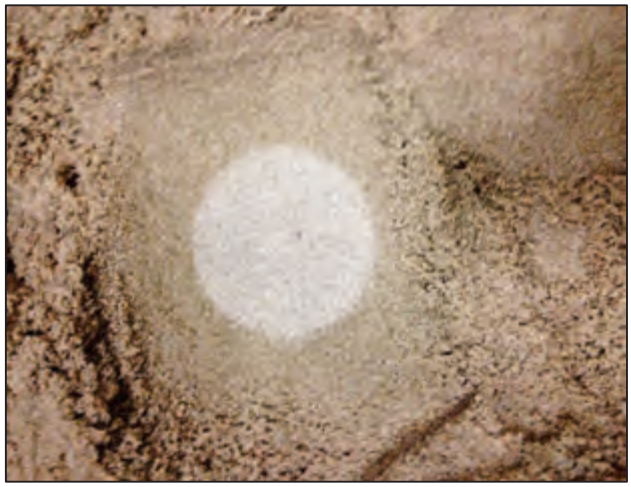

Figure 3-20: Discoloured Zone Vertically above Orifice

Figure 3-21: Close up view of Discoloured Region

Figure 3-22: Measurement of Height above Orifice to Circular Discoloured Cross Section

3.5.2 Experiment 1: Effect of Soil Particle Size

The main aim of Experiment 1 was to investigate the effect of particle size on the rate of leakage-induced erosion. It was decided that this was an important factor to investigate since the literature suggests that erosion increases with increasing abrasive particle size for a range of applications (Briaud et al., 2001; Gentet al., 2012; Negonga, 2013).

There are a number of factors that influenced the choice of granular material in which the pipes were buried. Firstly, as discussed in Section 2.5, SABS (1983) states that pipes in distribution systems should be laid in singularly graded, free draining granular material graded between 0.6mm and 19mm. In order to replicate realistic conditions, three granular media fitting this description were selected.

As discussed in Section 2.6.5, both Briaud et al. (1999) and Gent et al. (2012) explain that the rate of erosion is a function of the abrasive material's particle size. Briaud et al. (1999) suggests that for sands in free flowing water, the rate of erosion on soil beds increased linearly with increasing particle size. While Gent et al. (2012) studied the effect of particle size in abrasive water jet cutting, somewhat different circumstances to those of Briaud et al.'s study, Gent et al. found that the rate of erosion increased logarithmically with increasing particle size. From the literature, it is evident that particle size has an influence on erosion rates. For this reason, it was decided that the effect of particle size on the rate of erosion in the context of this study would be investigated. It was decided to test three different particle sizes of the same type of sand, so that factors such as particle density, hardness, angularity and Bond Work Index remained approximately constant over the three setups. The three sand types that were used for this set of experiments were the same as those used for the Pilot experiment, the physical properties of which can be found in Table 3-5 above.

In this experiment, the soil particle size was varied in Experiments A and C.

The experiment was deemed complete once the fastest eroding sample had locally removed enough pipe material to erode completely through the pipe wall. At this point, the orifice size would begin to increase, thus exacerbating the initial leak.

3.5.3 Experiment 2: Effect of Soil Cover

The aim of Experiment 2 was to investigate the effect that the depth of soil cover has on the rate of leakage-induced pipe erosion. This factor was selected since it is a parameter that can be relatively easily controlled by contractors when installing new pipelines. It was also stated in the literature that greater water pressures and flow rates are required to initiate fluidisation in deeper soil beds, as described by Figure 2-29 (Alsaydalani & Clayton, 2014). Since the soil bed depth influences the flow rate at which fluidisation is initiated, it is speculated that the depth of the soil bed also influences the geometry of the fluidisation zone. If the bed depth affects the geometry of the zone, it may also affect fluid velocities, pressures, and energy dissipation. If the soil bed height affects the fluid velocities in the vicinity of the orifice, then the bed height has the potential to affect the rate of the erosion.

In this experiment, the depth of soil cover was varied in Experiments A and C.

3.5.4 Experiment 3: Effect of Flow Rate

The aim of Experiment 3 was to investigate the effect of leakage flow rate on the rate of leakage-induced erosion. This factor was selected for investigation since it is known from the literature that leakage flow rate increases the size (height and volume) of the fluidisation zone. It is also known that an increase in the leakage flow rate increases the velocity of the particles within the fluidisation zone (van Zyl et al., 2013; Alsaydalani & Clayton, 2014). Furthermore, it should be noted that increasing particle velocities and leakage flow rates increase the rate of erosion in various applications (Goddard, 1994; Negonga, 2013). Negonga (2013) demonstrated that for the case where a water jet was leaking parallel to the pipe surface from a leaking saddle connection, that the rate of erosion increased linearly with increasing leakage flow rate, as illustrated by Figure 2-56.

Furthermore, it is important to investigate the effect of leakage flow rate on the rate of erosion so as to highlight the importance of pressure management schemes in this context. Pressure management schemes reduce leakage flow rates, and hence have the potential to mitigate the effects of leakage-induced pipe erosion.

In this experiment, the leakage flow rate was varied in Experiments A and C.

3.5.5 Experiment 4: Effect of Leak Orientation

The aim of Experiment 4 was to determine the effect of leak orientation on the rate of leak-induced erosion. In the case of leakage-induced pipe erosion, the literature suggests that the orientation of a leak affects the scour pattern that forms around the orifice (Negonga, 2013; Pike, 2013). The orientation of the leak influences the motion of the sand particles, and

hence, different leak orientations form different scour patterns, and can change the rate of erosion. It was found in the literature that inclined and horizontal leaks (parallel to the pipe surface) have the ability to erode through the entire thickness of the pipe wall, however, it has not been demonstrated that a vertical leak (perpendicular to the pipe surface) can erode through the entire pipe wall (Negonga, 2013; Pike, 2013). The leak orientation was selected for investigation since it is clearly an influential factor in the development of leakage-induced pipe erosion.

The horizontal leak was selected to simulate a leaking saddle connection. Figure 3-23 shows how the saddle was modified in such a way that the size, shape and orientation of the leak could be controlled. Figure 3-23 shows that a circular slot was drilled into the wall of the saddle, into which a 3mm (inside diameter) stainless steel tube was fitted. The slot pierced the rubber O-ring so that the tube extended into the water's entry point in the saddle connection. The tube allowed water to leak from the saddle connection to the external pipe surface, as shown in Figure 3-23. Figure 3-24 shows how the leaking saddle emitted a circular jet across the pipe's surface.

Figure 3-23: Saddle Modification

Figure 3-24: Leaking Saddle with Horizontal Circular Jet

An additional test was conducted during this experiment, which was named Experiment 4A (ii). Experiment 4A (ii) was an adjusted version of Experiment 4A, where the flow rate was reduced to 200 l/h. As it will later be explained, this test was conducted because Experiment 4A eroded through the pipe surface in fewer than 20 hours, and hence the

progress of the scour could not be observed since the leak was aggravated before its first inspection.

3.5.6 Experiment 5: Effect of Pipe Material

The aim of Experiment 5 was to determine the effect of pipe material on the rate of leakage-induced pipe erosion. It is clear from the literature that pipe material has a significant influence on the rate at which abrasive action can cause pipe erosion. Different pipe materials have different hardnesses, and hence exhibit different resistance to abrasion (Goddard, 1994; Ha et al., 1998; Yang & Hlavacek, 1999). For this reason, the effect of pipe material on leakage-induced erosion was a parameter that was chosen to be investigated. Furthermore, this is a factor that can be easily controlled in the design and construction phases of water distribution systems.

In this experiment, the pipe material was varied in Experiments A and C. Experiments 4A and 4C used pipe materials of steel and HDPE respectively. These materials were selected because they are inherently different from each other, and they are commonly used in South Africa. Although many older systems are made up of materials such as asbestos cement (AC) and cast iron, these materials have been omitted from this investigation since they are no longer used in the construction of new systems.

As shown in Figure 3-25, a male thread was cut onto either end of the HDPE pipe, while female threads were cut into each of the end PVC caps. The end caps were then screwed onto the pipes. It can also be observed that rubber O-rings were fitted to the inside of the end caps to give the end caps a watertight seal. The thread was further sealed with silicon.

As shown in Figure 3-26, stainless steel end caps were manufactured to seal the steel pipe sample. The end caps were manufactured from stainless steel disks, and cut such that that half of the disk was inserted into the pipe as shown in Figure 3-27. Figure 3-27 is a schematic cross section showing how the end cap fitted the pipe. The end cap was then welded to the pipe as it can be seen in Figure 3-26.

Figure 3-25: HDPE Pipe and PVC End Cap Modifications

Figure 3-26: Steel Disk End Cap Welded to Pipe

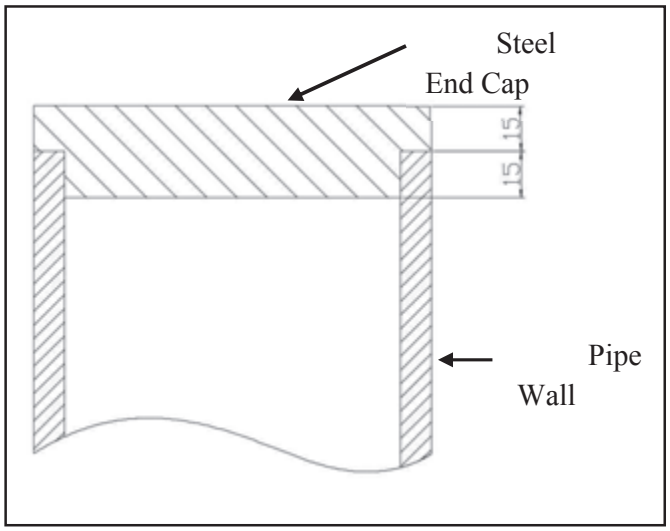

Figure 3-27: Cross-section of Manufactured Steel End Cap

4. Results and Discussion

4.1 Introduction

This chapter reports the results of the six sets of experiments that were described in Section 3.5., those experiments being five experiments designed to investigate the factors influencing erosion, plus the results of the pilot experiment. This chapter will begin by explaining the results of the control experiment that was repeated five times (once with each set of experiments), and hence demonstrate the repeatability of the testing method. This section will include an explanation of and an example of the data that was collected for each experiment. A sensitivity analysis will then be presented in which the results of the six experiments will be discussed. Experiments 1 and 2 will be discussed in greater detail than Experiments 3, 4, 5 and 6 to demonstrate how the data is presented and analysed in the rest of the study. The discussion of Experiment 1 will include a presentation and discussion of the four measurements taken at each inspection, namely Dimension A, Dimension B, scour volume and scour depth. Only scour volume will be reported and discussed for subsequent experiments.

This chapter will be concluded with a synthesis and discussion of the experimental results. The experimental data collected from this study has been presented in Appendix A.

4.2 Control Experiment

A control experiment was performed five times over the course of the testing. “Experiment B” in each set of tests was the control experiment, i.e. Experiment 1B, 2B, 3B etc. It was expected that all five control experiments would yield the same results and demonstrate repeatability in the testing procedure.

The orifice of each pipe sample was photographed at every inspection to visually monitor the progress of the scouring. Figure 4-1 shows a visual inspection of the scour progress from the time of 40 to 80 hours for Experiment 1B. The full range of photographs from the beginning to the end of each experiment can be found in Appendix A.

Table 4-1 shows the quantitative experimental data obtained for Experiment 1B. Table 4-1 gives an example of the data that was collected in this study. The experimental data for each experiment is not shown in the body of this study, but can be found in Appendix A.

Figure 4-2 shows the scour volume versus time for the five control experiments. Throughout the five experiments, logarithmic trend lines were fitted to the data to describe the relationships between time and the measured dimensions, i.e. Dimensions A, B, scour depth and scour volume. Logarithmic trend lines described the time-dependent growth of the measured dimensions quite well. It can be observed from Figure 4-2 that Experiments 2B to 5B generally appeared to follow a similar trend. The trends for Experiments 2B to 5B formed a logarithmic relationship with time.

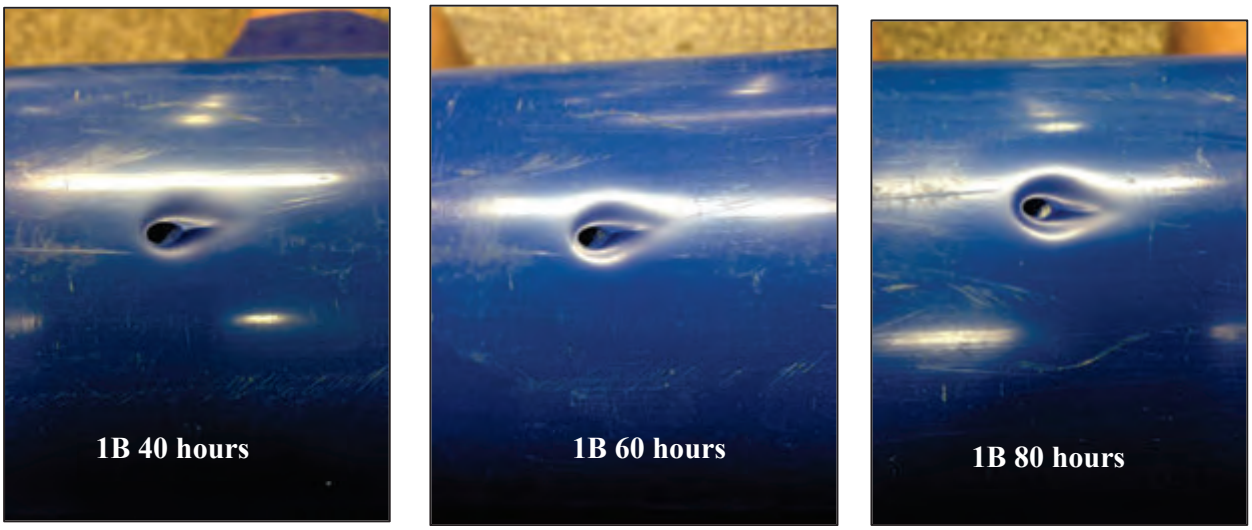

Figure 4-1: Visual Inspection of Experiment 1B from 40 to 60 hours

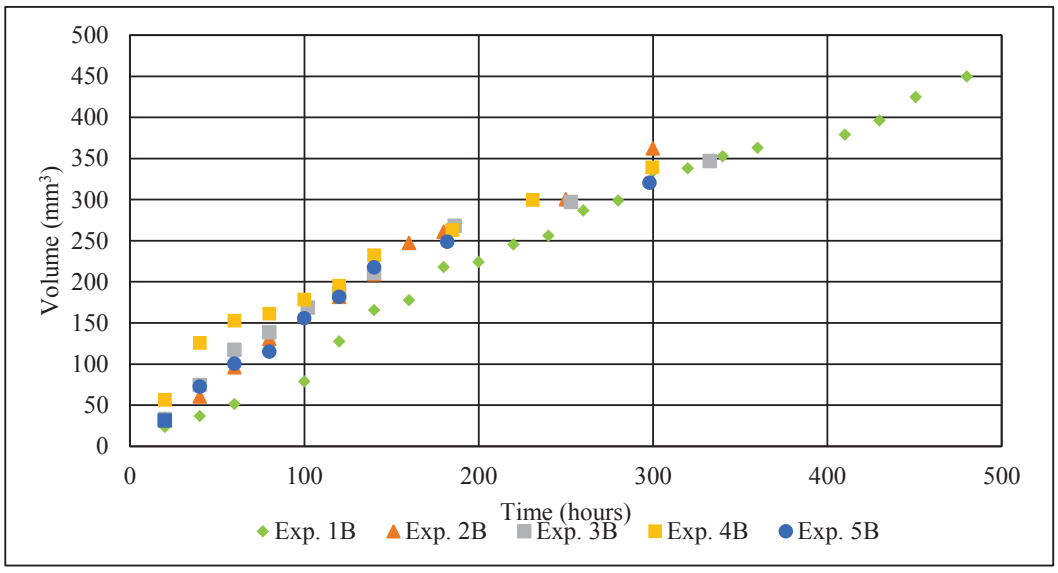

Figure 4-2: Comparison between Scour Volume of Five Control Experiments – Volume versus Time

It can also be observed that Experiment 1B seemed to progress significantly slower than the following four control experiments. It is suggested that this discrepancy in results is a consequence of a change in the testing methods. During Experiment 1B, the procedure followed after the daily inspection included filling the container with sand, saturating the sand and then restarting the test. For Experiments 2 to 5, the container was filled with sand, saturated with water, and then the container was struck several times which caused the sand to settle significantly. It is proposed that this increase in the soil bed's bulk density is the reason for the accelerated scouring in Experiments 2 to 5.

Table 4-1: Experimental Data for Experiment 1B

Run Time (h)	Dimension A (mm)	Dimension B (mm)	Depth (mm)	Putty (g)	Volume (mm^3)
0	4.24	3.00	0.00	0.000	0.0
20	19.00	9.81	0.20	0.049	23.7
40	19.08	11.02	0.36	0.076	36.7
60	20.22	12.62	0.52	0.106	51.2
80	20.22	12.62	0.54	-	-
100	21.24	13.80	0.80	0.163	78.7
120	21.52	14.06	1.00	0.264	127.5
140	21.52	14.60	1.08	0.343	165.7
160	22.00	15.08	1.36	0.368	177.8
180	22.92	16.10	1.48	0.451	217.9
200	23.42	16.10	1.56	0.464	224.2
220	23.42	16.60	1.78	0.508	245.4
240	23.42	16.60	1.82	0.530	256.0
260	23.42	16.60	2.00	0.594	287.0
280	24.52	17.22	2.06	0.619	299.0
300	24.52	17.66	2.20	0.692	334.3
320	24.52	17.66	2.42	0.700	338.2
340	24.52	17.66	2.50	0.730	352.7
360	24.52	17.66	2.64	0.751	362.8
410	24.52	17.66	3.36	0.785	379.2
430	24.52	17.66	3.60	0.820	396.1
450	24.52	17.66	3.70	0.879	424.6
480	24.52	18.32	3.78	0.931	449.8

Figure 4-3 shows the scour depth versus time for the five control experiments. It can be observed from Figure 4-3 that Experiments 2B to 5B generally appeared to follow a similar trend. Again, the trends for these four experiments appeared to be logarithmic in nature.

It can be observed that in terms of scour depth, Experiment 1B appeared to erode significantly slower than Experiments 2B to 5B. Again it is suggested that the discrepancy between Experiment 1B and the remaining four control experiments is a result of the change in testing procedure that was previously described.

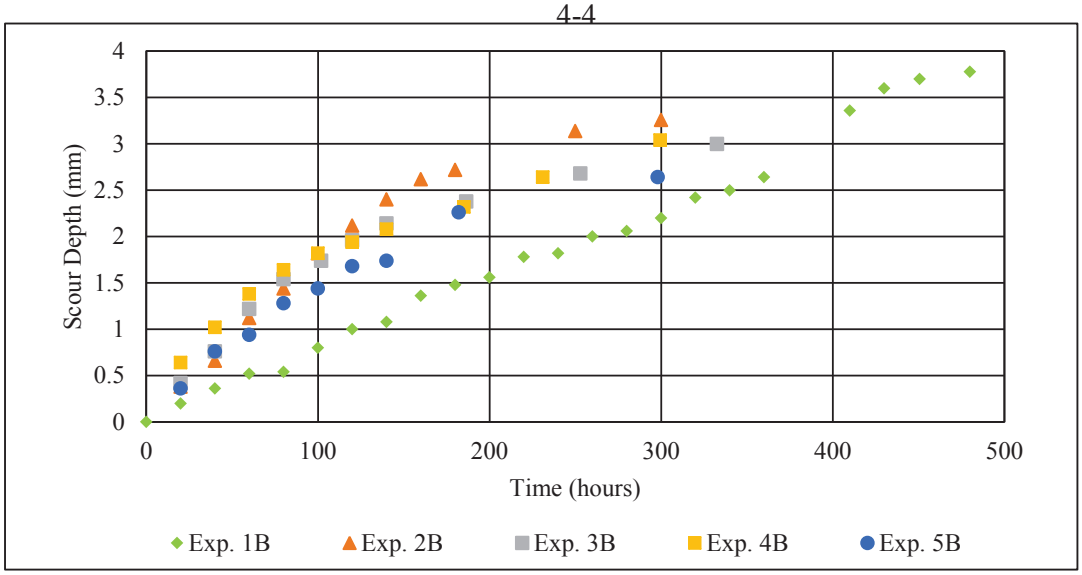

Figure 4-3: Comparison between Scour Volume of Five Control Experiments – Scour Depth versus Time

4.3 Sensitivity Analysis

4.3.1 Introduction

This section reports the results of the six experiments that were carried out in this study. The first five experiments were performed to investigate the effects of five parameters on the leakage-induced pipe erosion process. The parameters that were investigated were soil particle size, cover depth, leakage flow rate, leak orientation and pipe material. The five experiments that were conducted to investigate these parameters have been named Experiments 1 to 5 respectively. Experiment 6 in this sensitivity analysis investigates the effect of soil particle size on the size of a vertical fluidisation zone. The sensitivity analysis is concluded with a discussion of the effects of these five parameters on the process of leakage-induced pipe erosion.

4.3.2 Experiment 1: Soil Particle Size

4.3.2.1 Results

4.3.2.1.1 Development of Leak Opening

Figure 4-4 shows an example of the initial orifice condition for the experiments that were performed using uPVC pipe, with a 3mm diameter orifice inclined at 45°. For this set of tests where the initial leak was leaking at an inclination of 45° to the horizontal, the scour pattern that formed on all three of the pipe samples can best be described as a "teardrop" shape, symmetrical about the pipe's longitudinal axis as shown in Figure 4-5. Figure 4-5 shows a visual comparison between the scour patterns of tests 1A, 1B and 1C after 100 hours of exposure to the scouring. It was observed that pipe material had been removed from all sides of the initial orifice, however, the scouring effects were the most prominent on the right

hand side of the orifice as seen in Figure 4-5. This is the side of the orifice to which the jet was inclined.

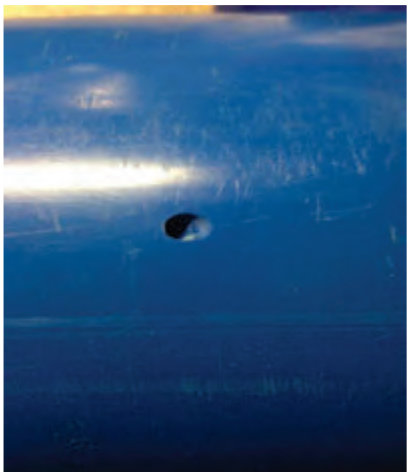

Figure 4-4: Initial Orifice Condition of Experiment 1

It should be noted that only the portion of the orifice located on the external surface of the pipe was widened due to the scouring process, while the portion extending into the pipe wall remained circular until the final stages of the experiment. Towards the end of the experiment, the indentation was deep enough to start affecting the shape of the cross sectional flow area.

As it can also be observed in Figure 4-5, the scour pattern formed an elevated ridge in the longitudinal direction of the pipe, just downstream of the orifice. The deepest indentation into the pipe wall was found on either side of this ridge towards the orifice.

As the erosion progressed and the indentation deepened, it was observed that the jet orientation became increasingly more vertical when flowing into air. This was observed while filling the pipe with water before burying it after each inspection. The rate at which the jet inclination increased was not quantified.

Furthermore, it is evident, even from visual inspections, as shown in Figure 4-5, that the larger the abrasive's grain size, the more severe the effect of the erosion.

Figure 4-6 shows the visual inspection of the pipes after 668 hours of exposure to the scouring. By visual comparison between Figures 4-5 and 4-6, it can be seen that the scouring action had deepened the indentation over time. It can further be observed in pipe sample 1A in Figure 4-6 that the scouring had eroded the entire way through the pipe wall, thus creating a second orifice. This demonstrated that this scouring phenomenon can increase a leak's initial area, and hence aggravate the initial leak.

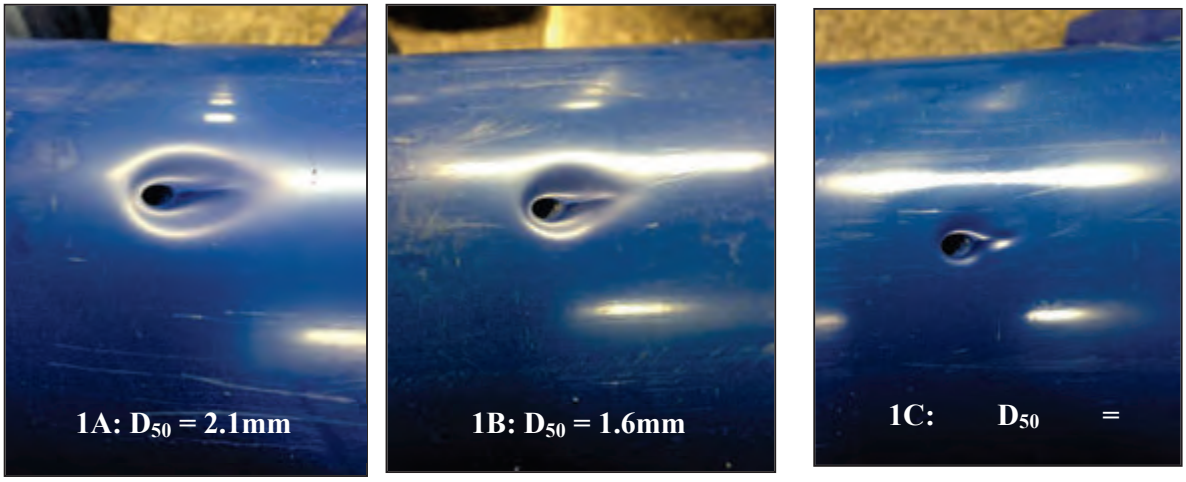

Figure 4-5: Visual Inspection of Tests 1A, 1B and 1C after 100 hours of Exposure to Scouring

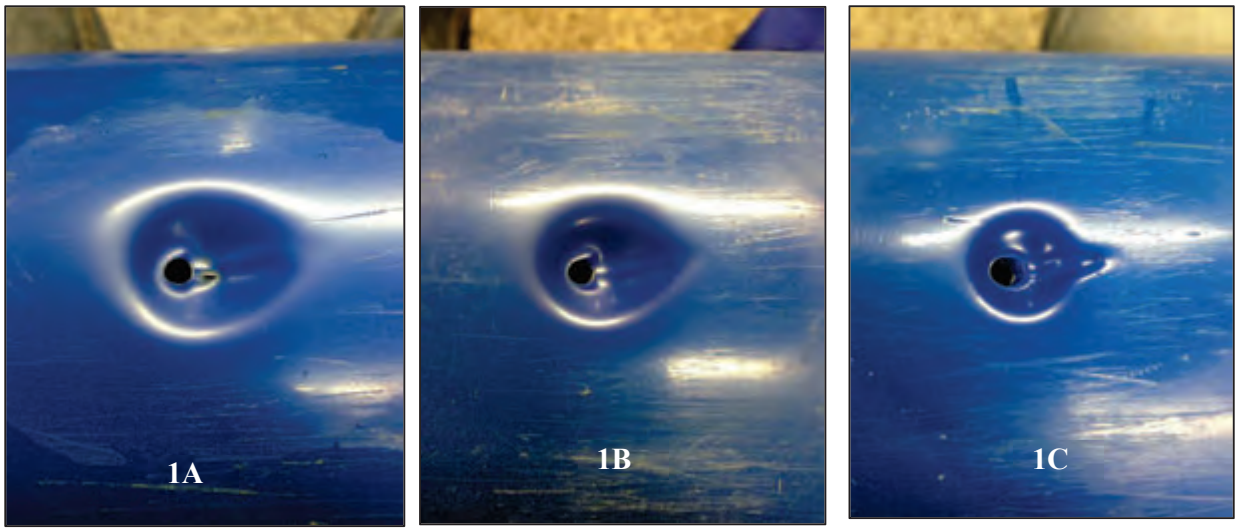

Figure 4-6: Visual Inspection of Tests 1A, 1B and 1C after 668 hours of Exposure to Scouring

The dimensions that were measured to describe the formation of the scour pattern for Experiment 1 were Dimensions A and B. Figures 4-7 and 4-8 describe the growth of Dimensions A and B respectively for all three tests conducted in Experiment 1. In all three cases, Dimensions A and B grew rapidly in the initial stages of the experiment (until approximately 40 hours), after which the scour-affected areas continued to grow at a decreasing rate. In both Figures 4-7 and 4-8, it can be seen that the larger the grain size, the greater the rate of erosion. It appeared that logarithmic trend lines generally described the growth of Dimensions A and B quite well throughout the experiments. For this reason, it can be seen that logarithmic trend lines were fitted to the data in Figures 4-7 and 4-8. It should be noted that the points (0; 4.24) and (0; 3) have been omitted from the trend lines since the logarithm of 0 is undefined.

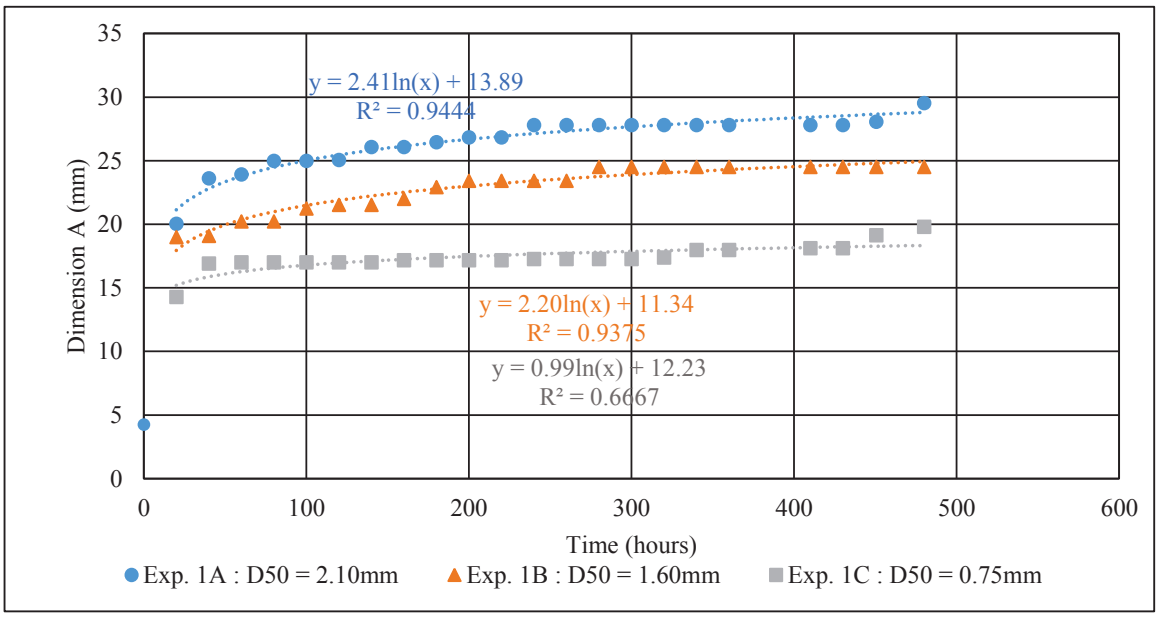

Figure 4-7: Development of Dimension A for Experiment 1

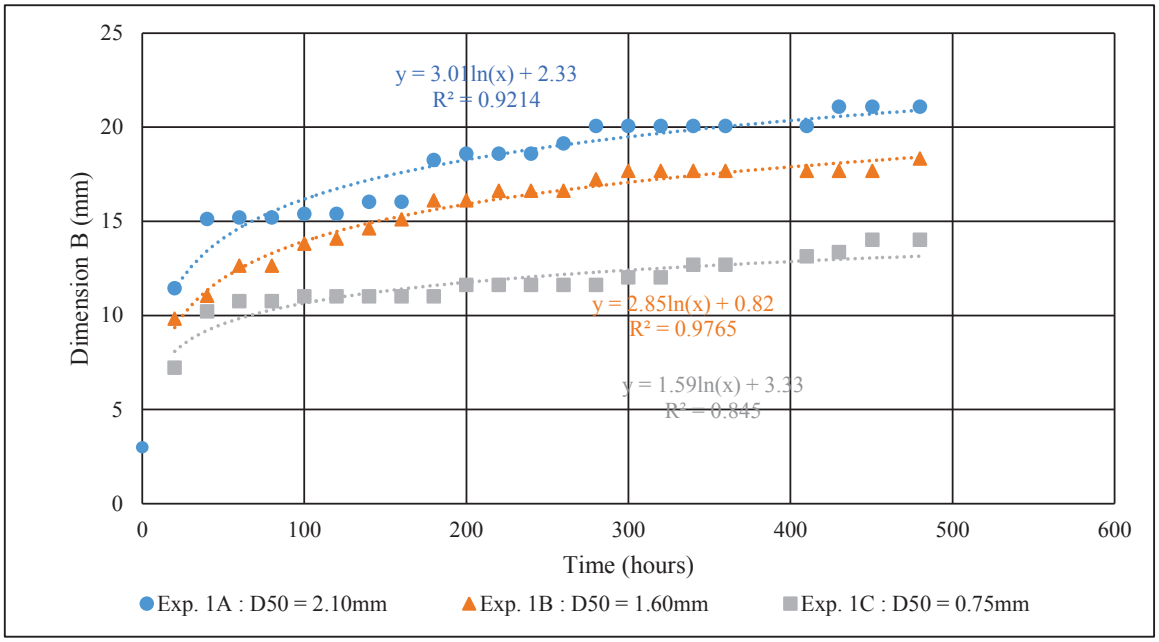

Figure 4-8: Development of Dimension B for Experiment 1

4.3.2.1.2 Volume of Removed Material

Figure 4-9 shows the volume of material removed plotted against time. As shown in Figure 4-9, logarithmic trend lines were fitted to the data. While linear trend lines appeared to fit the data better, logarithmic trend lines were selected for consistency since it was observed in Experiments 2 to 5 that logarithmic trend lines fitted the data the best. It is assumed that this was the case because the experimental procedure was refined after Experiment 1. For Experiment 1A, 1B and 1C, the logarithmic trend lines fitted the data with R^2 values of

greater than 0.80. Figure 4-9 demonstrates that the larger the grain size, the greater the rate of material removal.

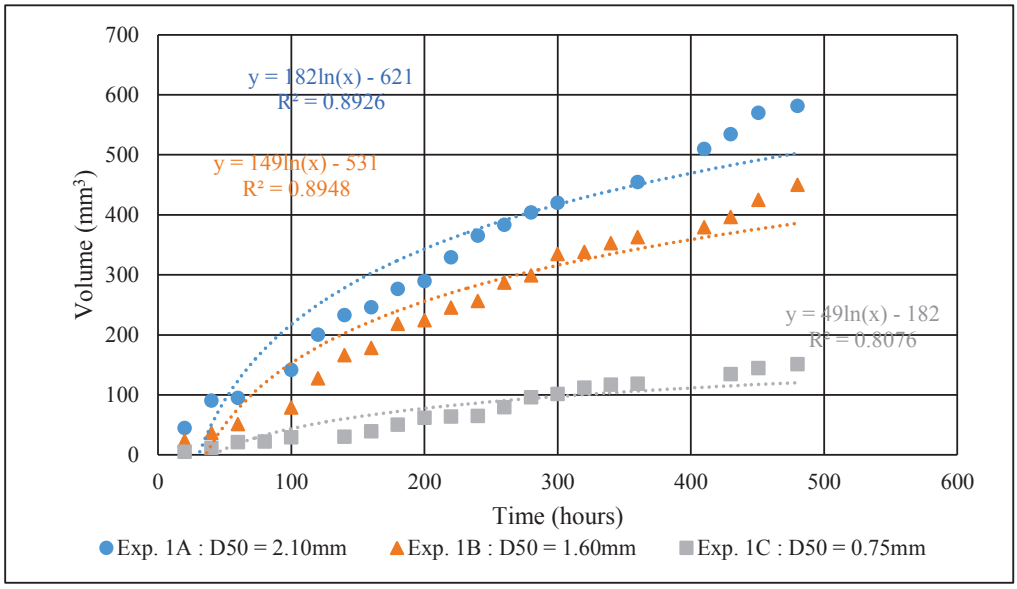

Figure 4-9 Volume of Pipe Material Removed over Time for Experiment 1

4.3.2.1.3 Development of Scour Depth

The depth of scour into the pipe wall was monitored for the duration of the tests. This dimension gives an indication of when the leak is going to be aggravated from its initial condition. When the scour depth equals the pipe wall thickness, then the leak area begins to increase. Another implication of the thinning of the pipe wall is that the stress within the pipe wall will increase locally, and could therefore leave the pipe more susceptible to cracking in cases where the internal water pressure is relatively high. This was not, however, observed during this study.

As shown in Figure 4-10, the depth of the erosion into the pipe wall was plotted against time. Again it can be seen that although the data appears to form a linear trend, logarithmic trend lines were fitted to the data for consistency between the 5 experiments. It was found in the subsequent experiments, Experiments 2 to 5, that the scour depth appeared to increase logarithmically with time, and hence logarithmic trend lines were selected for Experiment 1. These trend lines fitted the data well, with R^2 values of greater than 0.77 for all three experiments. Again it can be seen that the effect of the erosion becomes more severe with an increase in D_{50}.

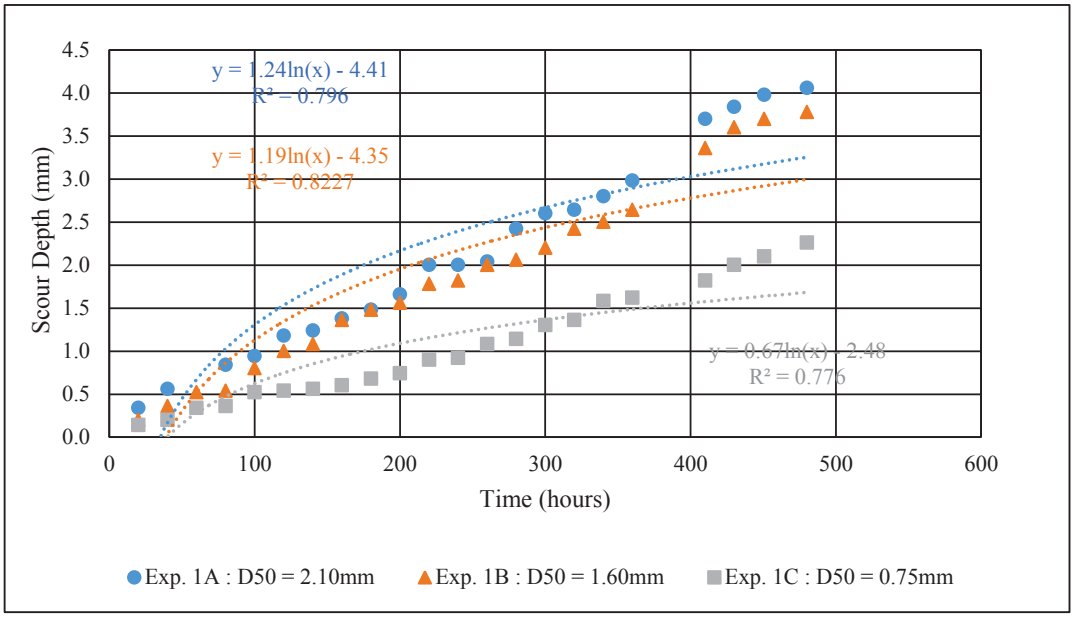

Figure 4-10: Progress of Scour Depth with respect to Time for Experiment 1

4.3.2.2 Discussion

The visual inspection showed that the orifice conditions were consistent with those found in literature. As discussed in Section 2.9.1, the smooth and polished conditions of the surfaces adjacent to the orifice have been observed by de Kater (2014), Negonga (2013) and Pike (2013).

The growth rates of Dimensions A and B decreased over time for two reasons. The first reason is that the jet orientation became more and more vertical as time progressed. As it will be further discussed in Section 4.3.5, the more vertical the jet is, the slower the growth rate of the area of influence. Secondly, the pipe material closer to the orifice is more likely to be eroded than material further from the orifice, and hence, as the material closer to the orifice is removed, the slower the rate of erosion will become.

While Figure 4-9 and 4-10 give an indication that the rate of erosion increases when the abrasive particle is larger, it is difficult to quantify exactly what effect the grain size has on the rate of scour from these plots. It can be observed that logarithmic trend lines were fitted to the data in these figures. It can therefore be said that the relationships between scour volume and scour depth with respect to time can be described by an equation in the form

$$y = a \cdot \ln(t) + b \tag{4.1}$$

Where y is either volume of material removed (mm^3) or scour depth (mm); t is time (hours); *a* and *b* are constants.

For a logarithmic function in this form, the derivative is given by

$$\frac{\partial y}{\partial t} = \frac{a}{t} \tag{4.2}$$

Therefore, the *a* value has a direct impact on the gradient of the function. It can be said that the *a* value is the gradient of a function in which the scour (volume or depth) is plotted against the logarithm of time. It should be noted that the units for the *a* value are mm^3/ln(hour), or mm/ln(hour) for the scour depth and scour volume respectively. Furthermore, for dimensional homogeneity, the *b* values for the scour volume and depth relationships with time are mm^3 and mm respectively. It is difficult to attach a physical meaning to the *b* value at this early stage of research within the field of leakage-induced pipe erosion. For the purposes of this study, this *b* value is purely for descriptive purposes. For this reason, it will not be discussed or evaluated further.

In order to quantify the effects of cover depth on the erosion process, the *a* values from the scour volume versus time graph (Figure 4-9) have been plotted against their respective D_{50} values in Figure 4-11. As it can be seen in Figure 4-11, The *a* value for the volume versus time function increases with increasing grain size.

A logarithmic trend line was fitted to the data in Figure 4-11. This logarithmic trend lines fitted the data well, with R^2 values greater than 0.99. Albeit under somewhat different circumstances, in the case of abrasive water jet cutting, Gent et al. (2012) similarly found that the rate of erosion increases logarithmically with increasing abrasive particle size.

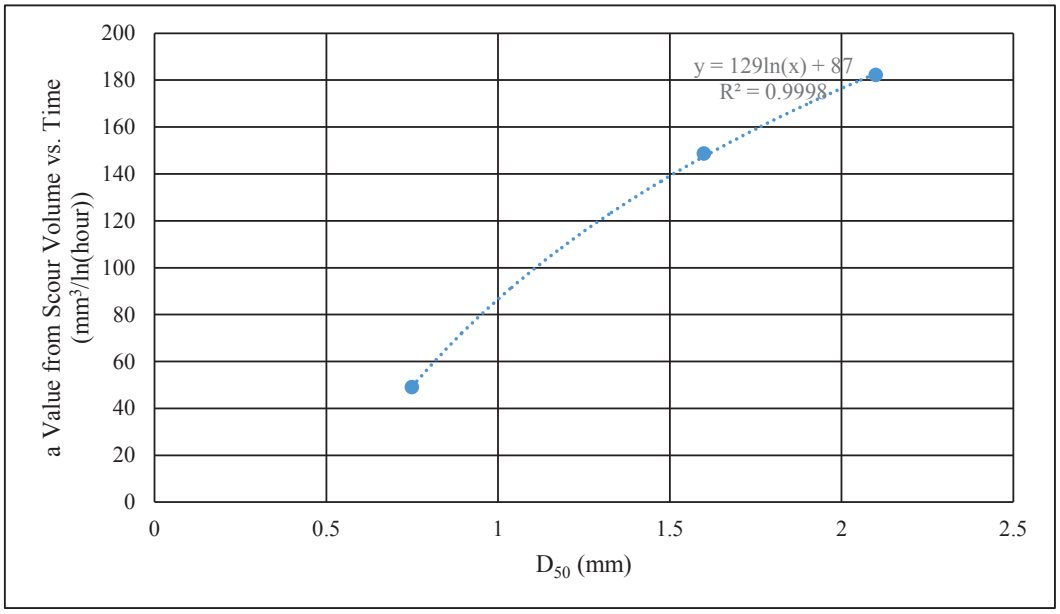

Figure 4-11: Logarithmic Trend Line a Values from Figure 4-11 vs. D_{50}

It was further noted by Gent et al. (2012), that in the case of abrasive water jet cutting, the rate of erosion increases with increasing particle size up until a certain size. When that certain abrasive particle size is exceeded, the rate of erosion begins to decrease with

increasing grain size. In the case of leakage induced pipe erosion, it is suspected that a similar phenomenon could occur when the grain sizes exceed a certain (unknown) size. This has been postulated because it is unlikely that a bed of larger particles, potentially in the gravel range (D_{50} between 2mm and 60mm), will be able to experience fluidisation. Based on the conditions stated by Niven & Khalili (1998), for fluidisation to occur, the granular bed needs to be able to expand, and the fluid flow needs to be able to create a sufficient drag force to support the weight of the particles. It is suspected that fluidisation would not occur in large-grained granular beds, because the flow would not create sufficient drag force to support the weight of many large particles. Larger particles also tend to have greater interlocking effects than smaller particles, making them more difficult to dislodge from the bed.

4.3.3 Experiment 2: Cover Depth

4.3.3.1 Results

4.3.3.1.1 Development of Leak Opening

As with Experiment 1, the initial leak condition caused a "teardrop" shaped scour pattern on all three tests as shown in Figure 4-12 below. This teardrop shape was symmetrical about the longitudinal axis of the pipe. Figure 4-12 shows a visual comparison between the scour patterns of tests 2A, 2B and 2C after 100 hours of exposure to the scouring. It was observed that pipe material had been removed from all sides of the initial orifice, with the most amount of material having been removed from the right of the orifice (as seen in Figure 4-12), and the least amount being removed from the left of the orifice (as seen in Figure 4-12). The right hand side of the orifice, as seen in Figure 4-12, is the side to which the jet was inclined. Again, the condition of the pipe surface around the orifice was smooth and polished.

As it can also be observed in Figure 4-12, the scour pattern formed an elevated ridge in the longitudinal direction of the pipe, just downstream of the orifice. The deepest indentation into the pipe wall was found on either side of this ridge towards the orifice.

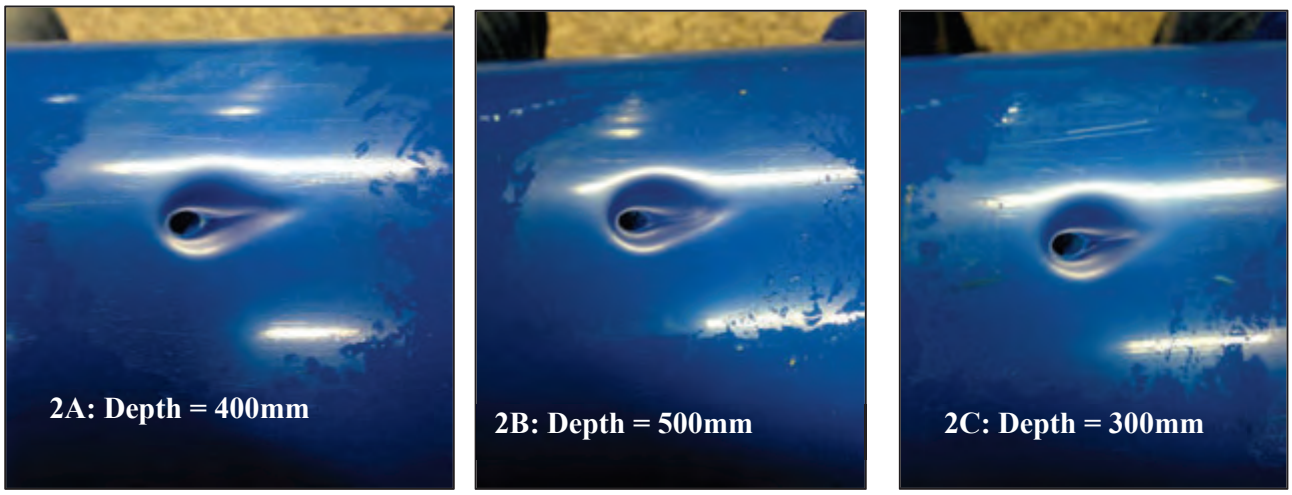

Figure 4-12: Orifice Conditions after 100hours of erosion

As the depth of the scour increased into the pipe wall, it was observed on all three pipe samples that the orientation of the jet became more and more vertical when flowing into air. The orifices of Experiments 2A and 2C maintained their circular cross sections for the full duration of the test. Experiment 2B, however, experienced enough erosion in the front and sides of the orifice to cause a change in the shape of the orifice as shown in Figure 4-13. Figure 4-13 shows the orifice condition of Experiment 2B after 344 hours of exposure to the scouring action, which was the end of the test's run time. Firstly, Figure 4-13 shows that the orifice became more vertical towards the end of its scour duration. Secondly, it shows that the orifice began to lose its circular cross section, and began to form dents in the sidewalls of the orifice.

Upon visual inspection, it was clear that Experiment 2B, the experiment with the greatest soil bed depth, experienced the most erosion out of the three tests. It was not conclusive upon visual inspection which pipe sample experienced more erosion between Experiments 2A and 2C.

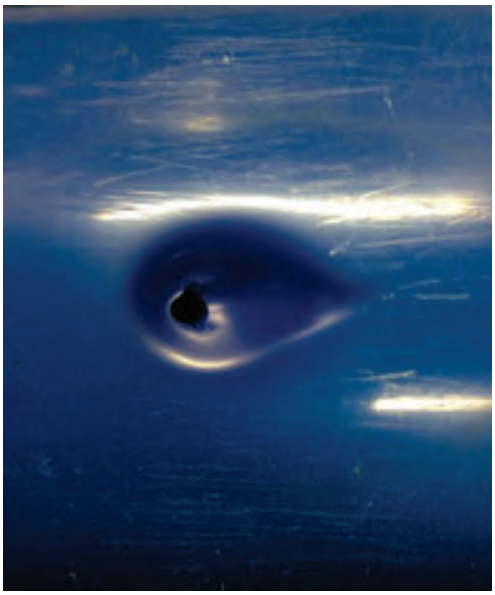

Figure 4-13: Final condition of Experiment 2B (344 hours)

4.3.3.1.2 Volume of Removed Material

Figure 4-14 illustrates how the volume of pipe material was removed from the pipe surface adjacent to the orifice over time. Plotting this data on a linear time scale showed that pipe material was removed rapidly in the initial stages of the experiment, and it appeared that the rate of material removal decreased with increasing time. For this reason, logarithmic trend lines were fitted to the data. The (0; 0) points have therefore been excluded from the plots since the logarithm of 0 is undefined.

From Figure 4-14, it appeared that the rate at which the volume of material was removed from the pipe slowed down as the scour time increased. Logarithmic trend lines were fitted to these three sets of data. All three sets of data had R^2 values greater than 0.91.

During this initial phase of the experiment (0-160 hours), the rate of erosion was greatest for Experiment 2B with a cover depth of 500mm, followed by 2A with a cover depth of 400mm, and then 2C with a cover depth of 300mm. While the difference between the rates material removal are relatively small for these three tests, it does suggest that greater cover depths increase the initial rate of erosion in this range cover depths.

During the second phase, between the times of 160 and 344 hours, it appeared that the rate of pipe material removal decreased. While Experiment 2B continued to display the greatest amount of erosion during this period, 2A and 2C appeared to converge.

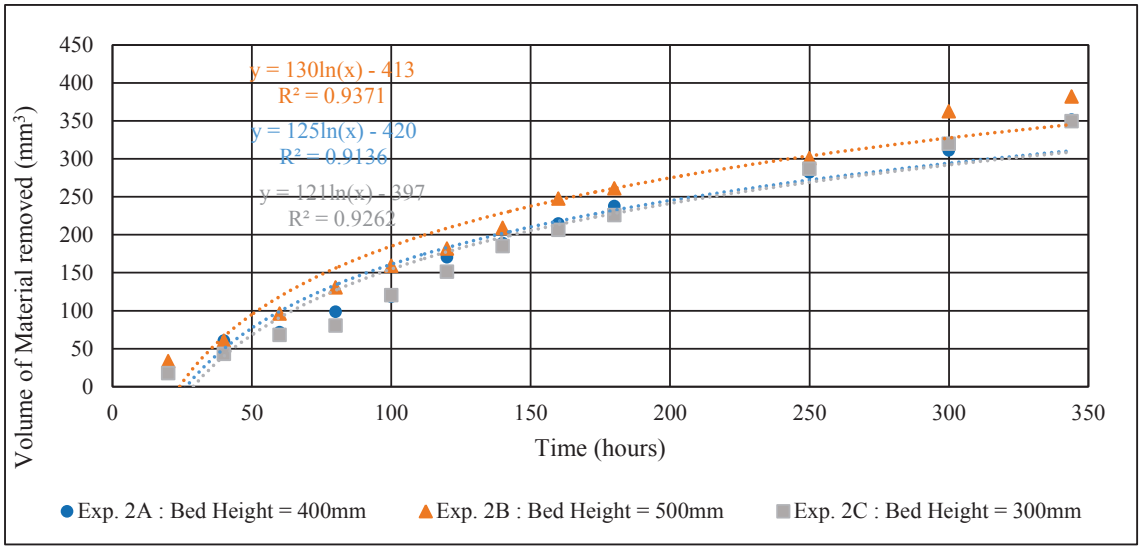

Figure 4-14: Volume of Removed Material for Experiment 2

4.3.3.2 Discussion

As shown in Figure 4-14, the scour volume appeared to increase logarithmically over time. This type of data has also been observed in the time-dependent scour of alluvial beds around infrastructure in open channel flow, as discussed in Section 2.6.4. Logarithmic trend lines were then fitted to the data as shown in Figure 4-14.

In terms of scour volume, the test with the greatest cover depth (Experiment 2B) consistently showed the greatest degree of erosion of the three. There was no obvious difference between Experiments 2A and 2C (cover depths 400mm and 300mm respectively). As previously discussed, Bailey (2015) observed that an increased pressure in the soil bed decreases the size of the fluidisation zone. Given a constant flow rate, a decreased flow area (fluidisation zone) would result in a greater fluid and particle velocity within the fluidisation zone. This explains why an increase in cover depth should increase the rate of erosion.

As it was seen in Figure 4-14, the rate of erosion differed with varying cover depths. Furthermore, it can be observed that logarithmic trend lines were fitted to this data. In order to quantify the effects of cover depth on the erosion process, the *a* values of the logarithmic trend line from the scour volume versus time graph (Figure 4-14) have been plotted against their respective cover depths in Figure 4-15. As it can be seen in Figure 4-15, there is no discernible correlation between the cover depth and the *a* values. This is because the difference between the results from 2A and 2C were not clearly distinct from one another. From Figure 4-15, it appears that the range of the *a* values was relatively small, suggesting that this range of cover depths has a relatively small effect on the rate of erosion.

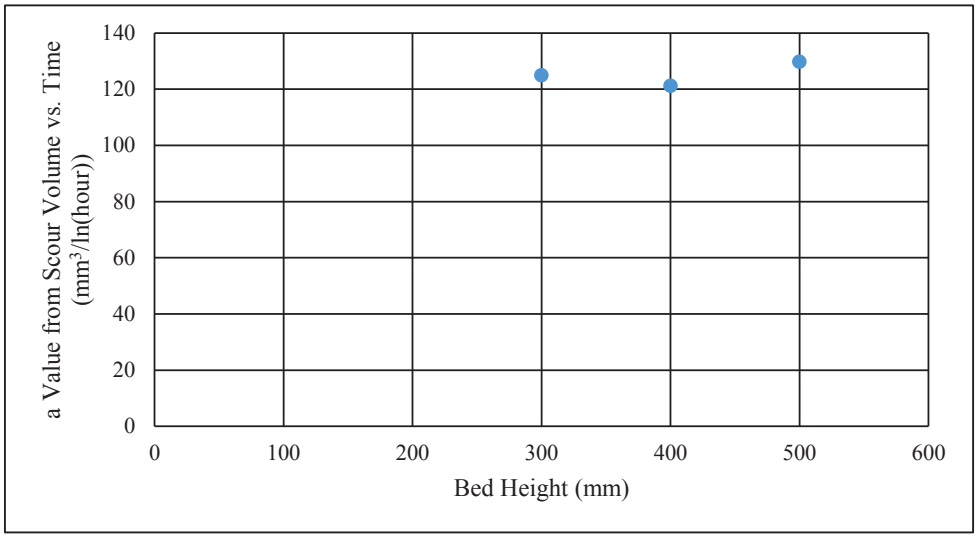

Figure 4-15: Logarithmic Trend Line *a* Values from Figure 4-20 vs. Bed Height

4.3.4 Experiment 3: Flow Rate

4.3.4.1 Results

4.3.4.1.1 Development of Leak Opening

As with Experiment 1 and 2, the initial leak condition initially caused a "teardrop" shaped scour pattern on all three tests. This teardrop shape was symmetrical about the longitudinal axis of the pipe. Figure 4-16 shows a visual comparison between the scour patterns of tests 3A, 3B and 3C after 80 hours of exposure to the scouring. It was observed that pipe material had been removed from all sides of the initial orifice, with the most amount of material having been removed from the right of the orifice (as seen in Figure 4-16), and the least amount being removed from the left of the orifice (as seen in Figure 4-16). The right hand side of the orifice, as seen in Figure 4-16, is the side to which the jet was inclined.

It was clear upon visual inspection that the test with the greatest flow rate (3A), was causing the erosion to happen at a far greater rate than that of 3B, while 3C (with the lowest flow rate) showed minor signs of erosion.

As it can be seen in Figure 4-17, the scour pattern of 3A (flow rate = 600 l/hour) became more rounded as the test progressed. This is due to the fact that the water jet became more and more vertical as the material in front of the orifice was removed. The effect of the leak orientation on the scour pattern will be discussed in further detail in Section 4.3.5. At 102 hours of erosion, it was observed that the erosive action had eroded the entire way through the pipe wall, creating a second orifice, as shown in Figure 4-17(ii). After 253 hours of scouring, the second orifice had enlarged enough to join the initial orifice, as shown in Figure 4-25 (iii).

Experiment 3B continued to exhibit a similar elongated teardrop shaped scour pattern, as it has been seen in Experiments 1 and 2.

Experiment 3C, with a flow rate of 200 l/h, showed very little erosion over the course of the testing period. It showed a slow development of the teardrop scour pattern, as shown in Figure 4-18 below.

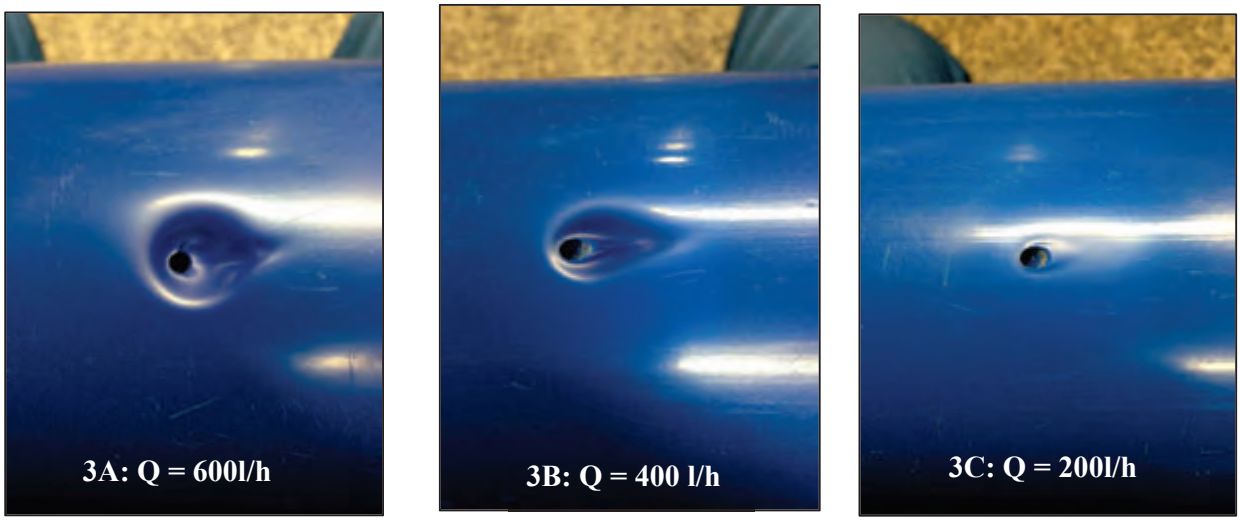

Figure 4-16: Orifice Conditions of Experiment 3 after 80 Hours of Erosion

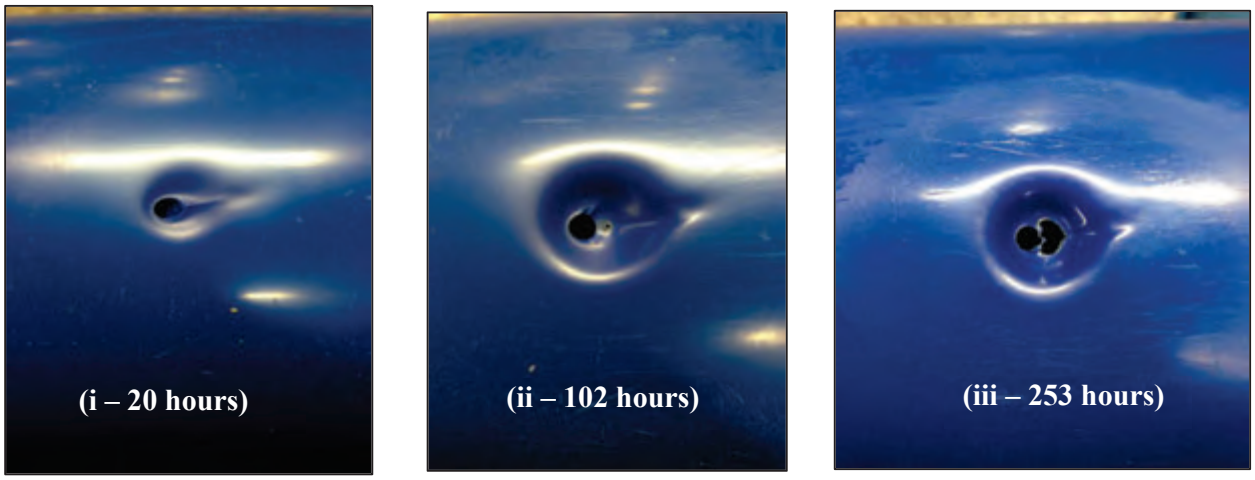

Figure 4-17: Visual Progression of Experiment 3A Scour Pattern

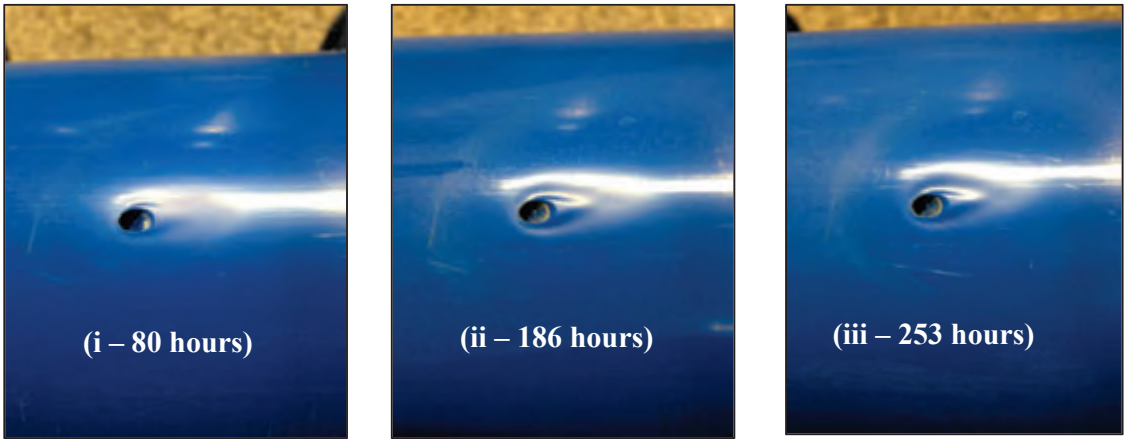

Figure 4-18: Visual Progression of Experiment 3C Scour Pattern

4.3.4.1.2 Volume of Removed Material

Figure 4-19 illustrates how the volume of pipe material was removed from the pipe surface adjacent to the orifice over time. Logarithmic trend lines were fitted to the volume removed versus time data for Experiment 3. These logarithmic trend lines fitted the data well for Experiments 3A and 3B, with R^2 values of greater than 0.92. A logarithmic trend line did not fit the data for Experiment 3C as well as it did for 3A and 3B. This is a result of the slow nature of the erosion at this flow rate. In the previous experiments (2A, 2B and 2C) it was observed that the pipe material was removed rapidly in the initial stages, and slowed down towards the end of the test. Due to the slow nature of the scour in Experiment 3C, the test did not have time to reach its slower phase of material removal. For this reason, a linear trend line fit the data for 3C better than a logarithmic trend line; however, a logarithmic trend line has been selected for consistency between experiments 3A, 3B an 3C.

Figure 4-19 clearly shows that the greater the leakage flow rate, the faster material is removed from the pipe surface.

Again it can be seen that for Experiments 3A and 3B that the rate of material removal decreases towards the latter stages of the test.

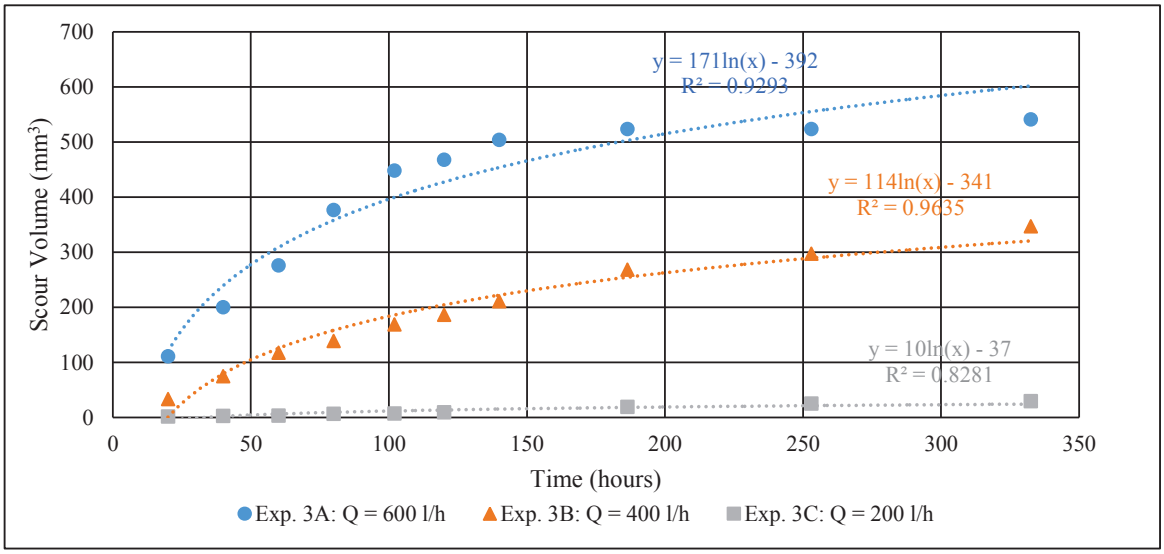

Figure 4-19: Volume of Removed Material for Experiment 3

4.3.4.2 Discussion

As it was seen in Figure 4-29, the rate of erosion increased with increasing flow rate. It is suggested that the increase in flow rate increases the velocity of the abrasive particles in the mobile bed zone. As suggested by both Archard's Law of abrasive wear and Preston's Equation (discussed in Sections 2.6.1 and 2.6.2 respectively), the rate of should be linearly proportional to the velocity of the abrasive particles.

In order to develop an empirical equation to describe how flow rate affects the scour volume, the *a* values found in Equation 4.1 were plotted against their respective flow rates. A linear trend line was then fitted to this plot. From this graph it can be seen that the *a* value in Equation 4.1 can be expressed as a function of flow rate.

Figure 4-20 shows the *a* values plotted against their respective flow rates. This constant was obtained from the scour volume versus time curves found in Figure 4-19.

From the trend line found in Figure 4-32, an empirical equation can be formulated. Equation 4.3 describes how material is removed from the pipe surface over time where the leakage flow rate is the only variable:

$$V_s = (0.4 \cdot Q - 62) \cdot \ln(t) + b \tag{4.3}$$

Where V_s= Scour volume (mm^3); Q = Flow Rate (l/h); t = time (hours)

It should be noted that this empirical equation is intended for descriptive purposes, and a potential starting point for future researchers to develop a more scientifically valid equation. This equation should not be interpreted as an accurate predictive model due to the insufficient number of data points used to formulate it.

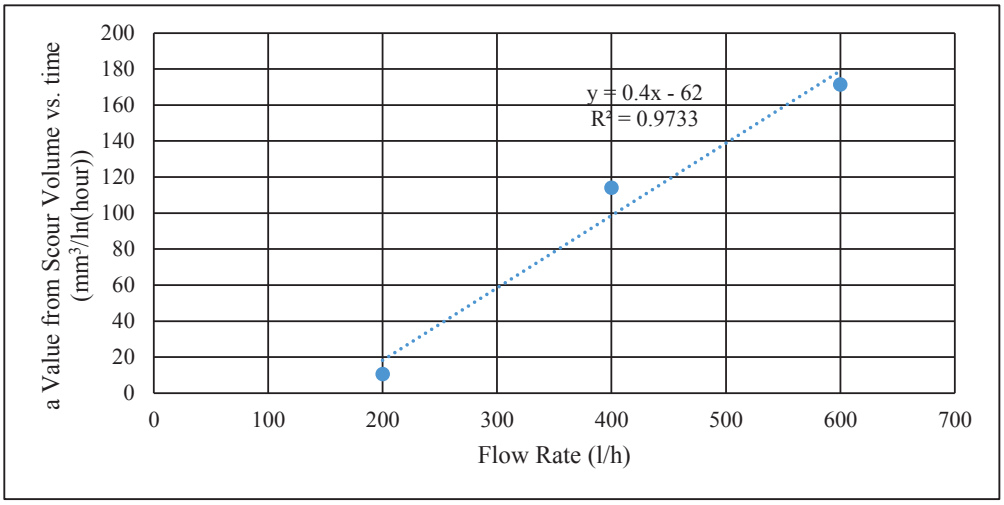

Figure 4-20: Logarithmic Trend Line *a* Values from Figure 4-19 vs. Flow Rate

4.3.5 Experiment 4: Leak Orientation

4.3.5.1 Results

4.3.5.1.1 Development of Leak Opening

The initial orifice conditions and pipe surface conditions for Experiments 4A, 4B and 4C can be seen in Figure 4-21. Experiment 4A has a horizontal leak (0°), simulating a saddle leak. The pipe surface that the leak runs across is initially clean and smooth. Figure 4-35 also shows the shapes and initial orifice orientations of Experiment 4B (45°) and 4C (90°).

Experiment 4A(i) produced an elongated scour pattern as shown in Figure 4-22. This experiment was inspected for the first time after 20 hours of exposure to the abrasion mechanism. Upon this inspection, it was observed that the scouring action had already eroded the entire way through the pipe surface, creating a new orifice on the pipe surface, as shown in Figure 4-22. After 60 hours of exposure to the erosion process, it was noted that there were no observable or measurable differences between the 20 hour and the 60 hour scour pattern. The flow pattern of Experiment 4A when flowing into air was investigated, and shown in Figure 4-23. It was observed that the new orifice was creating a vertical jet that the original horizontal jet was unable to penetrate. For this reason, the original horizontal jet was being deflected away from the pipe surface, which prevented any further erosion from taking place. The indentation caused by the horizontal jet was smooth and polished, as it has been observed with previous experiments.

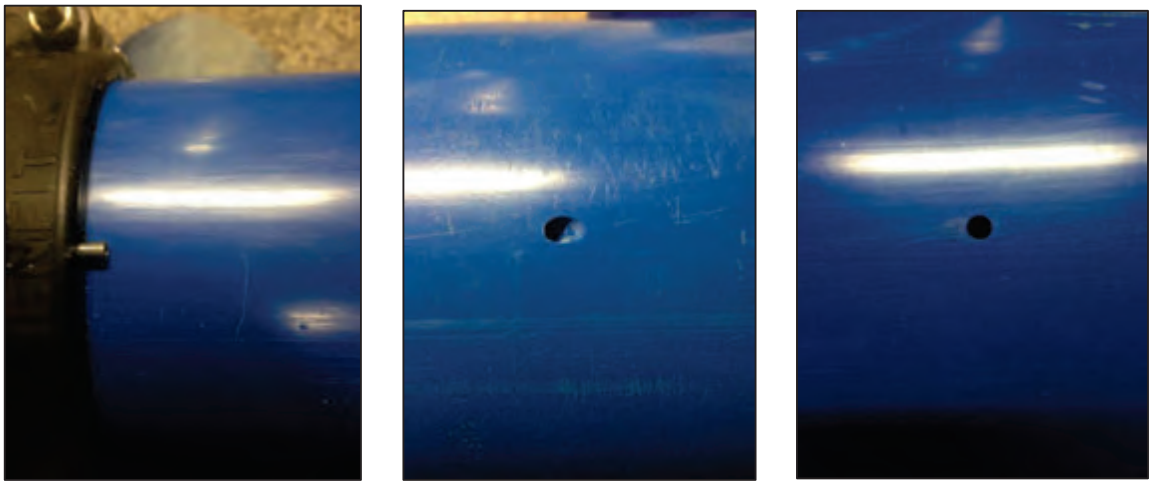

Figure 4-21: Initial Orifice Conditions of Experiment 4

Experiment 4A(ii) was a repeat of experiment 4A(ii), with a reduced flow rate (Q=200 l/h). Since Experiment 4A(i) caused the pipe to fail before the first inspection, Experiment 4A(ii) was performed in order to obtain a time-dependent relationship for the various scour parameters. As shown in Figure 4-23, Experiment 4A(ii) developed an ellipse-like scour pattern after 20 hours of exposure to the scouring. It was first observed that a new orifice had been created after 120 hours, and had progressed to the condition that can be seen in Figure4-25 after 140 hours. It should be noted that fluidisation could not be initiated for the horizontal

orifice at a flow rate of 200 l/h. For this experiment, the flow rate had to be temporarily increased to approximately 300 l/h to initiate fluidisation, after which the flow rate was reduced to 200 l/h where the fluidisation mechanism could be sustained.

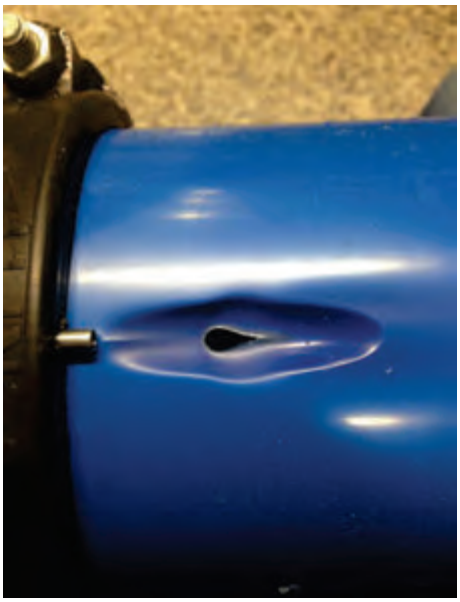

Figure 4-22: Orifice Condition of Experiment 4A(i) after 20 hours

Figure 4-23: Experiment 4A(i) Flow Pattern when Flowing into Air

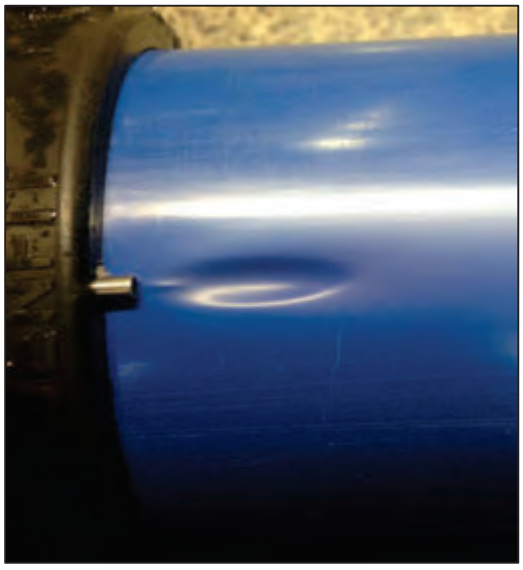

Figure 4-24: Orifice Condition of Experiment 4A(ii) after 20 hours

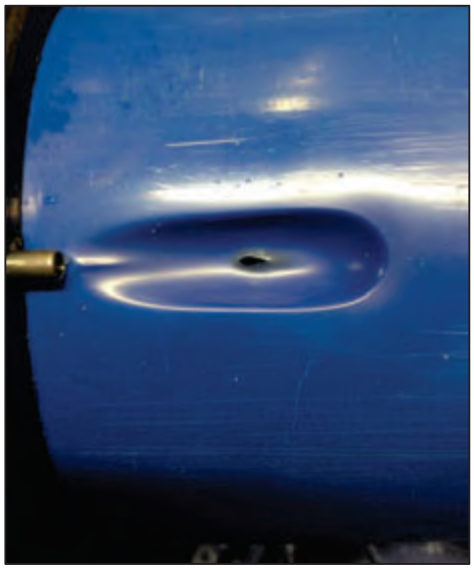

Figure 4-25: Orifice Condition of Experiment 4A(ii) after 140 hours

Experiment 4B showed a similar scour pattern to those shown in experiments 1B, 2B and 3B, however, the "teardrop" shape appeared to be skewed, and was not symmetrical about the pipe's longitudinal axis, as shown in Figure 4-26. It is suspected that this skewed scour pattern is a result of a manufacturing error.

As shown in Figure 4-27, Experiment 4C produced circular a scour pattern that was concentric with the original orifice. Figure 4-28 shows the growth of Experiment 4C's orifice diameter in during the latter stages of the test. The orifice maintained its original 3mm diameter for the first 185 hours of the experiment. It was first observed at the 231 hour inspection that the orifice had increased in diameter. After 299.5 hours of scouring, the indentation caused by the scouring had scoured deep enough to enlarge the diameter of the initial diameter from 3mm to 4.74mm as shown in Figures 4-28.

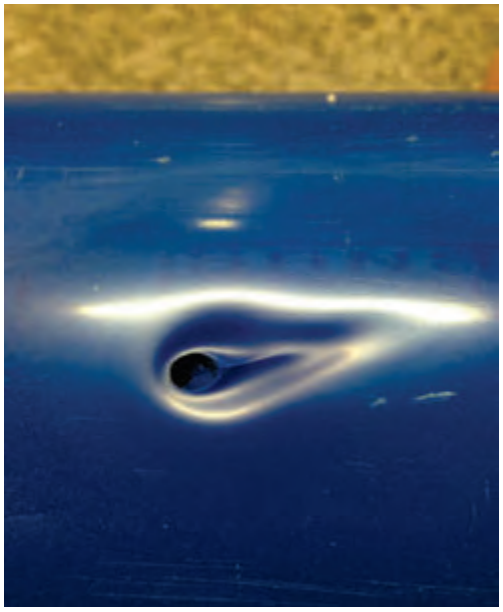

Figure 4-26: Orifice Condition of Experiment 4B after 60 hours

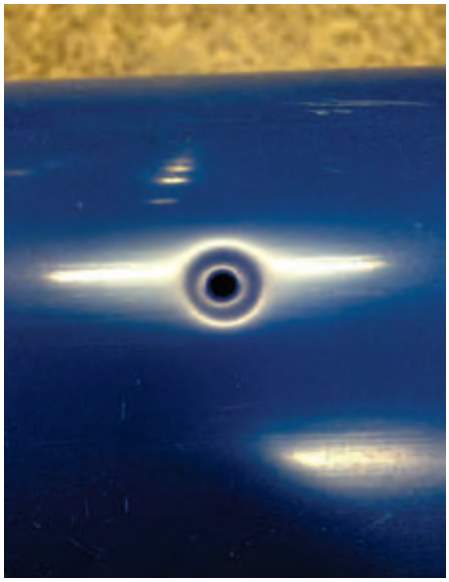

Figure 4-27: Orifice Condition of Experiment 4C after 60 Hours

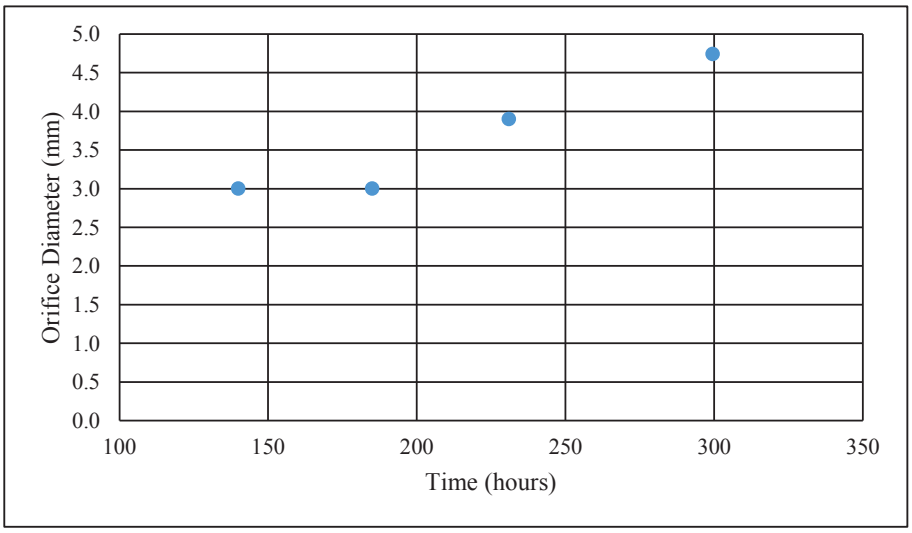

Figure 4-28: Experiment 4C's Orifice Diameter

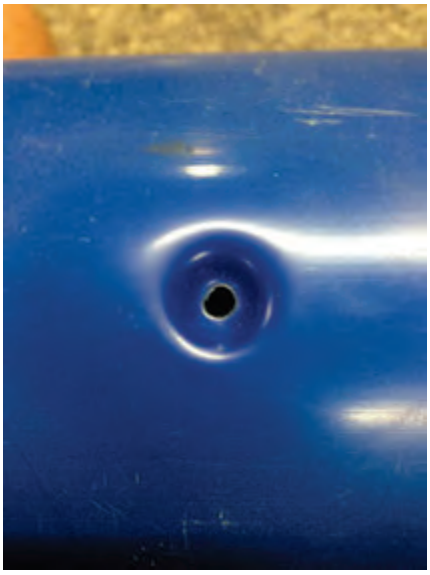

Figure 4-29: Orifice Condition of Experiment 4C after 229.5 Hours

4.3.5.1.2 Volume of Removed Material

Figure 4-30 illustrates how the volume of pipe material was removed from the pipe surface adjacent to the orifice over time. In terms of volume, the material appeared to be removed in a logarithmic fashion with respect to time.

Although it appeared that dimensions A and B stopped growing for Experiment 4A(i) after 20 hours, it appeared that the volume of the void increased between the times of 20 and 40 hours, after which it remained constant. A logarithmic trend line was fitted to the volume versus time data for Experiment 4A(i). This trend line was not a good fit for the data, and should not be trusted since there are only three data points available for this test. The volume of Experiment 4A(i)'s indentation grew the most rapidly out of the four tests in Experiment 4.

The volume of removed pipe material increased the second fastest for Experiment 4A(ii), as shown in Figure 4-30. A logarithmic trend line fitted the data for this test well, with an R^2 value of 0.95.

Experiment 4B (45° orifice orientation) eroded faster than 4C (90° orifice orientation) for the first 140 hours of the test, however, as it can be seen in Figure 4-30, the pipe material was removed from Experiment 4C in two distinct phases. During the first phase (0-140 hours), material was removed from the pipe approximately logarithmically at the slowest rate out of the four tests. During the second phase (140-300 hours), the rate of material removal increased significantly, also in a logarithmic manner. Separate logarithmic trend lines have been fitted to these two separate phases. During the second phase of Experiment 4C's volume removal, the scour depth increased more rapidly than in the initial phase. This would suggest that the scouring mechanism was somehow altered at this point. Since this process takes place below the soil surface and therefore cannot be observed, it is difficult to know exactly what caused this accelerated scouring. Two possibilities have been proposed to explain this increased rate of scouring. The first possibility is that the indentation caused by the scouring made the orifice a divergent orifice, as opposed to its original square edge shape. This could

have potentially affected the flow pattern, as demonstrated in the conic edged orifice in Figure 4-31. Figure 4-31 compares the flow lines of water exiting a square edged orifice to those of water exiting a conic edged orifice. It can be seen that the flow lines expand out of the conic edged orifice, as opposed to the flow lines out of the square edged orifice which flow straight. If the flow were to expand in this manner, it is suggested that the abrasion would influence a wider area of the pipe surface more vigorously, which would explain why the rate of erosion in terms of scour volume would begin to increase. This would not, however, explain why the rate of erosion in terms of scour depth would increase

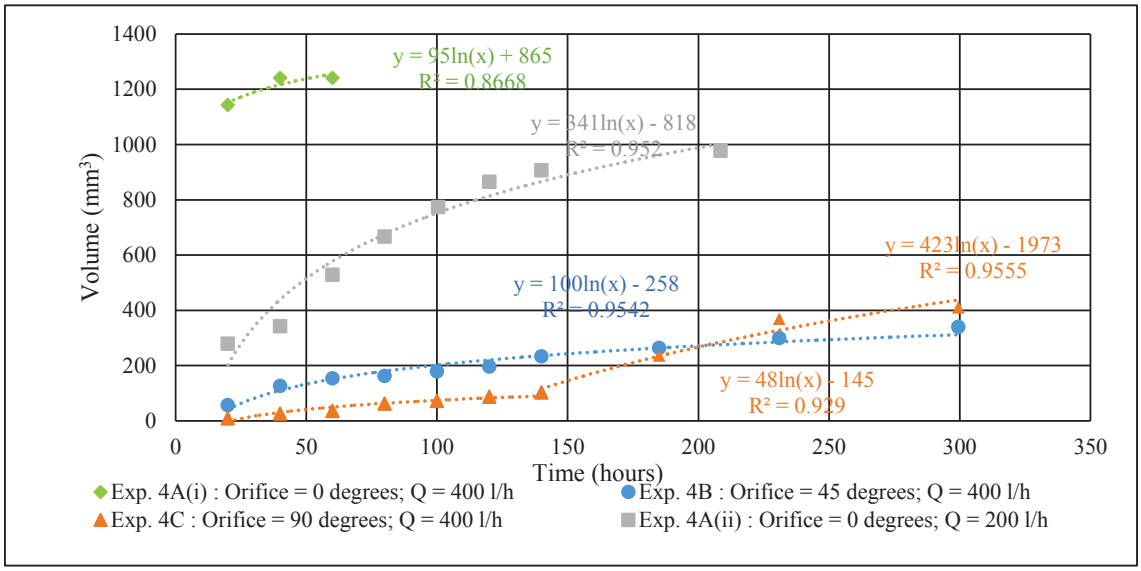

Figure 4-30: Volume of Removed Material for Experiment 4

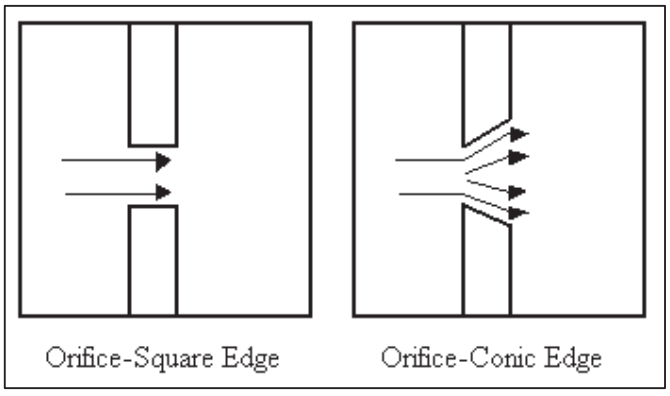

Figure 4-31: Types of Orifices (Miryala et al., 2013)

The second proposed possibility is that the eroded shape of the pipe surface changed the travel path of the soil particles. Figure 4-49 below gives a schematic interpretation of the

shape of Experiment 4C's orifice at the beginning of the second phase. As depicted in Figure 4-32, the orifice indentation formed a smooth, curved profile. It is postulated that the soil particles initially moved horizontally across the pipe surface, as indicated in Figure 4-32. As the erosion became more pronounced, it is assumed that the soil particles followed the indented pipe surface when being pulled in towards the orifice. This curved surface increased the length of the particles travel path. Increasing the length of the particles' travel path would have increased the particles' velocity given the same travel time. Therefore, the increased particle velocity increased the rate of erosion, thus producing a phase of increased rate of erosion

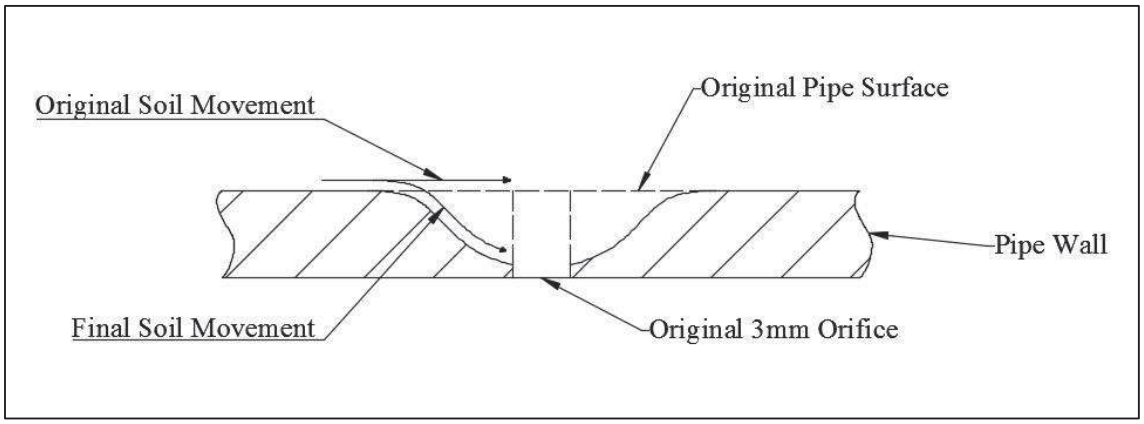

Figure 4-32: Schematic Interpretation of Experiment 4C's orifice Shape

4.3.5.2 Discussion

As it was seen in Figure 4-30, the rate of erosion increased with decreasing orifice inclination. In order to quantify the effect of the flow rate on the rate of erosion (in terms of scour volume), the trend lines of the scour depth versus time data were analysed.

In order to develop an empirical equation to describe how leak orientation affects the scour depth, the *a* values found in Equation 4.1 were plotted against the leak angles of inclination. A linear trend line was then fitted to this plot. From this graph it can be seen that *a* in Equation 4.1 can be expressed as a function of leak angle. It should be noted that only three data points were measured for the development of scour volume over time in Experiment 4A(i); these points did not produce a trend line with an appropriate *a* value that aligned with the hypothesis that *a* values can be used to describe the rate of erosion.

Figure 4-33 shows the *a* values plotted against their respective leak angles. These constants were obtained from the scour volume versus time curves found in Figure 4-30. The *a* value plotted at 90° is the *a* value from the first phase of the scour depth development seen in Figure 4-47. It should also be noted that the a value plotted for Experiment 4A was that from the data for Experiment 4A(ii). This was selected because the three measured data points from Experiment 4A(i) were considered insufficient to perform any reliable regression

analysis. Furthermore, the regression line from these three points did not align with the hypothesis that the *a* values can be used to describe the rate of erosion.

It can be seen in Figure 4-33 that a quadratic trend line was fitted to the data for *a* versus orifice orientation. A quadratic trend line was selected because it was obvious from visual inspections that the damage caused by the horizontal leak was far greater than that caused by the 45° and 90° leaks. This trend line therefore suggests that the effects of the scouring are not linearly proportional to the leak inclination.

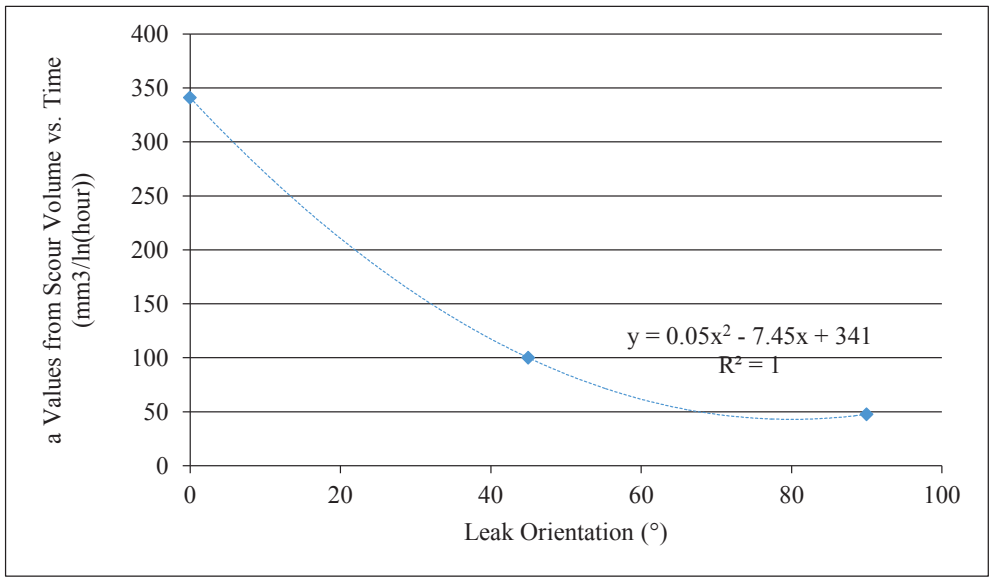

Figure 4-33: Logarithmic Trend Line *a* Values from Figure 4-30 vs. Flow Rate

It is suggested that the effects of the horizontal jet were much more severe than those of the 45° and 90° leaks because it is suspected that the horizontal leak forms a different erosion mechanism to the inclined and vertical leaks. As observed by Bailey (2015) and Pike (2013), for vertical and inclined leaks in a fluidised granular bed, granular particles are drawn in towards the jet adjacent to the orifice which causes the erosion of the pipe surface. It is suspected, however, that in the case of a horizontally leaking jet, the granular particles are entrained in the jet and scraped along the pipe surface with the same velocity as the jet exiting the orifice. Although particles are still drawn into the jet where they scrape along the pipe surface, the particle velocity inside the jet is far greater than that of the particles adjacent to the jet. For this reason, the particles inside the jet have a far greater erosive capacity than those adjacent to the jet. In the case of the horizontal leak, the jet comes into direct contact with the pipe surface, whereas jets at any other inclination are directed away from the pipe surface. The inclination at which the particles entrained in the jet begin to have an effect on the erosion process is unknown.

4.3.6 Experiment 5: Pipe Material

4.3.6.1 Results

4.3.6.1.1 Development of Leak Opening

As it was observed in Experiments 1, 2 and 3, the leaks with 45° orifice orientations in Experiment 5 formed scour patterns with teardrop shapes that were symmetrical about the longitudinal axis of the pipe. This is demonstrated in Figure 4-52. Figure 4-52 shows a comparison between the scour patterns formed on Experiments 5A, 5B and 5C after 80 hours of exposure to the scouring mechanism.

As it can be observed in Figures 4-34 and 4-35, two regions can be identified on the steel pipe's (Experiment 5A) scour pattern. The two regions have been identified in Figure 4-35. The inner region, indicated with an orange ellipse in Figure 4-35, is the same scour pattern that has been observed in the previous experiments on uPVC pipes with a 45° orifice orientation. This is the pattern whose longitudinal and transverse dimensions are the Dimensions A and B that have been measured for all of the previous experiments. In Experiment 5A, this region again exhibited a teardrop shaped pattern that was symmetrical about the pipe's longitudinal axis, with a smooth and polished surface and with an elevated ridge to the right of the orifice. It can also be observed in this inner region that there is a brownish discolouration in the base material. It is assumed that this is a result of corrosion, which may have accelerated the scouring process in this experiment.

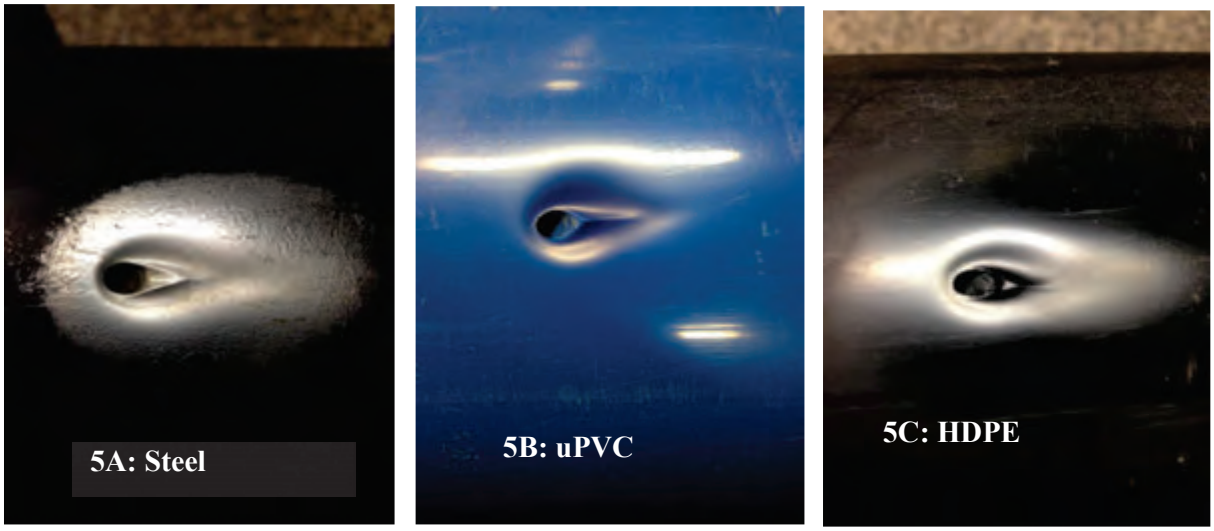

Figure 4-34: Orifice Conditions of Experiment 5 after 80 Hours of Erosion

The outer region of Experiment 5A's scour pattern has been indicated with a blue ellipse in Figure 4-53. This outer region was identified by the removal of the steel's black corrosion-resistant coating. The removal of this coating left the original silver colour of the steel exposed, making it easy to identify this outer region. The outer region of this scour pattern appeared slightly rougher than the inner region since it had not experienced the same aggressive material removal mechanism as that of the inner region. This surface roughness

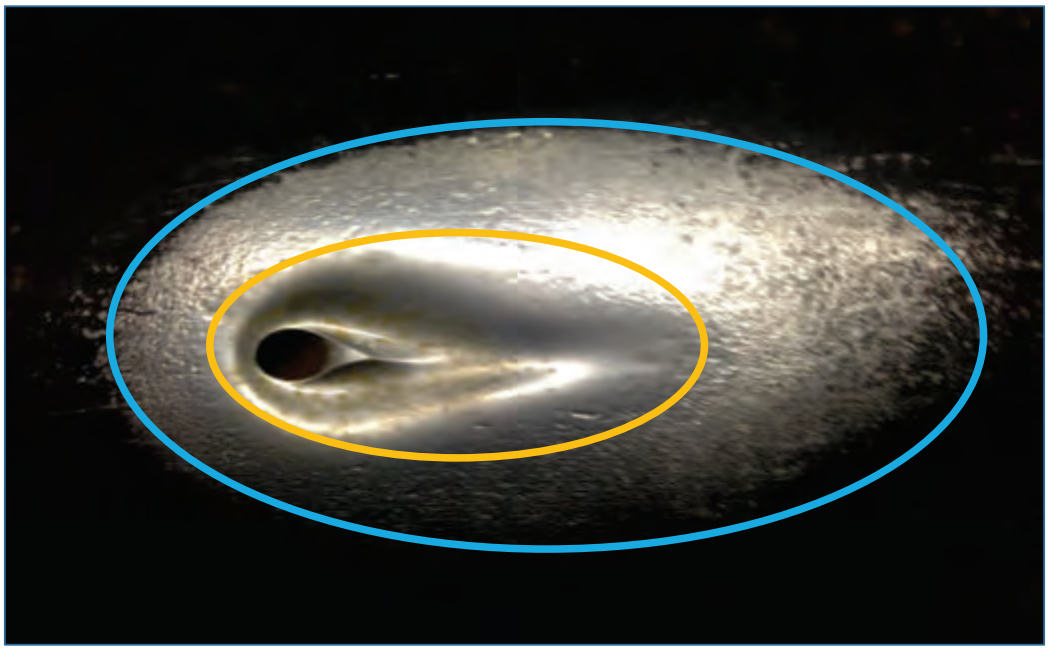

Figure 4-35: Regions of Scour Pattern on Steel Pipe

that can be observed in the outer region of the scour pattern is the pipe material's natural surface condition. It is proposed that further away from the orifice, the slower moving particles in the mobile bed zone had a lesser effect on removing pipe material than that of the fast moving particles adjacent to the orifice in the fluidised zone. The scour depth in this outer region is presumably in the order of microns, and was not observable to the naked eye in previous experiments where uPVC was used. In terms of mechanical future pipe failure, the scour depth in the outer region is negligible, however, this does leave the pipe material vulnerable to corrosion. The longitudinal and transverse dimensions of this outer region were measured, and can be found in Appendix A.

Figure 4-36 shows a visual inspection of the development of Experiment 5A's scour pattern over time. As shown in Figure 4-54, both the inner and the outer regions of the scour pattern grew over time. It can also be observed visually that the scour depth of the inner region increased over time.

Experiment 5C (HDPE pipe) displayed similar scour patterns to those that have been previously observed in experiments with 45° orifice orientations. Figure 4-37 gives a visual inspection of the development of the scour pattern for Experiment 5C. It can be seen that this test yielded a teardrop shape that was symmetrical about the pipe's longitudinal axis. The surface of the pipe in the scour-affected region was smooth and polished. It can be observed from the visual inspection that the scour pattern did not form clearly in the first 20 hours of exposure to the scouring.

Figure 4-36: Visual Development of Experiment 5A's Scour Pattern

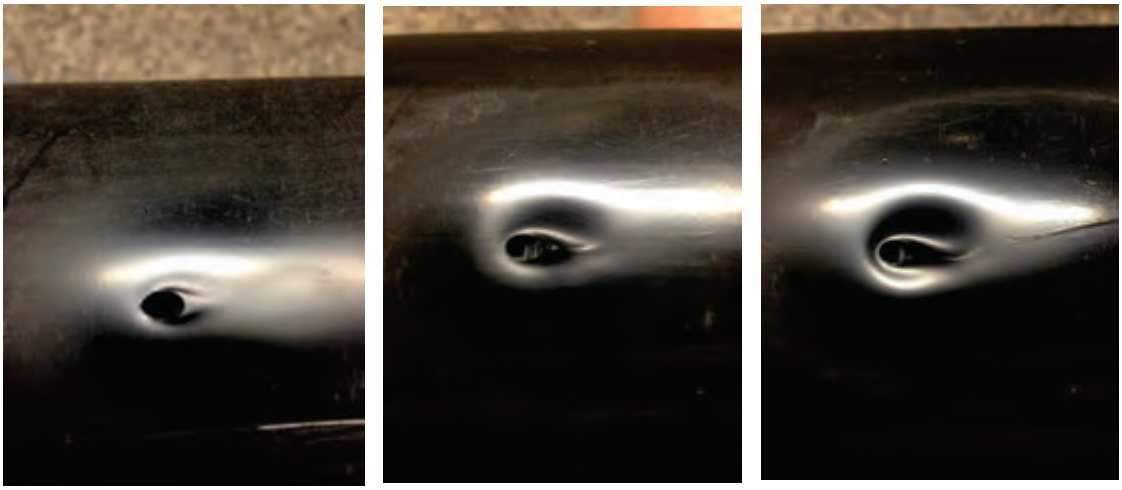

Figure 4-37: Visual Development of Experiment 5C's Scour Pattern

4.3.6.1.2 Volume of Removed Material

Figure 4-38 illustrates how the volume of pipe material was removed from the pipe surface adjacent to the orifice over time. Logarithmic trend lines were fitted to the volume removed versus time data for Experiment 5. These logarithmic trend lines fitted the data well for all three experiments, with R^2 values of greater than 0.93. The final point of the data for Experiment 5C was excluded from this trend line, since appeared to be an anomaly in this data set. Up until the time of 182 hours, material was being removed from this pipe sample the slowest of the three tests. Between the times of 182 and 298 hours, however, the volume of material removed from pipe sample 5C increased to greater than that of 5A, as shown in Figure 4-38. It is suspected that an experimental error occurred during this period of the testing, since it is expected that the rate of material removal would continue to be the slowest of the three tests during this period. Including this final data point in the calculation of the trend line for Experiment 5C gives an R^2 value of 0.84, as opposed to 0.93 without it.

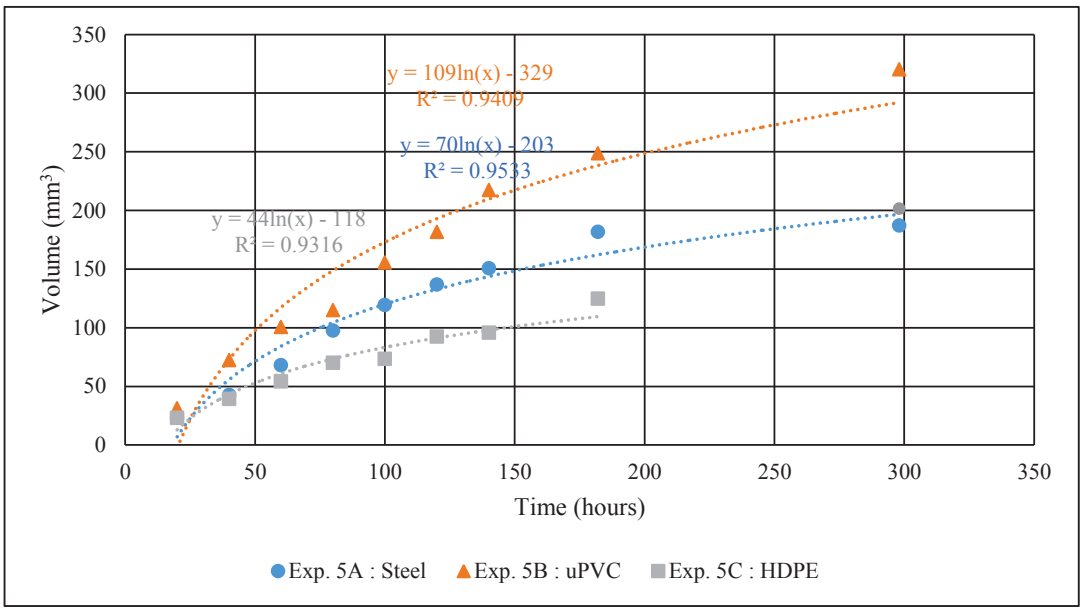

Figure 4-38: Volume of Removed Material for Experiment 5

Figure 4-38 shows that uPVC was the most erodible in terms of removal of pipe material. It also shows that steel eroded the second fastest, and that HDPE was the least susceptible to the effects of the scouring

4.3.6.2 Discussion

Figure 4-38 indicates that uPVC erodes faster than HDPE in terms of scour volume. As shown by Figures 2-21 and 2-23 in Section 2.7, this concurs with the findings of Goddard (1994) and ADS (2012). It is clearly illustrated in Figures 2-21 and 2-23 that HDPE exhibits a greater resistance to abrasion than PVC. Figure 2-20 also suggests that steel is more erodible than polyethylene (PE). This figure does not specify which type of polyethylene was tested (HDPE, LDPE, MDPE etc.), however, it does agree with the results displayed in Figure 4-38, in that material was removed faster from the steel pipe than the HDPE Pipe

In order to compare and build an empirical equation to describe how scour depth and volume removal increase with time, it is necessary to compare the *a* values from the scour volume removed versus time graphs.

The *a* values for the volume removed versus time graph is summarised in Table 4-2.

If it is assumed that uPVC is the standard or "normal" condition, then the *a* values of the steel and HDPE pipes can be expressed as a ratio to those values of uPVC. These ratios can then be used as "material coefficients" in an empirical equation describing how the scouring process progresses with time. Table 4-8 summarises the ratios of each material's *a* and *b* values to those of uPVC's.

Table 4-2: *a* Values for Scour Volume versus Time from Experiment 5

	a Value	Material Coefficient
Steel	70.214	0.644
uPVC	109.02	1
HDPE	43.708	0.401

4.3.7 Experiment 6: Shape of Suspended Zone

4.3.7.1 Introduction

Three experiments were performed simultaneously as described in Section 3.5.1., namely Experiments 6A, 6B and 6C. The primary purpose of these experiments were to test that the apparatus was working adequately for the investigation to come, and that the proposed methods of data collection were satisfactory. The operating conditions of the three tests are given in Table 4-10. It should be noted that the orifice orientation was vertical (90°) for all three of these tests.

The primary difference between these three experiments was the grain size of the bedding material as indicated in Table 4-10. It should also be noted in Table 4-10 that the flow rates differ between the three tests. This is because there were no PRV's on the individual test boxes. The only pressure control device was a PRV at the inlet of the delivery pipe. For this reason, a head loss was experienced between the water supply and the three test boxes, and hence, the test box furthest from the supply had a lower flow rate than the test closest to the supply. The average recorded operating flow rate for each test is quoted in Table 4-10 below.

Table 4-3: Operating Conditions for Experiment 4

Experiment	Flow Rate (l/h)	Grain Size (D_{50}) (mm)	Cover Depth (mm)	Pipe Material -	Leak Orientation (°)	Orifice Diameter (mm)
6A	395	**2.10**	500	uPVC	90	3
6B	375	**1.60**	500	uPVC	90	3
6C	352	**0.75**	500	uPVC	90	3

4.3.7.2 Results

Upon excavation, discoloured regions of sand were observed vertically above the orifices of the three tests, which were assumed to represent the mobile bed zones. Figure 4-39 below is the result of plotting the measured diameters of the discoloured circles against their corresponding measured heights. It should be noted that in this graph, the orifice of each experiment is situated at the position (0; 0) on this set of axes.

It is interesting to note that despite test 0A running at a greater flow rate than tests 0B and 0C as shown in Table 4-3, the maximum height of the mobile bed zone for test 0A was significantly smaller than that of test 0B. Similarly, the maximum height of the mobile bed zone of test 0B was smaller than that of test 0C, despite its test 0B's greater flow rate. It is also interesting to note that the maximum width of the mobile bed zone for each case was

approximately the same, however, the larger the grain size, the wider the area of influence at the level of the orifice.

From this information, it seems evident that the fluidisation and mobile bed zones penetrate further into soil beds with smaller grain sizes.

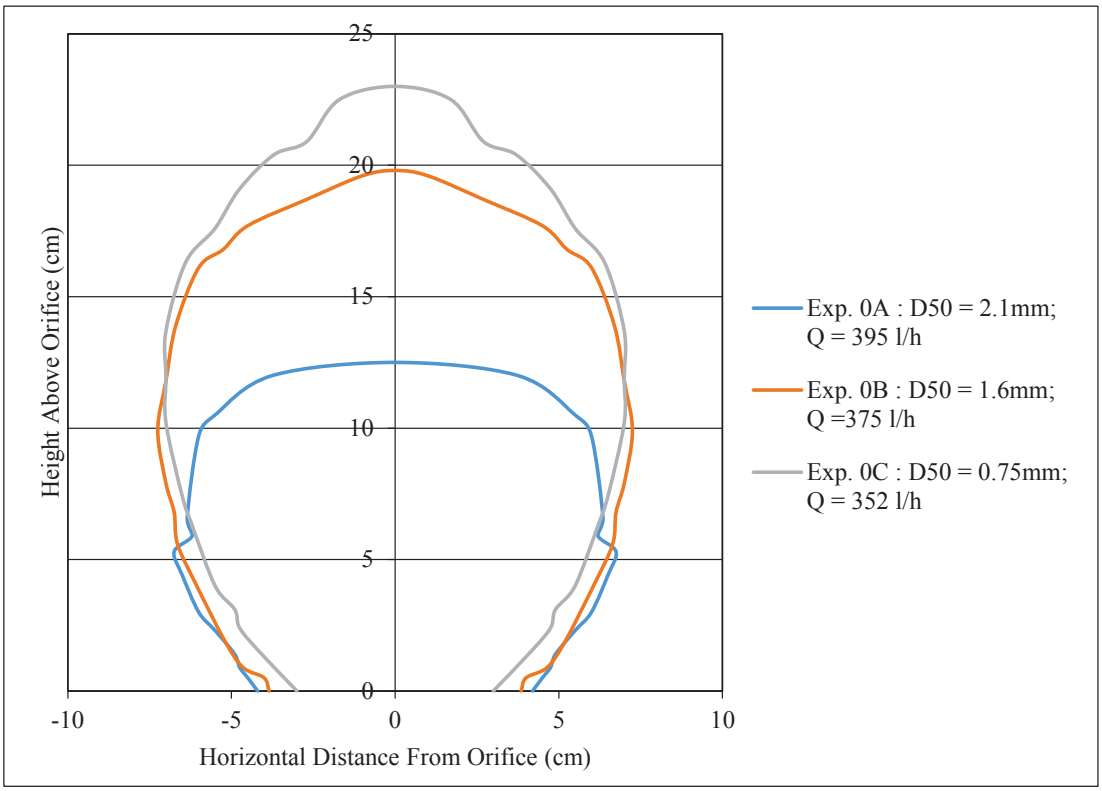

Figure 4-39: Shape of Mobile Bed Zone for Experiment 0

4.4 Discussion

4.4.1 General Observations

With the exception of Experiment 1, it was observed in all of the experiments that the scour progressed in a logarithmic fashion in terms of Dimensions A, B, scour volume and scour depth with respect to time. The erosion process happens faster during the initial phases of the testing because there is a lot of pipe material near the orifice to be removed. As the test progresses, there is less material to be removed from around the orifice, and hence the rate of erosion decreases. A similar trend can be observed in clear-water scour around abutments as previously discussed in Section 2.6.4. As material is removed from around the abutments, the rate of scour decreases, resulting in a logarithmic scour versus time relationship.

4.4.2 Sensitivity of Scour to Influencing Factors

This study demonstrated that five different factors have an effect on the rate of leakage-induced pipe erosion. It was found that the pipe material was removed logarithmically with time, both in terms of scour volume and scour depth. Equations in the form $y=a\cdot\ln(t)+b$ were used to describe how the scour depths and scour volumes increased with respect to time for the five experiments. The effect of each of the five factors was quantified in terms of the *a* values of the logarithmic trend.

Table 4-4 reports the *a* values of the scour volume versus time logarithmic trend lines for each of the experiments.

Table 4-4: *a* Values for Experiments 1 to 5 Scour Volume versus time Graphs

Experiment		Volume
1	A	182
	B	149
	C	49
2	A	121
	B	130
	C	125
3	A	171
	B	114
	C	10
4	A(i)	160
	A (ii)	341
	B	100
	C	48
5	A	70
	B	109
	C	44

Figure 4-40 is a spider plot which describe the sensitivity of *a* to the five factors that were tested, namely grain size, cover depth, flow rate, leak orientation and pipe material. In Figure 4-40, the x-axis shows the experiment ID (A, B or C), and the *a* values have been plotted on the y-axis against their corresponding experiment IDs. The *a* value plotted for Experiment 4A were those found in Experiment 4A(ii) rather than 4A(i), since a time-dependent scour relationship was not obtained for Experiment 4A(i). The *a* value plotted for Experiment B in each case was the average *a* value found by combining the data from Experiments 2 to 5 as shown in Figure 4-1.

Figure 4-40 shows clearly that the greatest range of *a* values was found in Experiment 4, which examined the effect of leak orientation. Figure 4-40 indicates that the horizontal leak (Experiment 4A) caused the greatest rate of erosion out of the 15 tests that were performed in this study. As it was discussed in Section 4.3.5, it is suggested that this was the case because the horizontal leak formed a different scouring mechanism to the remaining 14 tests.

It can also be observed in Figure 4-40 that changes in the grain size and leakage flow rate resulted in large ranges of *a* values. This suggests that variations in these parameters have significant effects on the rate of scour.

Figure 4-40 also indicates that variations in cover depth have a negligible effect on the rate of erosion. It should be noted, however, that a relatively small range of cover depths (300-500mm) was tested during this study.

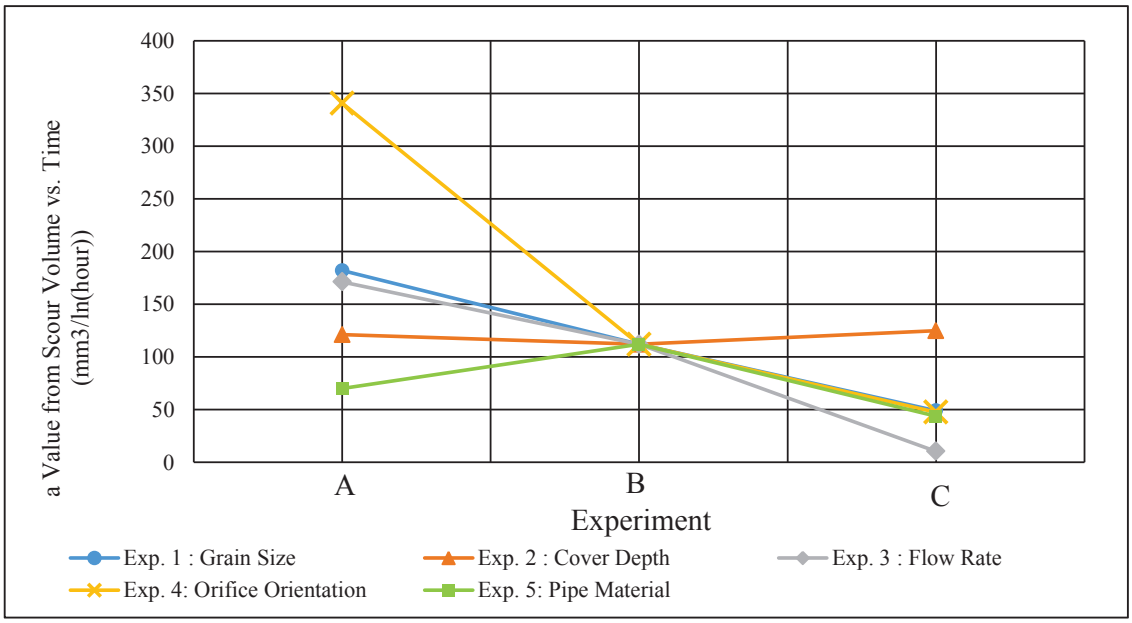

Figure 4-40: Sensitivity of a Value for Scour Volume versus Time

As expected from literature, the different pipe materials exhibited different amounts of resistance to erosion. However, as shown in Figure 4-40, the effects of the pipe material were relatively small in comparison to the effects of orifice orientation, grain size and cover depth.

A more intuitive parameter by which of quantifying the effect of each factor is to illustrate the volume of material removed from each experiment. Figure4-41 is a tornado diagram where each bar represents the range of scoured volume at 180 hours of exposure to the abrasion for each set of experiments. The mean value of material removed for the control experiment at 180 hours of scouring was 252mm^3. It can be observed in Figure that at 180 hours of scouring, the leak orientation had the largest range of removed scour volume. This suggests that the effect of leak orientation was the most influential factor in changing the rate of leakage-induced pipe erosion.

It can be said from Figure that the second most influential factor in changing the rate of leakage-induced pipe erosion is the flow rate, followed by grain size.

In the context of this experiment, the cover depth and pipe material had the least and second least significant impacts on leakage-induced pipe erosion respectively.

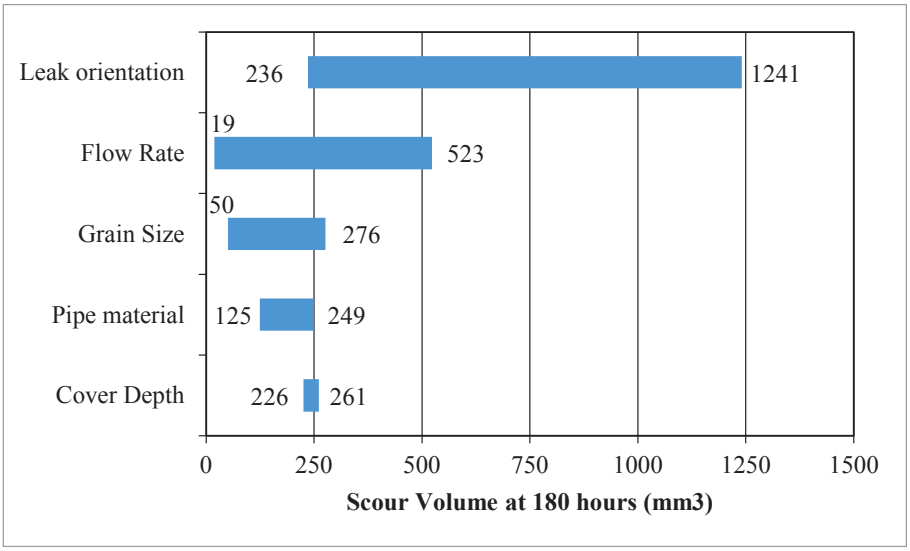

Figure 4-41: Tornado Plot of Maximum and Minimum Scour Volumes for each Experiment at 180 hours

4.4.3 Applications of Findings

The findings in this study are intended to have practical applications that aim to reduce leakage in water distribution systems. This study has identified five factors that have the potential to change the rate and the severity of leakage-induced pipe erosion. With this knowledge, leakage in water distribution systems can be reduced by either contractors or operation and maintenance teams.

The knowledge developed in this study can be used to the advantage of water authorities in one of two ways:

1. In water authorities who have regular active leak detection programmes, it would be advantageous to accelerate the leakage-induced pipe erosion process on existing leaks so that the leaks become easier to find.
2. In water authorities that do not implement active leak detection programmes, it would be beneficial to decrease the rate of leakage-induced pipe erosion so as not to exacerbate existing leak conditions.

It was found in this study that increasing the grain size of the bedding material increases the rate of erosion. With this in mind, it is suggested that during the construction of water distribution systems, the grain size be selected to compliment the local water authorities' operation and maintenance plan, i.e. if the water authority intends on implementing active leak detection, then a larger grain size should be used for the bedding material to increase the rate of leakage-induced pipe erosion, and vice versa.

While it was shown that the cover depth could change the rate of erosion, the spider plots in Section 4.4.2 show that the effect of a change in bed height (in the range of 300mm to 500mm) had a negligible effect on the rate of scour. By South African Standards, pressurised water pipes must have a minimum cover of 700mm (CSIR, 2011). While the experiments presented in this study utilised cover depths less than this depth, it is suggested that the range of cover depths used in this study (200mm) is typical of a water distribution system since cover depths are kept to a minimum during construction to minimize excavation costs. It is therefore suggested that adjusting the cover depth of a pipeline in a water distribution system for the sole purpose of benefitting from leakage-induced pipe erosion would not be feasible.

It was demonstrated in this study that the leakage flow rate has a significant influence on the rate of leakage-induced pipe erosion. The greater the flow rate, the greater the rate of erosion. This fact should further incentivise the utilisation of pressure management schemes in water authorities that do not make use of active leak detection techniques. Among other benefits, pressure management schemes will reduce the effects of leakage-induced pipe erosion. It is known that decreasing the pressure in a water distribution system will decrease the leakage flow rate, and hence reduce the effects the erosion. This is desirable if small leaks will be leaking for extended periods of time, so as not to aggravate the initial leak conditions.

It was also shown in this study that the orifice orientation has a significant effect on the development of the scour. While the formation and orientation of the leak is largely out of the control of the water authority, this study showed that leaks running parallel to the pipe's surface cause the most erosive damage. These types of leaks are most likely to form at saddle connections and uPVC socket connections. It is therefore suggested that when actively detecting leaks, that these types of connections be inspected first since these are the places where erosion is likely to be most severe.

Finally, it was shown that different pipe materials erode at different rates. It is suggested that an appropriate pipe material be selected during the design of water distribution systems. It is suggested that if the system is being designed for a water authority that utilises active leak detection techniques, that a more erodible material, e.g. uPVC, be selected.

Alternatively, in places where active leak detection will not be implemented, it is suggest that a less erodible material, e.g. HDPE, be selected for the construction of the system.

5. Conclusions

5.1 Introduction

An experimental study was performed to investigate the effects of five different factors on the process of leakage-induced pipe erosion. The five factors that were investigated were bedding material grain size, cover depth, flow rate, initial leak orientation and pipe material. The effects of these factors were investigated with five sets of experiments. Each set of experiments comprised three tests running simultaneously. The three tests in each experiment included one control test with defined standard conditions, and two tests in which one of the aforementioned factors was varied to different degrees.

The experimental setup consisted of a water supply feeding into a buried pipe specimen with a manufactured orifice to simulate a leak. The pipe sample was left to leak, and was excavated regularly to examine the orifice condition. The effects of the erosion were documented visually and quantitatively.

The most influential factors that affect the rate of leakage-induced pipe erosion were identified with a sensitivity analysis. It was then suggested how the findings of this study translate into practical applications.

5.2 Main Conclusions

The key findings from this study were the following:

- The testing procedure developed for this study provided consistent and repeatable results for four out of the five control experiments. It can be said that the discrepancy in the results from the first test was a result of a different bulk density. Therefore, although it was not explicitly tested, it can be said that the degree of compaction of a soil bed has an effect on the leakage-induced scouring process.
- In general, the four parameters that were measured to quantify the erosion (Dimension A, Dimension B, scour volume and scour depth) increased logarithmically with time. It was observed in the vast majority of cases that these four dimensions increased rapidly during the initial stages of each test, and continued to increase at a decreasing rate as the tests progressed. This is largely due to the fact that pipe material closer to the initial orifice is eroded more easily than pipe material further away. Once the close material has been eroded, the rate of material removal decreases.
- The process of leakage-induced pipe erosion has the potential to aggravate initial leak conditions. It was observed that leaks with different orifice orientations, flow rates and bedding material types were able to increase the initial orifice area, be it by enlarging the initial orifice or creating a second orifice nearby.

- It was found that the rate of leakage-induced pipe erosion increases with increasing bedding material particle size for the range of particle sizes that was tested in this study.
- It was found that the bedding material particle size influences the size of the suspended zone. It was shown that the larger the soil grain size, the smaller the suspended zone.
- This study showed that the effect of cover depth (within the tested range) on the rate of erosion was small in comparison to the effects of the other factors.
- The leakage flow rate also has a prominent effect on the rate of erosion. It was found that the greater the flow rate, the faster the pipe erodes.
- It was found that orifice orientation has a significant effect on the mechanism of leakage-induced pipe erosion. A leak running parallel to the pipe surface has the capacity to erode a pipe rapidly and exacerbate the initial leak. Inclined leaks and leaks normal to the pipe surface are also capable of causing damage to the pipe surface, but to a lesser degree than the parallel jet.
- This study showed that different pipe materials exhibit different amounts of scour resistance. Of the three pipe materials that were tested, uPVC was the most susceptible to erosion, while steel and HDPE displayed a lesser degree of erodibility.

5.3 Recommendations for Further Work

It was found in this study that the rate of erosion increased logarithmically with increasing bedding material grain size. It was suggested in the literature, however, that after the grain size increases beyond a certain size, the rate of erosion will begin to decrease. It is suggested that further work be undertaken to determine the grain size after which the rate of erosion will begin to decrease, and at what grain size erosion will no longer take place.

It is further suggested by the logarithmic relationship of the grain size and rate of erosion that there is a minimum grain size at which the erosion process will be initiated. It is recommended that further work be undertaken to determine this grain size.

In this study, the initial orifice was 3mm in diameter for all of the tests. It is recommended that the effects of different orifice shapes and sizes be explored.

All of the orifices in this study were situated on the upper-most surface of the pipe. It is recommended that further testing is done to investigate whether orifices situated on alternate locations e.g. the side or the bottom surfaces will experience the same type of erosion that was found in this study.

It is recommended that the effects of bulk density on the leakage-induced pipe erosion process be investigated in future work.

Lastly, the experiment examining the effect of cover depth showed inconclusive results. It is unknown whether these results were found because of the small range of cover depths

that were tested, or whether the cover depth has a negligible effect on the erosion process. It is recommended that a larger range of cover depths be tested.

6. References

ADS. 2012. *Abrasion Resistance of Polypropylene*. V. 43026. Available: http://www.ads-pipe.com/pdf/en/a4.03-abrasion_resistance_of_polypropylene.pdf.

Alcamo, J., Henrichs, T. & Rösch, T. 2000. *World Water in 2025 World Commission on Water for the 21 Century*. Kassel.

Alsaydalani, M.O.A. & Clayton, C.R.I. 2014. Internal Fluidization in Granular Soils. *Journal of Geotechnical and Geoenvironmental Engineering*. 140:1–10. DOI: 10.1061/(ASCE)GT.1943-5606.0001039.

American Concrete Pipe Association. 2011. *Concrete Pipe Design Manual*. Available: http://www.cement.org/cement-concrete-basics/concrete-products/concrete-pipe.

Anderson, A.G. 1963. Sediment transportation mechanics:erosion of sediment. *Journal of Hydraulic Division, American Society of Civil Engineers*. 89:237–248.

ASTM D4060-14. 2014. *Standard Test Method for Abrasion Resistance of Organic Coatings by the Taber Abraser*. West Conshohocken, PA. DOI: 10.1520/D4060-14.

ASTM International. 2006. *Standard Test Method for Permeability of Granular Soils (Constant Head) 1*. West Conshohocken, Pennsylvania. DOI: 10.1520/D2434-68R06.2.

ASTM International. 2015. *Standard Test Methods for Minimum Index Density and Unit Weight of Soils and Calculation of Relative Density*. West Conshohocken, Pennsylvania. DOI: 10.1520/D4254-14.2.

Bailey, N.D. 2015. Development and testing of experimental equipment to measure pore pressure and dynamic pressure at points outside a pipe leak. University of Cape Town.

Barbhuiya, A.K. & Dey, S. 2004. Local scour at abutments: A review. *Sadhana*. 29(5):449–476. DOI: 10.1007/BF02703255.

Bouzid, S. & Bouaouadja, N. 2000. Effect of impact angle on glass surfaces eroded by sand blasting. *Journal of the European Ceramic Society*. 20(May 1999):481–488.

Briaud, B.J., Ting, F.C.K., Chen, H.C., Gudavalli, R. & Perugu, S. 1999. SRICOS: Prediction of Scour Rate in Cohesive Soils at Bridge Piers. *Journal of Geotechnical and Geoenvironmental Engineering*. 125(April):237–246.

Briaud, J.L., Ting, F.C.K., Chen, H.C., Gudavalli, R., Peruga, S. & Wei, G. 1999. Sricos: Prediction of Scour Rate in Cohesive soild at Bridge Piers. *Journal of Geotechnical and Geoenvironmental Engineering*. 125(4):237–246.

Briaud, J.L., Ting, F.C.K., Chen, H.C., Cao, Y., Han, S.W. & Kwak, K.W. 2001. Erosion Function Apparatus for Scour Rate Predictions. *Journal of Geotechnical and Geoenvironmental Engineering*. 127(2):105–113.

British Standards Institution. 1990. *BS 1377-2:1990 Methods of test for soils for civil engineering purposes Part 2: Classification tests*.

Cardoso, A.H. & Bettess, R. 1999. Effects of Time and Channel Geometry on Scour at Bridge Abutments. *Journal of Hydraulic Engineering*. 125(April):388–399.

Cassa, a. M., van Zyl, J.E. & Laubscher, R.F. 2010. A numerical investigation into the effect of pressure on holes and cracks in water supply pipes. *Urban Water Journal*. 7(2):109–120. DOI: 10.1080/15730620903447613.

Clayton, C.R.I., Abbireddy, C.O.R. & Schiebel, R. 2009. A method of estimating the form of coarse particulates. *Géotechnique*. 59(6):493–501. DOI: 10.1680/geot.2007.00195.

Coetzer, A.J., van Zyl, J.E. & Clayton, C.R.I. 2008. Experimental Study of The Hydraulics of Small Circular Holes in Water Pipes . University of Johannesburg PO.

Consol. 2014. *Consol Mineral Products*. Available: http://www.consol.co.za/business/products/minerals [2015, October 13].

Craig, R.F. 2004. *Craig's Soil Mechanics*. Seventh Ed ed. London: Taylor and Francis.

CSIR. 2011. *Guidelines for human settlement planning and design: The red book*. Pretoria: Council for Scientific and Industrial Research. DOI: 10.1007/SpringerReference_85090.

Dumbleton, B. 1996. Hunting Down Water Leaks. *Water Engineering an Management*. 143(10):27–28.

Farley, M. & Trow, S. 2003. *Losses in Water Distribution Networks*. London: IWA Publishing.

Gent, M., Menéndez, M., Torno, S., Toraño, J. & Schenk, a. 2012. Experimental evaluation of the physical properties required of abrasives for optimizing waterjet cutting of ductile materials. *Wear*. 284-285:43–51. DOI: 10.1016/j.wear.2012.02.012.

Goddard, J.B. 1994. *Abrasion Resistance of Piping Systems*. Hilliard. Available: http://www.ads-pipe.com/pdf/detret/technical note 2.116 - abrasion resistance.pdf.

Greyvenstein, B. & van Zyl, J.E. 2005. An Experimental Investigation into the Pressure Leakage Relationship of some failed water pipes. *Journal of Water Supply Research and Technology*. 56(2):1–10.

Guo, S., Zhang, T., Shao, W., Zhu, D.Z. & Duan, Y. 2013. Two-dimensional pipe leakage through a line crack in water distribution systems. *Journal of Zhejiang University SCIENCE A*. 14(5):371–376. DOI: 10.1631/jzus.A1200227.

Ha, C.-S., Kim, Y., Lee, W.-K., Cho, W.-J. & Kim, Y. 1998. Fracture toughness and properties of plasticized PVC and thermoplastic polyurethane blends. *Polymer*. 39(20):4765–4772.

Haas, D.B. & Smith, L.G. 1975. *Erosion Studies - A Report to Dupont of Canada, Ltd*. Saskatchewan.

de Kater, H. 2014.

Kato, K. & Adachi, K. 2001. *Wear Mechanisms*.

Lahlou, Z.M. 2001. *Leak Detection and Water Loss Control*. Lynchburg.

Lambert, A. 2001. What do we Know about Pressure : Leakage Relationships In Distribution Systems ? In *IWA Conference System Approach to Leakage Control and Water Distribution Systems Management*. Brno, Czech Republic. 1–8.

Lambert, A. & Hirner, W. 2000. *Losses from Water Supply Systems: Standard Terminology and Recommended Performance Measures*.

Levin, J. 1989. Observations on the Bond standard grindability test , and a proposal for a standard grindability test for fine materials. *Journal of South African Institute for Mining and Metallurgy*. 89(1):13–20. DOI: 10.1016/0148-9062(89)91143-1.

Luo, J. & Dornfeld, D. a. 2001. Material removal mechanism in chemical mechanical

polishing: theory and modeling. *IEEE Transactions on Semiconductor Manufacturing*. 14(2):112–133. DOI: 10.1109/66.920723.

Ma, C.H. 2011. Internal Fluidisation due to Horizontal Seepage – A Laboratory Study. University of Southampton.

Majid, Z.A. & Mohsin, R. 2013. Multiple failures of API 5L X42 natural gas pipeline. *Engineering Failure Analysis*. 31:421–429. DOI: 10.1016/j.engfailanal.2013.02.012.

Majid, Z. a., Mohsin, R., Yaacob, Z. & Hassan, Z. 2010. Failure analysis of natural gas pipes. *Engineering Failure Analysis*. 17(4):818–837. DOI: 10.1016/j.engfailanal.2009.10.016.

Majid, Z. a., Mohsin, R. & Yusof, M.Z. 2012. Experimental and computational failure analysis of natural gas pipe. *Engineering Failure Analysis*. 19:32–42. DOI: 10.1016/j.engfailanal.2011.09.004.

Majid, Z.A., Mohsin, R. & Yusof, M.Z. 2011. Erosive Wear of Natural Gas Pipes Due to High Velocity Jet Impact: Computer Simulation Study. *Jurnal Teknologi*. 56(1):27–52.

Marunga, A., Hoko, Z. & Kaseke, E. 2006. Pressure management as a leakage reduction and water demand management tool: The case of the City of Mutare, Zimbabwe. *Physics and Chemistry of the Earth, Parts A/B/C*. 31(15-16):763–770. DOI: 10.1016/j.pce.2006.08.032.

Maury, A., Ouma, D., Boning, D. & Chung, J. 1997. Available: http://www-mtl.mit.edu/researchgroups/Metrology/PAPERS/AdvMetal97.pdf.

Mckenzie, R., Siqalaba, Z.N. & Wegelin, W.A. 2012. *The state of non-revenue water in South Africa*. Pretoria.

Melville, B.W. & Coleman, S.E. 2000. *Bridge Scour*. Highlands Ranch: Water Resources Publications.

Miryala, A., Scarlett, K., Zell, Z. & Kountz, B. 2013. *Flow Sensors*. Available: https://controls.engin.umich.edu/wiki/index.php?title=FlowSensors&oldid=77069 [2015, December 23].

Mohsin, R. & Majid, Z. 2014. Erosive Failure of Natural Gas Pipeline. *Journal of Pipeline Systems Engineering and Practice*.

Mora-Rodríguez, J., Delgado-Galván, X., Ramos, H.M. & López-Jiménez, P.A. 2013. An overview of leaks and intrusion for different pipe materials and failures. *Urban Water Journal*. 11(1):1–10. DOI: 10.1080/1573062X.2012.739630.

Mutikanga, H.E., Sharma, S.K. & Vairavamoorthy, K. 2013. Methods and Tools for Managing Losses in Water Distribution Systems. *Journal of Water Resources Planning and Management*. (April):166–174. DOI: 10.1061/(ASCE)WR.1943-5452.0000245.

Negonga, T. 2013. Investigation of the Effects of Soil Material Grade and Flow Rate on the Scouring of PVC Water Distribution Pipes due to Soil Fluidisation. University of Cape Town.

Niven, R.K. & Khalili, N. 1998. In situ fluidisation by a single internal vertical jet. *Journal of Hydraulic Research*. 36(2):199–228. DOI: 10.1080/00221689809498633.

O'Day, D.K., Weiss, R., Chiavari, S., Blair, D. & Clark, R.M. 1986. Water main evaluation for rehabilitation/replacemen. In *AWWA Research Foundation*. Denver.

Pike, S. 2013. Scouring Patterns of Pipes outside Leaks due to Soil Agitation.

University of Cape Town.

Preston, F. 1927. The theory and design of plate glass polishing machines. *Journal of the Society of Glass Technology*. 11:214–256.

Rajani, B., Zhan, C. & Kuraoka, S. 1996. Pipe-soil interaction analysis of jointed water mains. *Canadian Geotechnical Journal*. 33(3):393–404.

Raudkivi, B.A.J. & Ettema, R. 1983. CLEAR-WATER SCOUR AT CYLINDRICAL PIERS. *Journal of Hydraulic Engineering*. 109(3):338–350.

Richards, K.S. & Reddy, K.R. 2007. Critical appraisal of piping phenomena in earth dams. *Bulletin of Engineering Geology and the Environment*. 66(4):381–402. DOI: 10.1007/s10064-007-0095-0.

Rijsberman, F.R. 2006. Water scarcity: Fact or fiction? *Agricultural Water Management*. 80(1-3):5–22. DOI: 10.1016/j.agwat.2005.07.001.

Seago, C., Bhagwan, J. & Mckenzie, R. 2004. Benchmarking leakage from water reticulation systems in South Africa. 30(5):25–32.

Seckler, D., Amarasinghe, U., Molden, D., de Silva, R. & Barker, R. 1990. *World Water Demand and Supply, 1990 to 2025: Scenarios and Issues*. Colombo.

"South African Bureau of Standards Standardized Specification for Civil Engineering Construction Bedding (Pipes)". 1983.

Stabik, J., Makselon, M. & Tomanek, H. 2007. Erosion resistance testing of plastic pipes. *Journal of Achievements in Materials and Manufacturing Engineering*. 25(2):47–50.

van Thienen, P. 2014.

Vörösmarty, C.J., Green, P., Salisbury, J. & Lammers, R.B. 2000. Global Water Resources: Vulnerability from Climate Change and Population Growth. *Science*. 289(14 July 2000):284–288. Available: http://water-pire.uci.edu/wp-content/uploads/2013/08/1_Hao_Science-2000-Vörösmarty-284-8.pdf [2014, March 26].

Wallace, J.. 2000. Increasing agricultural water use efficiency to meet future food production. *Agriculture, Ecosystems & Environment*. 82(1-3):105–119. DOI: 10.1016/S0167-8809(00)00220-6.

Wallace, J.S. & Gregory, P.J. 2002. Water resources and their use in food production systems. *Aquatic Sciences*. 64(4):363–375. DOI: 10.1007/PL00012592.

Walski, T., Bazts, W., Posluszny, E.T., Weir, M. & Whitman, B.E. 2006. Modeling leakage reduction through pressure control. *American Water Works Association*. (April):147–155.

Walski, T., Whitman, B., Baron, M. & Gerloff, F. 2009. Pressure vs . Flow Relationship for Pipe Leaks. In *World Environmental and Water Resources Congress*. Kansas City, Missouri: American Society of Civil Engineers. 93–102.

Water Services Association of Australia. 2012. *Failure Modes in Pressurised Pipeline Systems*.

Wiebking, H. 1998. *Fillers in Pvc a Review of the Basics*. Easton, PA.

Yang, F. & Hlavacek, V. 1999. Improvement of PVC wearability by addition of additives. *Powder Technology*. 103(2):182–188.

Yang, H., Reichert, P., Abbaspour, K.C. & Zehnder, A.J.B. 2003. A water resources

threshold and its implications for food security. *Environmental science & technology*. 37(14):3048–54. Available: http://www.ncbi.nlm.nih.gov/pubmed/12901649.

Yang, Y., Zhang, T. & Zhu, D.Z. 2014. Influence of porous media on intrusion rate into water distribution pipes. *Journal of Water Supply: Research and Technology—AQUA*. 63:43. DOI: 10.2166/aqua.2013.213.

Zmitrowicz, A. 2006. Wear Patterns and Laws Of Wear – A Review. *Journal of Theoretical And Applied Mechanics*. 44(2):219–253.

Zok, F.W. & Miserez, a. 2007. Property maps for abrasion resistance of materials. *Acta Materialia*. 55(18):6365–6371. DOI: 10.1016/j.actamat.2007.07.042.

van Zyl, J.E. & Clayton, C.R.I. 2007. The effect of pressure on leakage in water distribution systems. *ICE - Water Management*. 160(2):109–114. DOI: 10.1680/wama.2007.160.2.109.

van Zyl, J.E., Alsaydalani, M.O. a, Clayton, C.R.I., Bird, T. & Dennis, A. 2013. Soil fluidisation outside leaks in water distribution pipes – preliminary observations. *Water Management*. 166(WM10):546–555. DOI: 10.1680/wama.11.00119.

7. Appendices

Appendix A : Experimental Data

Appendix B : Sand Characterisation

Appendix C : Volumetric Measurement

Appendix A: Experimental Data

7.1 Experiment 0: Pilot Experiment

Experiment	Flow Rate (l/h)	Grain Size (D_{50}) (mm)	Cover Depth (mm)	Pipe Material -	Leak Orientation (°)	Orifice Diameter (mm)
0A	395	**2.10**	500	uPVC	90	3
0B	375	**1.60**	500	uPVC	90	3
0C	352	**0.75**	500	uPVC	90	3

Operating Conditions of Pilot Experiment

7.1.1 Quantitative Data

Quantitative Data – Experiment 0A

Time (h)	Scour Diameter (mm)	Depth (mm)	Mass Putty (g)	Volume (mm^3)
0	3.00	0	0	0
20	9.90	0.12	-	-
40	11.22	0.18	0.052	25.12
60	13.30	0.22	0.074	35.75
80	13.80	0.28	0.125	60.39

Quantitative Data – Experiment 0B

Time (h)	Scour Diameter (mm)	Depth (mm)	Mass Putty (g)	Volume (mm^3)
0	3	0	0	0
20	7.24	0.08	-	-
40	8.90	0.12	0.027	12.85
60	10.62	0.18	0.049	23.33
80	10.72	0.24	0.072	34.29

Quantitative Data – Experiment 0B

Time (h)	Scour Diameter (mm)	Depth (mm)	Mass Putty (g)	Volume (mm^3)
0	3	0	0	0
20	5.62	0.04	-	-
40	8.24	0.06	0.021	10.00
60	8.82	0.12	0.024	11.43
80	9.14	0.18	0.028	13.33

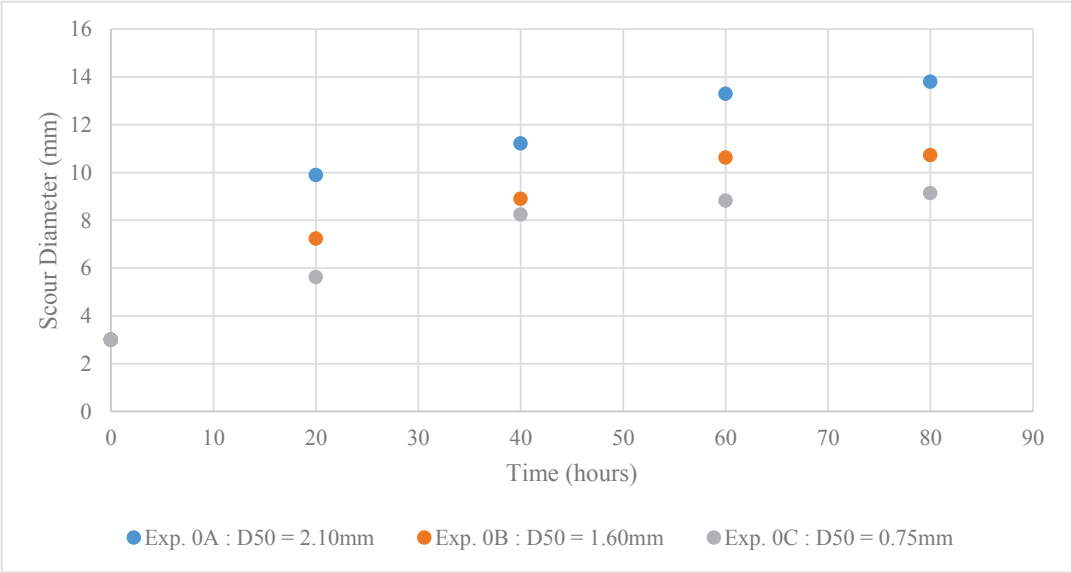

Development of Scour Diameter for Experiment 0

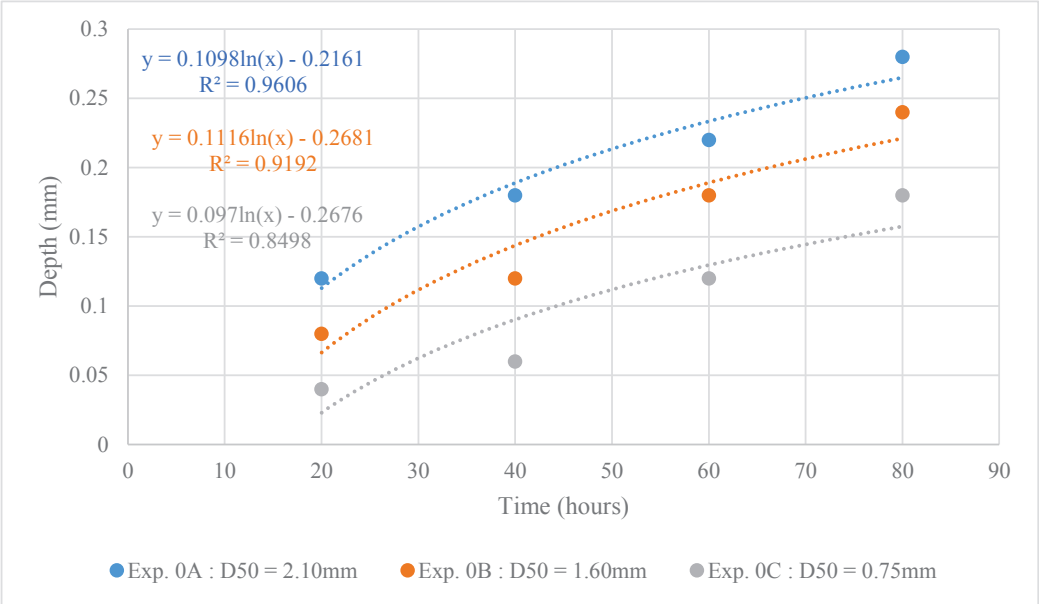

Development of Scour Depth for Experiment 0

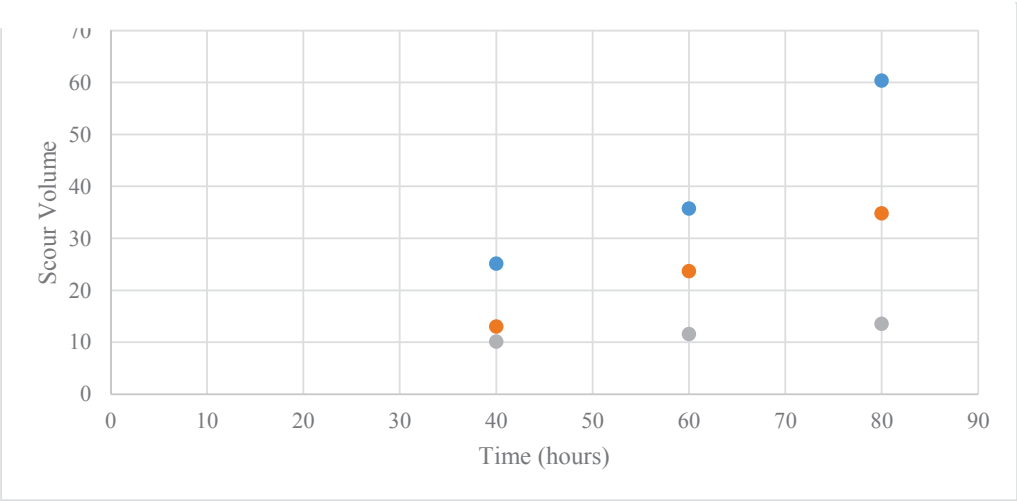

Development of Scour Volume for Experiment 0

7.1.2 Visual Inspection

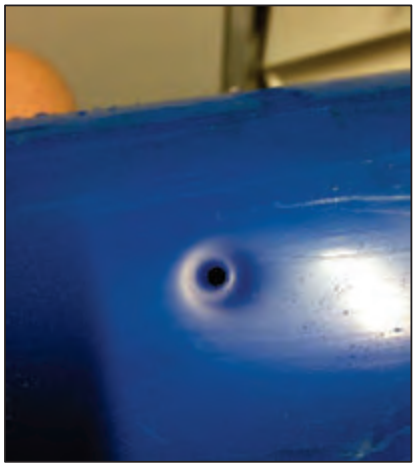

0A 80 hours

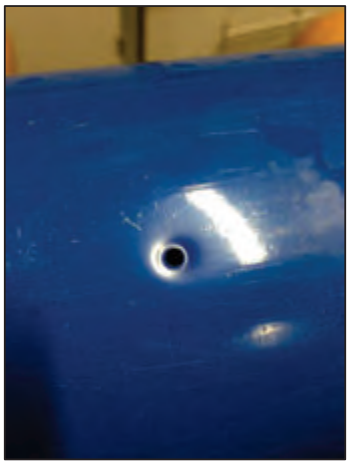

0B 80 hours

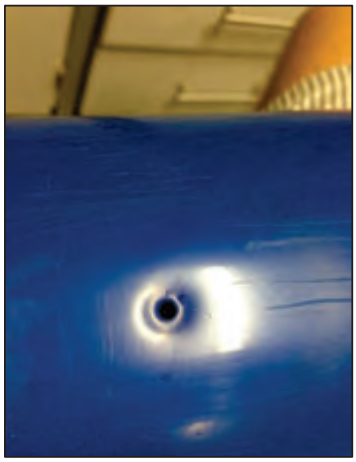

0C 80 hours

7.2 Experiment 1: Grain Size

Operating Conditions for Experiment 1

Experiment	Flow Rate (l/h)	Grain Size (D_{50}) (mm)	Cover Depth (mm)	Pipe Material -	Leak Orientation (°)	Orifice Diameter (mm)
1A	400	**2.10**	500	uPVC	45	3
1B	400	**1.60**	500	uPVC	45	3
1C	400	**0.75**	500	uPVC	45	3

7.2.1 Quantitative Data

Quantitative Data for Experiment 1A

Run Time (h)	Dimension A (mm)	Dimension B (mm)	Depth (mm)	Putty (g)	Volume (mm^3)
0	4.24	3.00	0.00	0.000	0.0
20	20.04	11.42	0.34	0.092	44.4
40	23.60	15.10	0.56	0.187	90.3
60	23.92	15.18	-	0.196	94.7
80	24.98	15.18	0.84	-	-
100	24.98	15.38	0.94	0.293	141.5
120	25.06	15.38	1.18	0.414	200.0
140	26.08	16.02	1.24	0.482	232.9
160	26.08	16.02	1.38	0.509	245.9
180	26.46	18.24	1.48	0.572	276.3
200	26.82	18.58	1.66	0.599	289.4
220	26.82	18.58	2.00	0.681	329.0
240	27.80	18.58	2.00	0.756	365.2
260	27.80	19.12	2.04	0.793	383.1
280	27.80	20.04	2.42	0.836	403.9
300	27.80	20.04	2.60	0.869	419.8
320	27.80	20.04	2.64	-	-
340	27.80	20.04	2.80	-	-
360	27.80	20.04	2.98	0.940	454.1
410	27.80	20.04	3.70	1.055	509.7
430	27.80	21.06	3.84	1.106	534.3
450.7	28.06	21.06	3.98	1.179	569.6
480	29.52	21.06	4.06	1.203	581.2

Quantitative Data for Experiment 1B

Run Time (h)	Dimension A (mm)	Dimension B (mm)	Depth (mm)	Putty (g)	Volume (mm^3)
0	4.24	3.00	0.00	0.000	0.0
20	19.00	9.81	0.20	0.049	23.7
40	19.08	11.02	0.36	0.076	36.7
60	20.22	12.62	0.52	0.106	51.2
80	20.22	12.62	0.54	-	-
100	21.24	13.80	0.80	0.163	78.7
120	21.52	14.06	1.00	0.264	127.5
140	21.52	14.60	1.08	0.343	165.7
160	22.00	15.08	1.36	0.368	177.8
180	22.92	16.10	1.48	0.451	217.9
200	23.42	16.10	1.56	0.464	224.2
220	23.42	16.60	1.78	0.508	245.4
240	23.42	16.60	1.82	0.530	256.0
260	23.42	16.60	2.00	0.594	287.0
280	24.52	17.22	2.06	0.619	299.0
300	24.52	17.66	2.20	0.692	334.3
320	24.52	17.66	2.42	0.700	338.2
340	24.52	17.66	2.50	0.730	352.7
360	24.52	17.66	2.64	0.751	362.8
410	24.52	17.66	3.36	0.785	379.2
430	24.52	17.66	3.60	0.820	396.1
450.7	24.52	17.66	3.70	0.879	424.6
480	24.52	18.32	3.78	0.931	449.8

Quantitative Data for Experiment 1C

Run Time (h)	Dimension A (mm)	Dimension B (mm)	Depth (mm)	Putty (g)	Volume (mm^3)
0	4.24	3.00	0.00	0.000	0.0
20	14.28	7.20	0.14	0.010	4.8
40	16.90	10.20	0.20	0.024	11.6
60	17.00	10.74	0.34	0.043	20.8
80	17.00	10.74	0.36	0.046	22.2
100	17.00	11.00	0.52	0.060	29.0
120	17.00	11.00	0.54	-	-
140	17.00	11.00	0.56	0.062	30.0
160	17.18	11.00	0.60	0.081	39.1
180	17.18	11.00	0.68	0.104	50.2

200	17.18	11.60	0.74	0.128	61.8
220	17.18	11.60	0.90	0.132	63.8
240	17.26	11.60	0.92	0.134	64.7
260	17.26	11.60	1.08	0.164	79.2
280	17.26	11.60	1.14	0.198	95.7
300	17.26	12.00	1.30	0.210	101.4
320	17.38	12.00	1.36	0.231	111.6
340	17.98	12.68	1.58	0.242	116.9
360	17.98	12.68	1.62	0.245	118.4
410	18.12	13.12	1.82	-	-
430	18.12	13.34	2.00	0.278	134.3
450.7	19.14	14.00	2.10	0.299	144.4
480	19.80	14.00	2.26	0.312	150.7

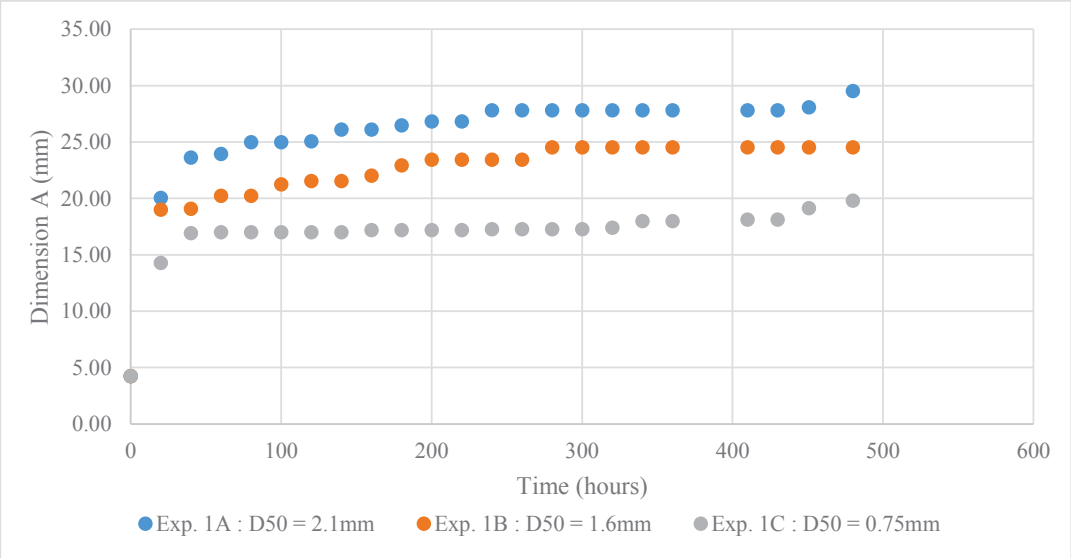

Development of Dimension A for Experiment 1

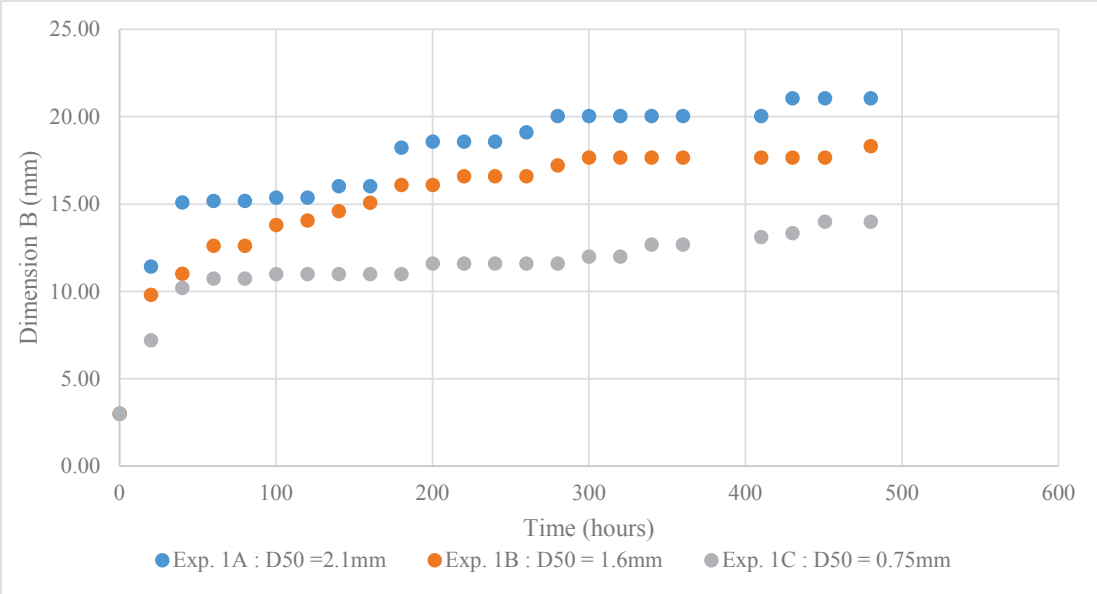

Development of Dimension B for Experiment 1

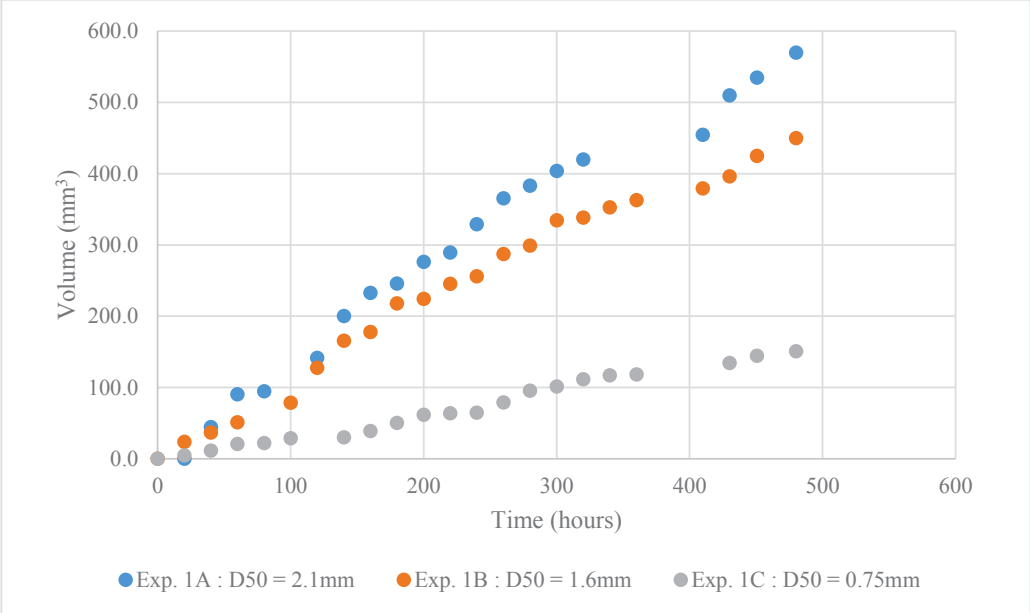

Volume of Pipe Material Removed over Time for Experiment 1

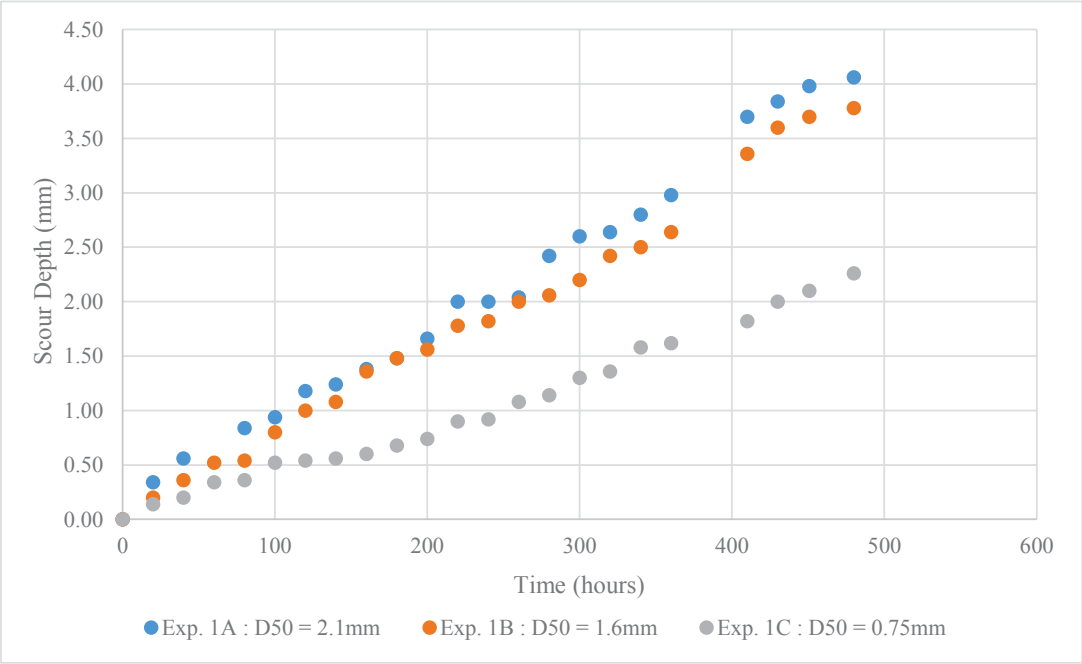

Figure 0-1: Progress of Scour Depth with respect to Time for Experiment 1

7.2.2 Visual Inspection

7.2.2.1 Experiment 1A

1A 20 hours

1A 40 hours

1A 60 hours

1A 80 hours

1A 100 hours

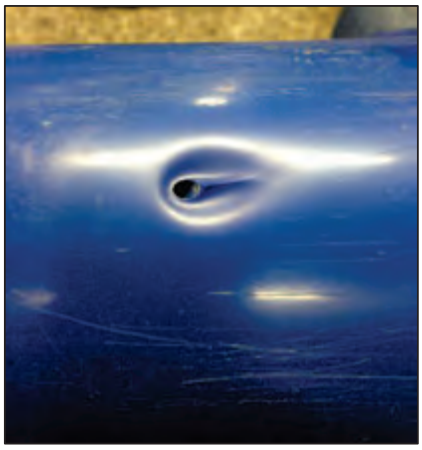

1A 120 hours

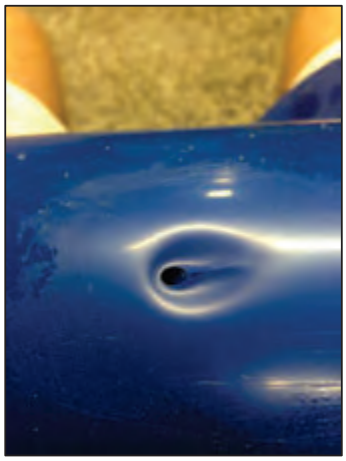

1A 140 hours

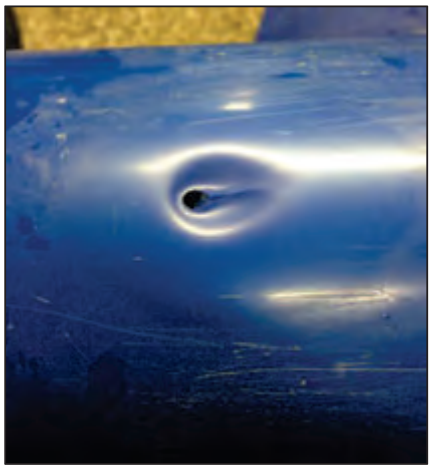

1A 160 hours

1A 180 hours

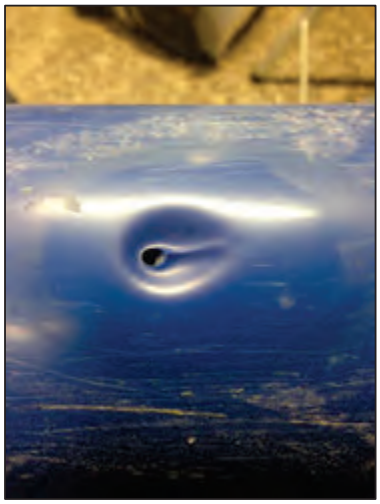

1A 260 hours

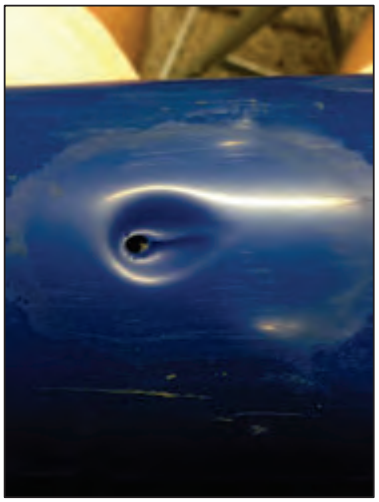

1A 280 hours

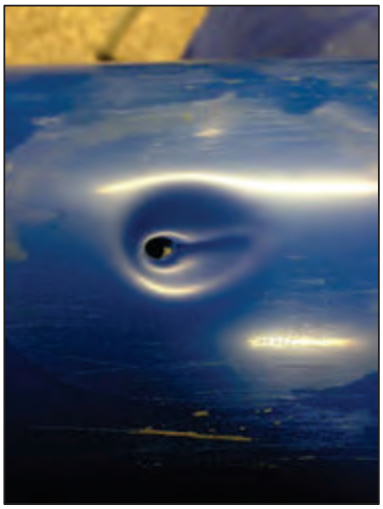

1A 300 hours

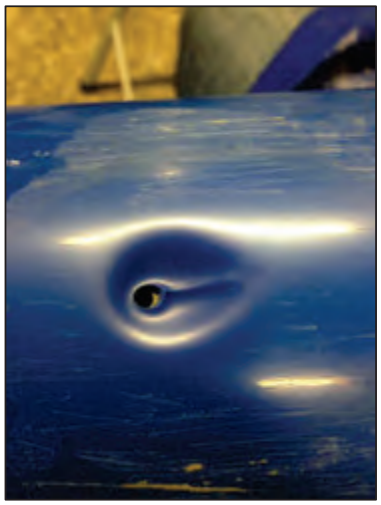

1A 320 hours

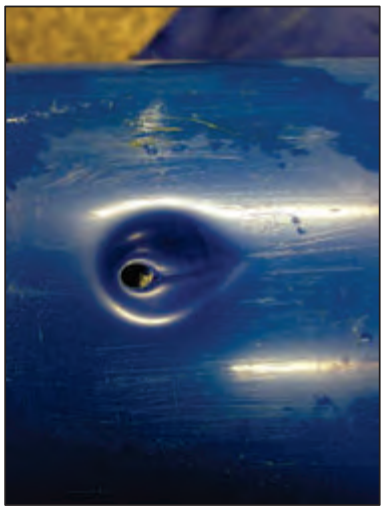

1A 340 hours

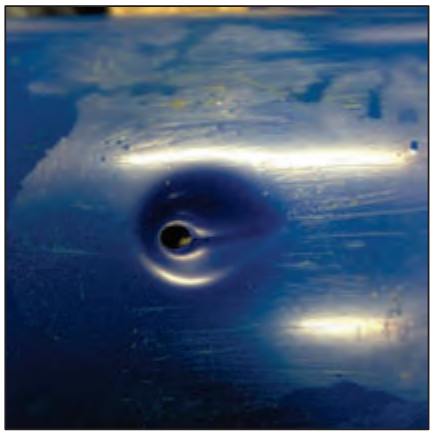

1A 360 hours

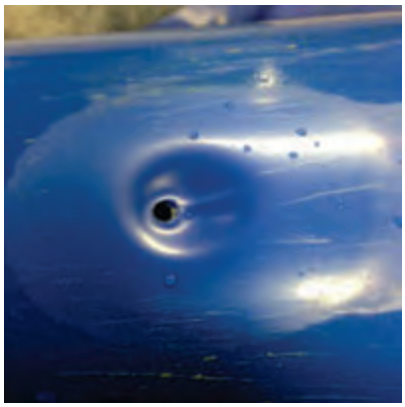

1A 410 hours

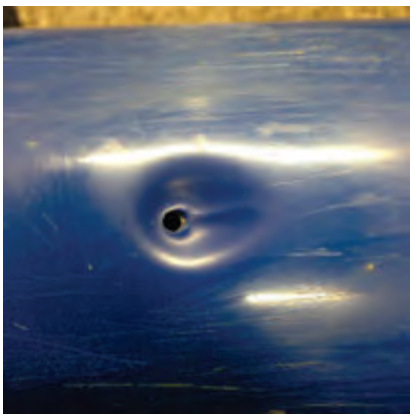

1A 430 hours

21A 450.7 hours

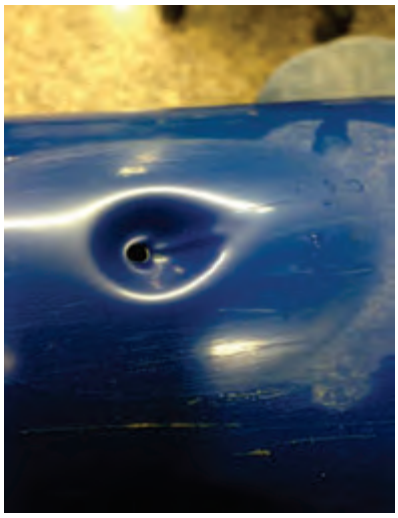

1A 620 hours

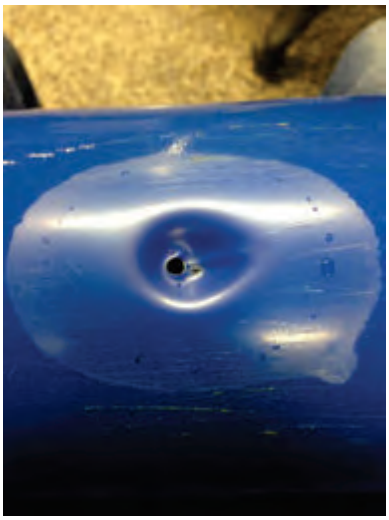

1A 639 hours

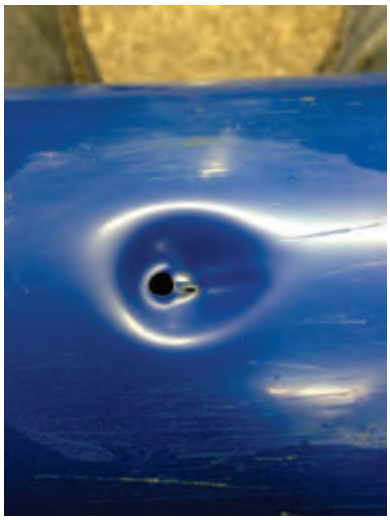

1A 668 hours

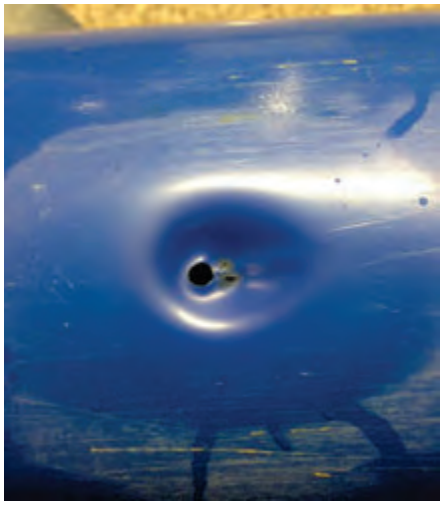

1A 685.1 hours

7.2.2.2 Experiment 1B

1B 40 hours

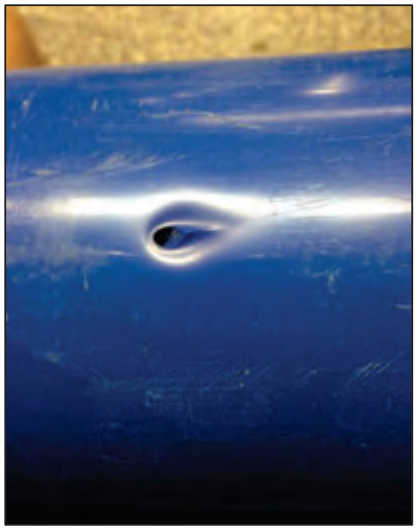

1B 60 hours

1B 80 hours

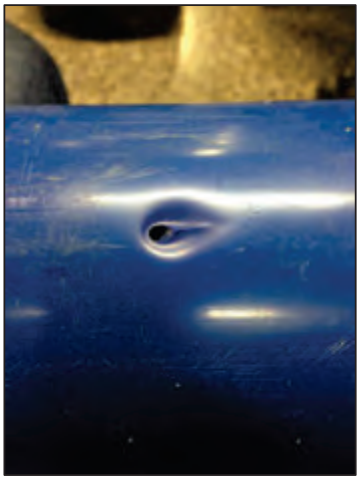

1B 100 hours

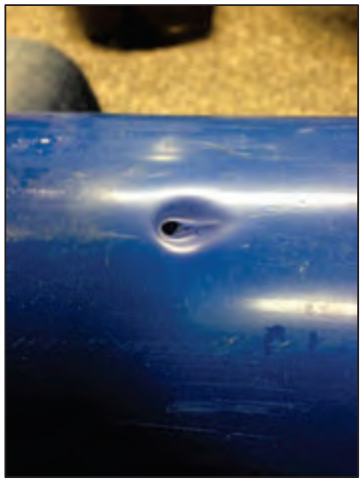

1B 120 hours

31B 140 hours

1B 160 hours

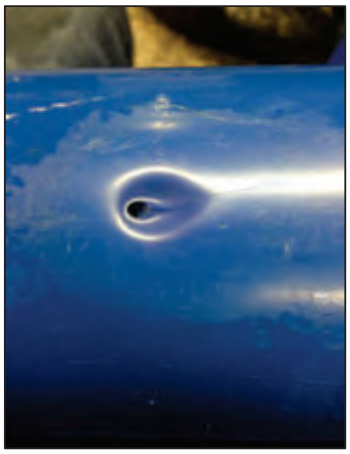

1B 180 hours

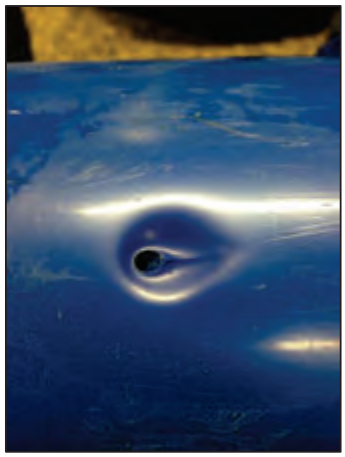

1B 200 hours

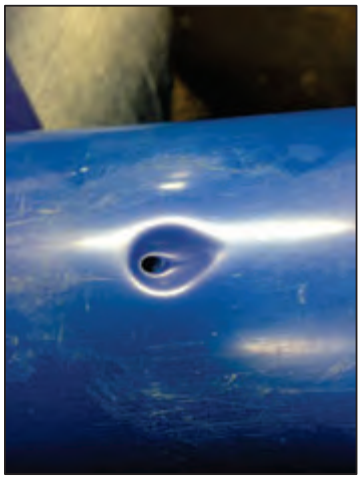

1B 220 hours

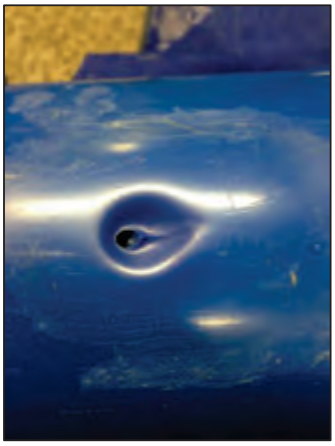

1B 240 hours

1B 260 hours

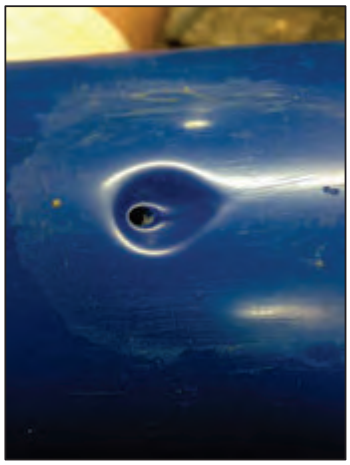

1B 280 hours

1B 300 hours

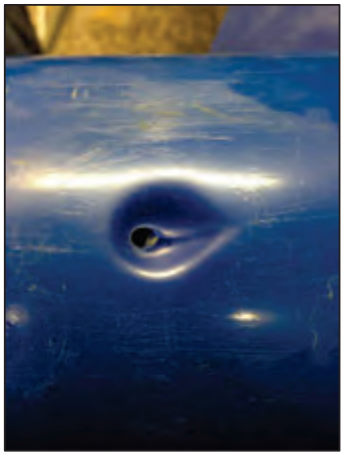

1B 320 hours

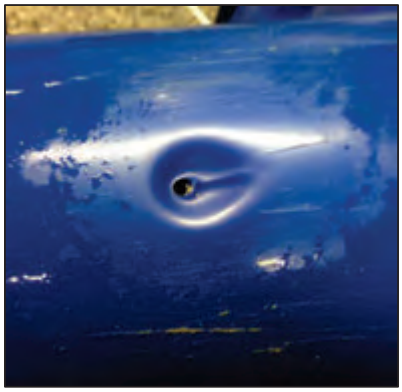

1B 340 hours

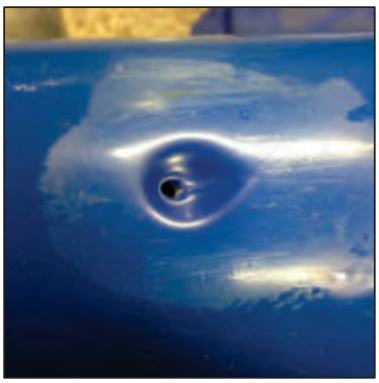

1B 410 hours

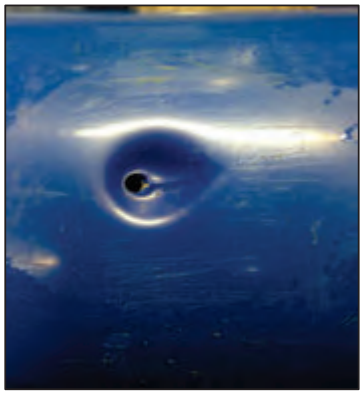

1B 430 hours

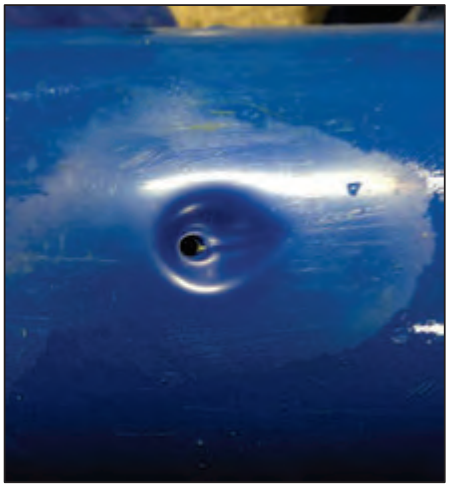

1B 450.7 hours

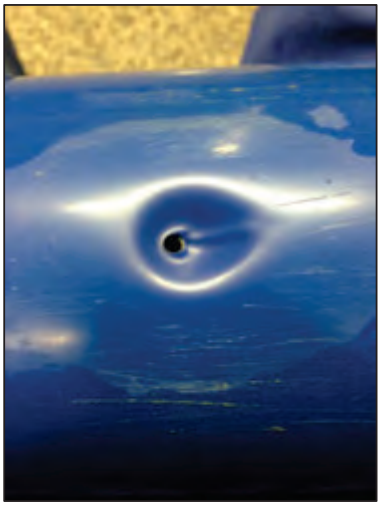

1B 480 hours

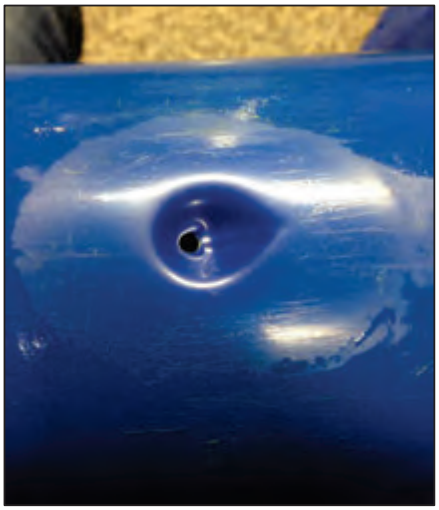

1B 620 hours

1B 639 hours

7.2.2.3 Experiment 1C

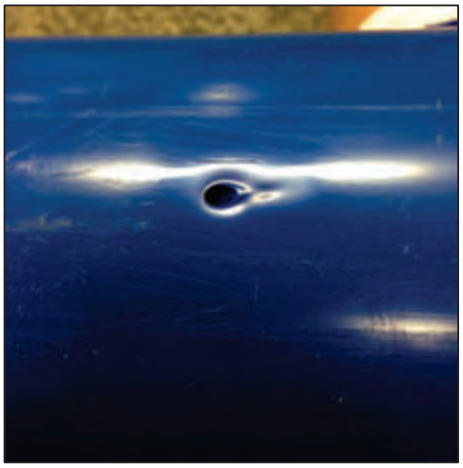

1C 40 hours

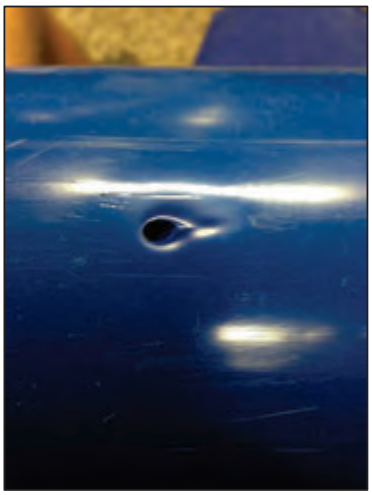

1C 60 hours

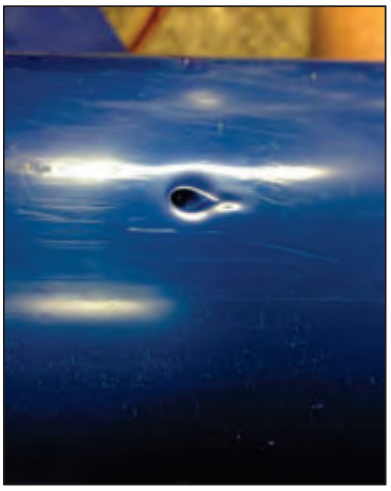

1C 80 hours

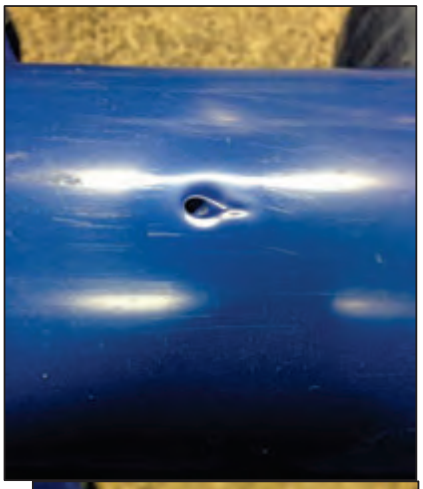

1C 120 hours

1C 140 hours

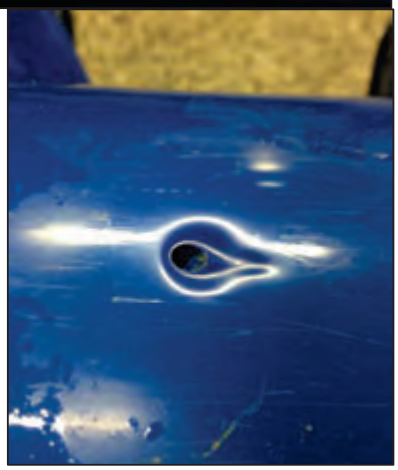

1C 160 hours

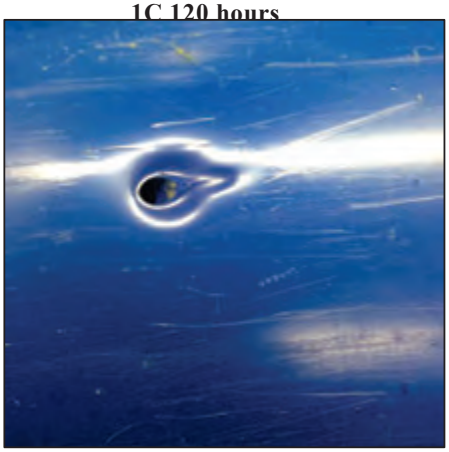

1C 180 hours

1C 200 hours

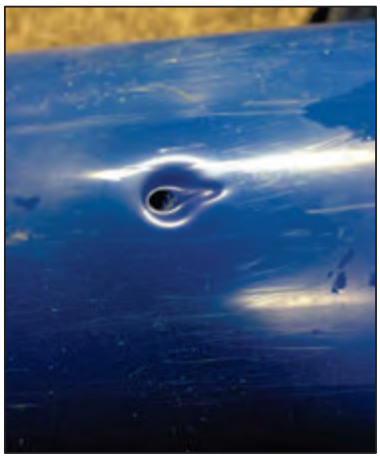

1C 220 hours

1C 240 hours

1C 260 hours

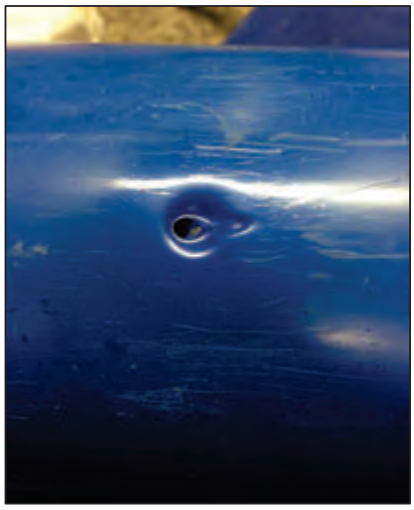

1C 280 hours

1C 300 hours

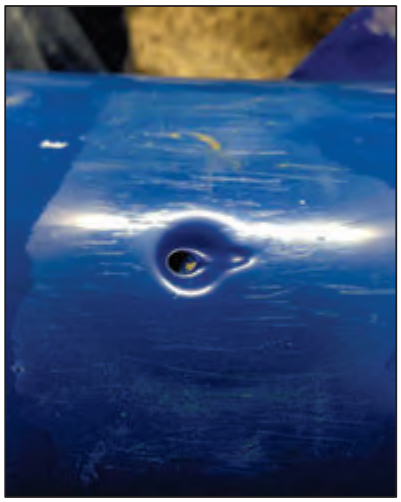

1C 320 hours

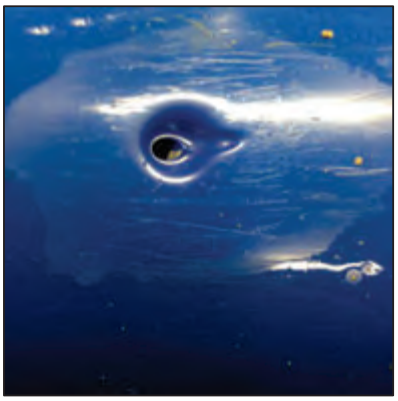

1C 360 hours

1C 410 hours

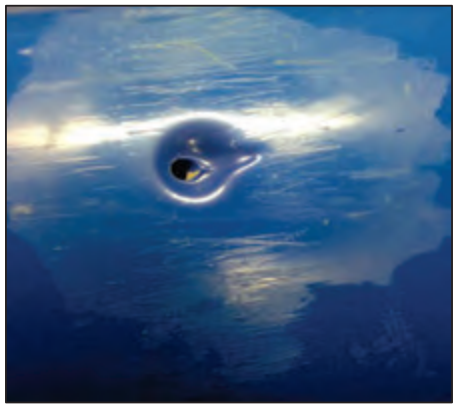

1C 410 hours

1C 450.7 hours

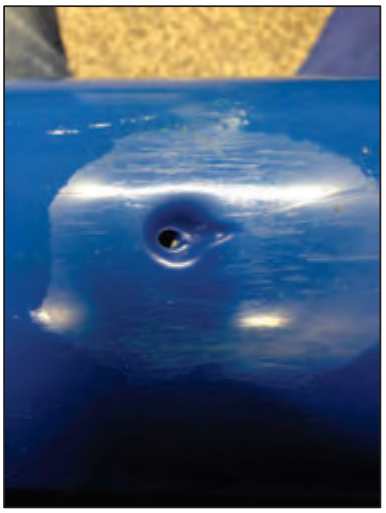

1C 480 hours

1C 620 hours

1C 639 hours

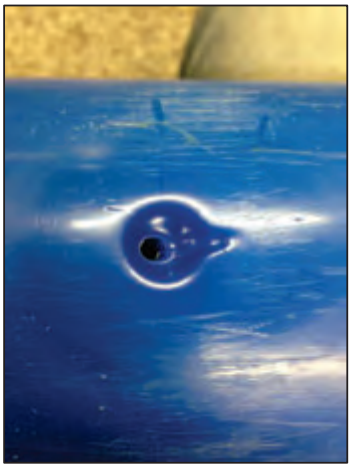

1C 668 hours

1C 685 hours

7.3 Experiment 2: Cover Depth

Operating Conditions for Experiment 2

Experiment	Flow Rate (l/h)	Grain Size (D_{50}) (mm)	Cover Depth (mm)	Pipe Material -	Leak Orientation (°)	Orifice Diameter (mm)
2A	400	1.60	**400**	uPVC	45	3
2B	400	1.60	**500**	uPVC	45	3
2C	400	1.60	**300**	uPVC	45	3

7.3.1 Quantitative Data

Quantitative Data – Experiment 2A

Run Time (h)	Dimension A (mm)	Dimension B (mm)	Depth (mm)	Putty (g)	Volume (mm^3)
0	4.24	3.00	0.00	0.000	0.0
20	19.24	9.74	0.28	0.039	18.8
40	21.14	10.28	0.66	0.125	60.4
60	22.84	11.38	0.98	0.148	71.5
80	22.84	13.12	1.28	0.204	98.6
100	23.28	13.50	1.50	0.245	118.4
120	23.28	14.20	1.68	0.352	170.0
140	23.74	14.28	1.80	0.391	188.9
160	24.82	15.40	2.00	0.444	214.5
180	24.80	15.40	2.12	0.492	237.7
250	26.18	16.30	2.60	0.584	282.1
300	26.80	16.96	2.98	0.644	311.1
344	29.64	17.36	3.12	0.727	351.2

Quantitative Data – Experiment 2B

Run Time (h)	Dimension A (mm)	Dimension B (mm)	Depth (mm)	Putty (g)	Volume (mm^3)
0	4.24	3.00	0.00	0.000	0.0
20	19.20	8.86	0.38	0.069	33.3
40	21.02	10.78	0.66	0.125	60.4

60	22.16	11.96	1.12	0.199	96.1
80	24.42	13.58	1.44	0.270	130.4
100	24.78	14.14	1.82	0.329	158.9
120	25.86	14.86	2.12	0.376	181.6
140	25.86	15.28	2.40	0.433	209.2
160	26.26	16.62	2.62	0.512	247.3
180	26.26	16.62	2.72	0.540	260.9
250	27.50	16.92	3.14	0.622	300.5
300	27.50	17.52	3.26	0.750	362.3
344	29.00	18.50	3.92	0.791	382.1

Quantitative Data – Experiment 2C

Run Time (h)	Dimension A (mm)	Dimension B (mm)	Depth (mm)	Putty (g)	Volume (mm^3)
0	4.24	3.00	0.00	0.000	0.0
20	18.84	9.18	0.24	0.036	17.4
40	18.84	10.00	0.52	0.089	43.0
60	18.96	11.28	0.80	0.141	68.1
80	20.14	12.64	1.02	0.166	80.2
100	20.18	13.26	1.28	0.249	120.3
120	20.22	14.12	1.62	0.313	151.2
140	21.82	14.90	2.02	0.383	185.0
160	22.34	15.14	2.20	0.427	206.3
180	23.30	16.44	2.26	0.467	225.6
250	24.24	16.58	2.74	0.594	287.0
300	25.74	17.42	3.00	0.662	319.8
344	28.12	17.78	3.08	0.723	349.3

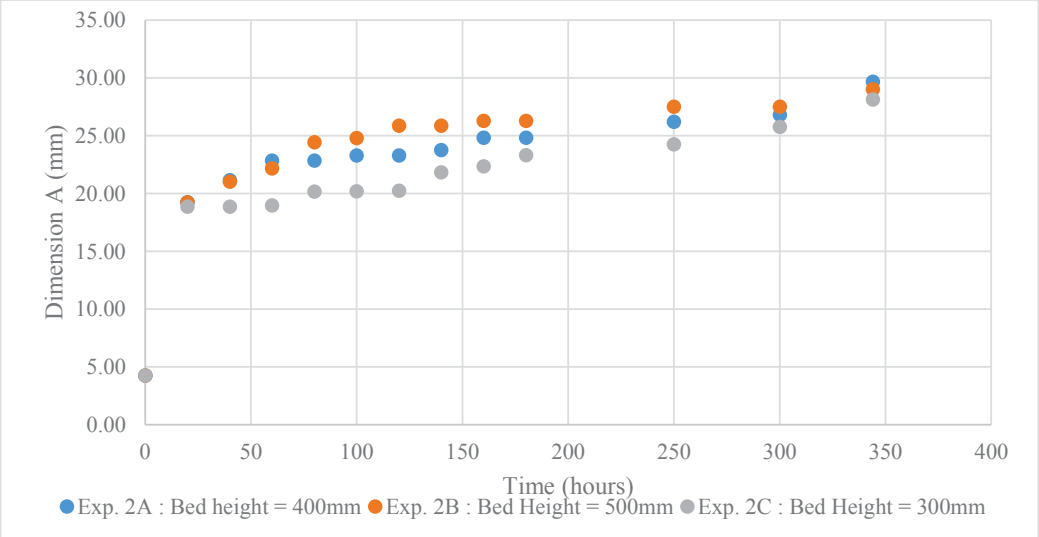

Development of Dimension A for Experiment 2

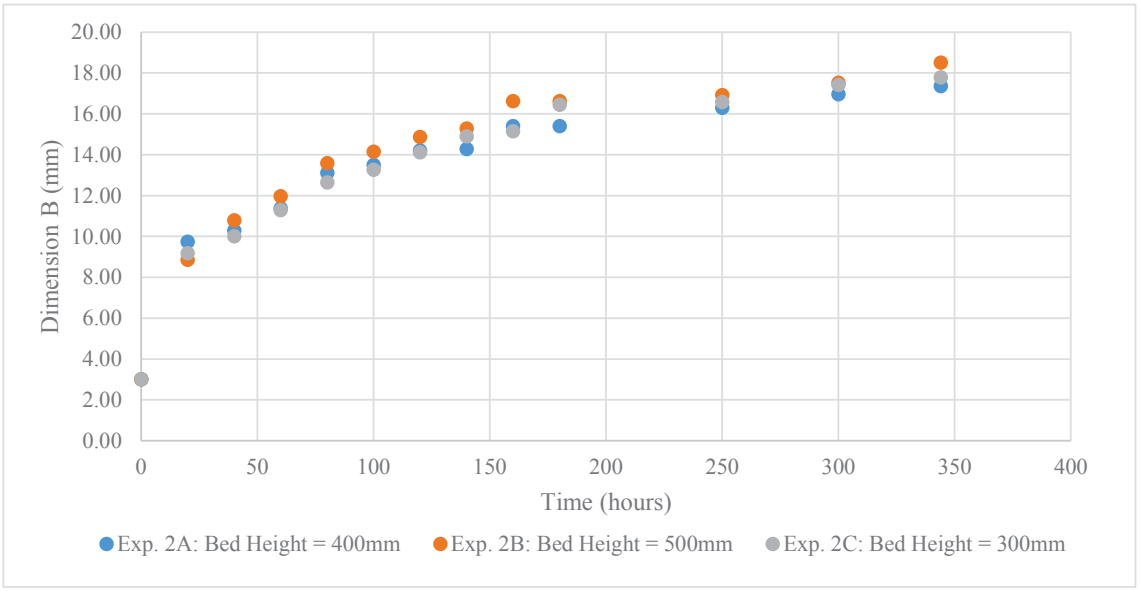

Development of Dimension B for Experiment 2

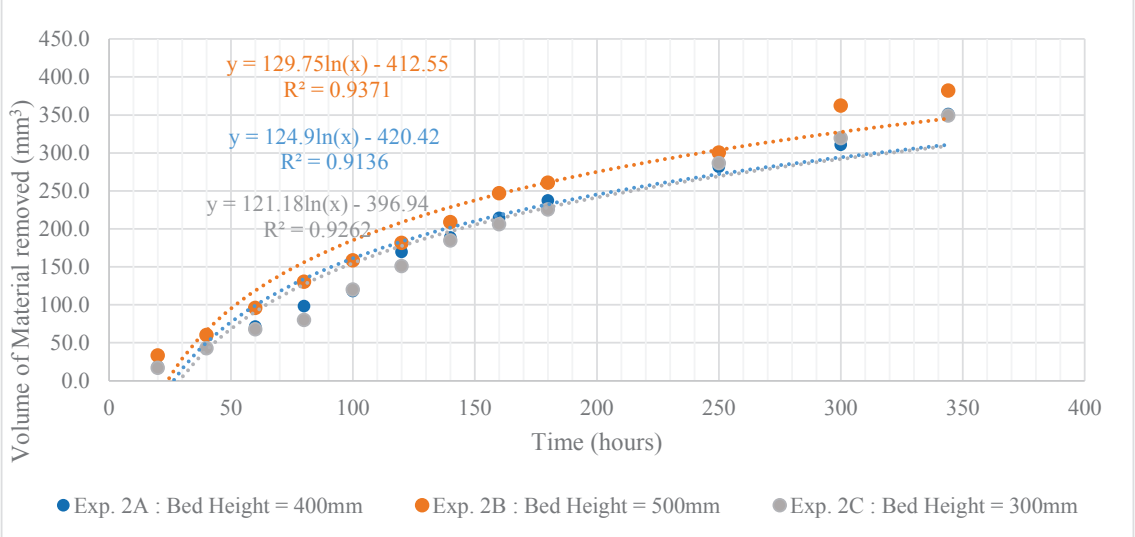

Volume of Removed Material for Experiment 2

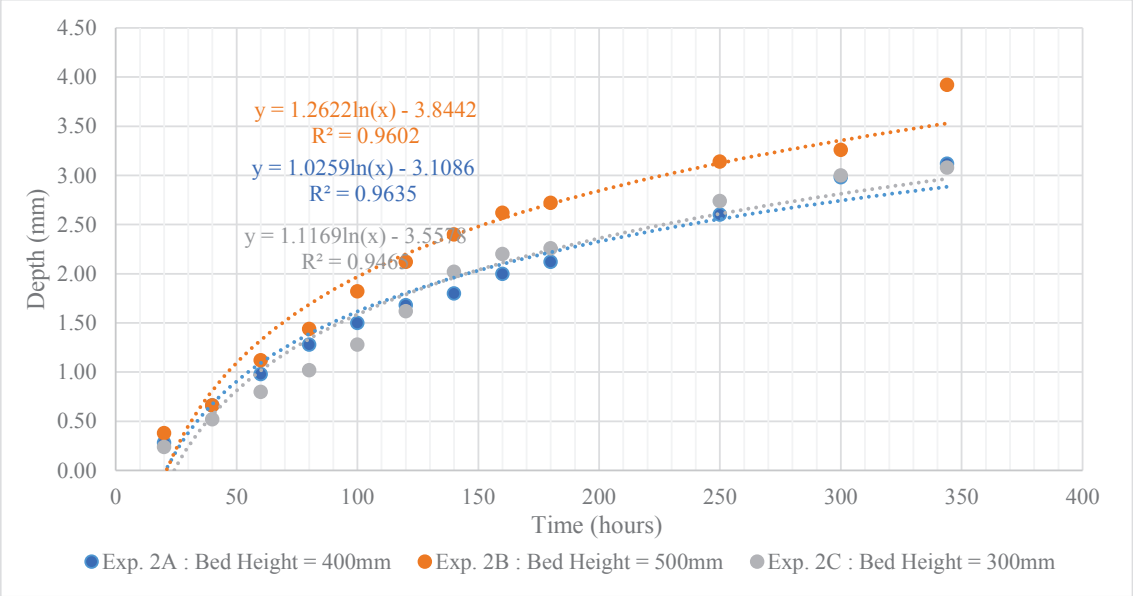

Figure 1: Development of Scour Depth over Time for Experiment 2

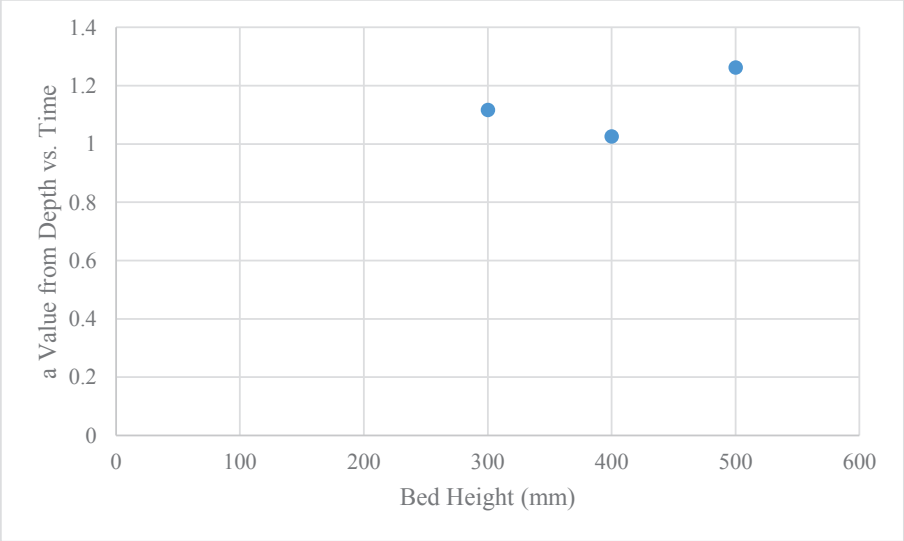

Figure 4: Logarithmic Trend Line a Values from Figure 4-27 vs. Bed Height

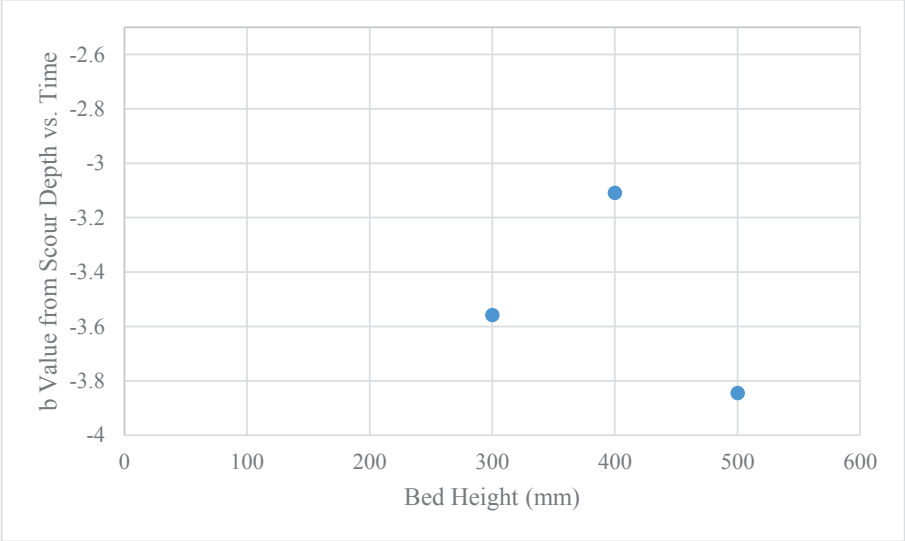

Figure 5: Logarithmic Trend Line b Values from Figure 4-27 vs. Bed Height

7.3.2 Visual Inspection

7.3.2.1 Experiment 2A

2A 20 hours

2A 40 hours

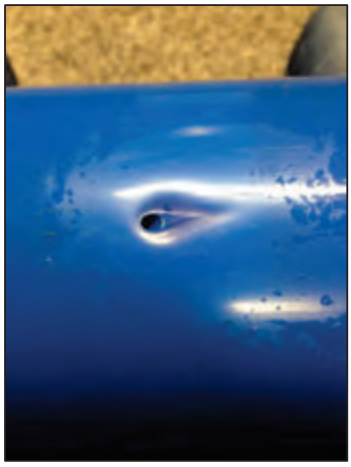

2A 60 hours

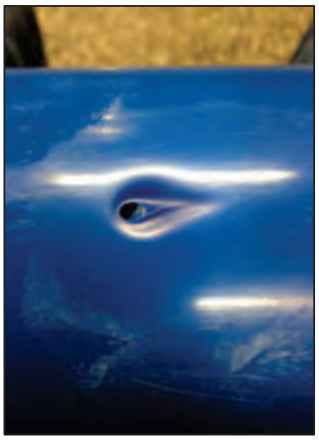

2A 80 hours

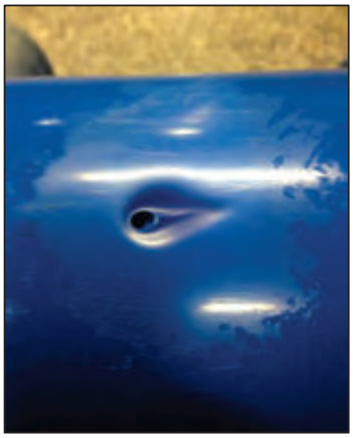

2A 100 hours

2A 120 hours

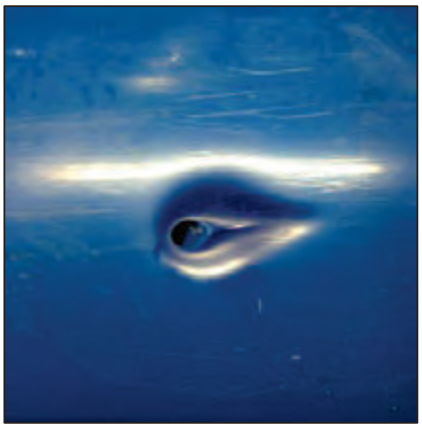

2A 140 hours

2A 160 hours

2A 180 hours

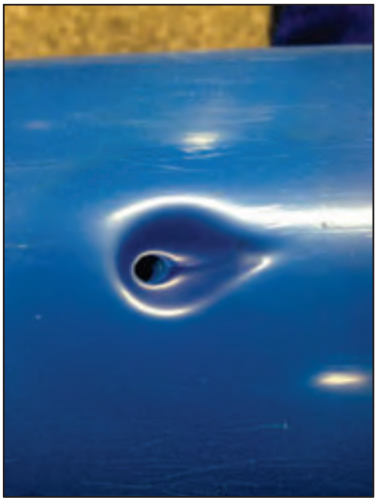

2A 250 hours

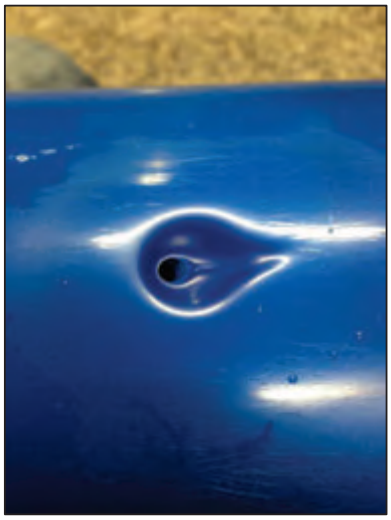

2A 300 hours

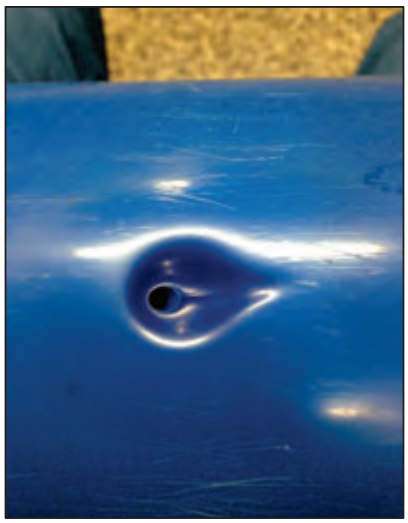

2A 344 hours

7.3.2.2 Experiment 2B

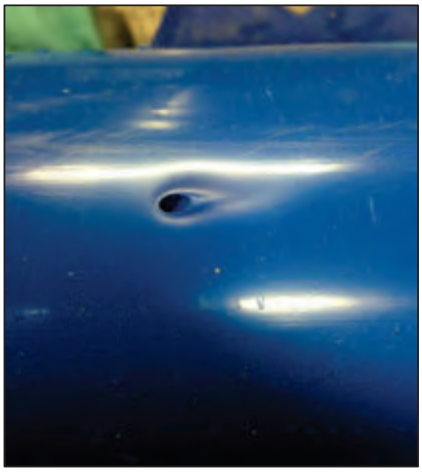

2B 20 hours

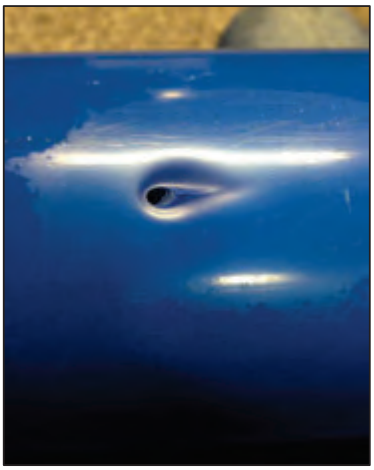

2B 60 hours

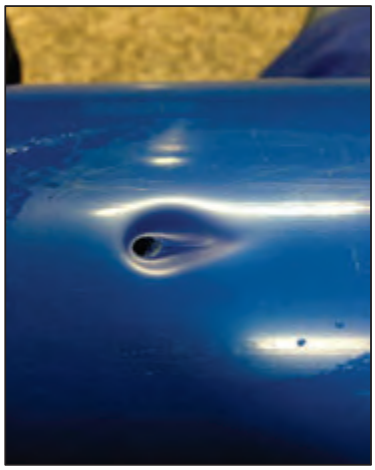

2B 80 hours

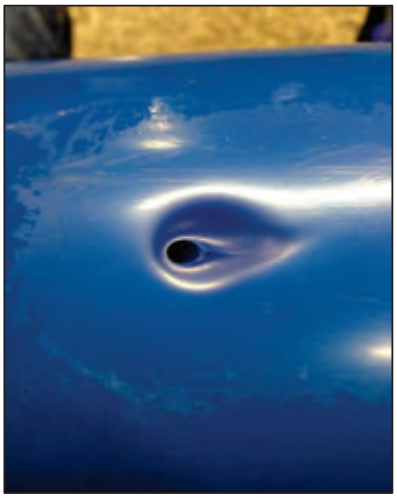

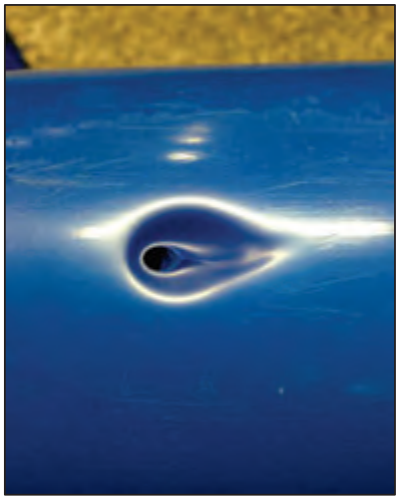

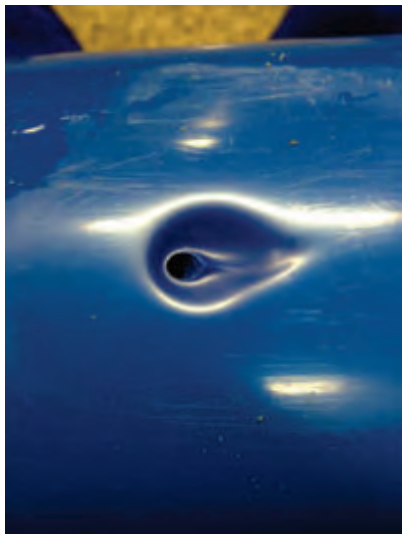

2B 160 hours

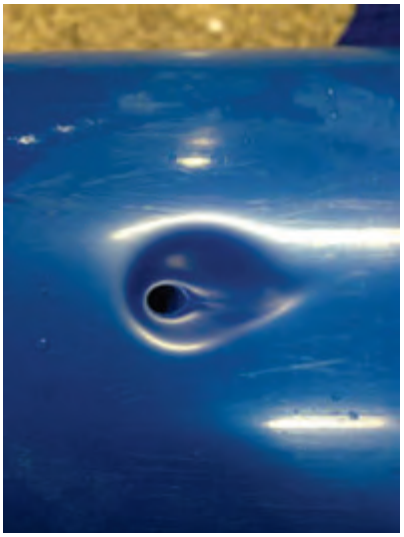

2B 180 hours

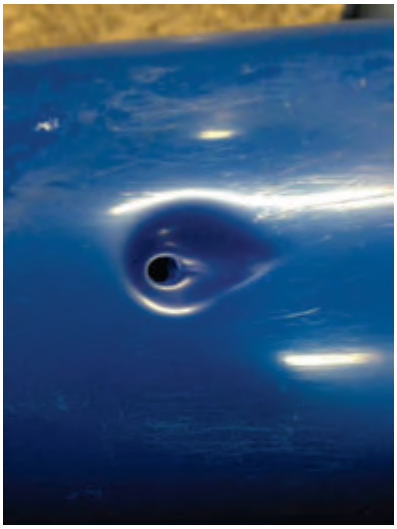

2B 250 hours

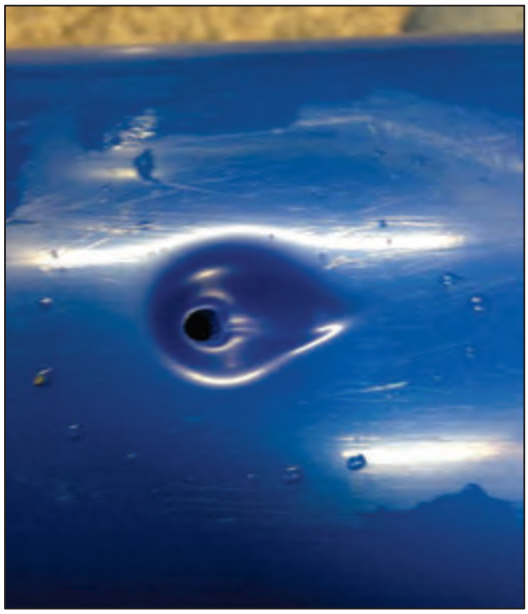

2B 250 hours

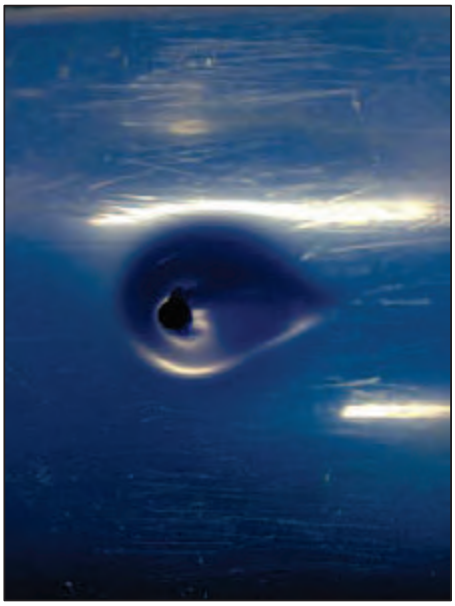

62B 250 hours

7.3.2.3 Experiment 2C

2C 20 hours

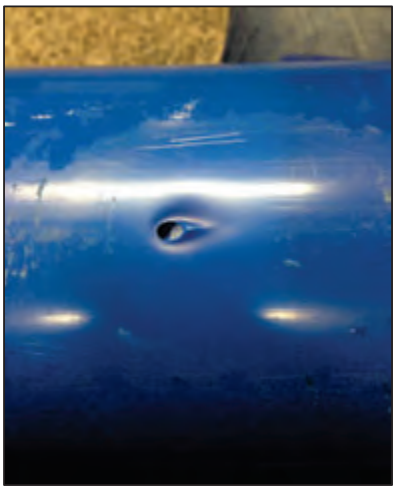

2C 40 hours

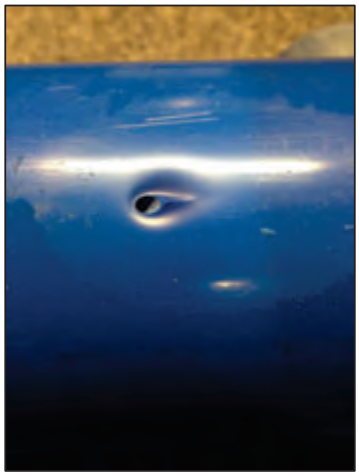

2C 60 hours

2C 80 hours

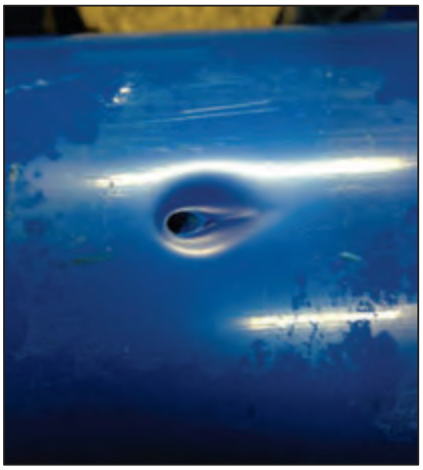

2C 100 hours

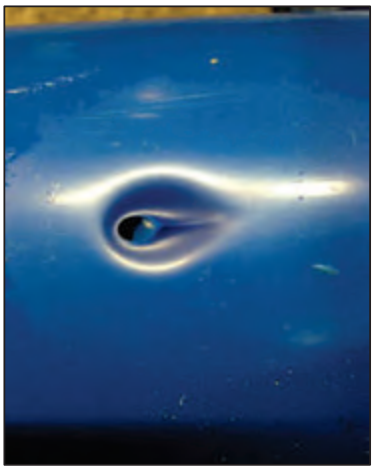

2C 120 hours

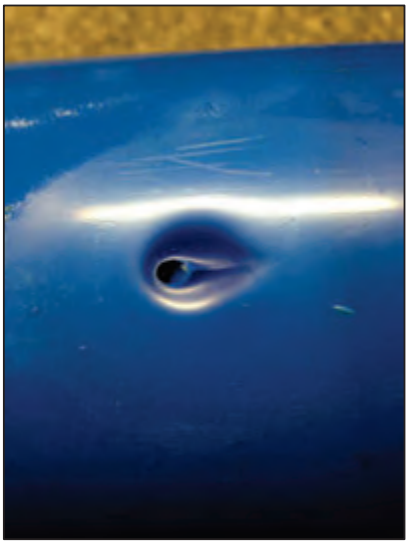

2C 140 hours

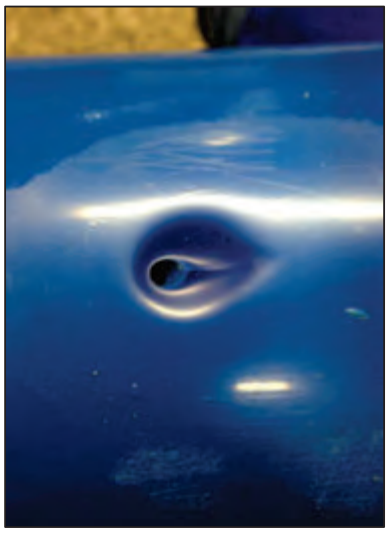

2C 160 hours

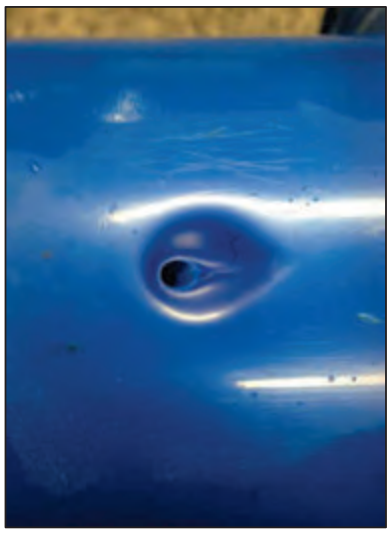

2C 180 hours

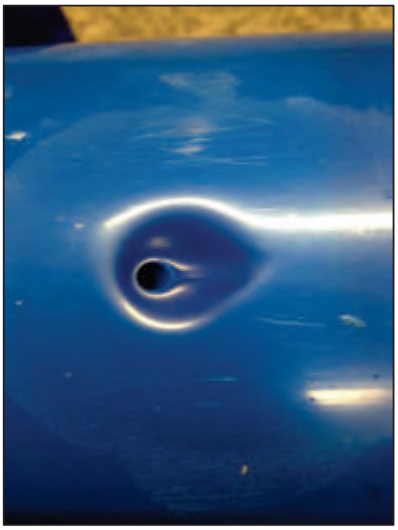

2C 250 hours

2C 300 hours

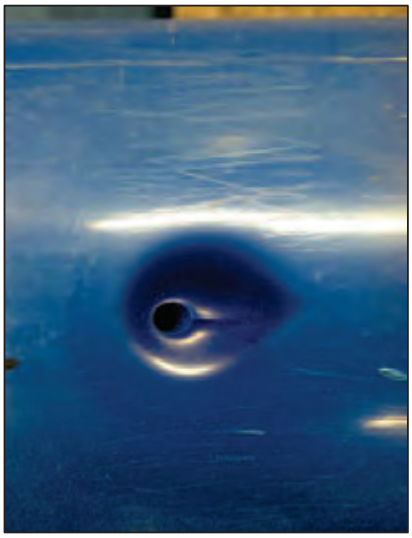

2C 344 hours

7.4 Experiment 3: Flow Rate

Table 0-1: Operating Conditions for Experiment 3

Experiment	Flow Rate (l/h)	Grain Size (D_{50}) (mm)	Cover Depth (mm)	Pipe Material -	Leak Orientation (°)	Orifice Diameter (mm)
3A	**600**	1.60	500	uPVC	45	3
3B	**400**	1.60	500	uPVC	45	3
3C	**200**	1.60	500	uPVC	45	3

7.4.1 Quantitative Data

In the table reporting the data collected for Experiment 3A, it can be observed that there are two additional columns labelled “Dimension A1” and “Dimension B1”. These are the longitudinal and transverse dimensions respectively of the new orifice opening. The visual development of the new orifice opening can be observed in Section 1.4.2.

Quantitative Data - Experiment 3A

Run Time (h)	Dimension A (mm)	Dimension B (mm)	Depth (mm)	Putty (g)	Volume (mm^3)	Dimension A1 (mm)	Dimension B1 (mm)
0.0	4.24	3.00	0.00	0.000	0.0	-	-
20.0	23.00	13.20	1.32	0.229	110.6	-	-
40.0	25.95	15.44	2.26	0.413	199.5	-	-
60.0	26.36	16.78	2.54	0.571	275.8	-	-
80.0	27.88	17.40	3.64	0.779	376.3	-	-
102.0	28.56	18.60	4.54	0.927	447.8	-	-
120.0	29.32	19.78	4.54	0.968	467.6	3.68	4.56
140.0	32.28	20.54	4.54	1.043	503.9	3.80	4.66
186.4	33.42	20.64	4.54	1.083	523.2	3.84	4.66
253.0	32.80	20.64	4.54	1.083	523.2	4.48	5.50
332.5	33.20	20.64	4.54	1.120	541.1	-	-

Quantitative Data – Experiment 3B

Run Time (h)	Dimension A (mm)	Dimension B (mm)	Depth (mm)	Putty (g)	Volume (mm^3)
0.0	4.24	3.00	0.00	0.000	0.0
20.0	24.02	9.08	0.42	0.068	32.9
40.0	27.06	11.76	0.76	0.154	74.4
60.0	28.24	12.64	1.22	0.243	117.4
80.0	28.32	13.42	1.54	0.287	138.6
102.0	28.64	14.18	1.74	0.349	168.6
120.0	29.64	15.02	1.96	0.385	186.0
140.0	29.74	15.54	2.14	0.436	210.6
186.4	29.80	16.22	2.38	0.555	268.1
253.0	29.90	17.30	2.68	0.615	297.1
332.5	30.92	17.64	3.00	0.718	346.9

Quantitative Data – Experiment 3C

Run Time (h)	Dimension A (mm)	Dimension B (mm)	Depth (mm)	Putty (g)	Volume (mm^3)
0.0	4.24	3.00	0.00	0.000	0.0
20.0	9.38	4.46	0.08	0.003	1.4
40.0	11.20	6.14	0.12	0.005	2.4
60.0	12.92	7.60	0.14	0.006	2.9
80.0	13.66	7.86	0.16	0.013	6.3
102.0	14.52	8.96	0.22	0.014	6.8
120.0	16.24	9.30	0.24	0.019	9.2
140.0	-	-	-	-	-
186.4	19.68	9.46	0.4	0.039	18.84058
253.0	19.70	10.26	0.46	0.052	25.12077
332.5	19.82	10.26	0.52	0.06	28.98551

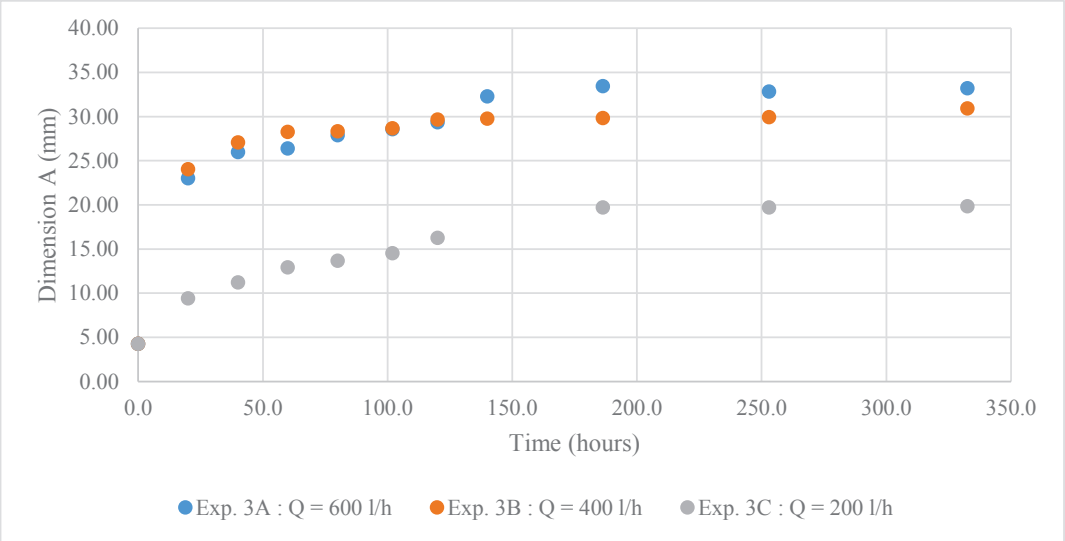

Development of Dimension A for Experiment 3

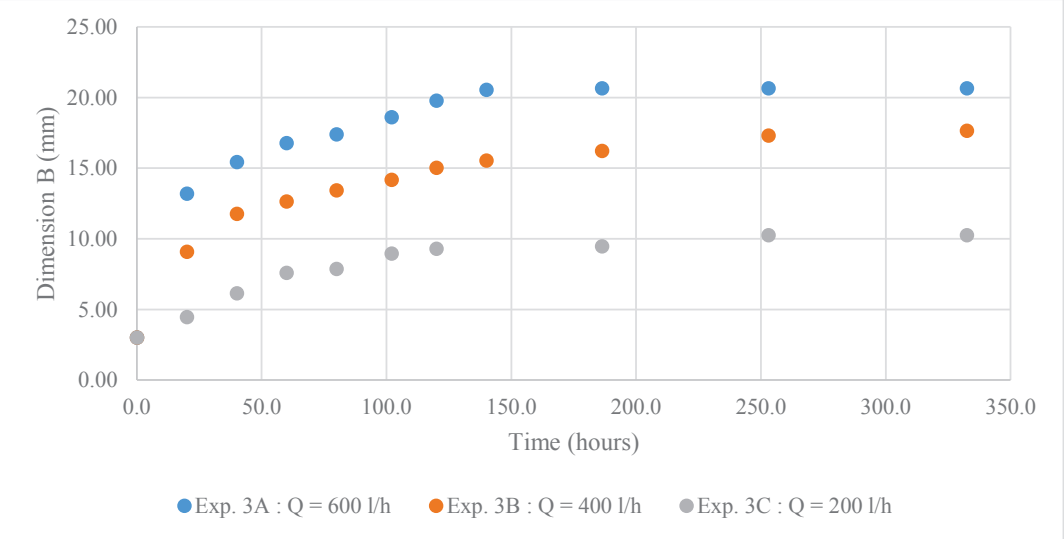

Development of Dimension B for Experiment 3

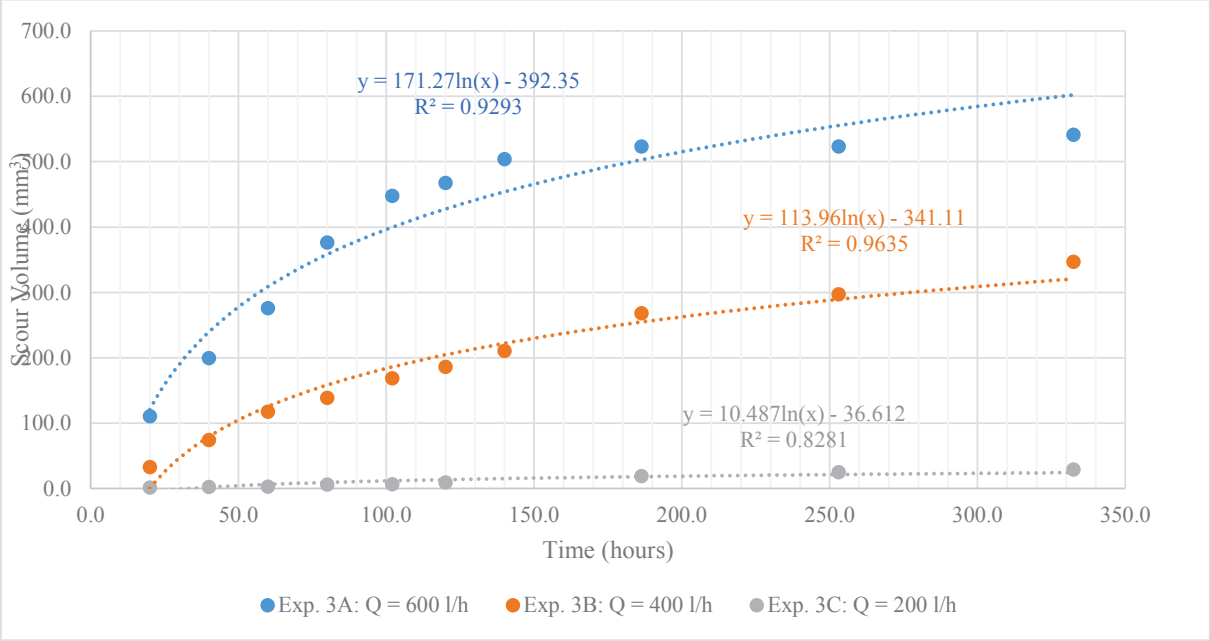

Volume of Removed Material for Experiment 3

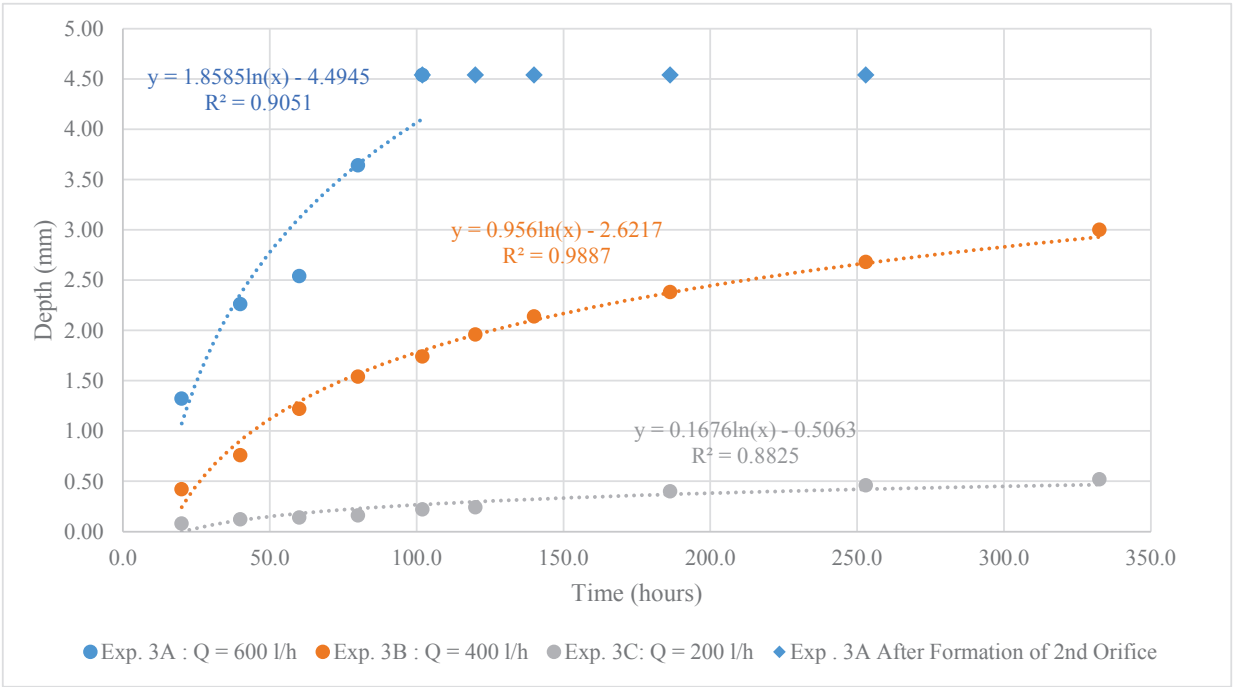

Development of Scour Depth into the Pipe Wall for Experiment 3

7.4.2 Visual Inspection

7.4.2.1 Experiment 3A

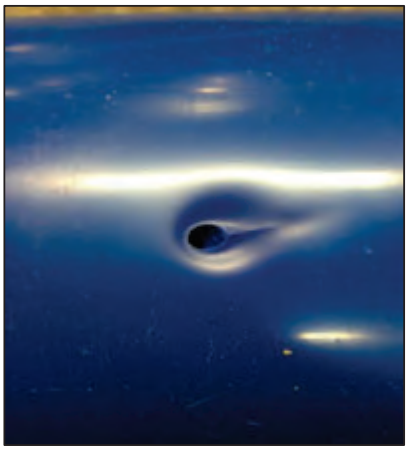

3A 20 hours

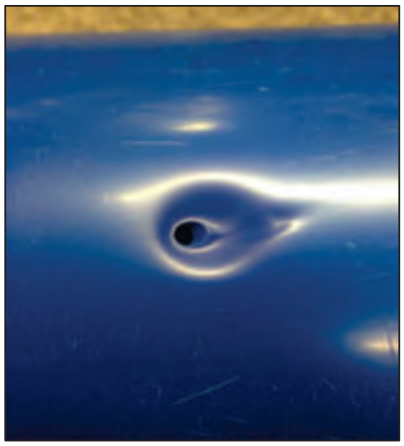

3A 40 hours

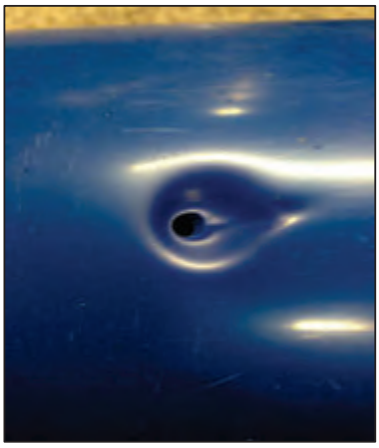

3A 60 hours

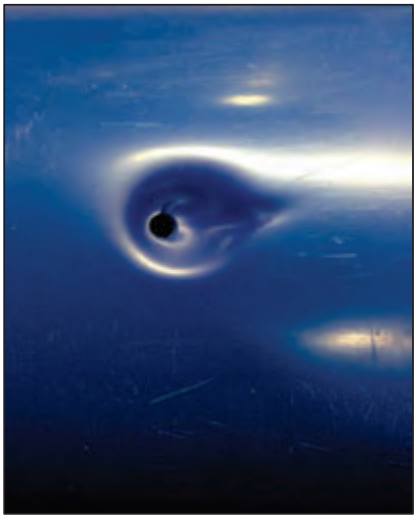

3A 80 hours

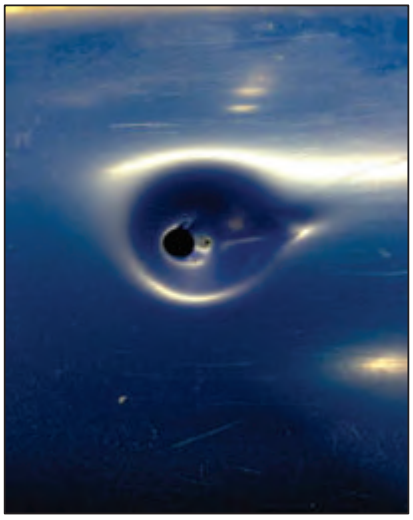

3A 102 hours

3A 120 hours

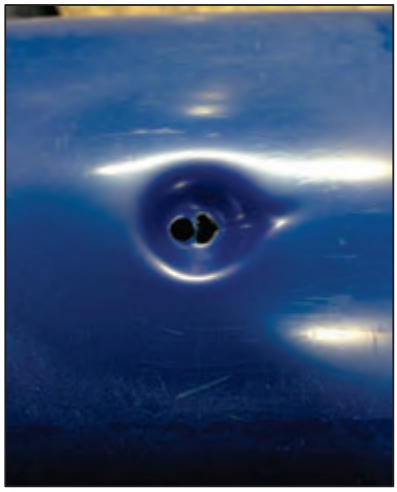

3A 140 hours

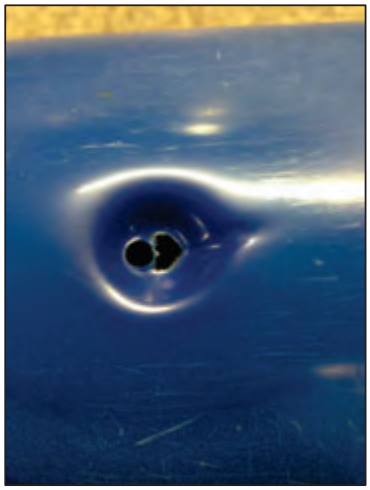

3A 186 hours

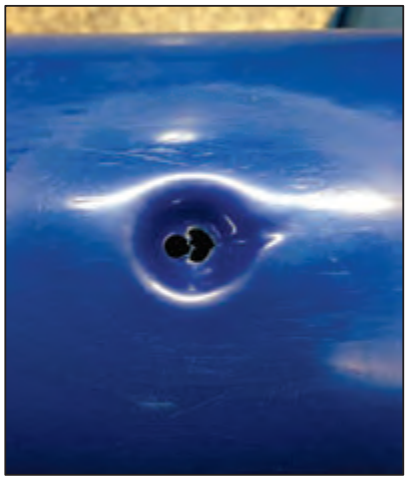

3A 253 hours

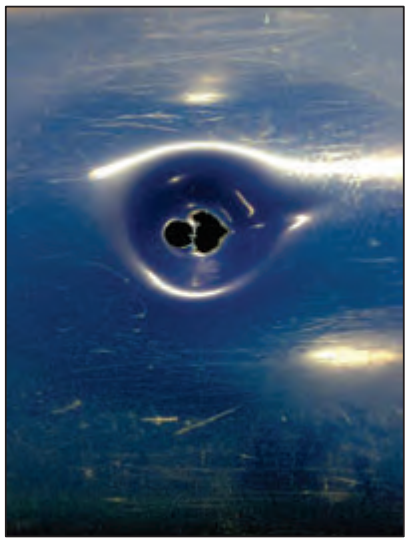

3A 332.5 hours

7.4.2.2 Experiment 3B

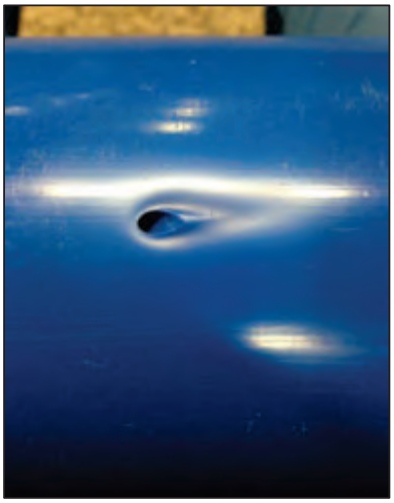

3B 20 hours

3B 40 hours

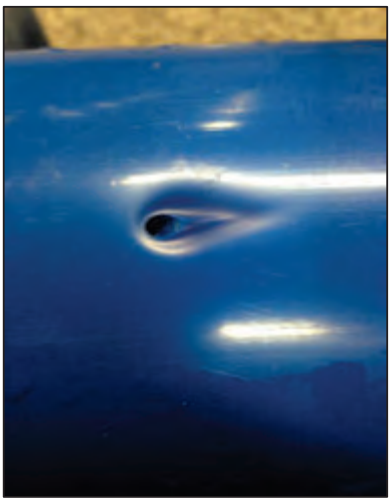

3B 60 hours

3B 80 hours

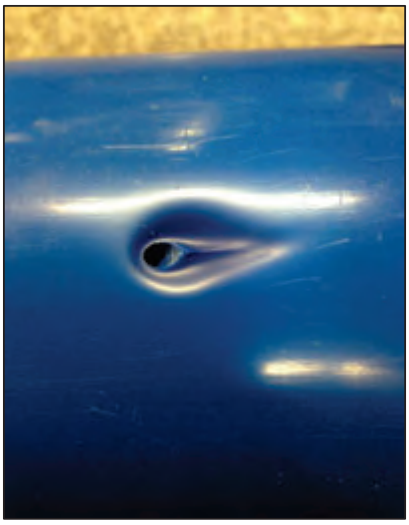

3B 102 hours

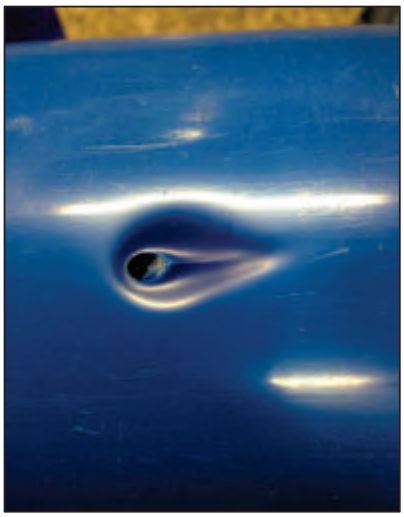

3B 120 hours

3B 140 hours

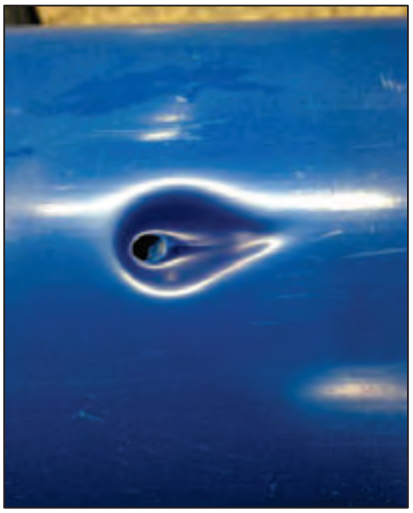

3B 186 hours

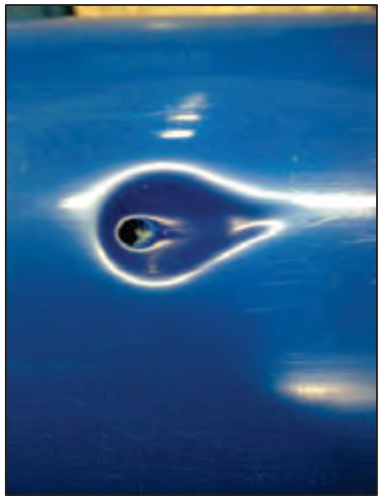

3B 253 hours

3B 332.5 hours

7.4.2.3 Experiment 3C

3C 20 hours

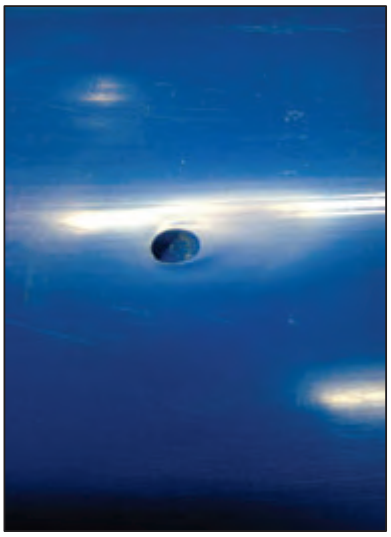

3C 40 hours

3C 60 hours

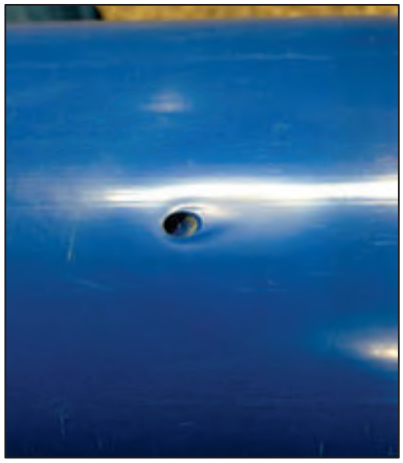

3C 80 hours

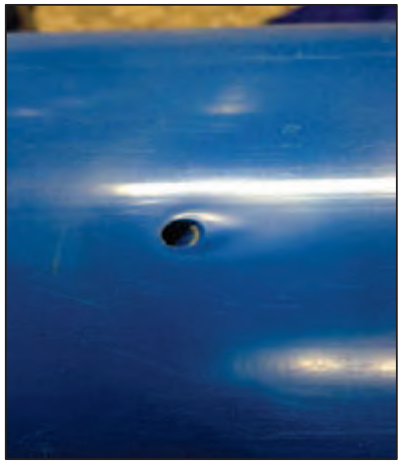

3C 102 hours

3C 120 hours

3C 186 hours

3C 253 hours

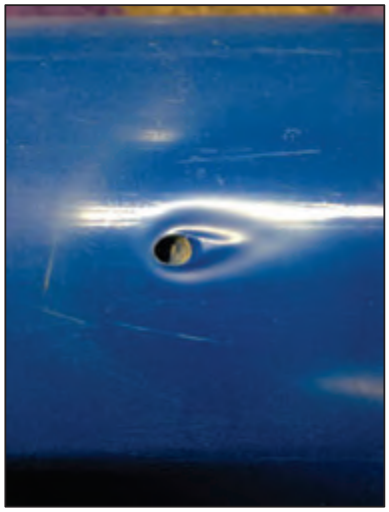

3C 332.5 hours

7.5 Experiment 4: Leak Orientation

Table 0-2: Operating Conditions for Experiment 4

Experiment	Flow Rate (l/h)	Grain Size (D_{50}) (mm)	Cover Depth (mm)	Pipe Material -	Leak Orientation (°)	Orifice Diameter (mm)
4A(i)	400	1.60	500	uPVC	**0**	3
4A(ii)	**200**	1.60	500	uPVC	**0**	3
4B	400	1.60	500	uPVC	**45**	3
4C	400	1.60	500	uPVC	**90**	3

7.5.1 Quantitative Data

In the tables reporting the data collected for Experiment 4A(i) and 4A(ii), it can be observed that there are two additional columns labelled "Dimension A1" and "Dimension B1". These are the longitudinal and transverse dimensions respectively of the new orifice opening. The visual development of the new orifice openings can be observed in Section 1.5.2.

It should also be observed that for Experiment 4C, there is an "Orifice Diameter" column. This indicates how the orifice enlarged in the latter stages of the test.

Quantitative Data for Experiment 4A(i)

Run Time (h)	Dimension A (mm)	Dimension B (mm)	Depth (mm)	Putty (g)	Volume (mm^3)	Dimension A1 (mm)	Dimension B1 (mm)
0	0.00	0.00	0.00	0.000	0.0	0.00	0.00
20	45.14	15.54	4.54	2.364	1142.0	8.48	3.88
40	45.14	15.54	4.54	2.568	1240.6	8.72	4.24
60	45.14	15.54	4.54	2.568	1240.6	9.78	4.24

Quantitative Data for Experiment 4A(ii)

Run Time (h)	Dimension A (mm)	Dimension B (mm)	Depth (mm)	Putty (g)	Volume (mm^3)	Dimension A1 (mm)	Dimension B1 (mm)
0.0	0.00	0.00	0.00	0.000	0.0	0	0
20.0	29.32	10.16	1.62	0.576	278.3	0	0
40.0	30.96	11.00	2.64	0.706	341.1	0	0
60.0	32.76	11.12	3.46	1.092	527.5	0	0
80.0	33.30	11.52	4.14	1.380	666.7	0	0
100.5	34.60	11.52	4.44	1.599	772.5	0	0
120.0	35.28	12.86	4.54	1.790	864.7	0	0
140.0	35.52	13.26	4.54	1.874	905.3	3.26	1.54
208.5	35.52	13.66	4.54	2.021	976.3	4.14	2.38

Quantitative Data for Experiment 4B

Run Time (h)	Dimension A (mm)	Dimension B (mm)	Depth (mm)	Putty (g)	Volume (mm^3)
0.0	4.24	3.00	0.00	0.000	0.0
20.0	23.46	10.58	0.64	0.117	56.5
40.0	23.58	11.24	1.02	0.260	125.6
60.0	26.22	13.73	1.38	0.316	152.7
80.0	28.46	14.16	1.64	0.334	161.4
100.0	28.46	14.70	1.82	0.369	178.3
120.0	28.64	15.28	1.94	0.404	195.2
140.0	28.64	15.84	2.08	0.481	232.4
185.0	28.64	17.56	2.32	0.544	262.8
231.0	29.98	17.64	2.64	0.620	299.5
299.5	31.00	17.76	3.04	0.702	339.1

Quantitative Data for Experiment 4C

Run Time (h)	Dimension A (mm)	Dimension B (mm)	Depth (mm)	Putty (g)	Volume (mm^3)	Orifice Diameter (mm)
0.0	3.00	3.0	0.00	0.000	0.0	3.00
20.0	10.24	10.2	0.36	0.017	8.2	3.00
40.0	12.58	12.6	0.64	0.053	25.6	3.00
60.0	13.18	13.2	0.82	0.074	35.7	3.00
80.0	14.66	14.7	1.00	0.127	61.4	3.00
100.0	14.70	14.7	1.38	0.148	71.5	3.00
120.0	15.68	15.7	1.56	0.179	86.5	3.00
140.0	16.00	16.0	2.30	0.210	101.4	3.00
185.0	18.16	18.2	4.16	0.489	236.2	3.00
231.0	20.28	20.3	4.54	0.763	368.6	3.90
299.5	20.28	20.3	4.54	0.850	410.6	4.74

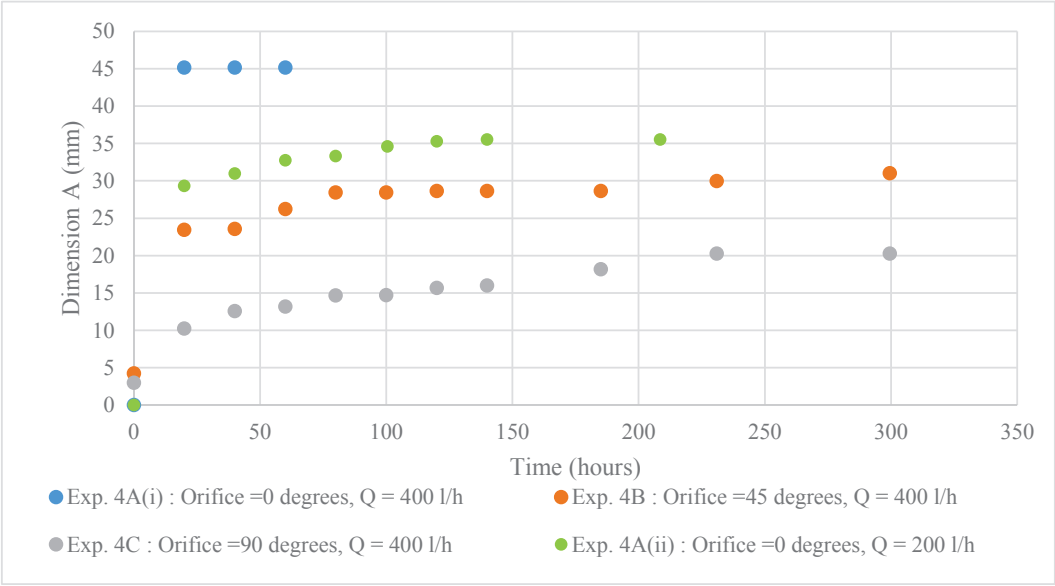

Development of Dimension A for Experiment 4

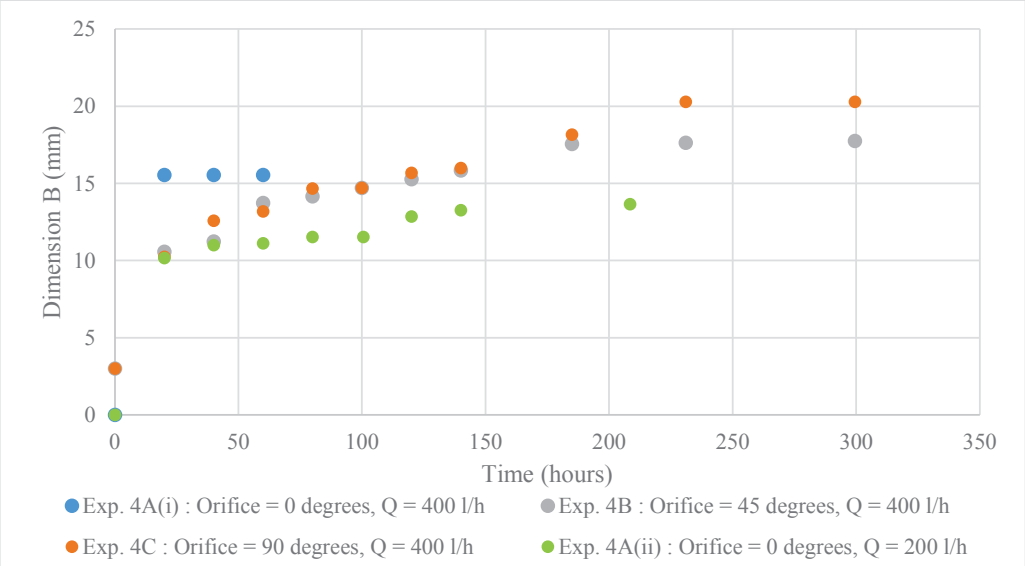

Development of Dimension B for Experiment 4

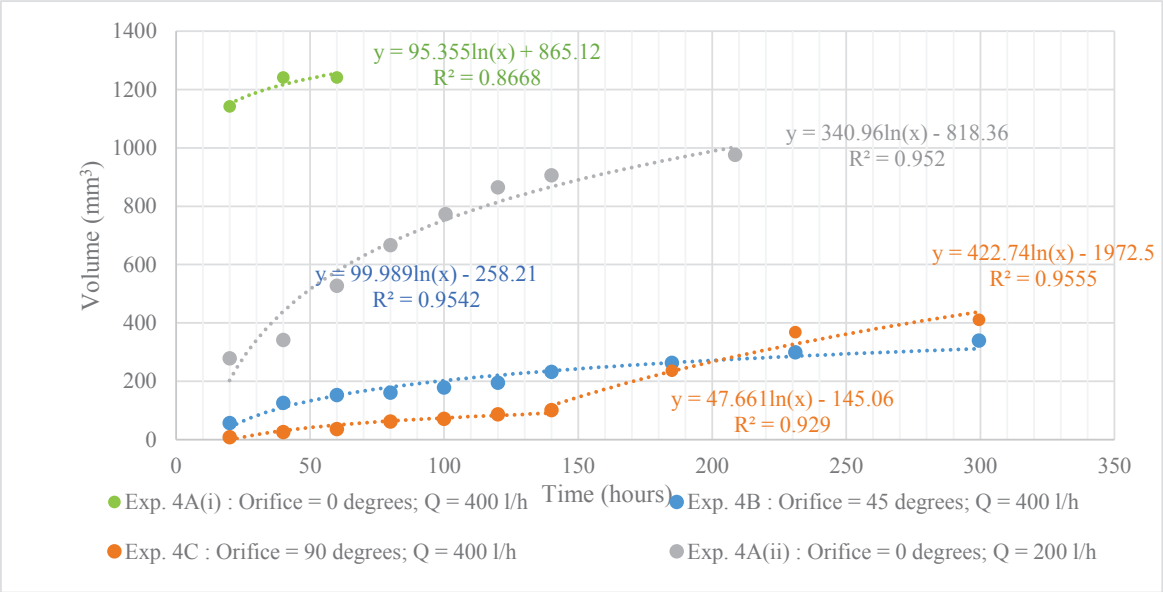

Volume of Removed Material for Experiment 4

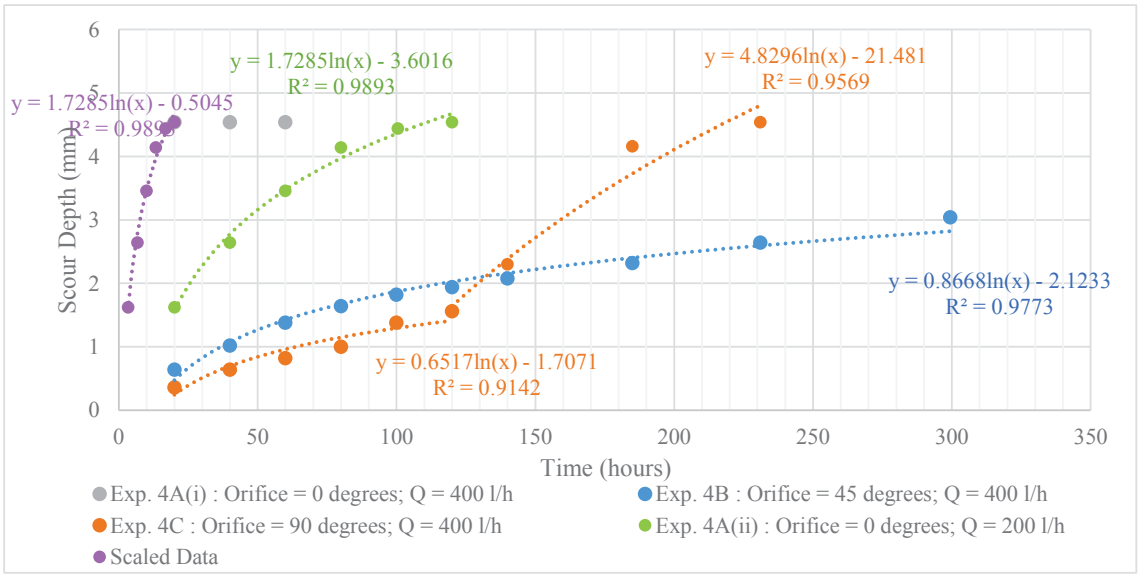

Development of Scour Depth into the Pipe Wall for Experiment 4

7.5.2 Visual Inspection

7.5.2.1 Experiment 4A(i)

4A(i) 0 hours

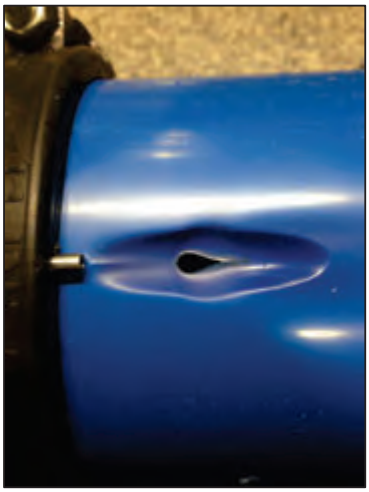

4A(i) 20 hours

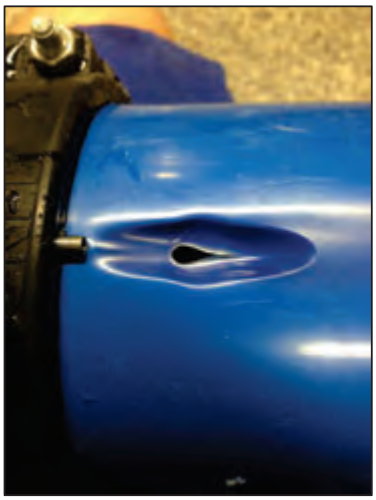

4A(i) 40 hours

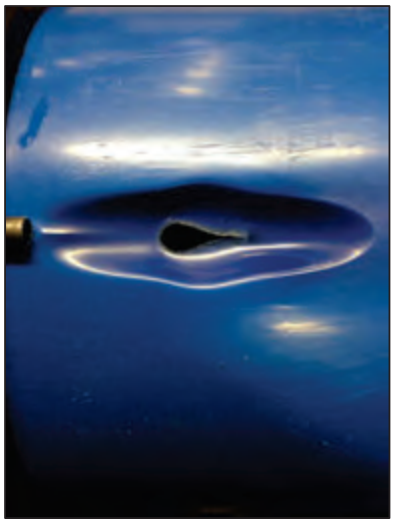

4A(i) 60 hours

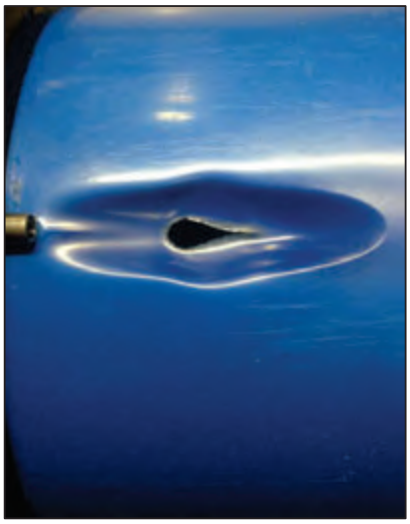

74A(i) 80 hours

7.5.2.2 Experiment 4A(ii)

4A(ii) 0 hours

4A(ii) 20 hours

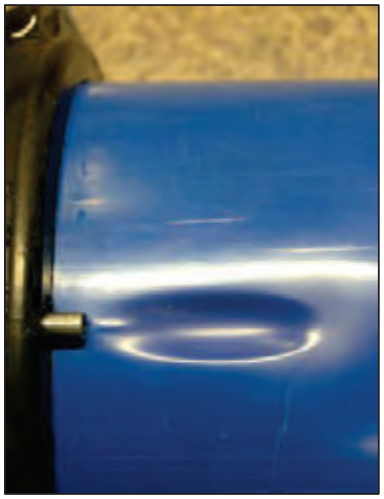

4A(ii) 40 hours

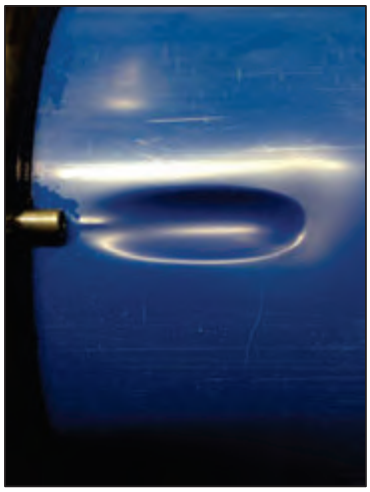

4A(ii) 60 hours

4A(ii) 80 hours

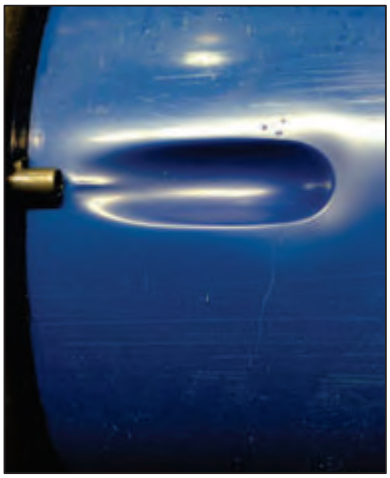

4A(ii) 100.5 hours

4A(ii) 120 hours

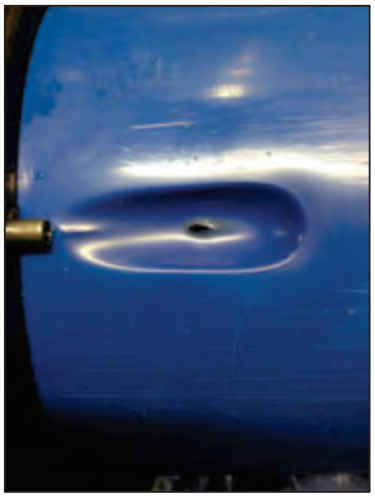

4A(ii) 140 hours

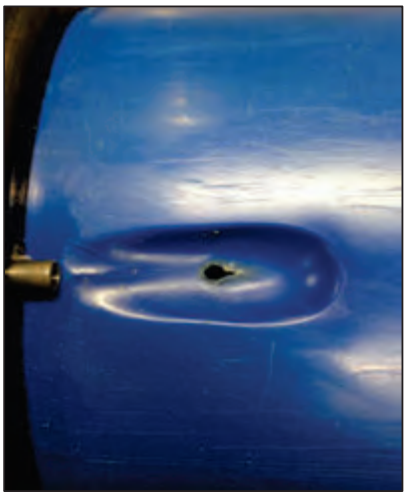

4A(ii) 208.5 hours

7.5.2.3 Experiment 4B

4B 20 hours

4B 40 hours

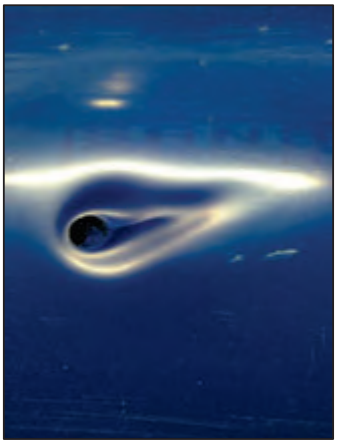

4B 60 hours

4B 80 hours

4B 100 hours

4B 120 hours

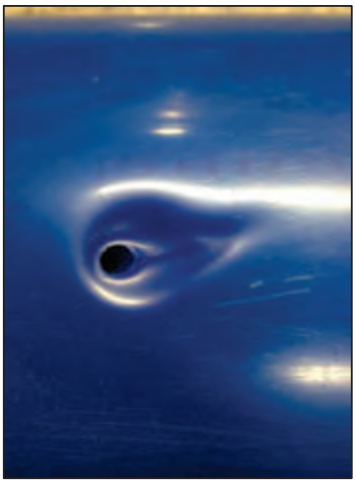

4B 140 hours

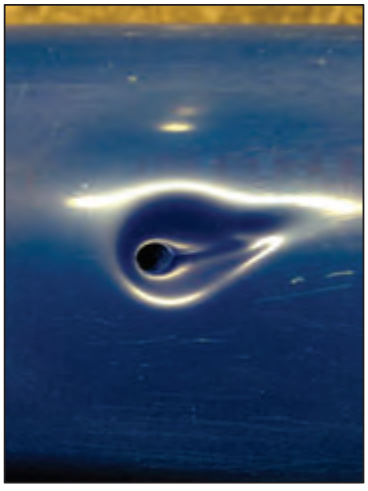

4B 185 hours

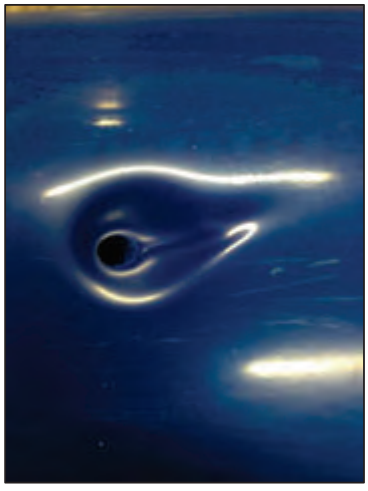

4B 231 hours

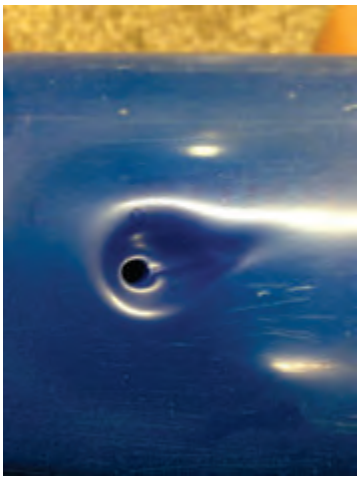

4B 299.5 hours

7.5.2.4 Experiment 4C

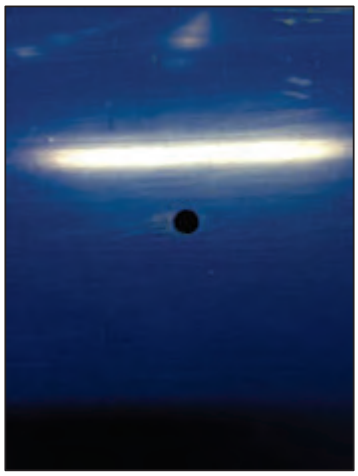

4C 0 hours

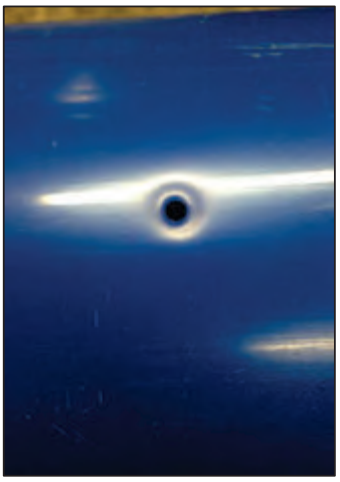

4C 20 hours

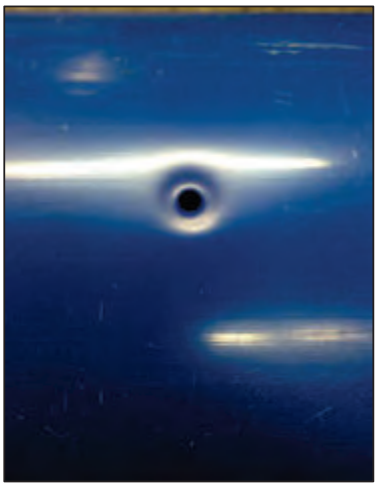

4C 40 hours

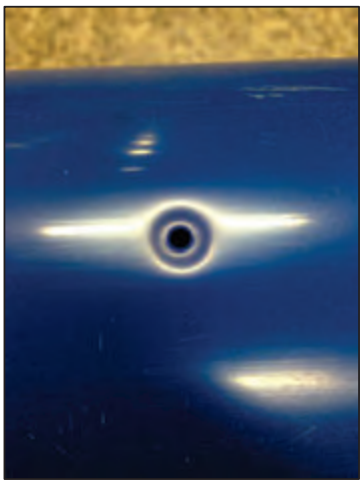

4C 60 hours

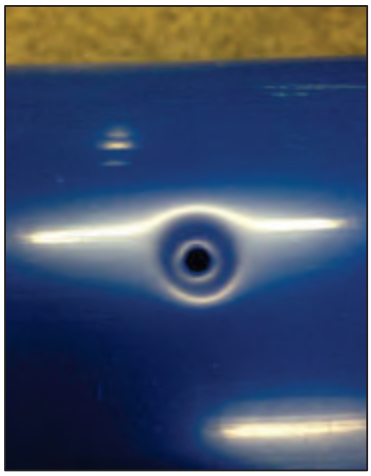

4C 80 hours

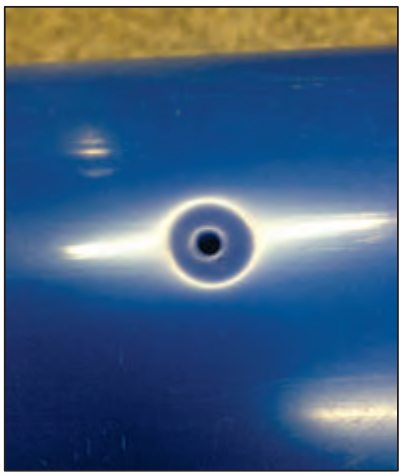

4C 100 hours

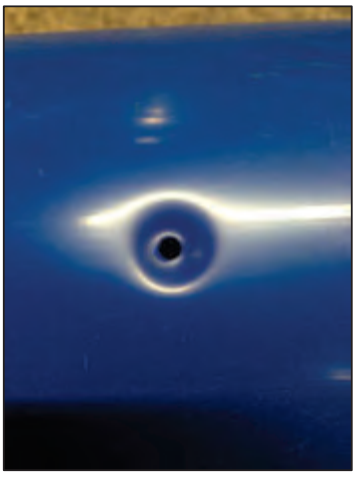

4C 120 hours

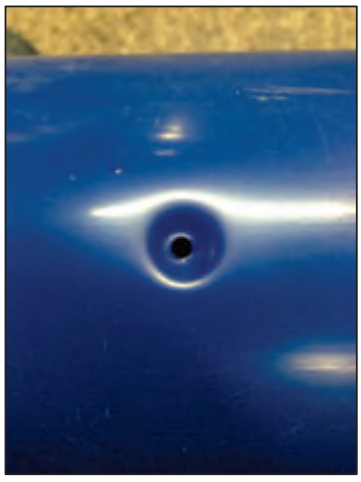

4C 140 hours

4C 185 hours

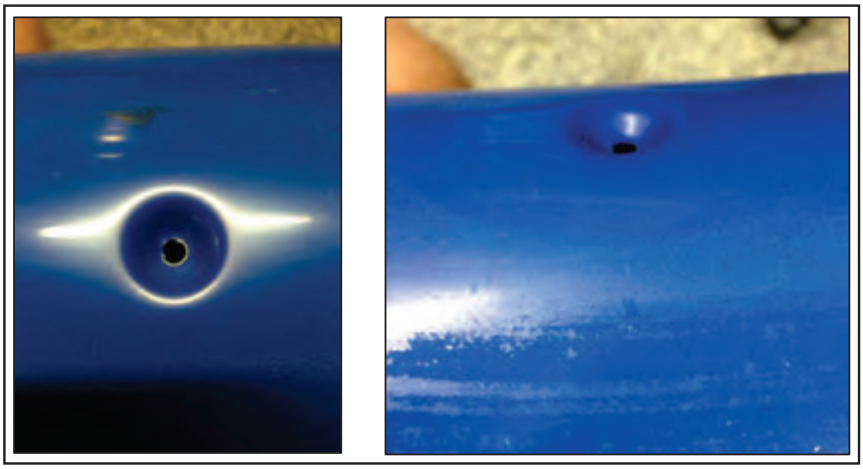

4C 231 hours

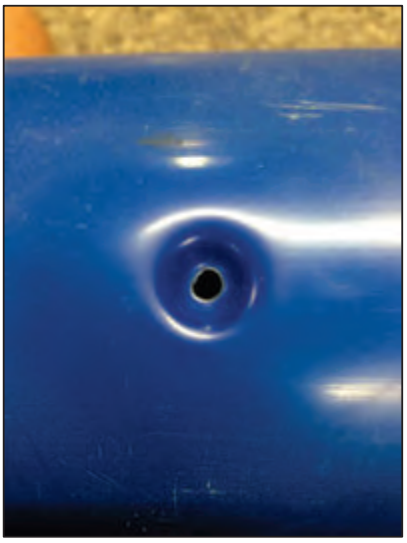

94C 299.5 hours

7.6 Experiment 5: Pipe Material

Operating Conditions for Experiment 3

Experiment	Flow Rate (l/h)	Grain Size (D_{50}) (mm)	Cover Depth (mm)	Pipe Material -	Leak Orientation (°)	Orifice Diameter (mm)
3A	400	1.60	500	**Steel**	45	3
3B	400	1.60	500	**uPVC**	45	3
3C	400	1.60	500	**HDPE**	45	3

7.6.1 Quantitative Data

In the table reporting the data collected for Experiment 5A, it can be observed that there are two additional columns labelled “Dimension A2” and “Dimension B2”. These are the longitudinal and transverse dimensions respectively of the scoured area that is defined by the area where the protective coating was removed from the steel. The visual development of this scour-affected area can be observed in Section 1.6.2.

Quantitative Data for Experiment 5A

Run Time (h)	Dimension A (mm)	Dimension B (mm)	Depth (mm)	Putty (g)	Volume (mm^3)	Dimension A2 (mm)	Dimension B2 (mm)
0.00	4.24	3.0	0.00	0.000	0.0	0.00	0.00
20.00	19.96	9.2	0.26	0.048	23.2	33.08	21.78
40.03	25.18	9.86	0.52	0.088	42.5	38.34	24.72
60.00	27.44	10.72	0.62	0.141	68.1	40.38	26.10
80.00	29.24	11.92	0.80	0.202	97.6	41.44	28.76
100.00	29.24	12.76	0.94	0.247	119.3	42.04	29.86
120.00	29.26	13.28	1.08	0.283	136.7	43.16	30.20
140.00	30.82	13.64	1.18	0.312	150.7	53.84	31.68
182.00	30.82	13.64	1.38	0.376	181.6	55.88	32.14
298.00	30.82	14.26	1.76	0.387	187.0	58.68	33.88

Quantitative Data for Experiment 5B

Run Time (h)	Dimension A (mm)	Dimension B (mm)	Depth (mm)	Putty (g)	Volume (mm^3)
0.00	4.24	3.00	0.00	0.000	0.0
20.00	22.30	10.38	0.36	0.065	31.4
40.03	24.76	11.96	0.76	0.150	72.5
60.00	25.00	12.92	0.94	0.208	100.5
80.00	25.16	13.34	1.28	0.238	115.0
100.00	26.08	14.18	1.44	0.322	155.6
120.00	26.18	14.78	1.68	0.376	181.6
140.00	26.38	15.74	1.74	0.450	217.4
182.00	27.06	16.20	2.26	0.515	248.8
298.00	27.60	17.30	2.64	0.663	320.3

Quantitative Data for Experiment 5B

Run Time (h)	Dimension A (mm)	Dimension B (mm)	Depth (mm)	Putty (g)	Volume (mm^3)
0.00	4.24	3.00	0.00	0.000	0.0
20.00	14.58	8.40	0.26	0.048	23.2
40.03	20.84	8.70	0.46	0.081	39.1
60.00	21.10	9.44	0.74	0.112	54.1
80.00	23.62	10.18	0.74	0.145	70.0
100.00	23.74	12.24	0.96	0.152	73.4
120.00	23.44	12.86	1.02	0.191	92.3
140.00	24.48	12.88	1.24	0.198	95.7
182.00	25.12	13.32	1.38	0.258	124.6
298.00	25.18	15.38	2.14	0.417	201.4

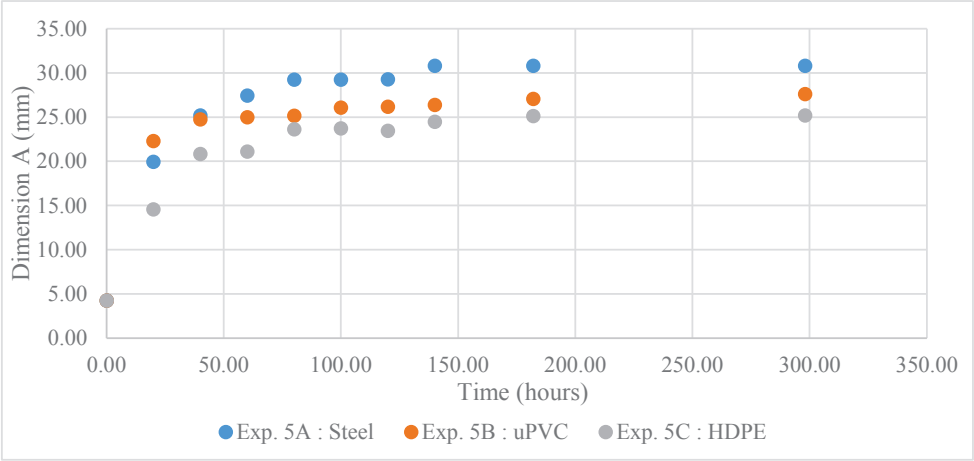

Development of Dimension A for Experiment 5

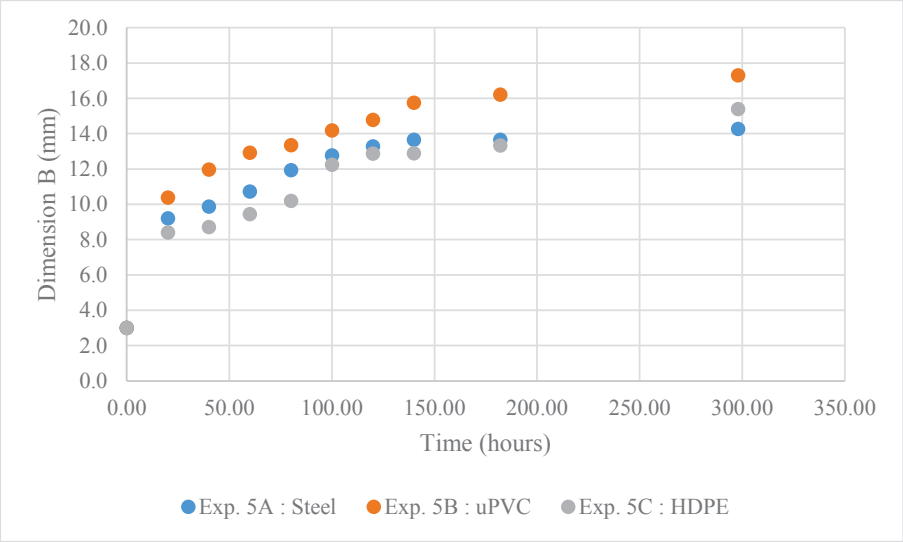

Development of Dimension B for Experiment 5

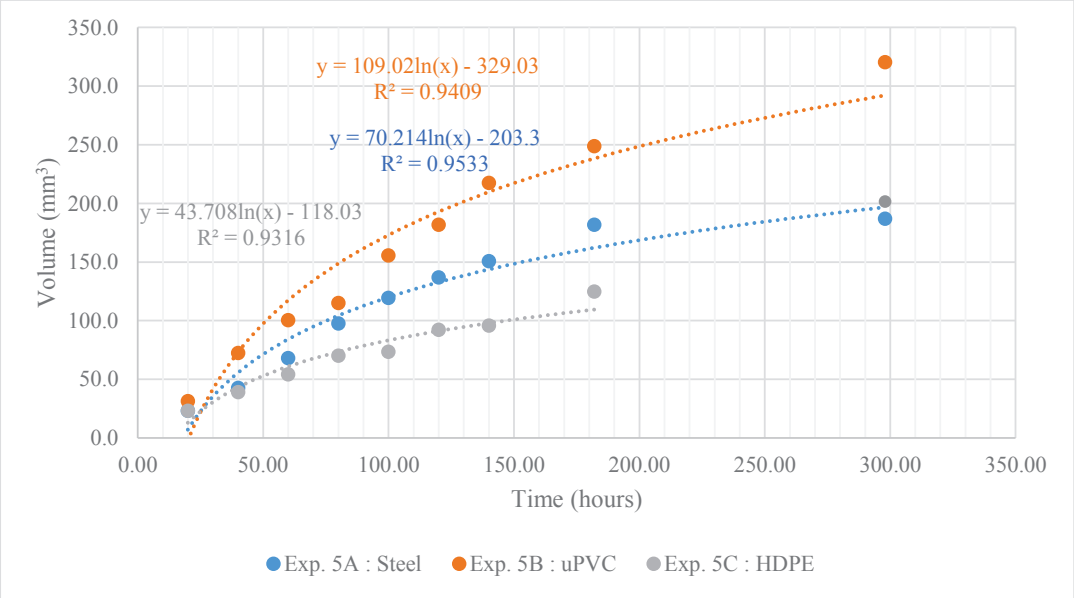

Volume of Removed Material for Experiment 5

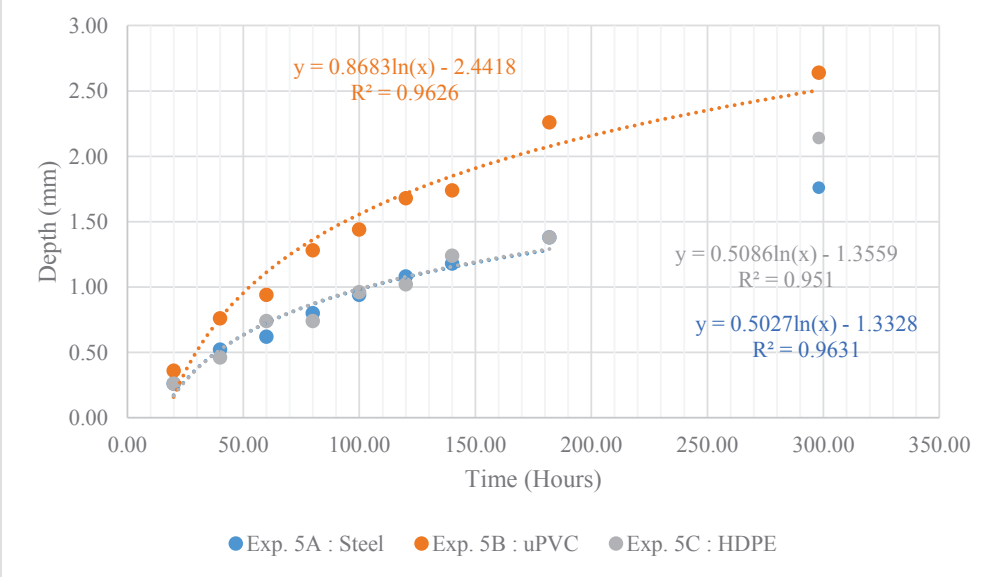

Development of Scour Depth into the Pipe Wall for Experiment 5

7.6.2 Visual Inspection

7.6.2.1 Experiment 5A

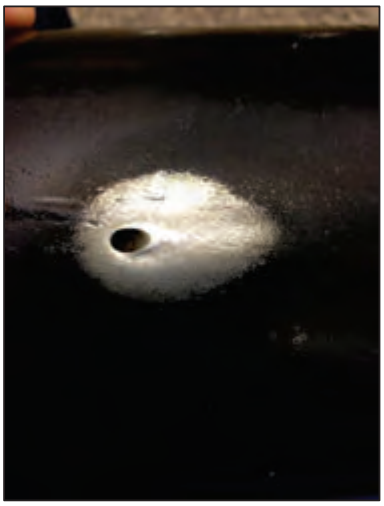

5A 20 hours

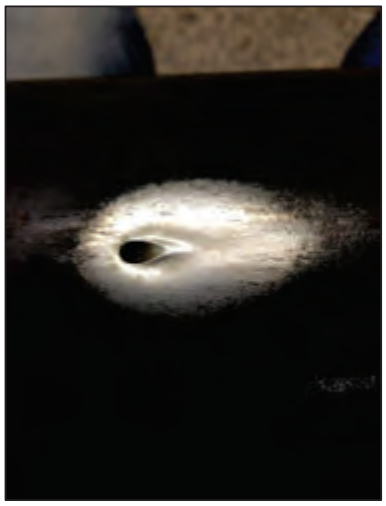

5A 40 hours

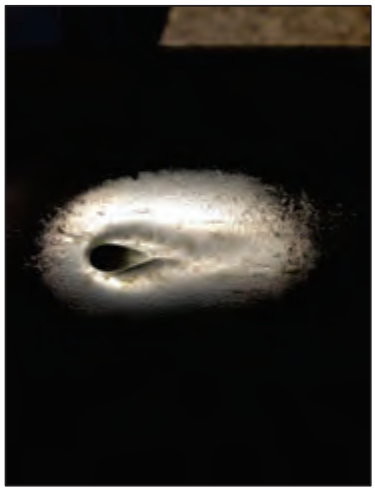

5A 60 hours

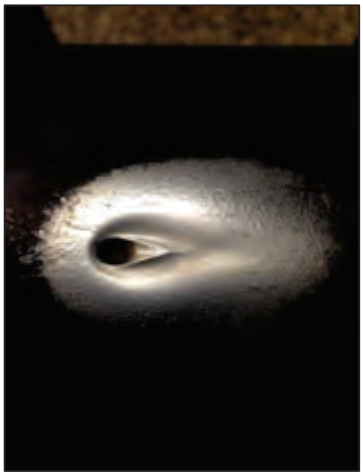

5A 80 hours

5A 100 hours

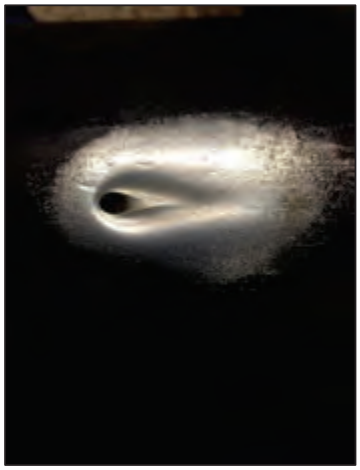

5A 120 hours

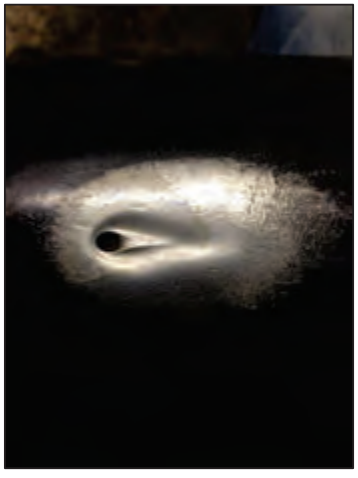

5A 140 hours

5A 182 hours

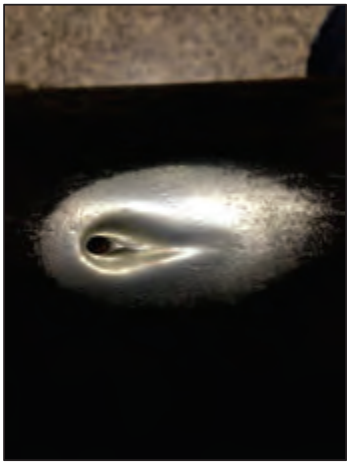

5A 253 hours

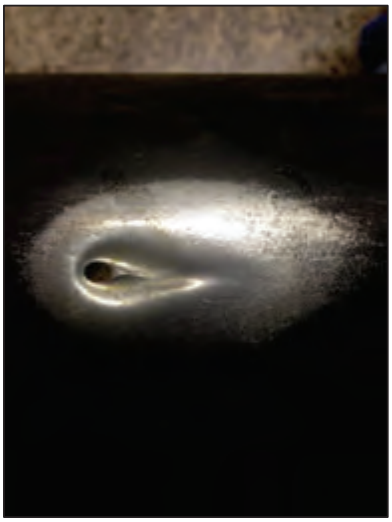

5A 298 hours

7.6.2.2 Experiment 5B

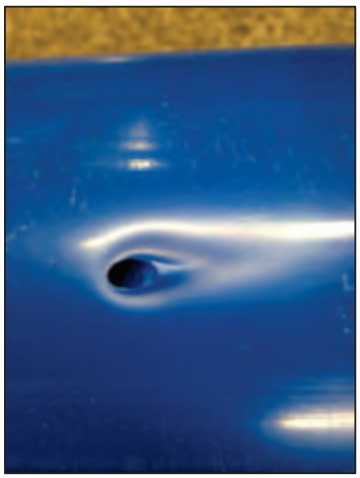

5B 20 hours

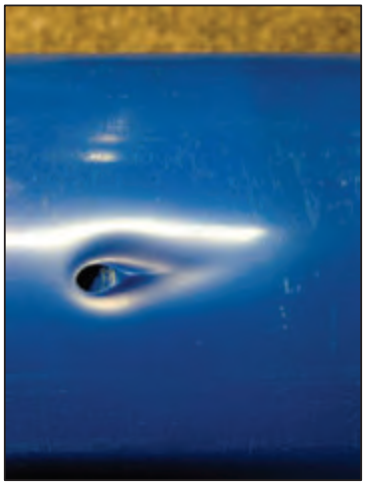

5B 40 hours

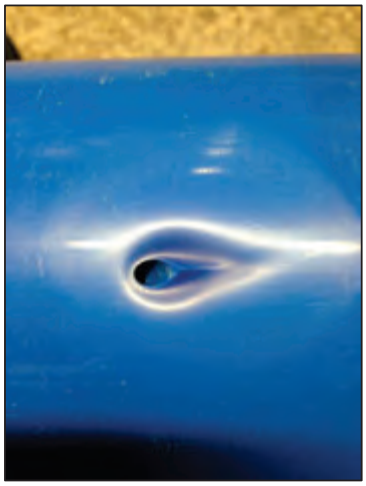

5B 60 hours

5B 80 hours

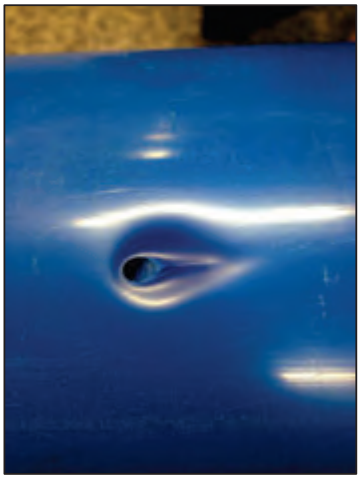

5B 100 hours

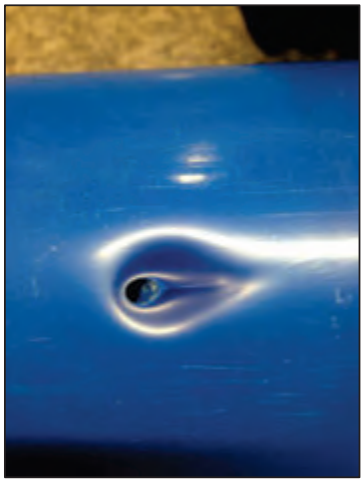

5B 120 hours

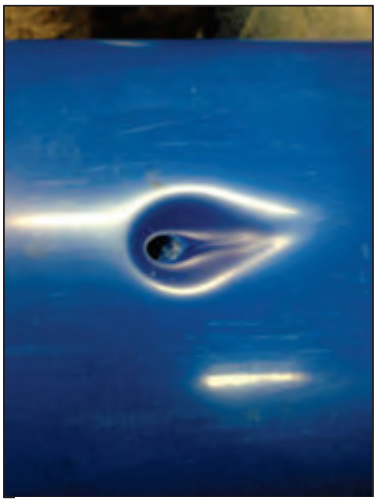

5B 140 hours

5B 182 hours

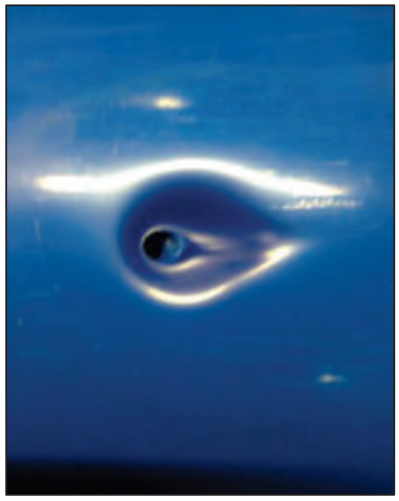

5B 253 hours

5B 298 hours

7.6.2.3 Experiment 5C

5C 0 hours

5C 20 hours

5C 40 hours

5C 60 hours

5C 80 hours

5C 100 hours

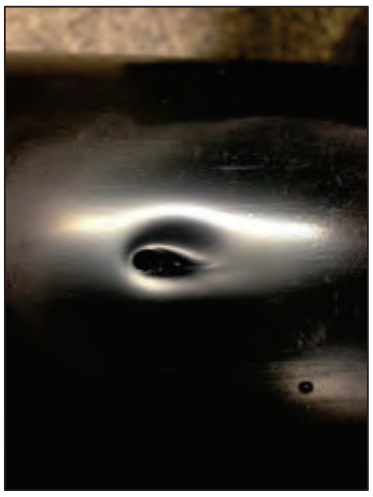

5C 120 hours

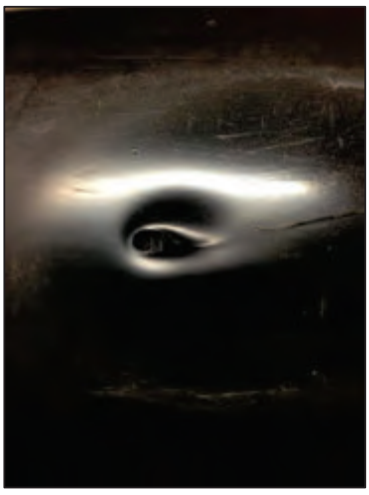

5C 140 hours

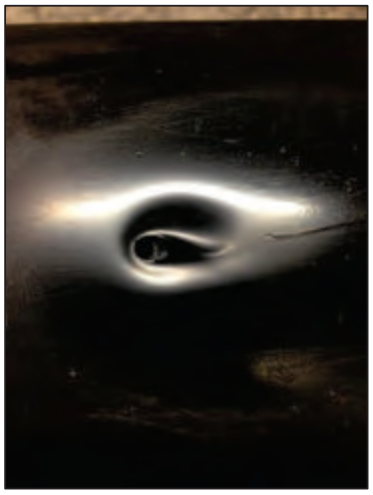

5C 182 hours

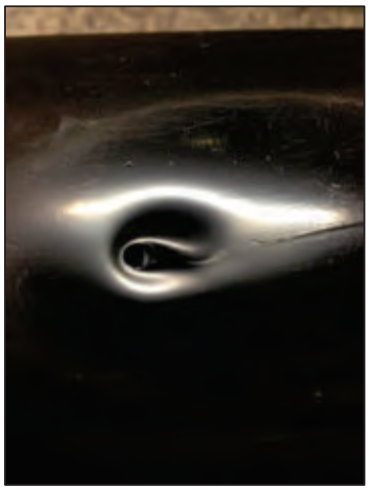

5C 253 hours

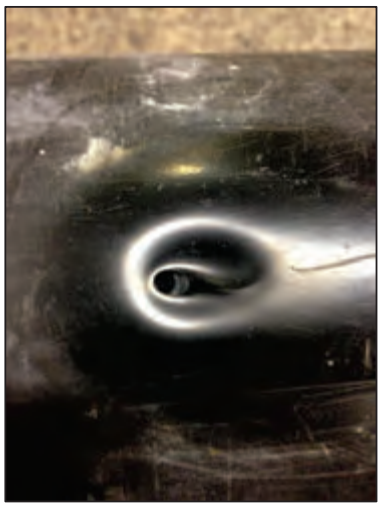

5C 298 hours

Appendix B: Sand Characterisation

1.1 Sand Origins and Compositions

The three sand types that were used for the pilot experiment differed only in median grain diameter size, D_{50}, but not in composition. The three sands used for this experiment were silica sands, originating from the Consol Industrial Mineral mine in Philippi, Western Cape, South Africa (Consol, 2014). This mine excavates natural silica deposits from a depth of up to 20m below ground level. All three sands were silica sands.

The three sands were supplied by Cape Silica Suppliers, Blackheath, Western Cape, South Africa.

In this dissertation, the three sand types were differentiated and named by their D_{50} grain size. Table shows the product name, as named by the supplier, the sands' corresponding D_{50} used in this dissertation, as well as the percentage chemical composition, as quoted by the supplier.

Table 1: Chemical Composition of Sands

Product Name	**Dissertation**	**D_{50} = 2.10mm**	**D_{50} = 1.60mm**	**D_{50} = 0.75mm**
	Manufacturer's Name	**Filter Grit 1.2mm-2.4mm**	**Filter Grit 0.8mm-1.4mm**	**No. 1 Sand**
Chemical Composition (%)				
SiO_2		98	98	99.75
Fe_2O_3		0.18	0.18	0.023
Al_2O3		-	-	0.070
TiO_2		-	-	0.024
ZrO_2		-	-	0.005
CaO		-	-	0.003

1.2 Particle Size Distribution

The Dry Sieve Method was used to determine the particle size distribution for the three sand samples. The test was carried out in accordance with BS 1377: Part 2: 1990. (British Standards Institution, 1990).

The results obtained for the sieve analyses for the three sands are given in Tables. Figure shows the grading curves for the three sands.

Table 2: Sieve Analysis for Sand D50 = 2.1mm

Sieve Opening (µm)	Sieve Weight (g)	Weight Sieve + Aggregate (%)	Aggregate Retained (g)	Mass Retained (%)	Total % Retained on Sieve	Cumulative % passing
3350	600.8	600.8	0.0	0.00	0.00	100.00
2000	577.6	813.5	235.9	52.80	52.80	47.20
1180	543.8	743.1	199.3	44.61	97.40	2.60
850	521.3	531.1	9.8	2.19	99.60	0.40
600	532.8	534.2	1.4	0.31	99.91	0.09
425	505.8	506.1	0.3	0.07	99.98	0.02
300	477.4	477.5	0.1	0.02	100.00	0.00
0	475.0	475.0	0.0	0.00	100.00	0.00
		Total	**446.8**			

Table 3: Sieve Analysis for Sand D50 = 1.6mm

Sieve Opening (µm)	Sieve Weight (g)	Weight Sieve + Aggregate (%)	Aggregate Retained (g)	Mass Retained (%)	Total % Retained on Sieve	Cumulative % passing
3350	600.8	600.8	0.0	0.00	0.00	100.00
2000	568.5	649.1	80.6	17.20	17.20	82.80
1180	543.6	862.1	318.5	67.98	85.19	14.81
850	521.5	585.2	63.7	13.60	98.78	1.22
600	533.2	538	4.8	1.02	99.81	0.19
425	506.0	506.8	0.8	0.17	99.98	0.02
300	477.5	477.6	0.1	0.02	100.00	0.00
0	475.2	475.2	0.0	0.00	100.00	0.00
		Total	**468.5**			

Table 4: Sieve Analysis for Sand D50 = 0.75mm

Sieve Opening (µm)	Sieve Weight (g)	Weight Sieve + Aggregate (%)	Aggregate Retained (g)	Mass Retained (%)	Total % Retained on Sieve	Cumulative % passing
2000	568.00	568.0	0.0	0.00	0.00	100.00
1180	551.90	556.7	4.8	1.17	1.17	98.83
850	521.00	635.7	114.7	27.90	29.07	70.93
600	513.50	744.9	231.4	56.29	85.36	14.64
425	505.80	556.2	50.4	12.26	97.62	2.38
300	476.60	481.2	4.6	1.12	98.74	1.26
250	505.60	507.2	1.6	0.39	99.12	0.88
150	469.30	471.7	2.4	0.58	99.71	0.29
63	457.00	458.2	1.2	0.29	100.00	0.00
0	474.80	474.8	0.0	0.00	100.00	0.00
		Total	**411.10**			

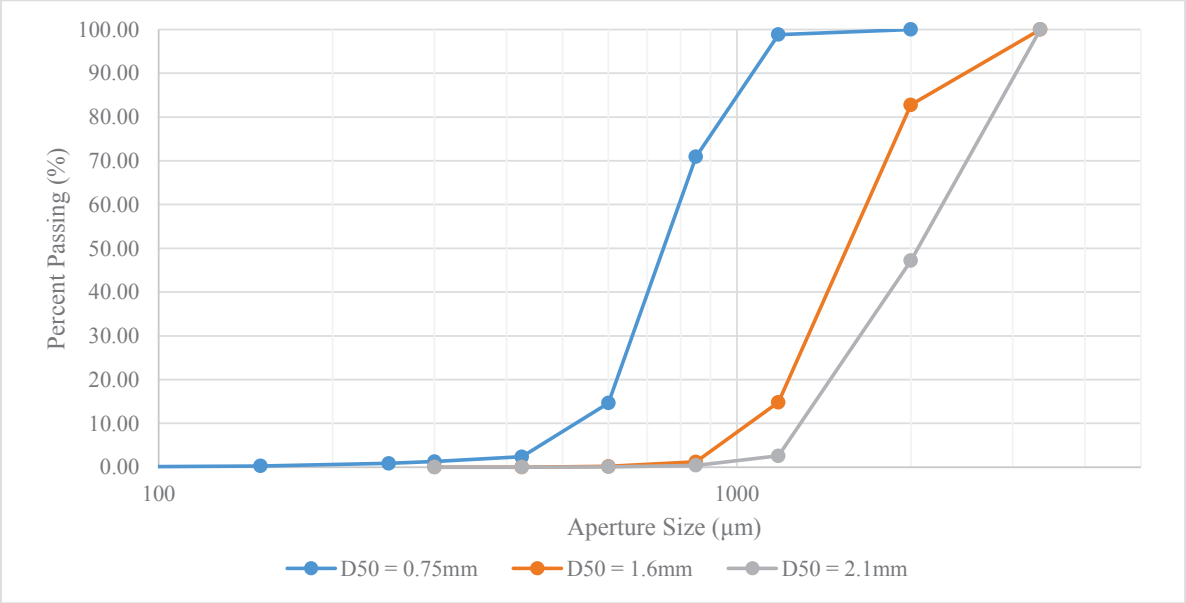

Figure 1: Grading Curves for three Sand Types used in Experiments

1.3 D_{50} and Coefficients of Uniformity

The D_{60}, D_{50} and D_{10} values of the three sand samples were read off of the grading curves as shown in Figure. Figure demonstrates how the D_{50} values of the sands were determined. The horizontal dashed line marks line where 50% of the soil sample passed through the sieve. The vertical dashed lines in Figure indicate the D_{50} grain size for each sand type.

Table Indicates the D_{60}, D_{50} and D_{10} that were read $_{off}$ the grading curve. The D_{60} and D_{10} were used to calculate the coefficient of uniformity, given by Equation. The coefficient of uniformity is also given in Table.

$$C_u = \frac{D_{60}}{D_{10}}$$

Where C_u = Coefficient of uniformity

Table 5: Characteristic Grain Sizes for Sands used in Experiments

D_{50} (mm)	D_{10} (mm)	D_{60} (mm)	C_u -
2.1	1.30	2.30	1.77
1.2	1.06	1.72	1.62
0.75	0.54	0.80	1.48

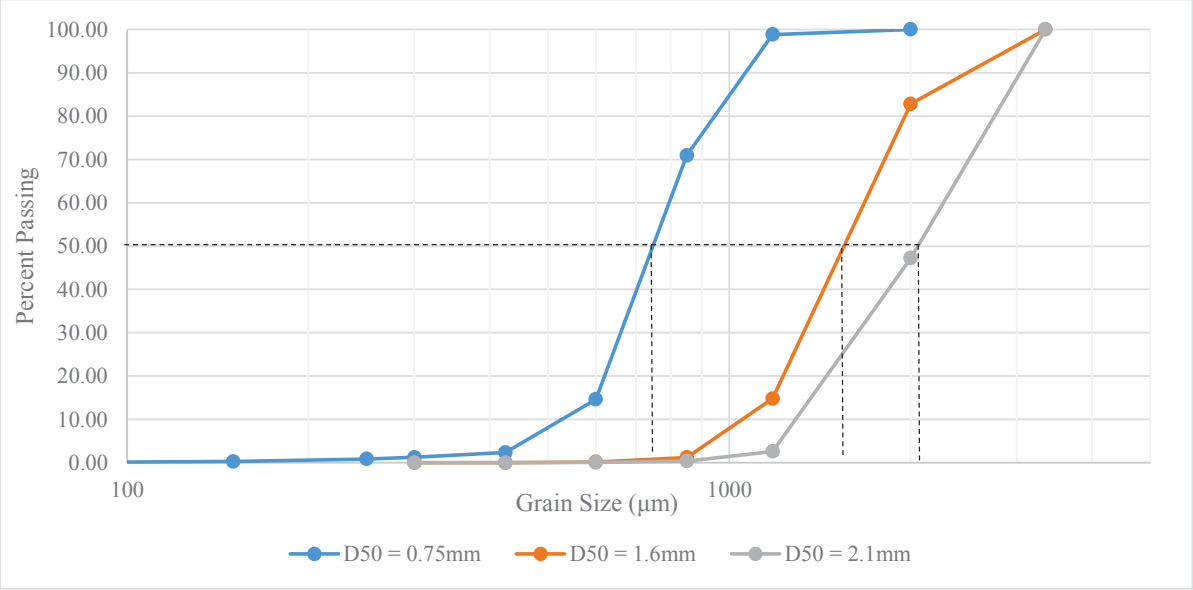

Figure 2: Reading Values off Grading Curve

1.4 Particle Density

The Small Pyknometer Method was used to determine the particle density of the three sands used in the experiments. The test was carried out in accordance with BS 1377: Part 2: 1990.

As specified in BS 1377: Part 2, the particle density was calculated with the following equation:

$$\rho_s = \frac{\rho_w \cdot (m_2 - m_1)}{(m_4 - m_1) - (m_3 - m_2)}$$

Where ρ_s = Soil particle density; ρ_w = Density of water; m_1 = Mass of bottle; m_2= Mass of soil and bottle; m_3 = Mass of bottle filled with soil and water; m_4 = Mass of bottle filled with water

The test was repeated three times for each soil sample, and the results were averaged. The results of these particle density tests are given in Tables.

Table 6: Particle Density Test for Sand D_{50} =2.1mm

	m_1 (g)	m_2 (g)	m_3 (g)	m_4 (g)	Density (kg/m^3)
Test 1	34.628	44.658	90.800	84.489	**2696.96**
Test 2	36.926	46.936	94.544	88.298	**2659.40**
Test 3	35.353	45.365	93.639	87.317	**2713.28**
				Average	**2690**

Table 7: Particle Density Test for Sand D_{50} =1.6mm

	m_1 (g)	m_2 (g)	m_3 (g)	m_4 (g)	Density (kg/m^3)
Test 1	37.264	47.318	95.145	88.854	**2671.80**
Test 2	35.355	45.415	93.572	87.296	**2658.56**
Test 3	34.622	44.674	90.731	84.467	**2653.64**
				Average	**2661**

Table 8: Particle Density Test for Sand D50 =0.75mm

	m_1 (g)	m_2 (g)	m_3 (g)	m_4 (g)	Density (kg/m^3)
Test 1	37.264	47.26	95.16	88.925	**2657.80**
Test 2	35.049	45.069	91.286	84.965	**2708.84**
Test 3	35.408	45.418	90.201	83.893	**2703.94**
				Average	**2690**

1.5 Dry Bulk Density

1.5.1 Loose/Minimum Dry Bulk Density

The method used to calculate the loose/minimum dry bulk densities of the three soils was *Method A* as described in ASTM International D4254 : 2015. A mould with alternate dimensions to those specified in the standard was used. The dimensions of the mould are given in Table. Each sample was tested three times and the results were averaged to calculate the loose bulk density.

Tables report the results of the results of the bulk density tests for soils D_{50}=2.10mm, D_{50}=1.60mm and D_{50}=0.75mm.

Table 9: Dimensions of Mould used for Bulk Density Test

Diameter (mm)	Height (mm)	Volume (litres)	Mass (kg)
152.55	156.10	2.85	3.03

Table 10: Minimum Dry Bulk Density of Sand D_{50} = 2.10mm

	Mass of Soil (kg)	Density (kg/m^3)
Test 1	4.250	1490
Test 2	4.275	1498
Test 3	4.265	1495
	Average	**1494**

Table 11: Minimum Dry Bulk Density of Sand D50 = 1.60mm

	Mass of Soil (kg)	Density (kg/m^3)
Test 1	4.335	1519
Test 2	4.320	1514
Test 3	4.290	1504
	Average	**1512**

Table 12: Minimum Dry Bulk Density of Sand D50 = 0.75mm

	Mass of Soil (kg)	Loose Density (kg/m^3)
Test 1	4.610	1616
Test 2	4.605	1614
Test 3	4.590	1609
	Average	**1613**

1.5.2 Compact/Maximum Dry Bulk Density

The method used to calculate the compact/maximum dry bulk densities of the three soils was *Method 2A* as described in ASTM International D4253 : 2015. The same mould was used for the minimum and the maximum bulk density tests, as described in Table.

Table reports the compact/maximum dry bulk densities of the three soils.

Table 13: Maximum Dry Bulk Density of Three Sand Types

Sand	Mass of soil (kg)	Average Height after Compaction (mm)	Volume (litres)	Density (kg/m^3)
D_{50}=2.10mm	4.265	147.650	2.70	**1580**
D_{50}=1.60mm	4.290	142.840	2.61	**1643**
D_{50}=0.75mm	4.590	140.295	2.56	**1790**

1.5.3 Void Ratio and Porosity

The maximum and minimum void ratios were calculated with the following equations:

$$e_{max} = \frac{\rho_w \cdot G}{\rho_{dmin}} - 1$$

$$e_{min} = \frac{\rho_w \cdot G}{\rho_{dmax}} - 1$$

Where e_{max}=Maximum void ratio; e_{min}=Minimum void ratio, G = Particle specific gravity; ρ_{dmax}=Maximum dry bulk density; ρ_{dmin}=Minimum dry bulk density.

The maximum and minimum porosity values were then calculated using the following equation:

$$n = \frac{e}{1 + e}$$

Where n = porosity.

The maximum and minimum void ratios and porosities of the three soils are given in Table.

Table 14: Void Ratios and Porosity

Sand	Minimum Void Ratio	Maximum Void	Minimum Porosity (%)	Maximum Porosity (%)
D_{50}=2.10mm	0.70	0.80	41.25	44.45
D_{50}=1.60mm	0.62	0.76	38.26	43.17
D_{50}=0.75mm	0.50	0.67	33.46	40.05

1.6 Permeability

The Constant Head Method was used to determine the permeability of the three soils used in this study. The test was carried out in accordance with ASTM International-D2434 : 2006.

Table gives the dimensions of the permeater, and the heights of the manometer outlets relative to the base of the permeater.

Table 15: Dimensions of Permeater

Permeater Diameter (mm)	Permeater Cross-sectional Area (cm^2)	Manometer Heights			
		L_1 (mm)	L_2 (mm)	L_3 (mm)	L_4 (mm)
113.58	101.3	108	208	308	408

1.6.1 Permeability for Sand D_{50}=2.10mm

The flow rate was measured and calculated three times for this test, and the average of the three measurements was for the permeability calculations. The volume of water flowing out of the permeater over a measured time period was used to calculate the flow rate. Table reports the flow rates used to calculate the permeability of the D_{50}=2.10mm soil.

The permeability was then calculated between the manometers using Darcy's Law of permeability as follows:

$$K = \frac{Q \cdot L}{A \cdot h_s}$$

Where K= Coefficient of permeability; Q = Volumetric flow rate; L = Distance between manometers; h = Headloss between manometers

Table reports the measured water heights in the manometers. These readings were used to calculate the headloss between the manometers.

Table reports the results of the permeability of the D_{50}=2.10mm soil. It should be noted that the highlighted rows were note used in the calculation of the average permeability as they appear to be outliers.

Table 16: Flow Rate for D_{50} = 2.10mm Permeability Test

Measurement	Volume (ml)	Time (s)	Flow Rate (l/min)	Flow Rate (m^3/s)
1	3301	21.13	9.37	1.56×10^{-4}

2	3239	21.03	9.24	$1.54x10^{-4}$
3	3417	22.68	9.04	$1.51x10^{-4}$
		Average	**9.22**	**$1.54\ x10^{-4}$**

Table 17: Manometer Readings for D_{50} = 2.10mm Permeability Test

Manometer Number	Manometer Reading, *h* (mm)
1	1070
2	970
3	890
4	829

Table 18: Permeability of Soil D_{50} = 2.10mm

Manometers	Length, L (mm)	Headloss, h (mm)	Permeability	
			K (m/s)	K (cm/s)
1 to 2	100	100	0.015	1.52
2 to 3	100	80	0.019	1.90
***3 to 4**	100	61	0.025	2.49
1 to 3	200	180	0.017	1.68
1 to 4	300	241	0.019	1.89
***2 to 4**	200	141	0.022	2.15
			Average	**1.75**

***Highlighted rows have been excluded from calculated average permeability**

1.6.2 Permeability for Sand D_{50}=1.6mm

The flow rate was measured and calculated three times for this test, and the average of the three measurements was for the permeability calculations. The volume of water flowing out of the permeater over a measured time period was used to calculate the flow rate. Table reports the flow rates used to calculate the permeability of the D_{50}=1.60mm soil.

The permeability was then calculated between the manometers using Darcy's Law of permeability as follows:

$$K = \frac{Q \cdot L}{A \cdot h_s}$$

Where K= Coefficient of permeability; Q = Volumetric flow rate; L = Distance between manometers; h = Headloss between manometers

Table reports the measured water heights in the manometers. These readings were used to calculate the headloss between the manometers.

Table reports the results of the permeability of the D_{50}=1.60mm soil.

Table 19: Flow Rate for D50 = 1.60mm Permeability Test

Measurement	Volume (ml)	Time (s)	Flow Rate (l/min)	Flow Rate (m^3/s)
1	3287	24.58	8.02	1.34×10^{-4}
2	3581	26.61	8.07	1.35×10^{-4}
3	3511	25.86	8.15	1.36×10^{-4}
		Average	**8.08**	$\mathbf{1.35 \times 10^{-4}}$

Table 20: Manometer Readings for D50 = 1.60mm Permeability Test

Manometer Number	Manometer Reading, h (mm)
1	1145
2	873
3	565
4	224

Table 21: Permeability of Soil D50 = 1.60mm

Manometers	Length, L (mm)	Headloss, h (mm)	Permeability	
			K (m/s)	K (cm/s)
1 to 2	100	272	0.005	0.49
2 to 3	100	308	0.004	0.43
3 to 4	100	341	0.004	0.39
1 to 3	200	580	0.005	0.46
1 to 4	300	921	0.004	0.43
2 to 4	200	649	0.004	0.41
			Average	**0.44**

1.6.3 Permeability for Sand D_{50}=0.75mm

The flow rate was measured and calculated three times for this test, and the average of the three measurements was for the permeability calculations. The volume of water flowing out of the permeater over a measured time period was used to calculate the flow rate. Table reports the flow rates used to calculate the permeability of the D_{50}=0.75mm soil.

The permeability was then calculated between the manometers using Darcey's Law of permeability as follows:

$$K = \frac{Q \cdot L}{A \cdot h_s}$$

Where K= Coefficient of permeability; Q = Volumetric flow rate; L = Distance between manometers; h = Headloss between manometers

Table reports the measured water heights in the manometers. These readings were used to calculate the headloss between the manometers. It should be noted that Table does not report a measured manometer height for manometer 4. This is because the fine soil particles entered the manometer, and hence obstructed the water from rising in the sight tube.

Table reports the results of the permeability of the D_{50}=0.75mm soil.

Table 22: Flow Rate for D50 = 0.75mm Permeability Test

Measurement	Volume (ml)	Time (s)	Flow Rate (l/min)	Flow Rate (m^3/s)
1	4108	65.19	3.78	$6.30x10^{-5}$
2	3433	55.07	3.74	$6.23x10^{-5}$
3	3783	60.06	3.78	$6.30x10^{-5}$
		Average	**3.77**	**$6.28x10^{-5}$**

Table 23: Manometer Readings for D50 = 0.75 mm Permeability Test

Manometer Number	Manometer Reading, h (mm)
1	1172
2	838
3	363
4	-

Table 24: Permeability of Soil D50 = 0.75mm

Manometers	Length, L (mm)	Headloss, h (mm)	Permeability	
			K (m/s)	K (cm/s)
1 to 2	100	334	0.002	0.19

2 to 3	100	475	0.001	0.13
1 to 3	200	809	0.002	0.15
			Average	**0.16**

1.7 Particle Form Factor

While there are a multitude of methods and techniques for estimating the shape of form factor of a particle, the Scalene Ellipsoid Equivalent Sphericity (SEES) method was selected for these sand samples (Clayton, Abbireddy & Schiebel, 2009). The advantage of this method is that it considers three dimensions to estimate the particle's form (where most other methods only consider two dimensions of the particle), and can therefore differentiate between bulky and platy particles.

The SEES form factor can be calculated in two different ways described by Clayton et al. (2009). Either of the methods is acceptable, but one method may be preferable to the other depending on the equipment that is available.

The first method requires the major (L) and intermediate (I) dimensions to be obtained, while the second method requires the major (L) and the smallest dimension (S). The major dimension (L) is defined as the diameter of the smallest circumscribed circle around the projection of a particle onto a plane normal to the imaging system. The intermediate dimension (I) is defined as the largest inscribed circle within the projection of a particle onto a plane normal to the imaging system. The smallest dimension (S) is defined as the smallest inscribed circle within a projection of the soil particle on a plane orthogonal to the major dimension.

The method used to calculate the form factor for the three soils was the following:

1. A soil particle was dropped onto a horizontal surface. and The particle was then fixed to a small right-angled block using double sided adhesive tape by gently pressing the block against the particle's surface.
2. The particle's image was then captured in plan view with static imaging apparatus.
3. The block was then rotated 90° such that the particle was viewed orthogonally to the plan view. The orthogonal view was then captured.
4. Using the projections of these two views, the L, I and S dimensions were measured using Autocad.
5. The SEES was calculated using Equation. While the I dimension was not used in this calculation, it has been recorded.
6. This test was performed on 3 randomly selected particles for each sand type, and the SEES was averaged.

$$SEES = \frac{S}{L}$$

Where S = Smallest particle dimension; L = Major particle dimension.

Tables show the L, I and S dimensions for the three sand types, as well as the SEES. The Figures below each table show the visual representations of the L, I and S dimensions for the sand types in their corresponding tables.

Table 25: L, I and S Dimensions for SEES, D_{50}=2.1mm

Sample	Front View		Side View	SEES S/L
	L (mm)	I (mm)	S (mm)	
1	0.8164	0.5650	0.4537	0.56
2	0.8205	0.5588	0.4900	0.60
3	0.8170	0.5648	0.4505	0.55
			Average	**0.57**

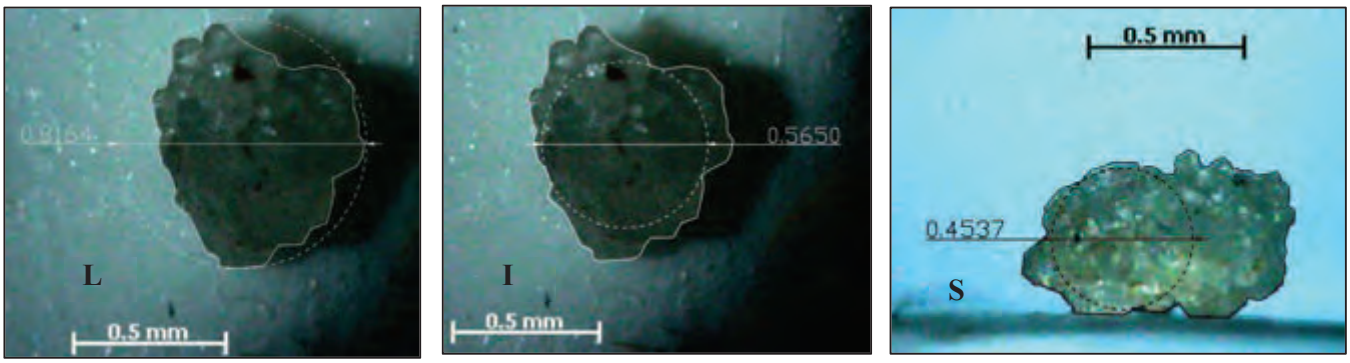

Figure 4: D50 = 2.1mm -Sample 1

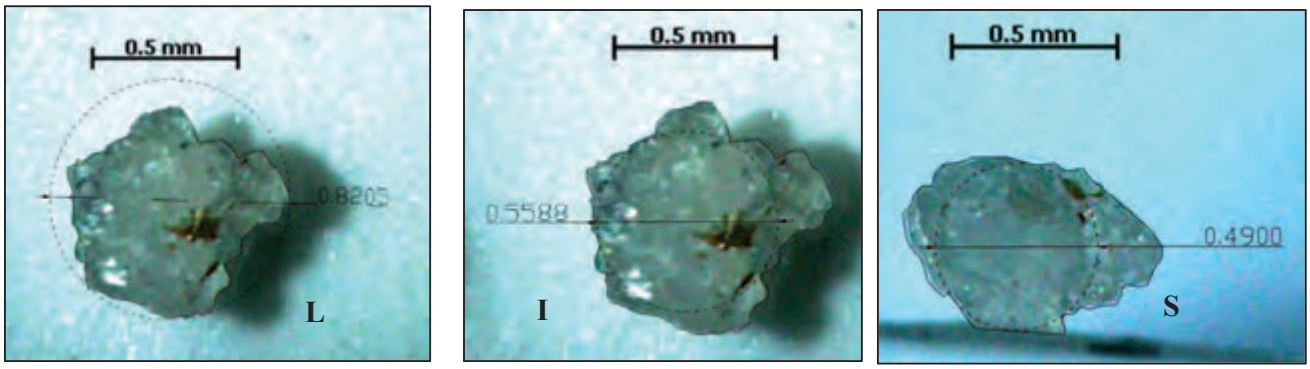

Figure 5: D50 = 2.1mm -Sample 2

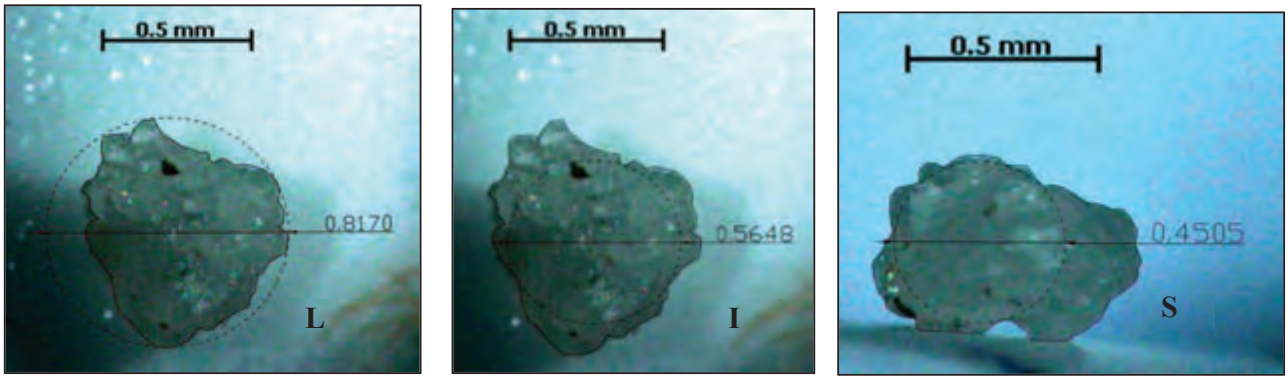

Figure 3: D50 = 2.1mm -Sample 3

Table 26: L, I and S Dimensions for SEES, D50=1.6mm

Sample	Front View		Side View	SEES S/L
	L (mm)	I (mm)	S (mm)	
1	0.7669	0.4843	0.3960	0.52
2	0.6252	0.4508	0.2912	0.47
3	0.7314	0.4572	0.3563	0.49
			Average	**0.49**

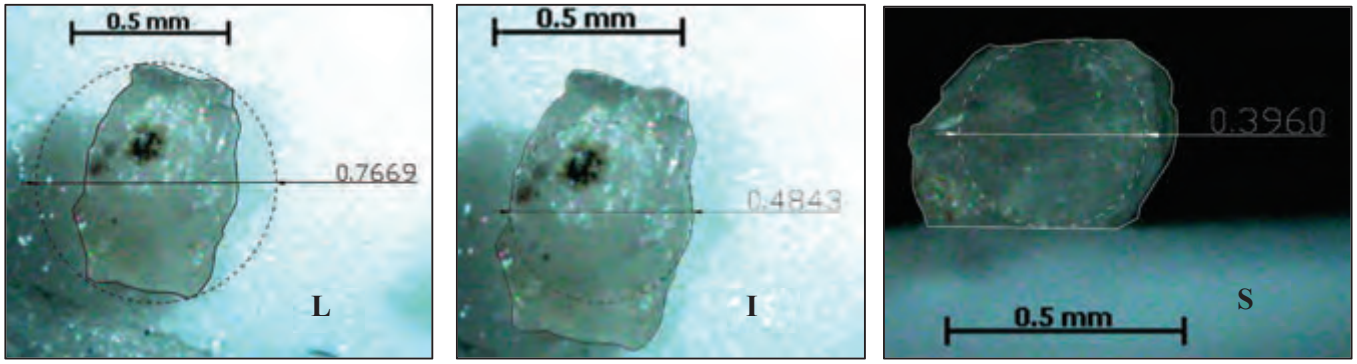

Figure 7: D50 = 1.6mm -Sample 1

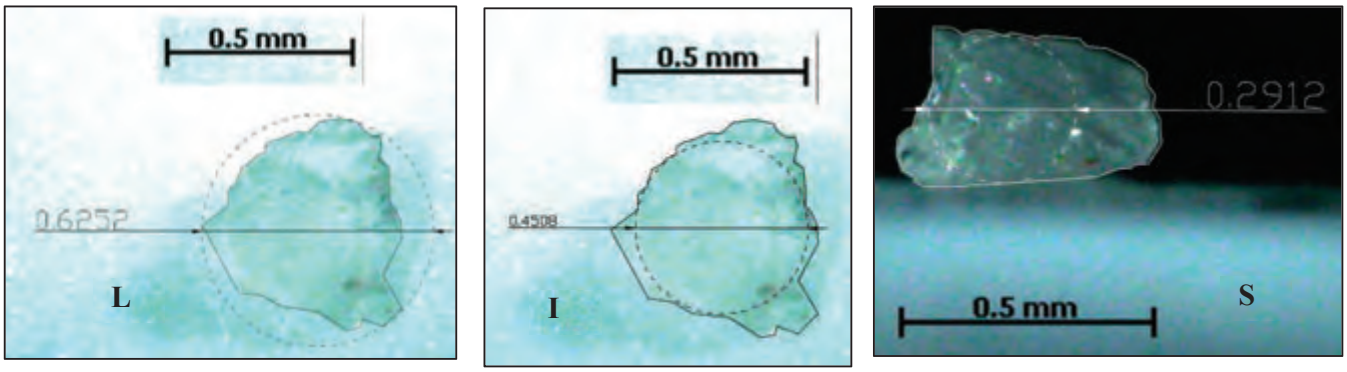

Figure 8: D50 = 1.6mm -Sample 2

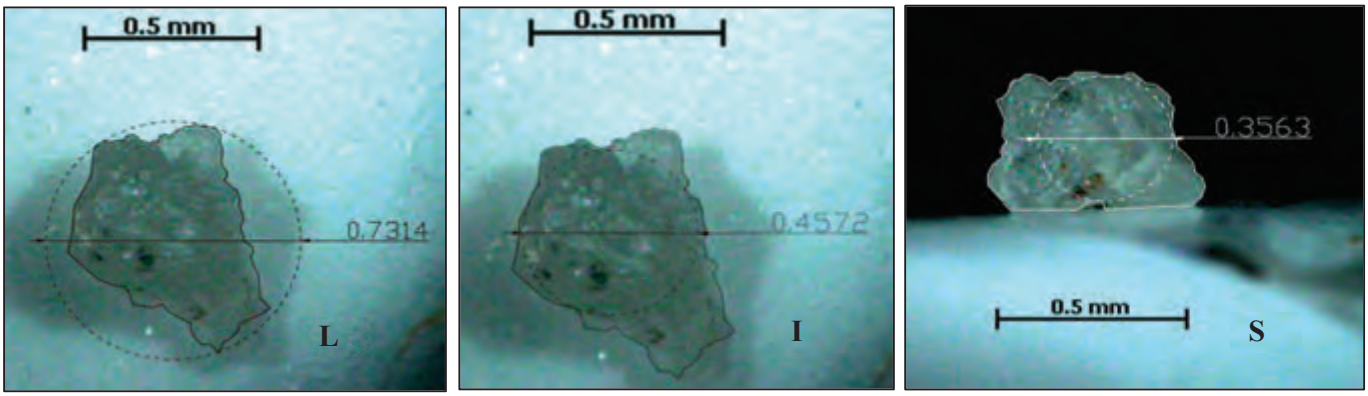

Figure 6: D50 = 1.6mm -Sample 3

Table 27: L, I and S Dimensions for SEES, D50=0.75mm

Sample	Front View		Side View	SEES
	L (mm)	I (mm)	S (mm)	
1	0.5133	0.3066	0.2777	0.54
2	0.4243	0.2990	0.2431	0.57

3	0.4531	0.2608	0.2508	0.55
			Average	**0.56**

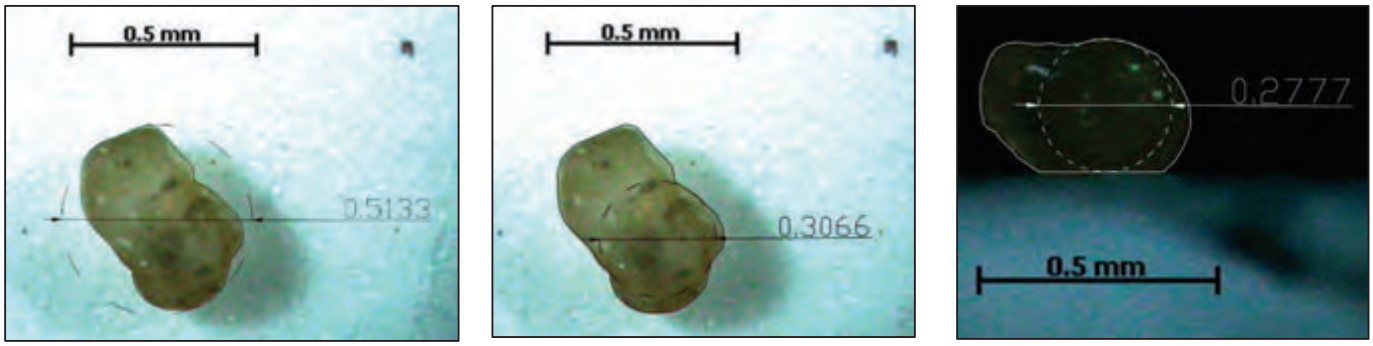

Figure 9: D50 = 0.75mm -Sample 1

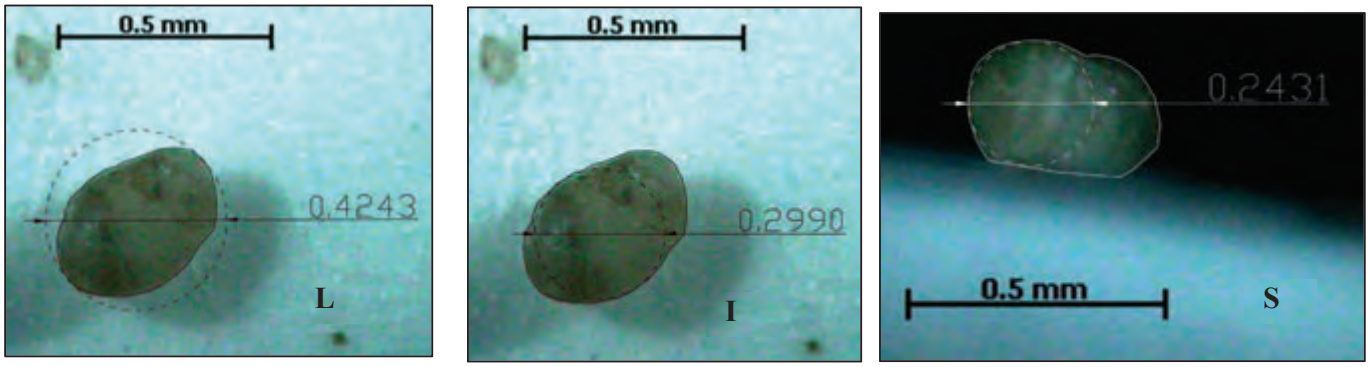

Figure 10: D50 = 0.75mm -Sample 2

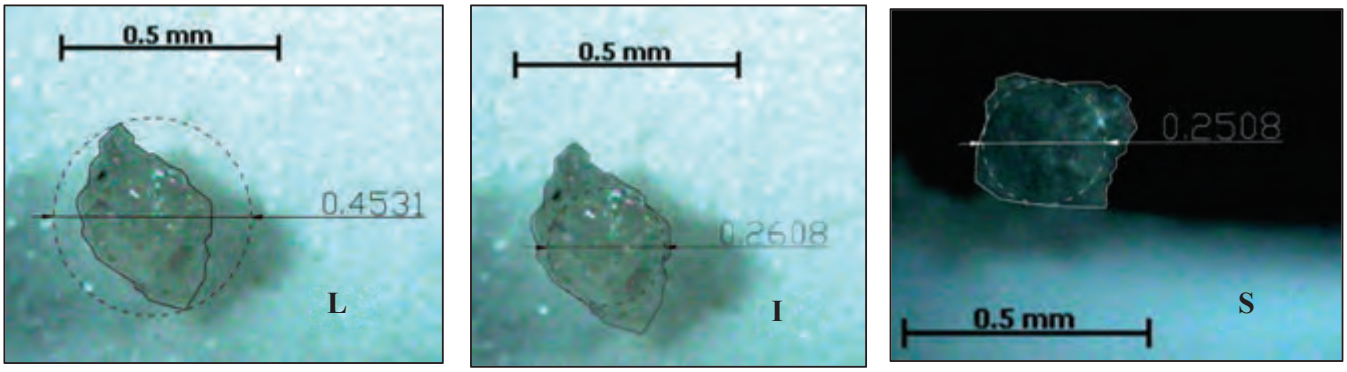

Figure 11: 0.75mm -Sample 3

Appendix C: Volumetric Measurement

1.8 Density of Putty

The putty that was used for the measurements of the scour volume was called Powafix Multi-Purpose Glazing Putty – White.

The specific gravity of this putty, as quoted by the manufacturer, was S.G. = 2.1. However, since the value of the putty's specific gravity/density was critical to the measurement of the scour volume, the specific gravity was determined independently for this study.

The following method was used to determine the putty's density:

1. A 10ml measuring cylinder was partially filled with a random amount of water. The measuring cylinder was marked with 0.2ml graduations.
2. The initial volume of water was measured and recorded (V_1).
3. A randomly sized piece of putty was then weighed and the mass was recorded (m).
    a. The putty was then dropped into the measuring cylinder with the water. The new volume of water was then measured and recorded (V_2).
4. The density of the putty was then calculated with Equation.
5. This process was repeated three times, and the results were averaged.

$$\rho_{putty} = \frac{m}{V_2 - V_1}$$

The results of this test are given in Table. The density of the putty used for this study was 2066kg/m^3.

Table 0-1: Putty Density Test

Test	V_1	V_2 (ml)	Mass (g)	Density (kg/m^3)
1	5.8	6.5	1.435	**2050**
2	5.2	6.2	2.120	**2120**
3	5	6.1	2.232	**2029**
			Average	**2066**

1.9 Repeatability of Volumetric Measurement

In order to determine the accuracy and repeatability of the scour volume measurement method, an eroded pipe sample was selected and its scour volume was measured 10 times,

and the mass of the putty was recorded. The results of these measurements are recorded in Table.

From these 10 measurements, mean, range, and standard deviation were calculated. These values are reported in Table. Furthermore, the standard deviation was calculated as a percentage of the mean. This analysis shows that there was some variation in this method of measuring the scour volume, with an error of approximately 4.9%.

Table 0-2: Scour Volume Measurement Repeatability Test

Measurement	Mass (g)
1	0.751
2	0.754
3	0.745
4	0.744
5	0.739
6	0.746
7	0.751
8	0.776
9	0.770
10	0.766

Table 0-3: Scour Volume Measurement Analysis

Standard Deviation (g)	Range (g)	Mean (g)	% Standard deviation of mean
0.0123	0.037	0.7542	4.91

EBE Faculty: Assessment of Ethics in Research Projects

Any person planning to undertake research in the Faculty of Engineering and the Built Environment at the University of Cape Town is required to complete this form before collecting or analysing data. When completed it should be submitted to the supervisor (where applicable) and from there to the Head of Department. If any of the questions below have been answered YES, and the applicant is NOT a fourth year student, the Head should forward this form for approval by the Faculty EIR committee: submit to Ms Zakiya Chikte (Zakiya.chikte@uct.ac.za); New EBE Building, Ph 021 650 5739). Students must include a copy of the completed form with the dissertation/thesis when it is submitted for examination.

Name of Principal Researcher/Student: Stefan Pike **Department: Civil Engineering**

If a Student: **Degree: M.Sc. Eng.** **Supervisor: Prof. J.E. van Zyl**

If a Research Contract indicate source of funding/sponsorship: Water Research Commission

Research Project Title: Experimental Investigation of Leakage-Induced Pipe Erosion outside of Pipe Leaks

Overview of ethics issues in your research project:

Question 1: Is there a possibility that your research could cause harm to a third party (i.e. a person not involved in your project)?	YES	(NO)
Question 2: Is your research making use of human subjects as sources of data? If your answer is YES, please complete Addendum 2.	YES	(NO)
Question 3: Does your research involve the participation of or provision of services to communities? If your answer is YES, please complete Addendum 3.	YES	(NO)
Question 4: If your research is sponsored, is there any potential for conflicts of interest? If your answer is YES, please complete Addendum 4.	YES	(NO)

If you have answered YES to any of the above questions, please append a copy of your research proposal, as well as any interview schedules or questionnaires (Addendum 1) and please complete further addenda as appropriate.

I hereby undertake to carry out my research in such a way that

- there is no apparent legal objection to the nature or the method of research; and
- the research will not compromise staff or students or the other responsibilities of the University;
- the stated objective will be achieved, and the findings will have a high degree of validity;
- limitations and alternative interpretations will be considered;
- the findings could be subject to peer review and publicly available; and
- I will comply with the conventions of copyright and avoid any practice that would constitute plagiarism.

This application is approved by:

Supervisor (if applicable):		
HOD (or delegated nominee): Final authority for all assessments with NO to all questions and for all undergraduate research.		
Chair : Faculty EIR Committee For applicants other than undergraduate students who have answered YES to any of the above questions.		

ADDENDUM 1:
Please append a copy of the research proposal here, as well as any interview schedules or questionnaires:

ADDENDUM 2: To be completed if you answered YES to Question 2:

It is assumed that you have read the UCT Code for Research involving Human Subjects (available at http://web.uct.ac.za/depts/educate/download/uctcodeforresearchinvolvinghumansubjects.pdf) in order to be able to answer the questions in this addendum.

2.1 Does the research discriminate against participation by individuals, or differentiate between participants, on the grounds of gender, race or ethnic group, age range, religion, income, handicap, illness or any similar classification?	YES	NO
2.2 Does the research require the participation of socially or physically vulnerable people (children, aged, disabled, etc) or legally restricted groups?	YES	NO
2.3 Will you not be able to secure the informed consent of all participants in the research? (In the case of children, will you not be able to obtain the consent of their guardians or parents?)	YES	NO
2.4 Will any confidential data be collected or will identifiable records of individuals be kept?	YES	NO
2.5 In reporting on this research is there any possibility that you will not be able to keep the identities of the individuals involved anonymous?	YES	NO
2.6 Are there any foreseeable risks of physical, psychological or social harm to participants that might occur in the course of the research?	YES	NO
2.7 Does the research include making payments or giving gifts to any participants?	YES	NO

If you have answered YES to any of these questions, please describe how you plan to address these issues (append to form):

ADDENDUM 3: To be completed if you answered YES to Question 3:

3.1 Is the community expected to make decisions for, during or based on the research?	YES	NO
3.2 At the end of the research will any economic or social process be terminated or left unsupported, or equipment or facilities used in the research be recovered from the participants or community?	YES	NO
3.3 Will any service be provided at a level below the generally accepted standards?	YES	NO

If you have answered YES to any of these questions, please describe how you plan to address these issues (append to form)

ADDENDUM 4: To be completed if you answered YES to Question 4

4.1 Is there any existing or potential conflict of interest between a research sponsor, academic supervisor, other researchers or participants?	YES	NO
4.2 Will information that reveals the identity of participants be supplied to a research sponsor, other than with the permission of the individuals?	YES	NO
4.3 Does the proposed research potentially conflict with the research of any other individual or group within the University?	YES	NO

If you have answered YES to any of these questions, please describe how you plan to address these issues(append to form)